2015

THE DISPERSION AND SELECTIVE FLOCCULATION OF HEMATITE ORE

Howard James Haselhuhn III
Michigan Technological University

THE DISPERSION AND SELECTIVE FLOCCULATION OF HEMATITE ORE

By

Howard James Haselhuhn III

A DISSERTATION

Submitted in partial fulfillment of the requirements for the degree of

DOCTOR OF PHILOSOPHY

In Chemical Engineering

MICHIGAN TECHNOLOGICAL UNIVERSITY

2015

This dissertation has been approved in partial fulfillment of the requirements for the Degree of DOCTOR OF PHILOSOPHY in Chemical Engineering

Department of Chemical Engineering

Thesis Advisor:	*Dr. S. Komar Kawatra*
Committee Member:	*Dr. Tony Rogers*
Committee Member:	*Dr. Caryn Heldt*
Committee Member:	*Dr. Paul Sanders*
Department Chair:	*Dr. S. Komar Kawatra*

Table of Contents

List of Figures

List of Tables

Preface

This dissertation is a compilation of published journal articles, journals articles accepted for publication, and unpublished project reports developed by Howard Haselhuhn and Dr. S. Komar Kawatra. The layout of the journal articles have been edited to present a flow of topics throughout the dissertation. Unpublished project reports were stripped of intellectual property prior to their inclusion within this dissertation.

All experiments and measurements discussed within this dissertation were performed by Howard Haselhuhn with the assistance of the undergraduate researchers acknowledged in the acknowledgement section of this dissertation. The overall project oversight, experimental design, technical considerations, and presentation of results in both paper and visual form were prepared by both Howard Haselhuhn and Dr. S. Komar Kawatra.

The following peer reviewed publications have been included within this dissertation with permission from the Journals they have been published in or are soon to be published in:

Haselhuhn, H. J., and Kawatra, S. K., 2015, "The Role of Surface Chemistry in Iron Ore Beneficiation," *Minerals & Metallurgical Processing*, Accepted.

Haselhuhn, H. J., 2012, "Water Chemistry Effects on the Zeta Potential of Concentrated Hematite Ore," *Minerals & Metallurgical Processing*, Vol. 29, No. 2, pp. 135-136.

Haselhuhn, H. J, and Kawatra, S. K., 2015, "The Role of Water Chemistry in the Selective Flocculation and Dispersion of Iron Ore," *Minerals & Metallurgical Processing,* In Press

Haselhuhn, H. J., 2013, "Dispersant Adsorption and Effects on Settling Behavior of Iron Ore," *Minerals & Metallurgical Processing,* Vol. 30, No. 3, pp. 188-189.

Haselhuhn, H. J., Kawatra, S. K., 2015, "Design of a Continuous Pilot Scale Deslime Thickener," *Minerals & Metallurgical Processing*, Accepted.

Acknowledgements

I would first like to thank Dr. S. Komar Kawatra for his extensive role in the research projects that were accomplished for this dissertation. Without his advice, support and most of all, patience, this work would not have been possible.

I would also like to thank Dr. Timothy Eisele for his time in reading and giving feedback on all of my work. He has been a great friend throughout the past five years.

I would like to thank Cliffs Natural Resources, and particularly, Dr. Joshua Carlson, Scott Rasmussen, and Mathew Rea for providing the materials, advice and partial financial support for the research in this dissertation. I would also like to thank the U.S. Department of Education for financial support and ASISC for laboratory use and financial support. A special thanks goes out to all of the undergraduate students who put in time on the research projects I have been working on. In particular, I would like to thank Shannon Ennis for her time assisting with pilot thickener studies.

Finally, I would like to thank my wife, Amberlee Haselhuhn, for putting up with me over the past five years.

Abstract

Iron ore is one of the most important ores in the world. Over the past century, most mining of iron ore has been focused on magnetite (Fe_3O_4). As the name suggests, magnetite is magnetic in nature and is easily separated from gangue (unwanted) minerals through magnetic separation processes. Unfortunately, the magnetite ore bodies are diminishing. Because of this, there has been a recent drive to pursue technology that can economically separate hematite (Fe_2O_3) from its gangue minerals as hematite is a much more abundant source of iron. Most hematite ore has a very small liberation size that is frequently less than 25µm. Beneficiation of any ore with this fine of a liberation size requires advanced processing methods and is seldom pursued.

A single process, known as selective flocculation and dispersion, has been successfully implemented at a plant scale for the beneficiation of fine liberation size hematite ore. Very little is known about this process as it was discovered by the U.S. Bureau of Mines by accident. The process is driven by water chemistry and surface chemistry modifications that enhance the separation of the hematite from its gangue minerals. This dissertation focuses on the role of water chemistry and process reagents in this hematite beneficiation process. It has been shown that certain ions, including calcium and magnesium, play a significant role in the process. These ions have a significant effect on the surface chemistry as reported by zeta potential studies. It was shown that magnesium ions within the process water have a more significant impact on surface chemistry than calcium ions due to steric hindrance effects at the hematite surface. It has also been

shown that polyacrylic acid dispersants, if used in the process, can increase product quality (increase iron content, decrease phosphorus content, decrease silica content) substantially.

Water, surface and reagent chemistry experiments were performed at a laboratory, pilot, and full plant scale during the course of this work. Many of the conclusions developed in the laboratory and pilot scale were found to be true at the full plant scale as well. These studies are the first published in history to develop theories of water chemistry and surface chemistry interactions at a full plant scale.

Introduction

Iron ore is one of the most important ores to the global society. It primarily consists of two minerals: magnetite (Fe_3O_4) and hematite (Fe_2O_3). Currently, magnetite is heavily mined and concentrated using magnetic separators. Hematite is rarely mined because it cannot be separated easily from its gangue minerals (silica, clay, etc…). Most of the world's iron ore is in the form of hematite; therefore, as the grade of magnetite ore continues to decline, it is important to develop new and better technology to concentrate hematite ore.

One process exists that can economically and industrially concentrate hematite ore. It uses a combination of selective flocculation and dispersion desliming and reverse cationic froth flotation. This process was developed by the U.S. Bureau of Mines and has only been implemented at one plant in the world. It is a complicated process relying on both surface chemistry and water chemistry to separate hematite from other minerals. The surface chemistry, water chemistry, and reagent selection in this process is the topic of this dissertation.

Surface chemistry play a very important role in the hematite beneficiation process. Surface chemistry refers to the interactions of aqueous ions and reagents at the solid iron ore particle surfaces. These surfaces typically carry an electrical charge that attracts ions and reagents from the solution. The interaction between ions, reagents and the surface can result in either physical or chemical bonds that can affect how the particle behaves in the process. For example, a flocculant can be attracted to charged particle surfaces, form

chemical or physical bonds with surfaces on multiple particles, and thereby cause flocculation of those particles. This same phenomena can happen with aqueous ions. If particle surfaces are negatively charged and a positively charged cation exists nearby, the negatively charged surfaces will form either physical or chemical bonds with the cation, and thereby cause flocculation.

During the first step of the hematite beneficiation process, known as selective flocculation and dispersion desliming, reagent selection and water chemistry are very crucial. At this step, all particles, regardless of mineralogy, carry a negatively charged surface. It is important to remove positively charged ions such as calcium and magnesium in order to prevent flocculation of particles containing different mineralogies. This is accomplished using a dispersant and is discussed in depth in Chapter 3. It is also important to add a selective flocculant that only flocculates a particular mineral, in this case, hematite. If a dispersant is added to negate the effects of cations and a selective flocculant is added to flocculate only hematite, hematite flocs will settle while all other minerals will remain dispersed and can be removed.

Reagents selection, water chemistry and surface chemistry are also very important during the second step of the hematite beneficiation process, known as reverse cationic froth flotation. In this beneficiation process, a reagent is added to depress the surface charge of only hematite. Then a reagent, known as a collector, is added that has a cationic end group with a hydrophobic chain. Since the surface charge of the hematite has been depressed, the cationic end of the collector selectively adsorbs to the non-hematite particle surfaces. The hydrophobic end of the collector is easily attached to air bubbles

which are injected to allow the now-hydrophobic particles to float to the top of the vessel, while the flocculated and depressed hematite particles sink to the bottom and a removed as the product.

This dissertation discusses the surface phenomena occurring within this beneficiation process in detail. Experiments were performed to show the effects of water chemistry, surface chemistry, and reagent selection in the laboratory, in a pilot scale beneficiation process, and at a full scale hematite beneficiation plant. It is the first compilation of work on this process that relates surface phenomena on all three process scales.

Chapter 1 Introduction

Chapter 1 of this dissertation is a review of the common iron ore beneficiation processes. It serves as an in-depth introduction to the remainder of the dissertation. This chapter explains how the water chemistry and surface chemistry are linked in the process and discusses how changes in either can affect process performance.

Chapter 2 Introduction

Chapter 2 focuses on the water and surface chemistry required for an effective separation of hematite from its gangue minerals in hematite ore. Chapter 2 is split into three sections. The first section (2.1) details a laboratory analysis of the zeta potential of hematite ore and shows how different common ions in water can affect the zeta potential. Implications to process performance are also discussed. The second section (2.2) details the effects of these water chemistry factors on process performance in a pilot scale selective flocculation and dispersion deslime thickener. This thickener was constructed at

Michigan Tech and designed with the help of Chris Braun at FLSmidth. During this study, water chemistry as changed in the process and the resulting grade and recovery of hematite ore was measured. The third section (2.3) details a study of water chemistry and surface chemistry at the previously mentioned selective flocculation and dispersion full scale hematite beneficiation plant. In the first analysis, samples were taken throughout the plant and relationships between water chemistry, surface chemistry and plant performance were determined. In the second analysis, samples were taken and analyzed on site three times per day for five days. Relationships between water chemistry, surface chemistry, and process performance were used to give recommendations to the project sponsor.

Chapter 3 Introduction

Chapter 3 contains material concerning dispersant selection for the selective flocculation and dispersion process. Chapter 3 is split into two sections. The first section (3.1) discusses dispersant effectiveness at a laboratory scale. During this study, the effects of dispersant choice, dispersant dose, and water chemistry were determined. The effectiveness of each dispersant was compared. The second section (3.2) uses many of the dispersants from the first section (3.1) and applies them at a pilot scale to determine if the laboratory conclusions scaled to a pilot separation process.

1 The Role of Surface Chemistry in Iron Ore Beneficiation[1]

1.1 Iron Ore Beneficiation Processes

There are two principle types of ore bodies that are processed in the United States: Magnetite and Hematite. Magnetite (Fe_3O_4) is a magnetic iron oxide that is easily concentrated using a combination of magnetic separators and flotation. The reserves of magnetite ore are continuously diminishing due to its ease of beneficiation making technology that can process hematite ores extremely important. Hematite (Fe_2O_3) is a non-magnetic iron oxide that constitutes the majority of the worldwide iron ore reserves. Processing hematite ore typically requires advanced separation techniques including selective flocculation and dispersion, reverse froth flotation, or high-tension electrostatic separation.

Magnetite beneficiation typically takes place in a series of magnetic separators followed by reverse froth flotation. A flow sheet for the magnetite beneficiation process at a Minnesota plant is shown in Figure 1.1. During this process, a ~38% Fe magnetite ore is ground in a rod mill to ~3% passing at 400 mesh. The first stage of magnetic separators, known as cobbers, remove large siliceous particles from the process. The cobber concentrate is then ground to ~51% passing at 400 mesh. This ground material is then

[1] The material contained within this chapter has been published in the journal *"Minerals & Metallurgical Processing."* It is included in this dissertation with permission from the journal.
Citation:
Haselhuhn, H. J., and Kawatra, S. K., 2015, "The Role of Surface Chemistry in Iron Ore Beneficiation," *Minerals & Metallurgical Processing*, Accepted.

processed by a second stage of magnetic separators known as roughers. The roughers concentrate the iron oxides to ~59% Fe. The concentrate is passed through a cyclone to remove fine material (~61% passing at 400 mesh) for further processing. The course material is recirculated back into the ball mill for further grinding. The cyclone overflow is processed via thickening where fine silica is removed in the overflow. The concentrate from thickener typically contains ~67% Fe. The next beneficiation step is a magnetic separator known as the finisher. This step concentrates the iron up to ~68.5% Fe. (Reid, 1988) The final beneficiation step uses flotation to float the remaining silica from the magnetite. Once the beneficiation process is complete, the concentrated iron ore is then filtered and agglomerated into pellets in preparation for dry processing. Similar flow sheets are used in other Minnesota and Michigan magnetite beneficiation plants (Mular et al., 2002).

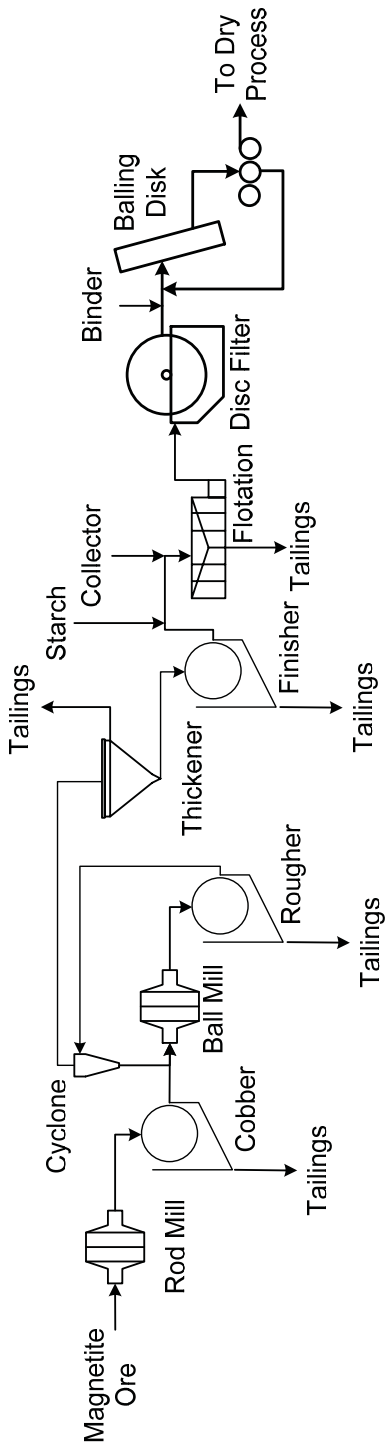

Figure 1.1: Example magnetite benefication process flow sheet used in Minnesota mining operation. Adapted from Mular et al. (2002) and Reid (1988).

Hematite beneficiation processes (aside from electrostatic separation) rely much more heavily on water chemistry and chemical reagents (flocculants and dispersants) to drive the separation processes. This type of process is typically known as selective flocculation and dispersion. This name stems from the use of corn starch as a selective flocculant for iron oxides and the use of inorganic phosphate and silicate general dispersants. An example of a flow sheet for this type of hematite beneficiation plant is shown in Figure 1.2. The incoming ore is ground with caustic soda (NaOH) in a ball mill (semi-autogenous) and pebble mill until liberation size is reached (~81% passing at 500 mesh). The fine material is removed by cyclones and the iron ore is initially concentrated to ~55% Fe in selective thickeners (deslime thickeners) using starch as a selective flocculant. The deslime thickener underflow is further concentrated via reverse cationic froth flotation using an etheramine collector. Carbon dioxide is added to the concentrate to reduce the alkalinity prior to filtration. A calcite/dolomite fluxing agent is also added at this stage for slag removal during downstream reduction processes. The concentrate is then filtered and agglomerated into pellets in preparation for dry processing.(Keranen, 1986) This type of beneficiation plant is seldom economical because it is difficult to control the surface chemistry that affect reagent selectivity (Department of Energy, 2001; Haselhuhn et al., 2012).

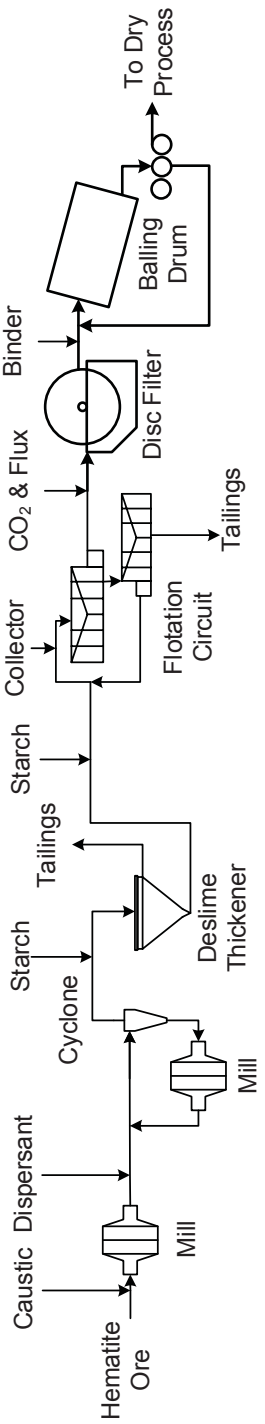

Figure 1.2: Example hematite beneficiation process flow sheet used in Michigan mining operation. Adapted from Keranen (1986).

The dry processing steps are very similar in most iron ore beneficiation plants. It consists of drying and sintering the pelletized concentrate using either a straight grate or a grate-kiln-grate furnace. Once dried, the pellets are shipped via railway or waterway to a smelting plant. Smelting can take place in a variety of ways including the blast furnace, electric arc furnace (EAF) or on a smaller scale, the rotary hearth furnace (RHF or Midrex ITmk3®). A flow-sheet for dry processing of iron ore is shown in Figure 1.3.

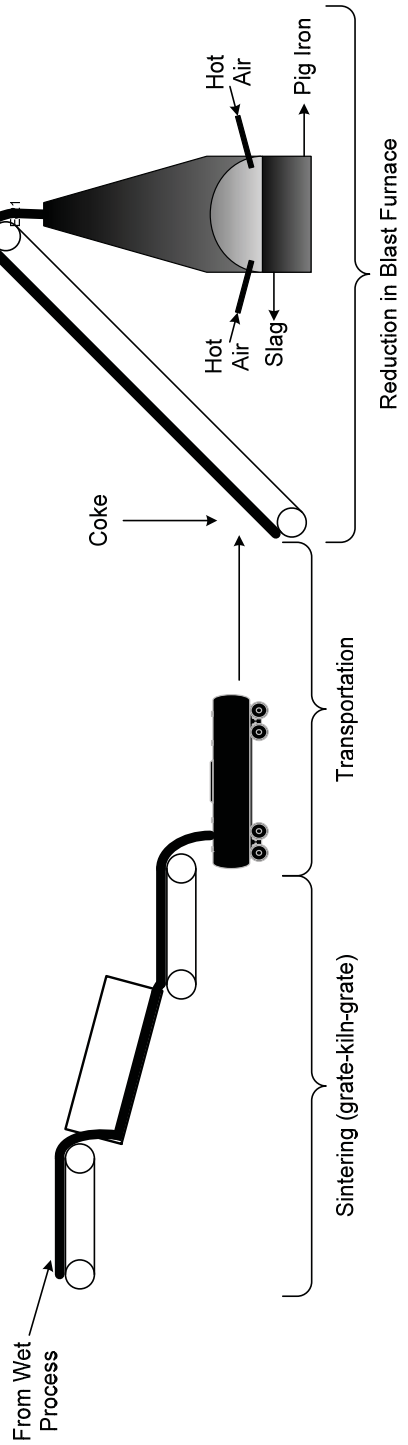

Figure 1.3: Dry processing of concentrated iron ores through a grate-kiln-grate sintering furnace and a blast furnace for pig iron production.

This dissertation focuses on the water chemistry, surface chemistry and reagents used during the selective flocculation and dispersion wet process described in Figure 1.2.

1.2 Relationship of Water Chemistry, Surface Chemistry and the Selective Flocculation and Dispersion Process

Ionic equilibrium and surface chemistry play vital roles during the selective flocculation and dispersion process of hematite beneficiation (Eisele et al., 2005; Engesser, 2003; Ripke et al., 2003). Ions in the process water are attracted to the solid particle surfaces during the separation process. These interactions affect the electrostatic charge of the particle in solution (zeta potential) and the ability of chemical reagents to act on the surfaces in a way that promotes their separation. To study the effects of these ions in the process, it is important to understand where these ions come from; i.e. what is dissolving in the water to produce these ions and what ions are already present in the fresh and recycled process waters. It is also important to understand how these dissolved ions interact with the surfaces during processing; i.e. which ions can cause issues during selective flocculation and dispersion.

1.2.1 Dissolution of Iron Ore Minerals

United States iron ores primarily consist of magnetite (Fe_3O_4). As the reserves of magnetite continue to diminish, other ores including hematite (Fe_2O_3), goethite ($FeO(OH)$), pyrite (FeS_2), and siderite ($FeCO_3$) will need to be mined to meet the worldwide iron demand. These minerals behave differently during the concentration process. Magnetite, hematite and goethite are, for the most part, insoluble iron oxides

during the concentration process; whereas, pyrite and siderite dissolve to form sulfate ions and carbonate ions, respectively:

Pyrite Dissolution in Process Water (Engesser, 2003):

$$4FeS_{2(s)} + 15O_2 + 14H_2O \rightarrow 4Fe(OH)_3 + 16H^+ + 8SO_4^{-2}$$

Siderite Dissolution in Process Water (Bénézeth et al., 2009):

$$FeCO_{3,(s)} \rightarrow Fe^{+2} + CO_3^{-2}$$

The sulfuric acid generation from the oxidation reaction of pyrite is neutralized in the process water by calcite ($CaCO_3$) and dolomite ($CaMg(CO_3)_2$) present in the ore. This neutralization reaction results in an increase in the ionic concentrations of calcium, magnesium, carbonate and sulfate ions in the process water (Engesser, 2003). Gangue minerals found in the ore, such as the aforementioned calcite and dolomite, also dissolve to contribute calcium, magnesium and carbonate to the ionic content of the process water:

Calcite Dissolution in Process Water:

$$CaCO_{3,(s)} \rightarrow Ca^{+2} + CO_3^{-2}, \text{ or}$$

$$H^+ + CaCO_{3,(s)} \rightarrow Ca^{2+} + HCO_3^-$$

Dolomite Dissolution in Process Water

$$CaMg(CO_3)_{2,(s)} \rightarrow Ca^{+2} + Mg^{+2} + 2CO_3^-, or$$

$$2H^+ + CaMg(CO_3)_{2,(s)} \rightarrow Ca^{+2} + Mg^{+2} + 2HCO_3^-$$

1.2.2 Ionic Contributions from Chemical Reagents

Most other ions that are contained within the process water are the result of adding reagents during the concentration process. Many reagents are added during the

concentration process that use sodium to solubilize their functional groups including sodium hydroxide (pH modifier and dispersant), sodium carbonate (pH modifier), sodium oleate (anionic collector), sodium silicate (dispersant), sodium phosphates (dispersant), and sodium dodecyl sulphate (anionic collector) (Arol et al., 2003; Haselhuhn et al., 2012; Iwasaki, 1983; Quast, 2000). There are also reagents that contribute anions to the process water including sodium silicate, sodium phosphate, sodium carbonate, carbon dioxide (pH modifier) and dodecylammonium chloride (cationic collector). These reagents, their functional groups and some typical dosage rates found in literature can be seen in Table 1.1.

Table 1.1: Process reagents that contribute cations and anions to the process water.

Chemical Name	Trade Name	Chemical Formula	Structure	Reagent Use	Typical Dosage (Units Specified)
Sodium Silicate	Water Glass	**Na**$_2$SiO$_3$	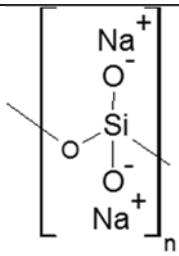	Dispersant	0.30 lb/ton[a] 0 – 4 lb/ton[b]
Sodium Tripolyphosphate	STPP	**Na**$_5$P$_3$O$_{10}$	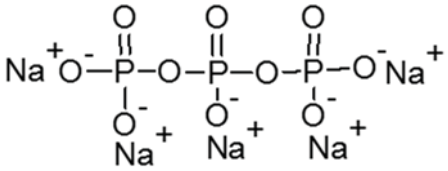	Dispersant/Water Softener	0 – 1 lb/ton[b]
Sodium Hydroxide	Caustic	**Na**OH	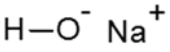	pH Modifier/Dispersant	2.45 lb/ton[a]
Sodium Carbonate	Soda Ash	**Na**CO$_3$	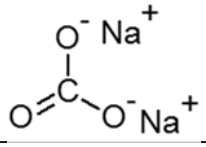	pH Modifier	
Carbon Dioxide	-	**CO$_2$**	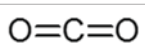	pH Modifier	
Sodium Oleate	-	**Na**C$_{18}$H$_{33}$O$_2$	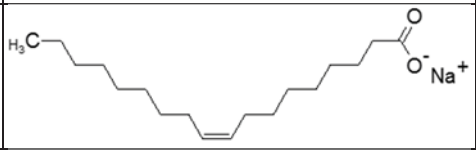	Anionic Collector	
Sodium Dodecyl Sulphate	-	**Na**C$_{12}$H$_{25}$SO$_4$	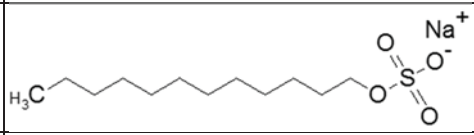	Anionic Collector	0.2 – 2.2 lb/ton[c]
Dodecyl-ammonium Chloride[d]	-	C$_{12}$H$_{25}$NH$_3$**Cl**	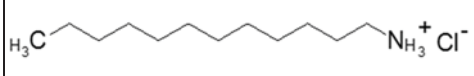	Cationic Collector	

References:

a - (Keranen, 1986) b - (Green et al., 1984) c - (Quast, 2000) d - (Choi et al., 1961)

1.2.3 Ionic Contributions from Fresh and Re-use water in Concentrator

Depending on the iron ore processing facility, the water used in the process can come from recirculating process water, fresh water or a combination of both. A recent study conducted by Haselhuhn et al., (2012) on process water chemistry throughout an iron ore concentrator showed the principle ions present in the process water at different location within a hematite ore concentrator. This study concluded that the process water changes drastically from the initial addition of water during comminution to the removal of water at filtration. This data is shown in Table 1.2. As shown, the incoming water has significant amounts of sodium, carbonate and chloride ions present. The sodium concentration slightly increases from 455 to 495 ppm due to reagent addition. The total carbonate concentration (bicarbonate plus carbonate) increases from 818 ppm to 1295 ppm due to the addition of a calcite/dolomite fluxing agent and the addition of carbon dioxide prior to filtration. The addition of the fluxing agent and CO_2 also cause an increase in the calcium and magnesium concentration of the process water because of the dissolution of the fluxing agent at the decreased pH. The high concentrations of ions seen at the filter feed can be detrimental to downstream balling, sintering and reduction processes. (Haselhuhn et al., 2012)

Table 1.2: Chemical analyses of process water at an operating hematite ore concentration plant at water addition and removal operations (Haselhuhn et al., 2012).

Description	Post Comminution Process Water	Filter Feed Process Water
Calcium (mg/L)	4.47	71
Magnesium (mg/L)	2.67	58
Sodium (mg/L)	455	495
Potassium (mg/L)	11.4	20.5
Iron (mg/L)	16.4	0.5
pH (WAL)	10.59	7.67
Chloride (mg/L)	110	100
Sulfate (mg/L)	90	100
Fluoride (mg/L)	4.1	4.2
Nitrate (mg/L)	16	0.1
Nitrite (mg/L)	0.29	0
Carbonate (mg/L)	724	0
Bicarbonate (mg/L)	94	1295
Hardness ($CaCO_3$ mg/L)	22	416

1.3 Surface Chemistry of Iron Ore

Interactions between process water ions and the surfaces of the slurry particles account for most variations in processing conditions during flotation and desliming operations in the selective flocculation and dispersion process. Understanding how specific ions interact with surfaces is essential to optimize process performance and predict downstream processing requirements.

The pH of the water is the primary factor determining the surface charge of particles in solution. (Laskowski et al., 1992; Stumm et al., 1992). At a low pH the surface is positively charged, whereas, at a high pH, the surface is negatively charged as shown in Figure 1.4. The pH at which the surface bears no charge is referred to as the point of zero charge (PZC).

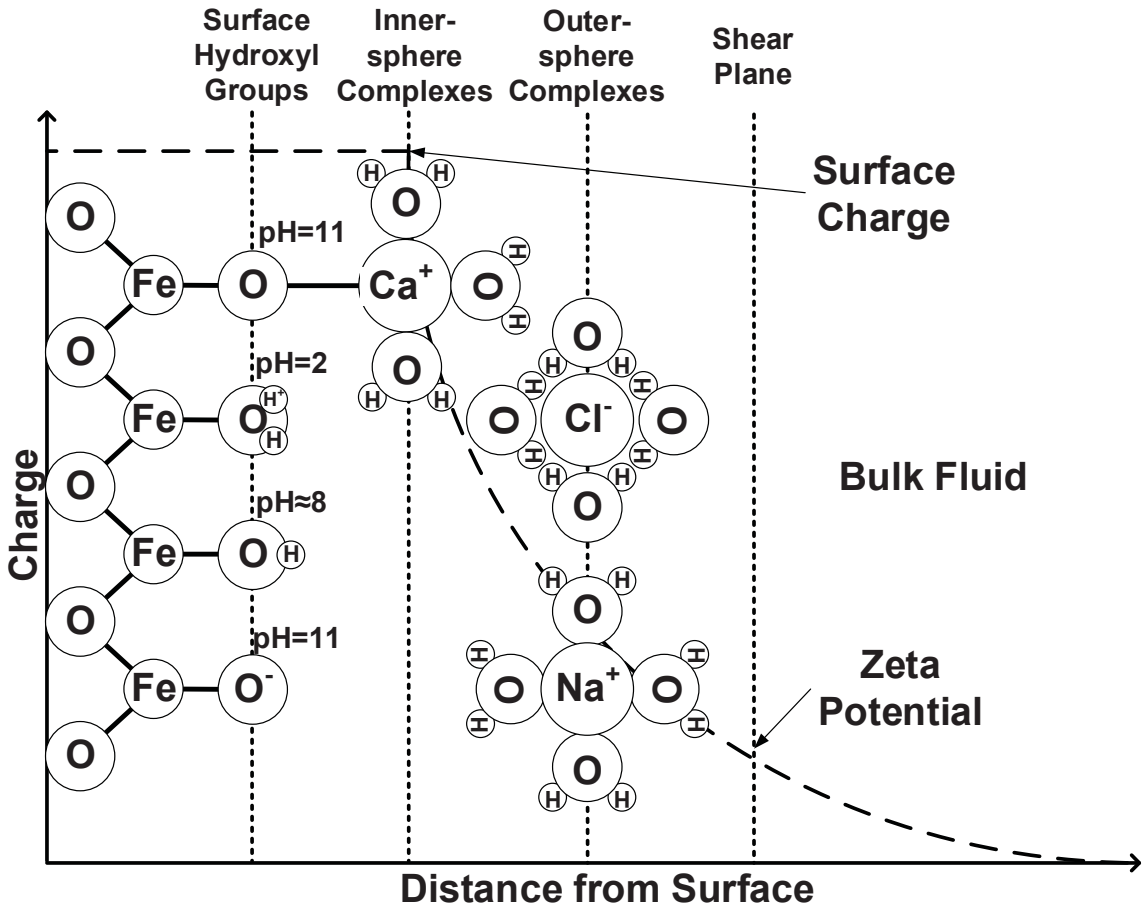

Figure 1.4: Water-solid interface of a hydrated iron oxide. As distance from surface hydroxyl groups increases, the charge with respect to the bulk fluid decreases. The charge at the shear plane is known as the zeta potential. pH: hydrogen from solution adsorbs to surface oxygen; depending on the pH of the solution, the hydroxyl surface can be positively, negatively, or neutrally charged. Complexes: inner sphere complexes exist at the hydroxyl surface if pH is adequate for formation; outer-sphere complexes exist due to coulombic forces away from surface. Adapted from Dzombak et al. (1990), Laskowski et al. (1992), Sparks et al. (1998), and Stumm et al. (1992).

The surface charge determines the charge of ions in solution that will be attracted to the surface. The ions that are attracted to the surface either form inner-sphere or outer-sphere complexes at the surface. An inner-sphere complex consists of a primarily single covalent bond between the ion and the surface. An outer sphere complex occurs when the ion approaches the surface through coulombic forces but is separated from the surface by one or more water molecules, see Figure 1.4 (Stumm et al., 1992).

The coulombic forces diminish with distance from the surface. As the coulombic forces diminish, the outer-sphere complexes can no longer be held to the surface and are merely present as diffuse ions in the bulk fluid. The distance at which the coulombic forces are too weak to hold outer-sphere complexes to the surface is referred to as the shear plane, see Figure 1.4. The potential difference between the shear plane (sometimes referred to as the slipping plane) and the bulk solution is referred to as the zeta potential. The zeta potential of particle surfaces is primarily a function of water chemistry and the underlying surface charge of the particle.

1.3.1 Surface Speciation and Surface Potential

Each oxide mineral in the iron ore has a unique relationship with the surrounding aqueous environment. This relationship creates an electrical charge at the surface of the particle. The magnitude and sign (positive or negative) of the surface charge is first and foremost a function of pH. For an oxide mineral, the 2 pKa model has been extensively used to define the surface charge of particles. It consists of chemical equations relating the concentration of negatively, neutrally, and positively charged surface sites to an

equilibrium constant. This model consists of the following equilibrium reactions and equations (Equations 1.1 and 1.2):

$$\equiv MOH_2^+ \overset{K_{a1}^{app}}{\Longleftrightarrow} \equiv MOH + H^+ \qquad K_{a1}^{app} = \frac{[\equiv MOH]\{H^+\}}{[\equiv MOH_2^+]} \qquad \textbf{\textit{Equation 1.1}}$$

$$\equiv MOH \overset{K_{a2}^{app}}{\Longleftrightarrow} \equiv MO^- + H^+ \qquad K_{a2}^{app} = \frac{[\equiv MO^-]\{H^+\}}{[\equiv MOH]} \qquad \textbf{\textit{Equation 1.2}}$$

$Where,$

$\equiv$ *denotes a solid material behind a surface*

M *denotes an atom bonded to oxide to form an oxide mineral*

$(ex: M = Fe\ for\ Fe_2O_3)$

K_{ax}^{app} *= Applied equilibrium constant for the given reaction*

$[\equiv MOH_2^+]$ *= Concentration of positively charged surface sites* $\left(\frac{mol}{L}\right)$

$[\equiv MOH]$ *= Concentration of neutrally charged surface sites* $\left(\frac{mol}{L}\right)$

$[\equiv MO^-]$ *= Concentration of negatively charged surface sites* $\left(\frac{mol}{L}\right)$

$\{H^+\}$ *= Activity of hydrogen in the process water* $\left(\frac{mol}{L}\right)$

The applied equilibrium constant, K_{ax}^{app}, is a function of the concentration of the reactive surface sites, the activity of the ions present in the process water, and the electrical potential between the surface and the bulk fluid surrounding the surface, denoted surface potential (ψ). It can be correlated to published values of intrinsic equilibrium constants using the following empirical relation (Equation 1.3):

$$K_{ax}^{app} = K_{ax}^{int} \cdot e^{\frac{Z \cdot F \cdot \psi}{R \cdot T}}$$ ***Equation 1.3***

$Where,$

$K_{ax}^{int} = Intrinsic\ equilibrium\ constant\ for\ the\ given\ reaction$

$Z = Change\ in\ surface\ charge\ for\ the\ given\ reaction$

$F = \ Farraday\ Constant \left(96485.34 \frac{C}{mol}\right)$

$\psi = Surface\ Potential\ (V)$

$R = Ideal\ Gas\ Constant\ \left(8.314\ \frac{kg \cdot m^2}{s^2 \cdot mol \cdot K}\right)$

$T = Temperature\ (K)$

To use these equations, both the intrinsic equilibrium constant and the surface potential at a given pH must be known. Literature values for the intrinsic equilibrium constant for common constituents of iron ore are shown in Table 1.3. The surface potential, can be calculated via the Gouy-Chapman theory (Equation 1.4) using the total ionic concentration of the slurry, c, the temperature of the slurry, T, the dielectric constant of the slurry, ε, and the valency of the ions in the slurry, Z and the charge of the surface, σ (Stumm et al., 1992):

$$\psi = \frac{2RT \cdot asinh\left(\frac{\sqrt{2}\sigma}{4\sqrt{RT\varepsilon\varepsilon_0 c}}\right)}{F \cdot z}$$ ***Equation 1.4***

$Where,$

$R = Ideal\ Gas\ Constant\ \left(8.314\ \frac{kg \cdot m^2}{s^2 \cdot mol \cdot K}\right)$

$T = Temperature\ (K)$

$\varepsilon = Dielectric\ Constant\ (78.5\ for\ water\ at\ 25°C)$

$\varepsilon_0 = Permittivity\ of\ Free\ Space\ \left(8.854 \cdot 10^{-12}\frac{C}{V \cdot M}\right)$

$c = Total\ Ionic\ Concentration\ of\ Slurry\ \left(\frac{mol}{m^3}\right)$

$z = Valency\ of\ ions\ in\ the\ slurry$

$\sigma = Surface\ Charge\ \left(\frac{C}{m^2}\right)$

The unknown variable in Equation 1.4 is the surface charge, σ. This electric charge attracts counter-ions in the solution forming a layer of charged ions surrounding the particle. This layer of ions can reduce or strengthen the effects of process reagents added to the slurry and thus have a large impact on mineral separation operations. The surface charge must be solved for iteratively using the following equation (Equation 1.5) in conjunction with Equation 1.1-1.4 and a mole balance on surface sites:

$$\sigma = \frac{F}{a \cdot s}([\equiv MOH_2^+] - [\equiv MO^-]) \qquad \textbf{\textit{Equation 1.5}}$$

$Where,$

$a = Concentration\ of\ Solids\ \left(\frac{kg}{L}\right)$

$s = Specific\ Surface\ Area\ \left(\frac{m^2}{kg}\right)$

Specific surface area can be measured for each case; however, in absence of technology to measure surface area, literature values are available for ranges of surface areas of each of the main constituents in iron ore (Cornell et al., 1996; Demchuk et al., 2005).

Table 1.3: Surface reactions of the constituents of iron ore in water and their associated equilibrium constants (Davis et al., 1986; Fuerstenau et al., 2007).

Surface Acidity Reaction & Equation	**Equilibrium Constants for Iron Ore Minerals**		
$\equiv MeOH_2^+ \overset{K_{a1}^{app}}{\Longleftrightarrow} \equiv MeOH + H^+$	$\boldsymbol{log(K_{a1}^{int})}$	$\boldsymbol{log(K_{a2}^{int})}$	**Mineral**
	-7.09	-11.11	Goethite (FeO(OH))
$K_{a1}^{app} = K_{a1}^{int} \cdot e^{\frac{Z \cdot F \cdot \psi}{R \cdot T}}$	-5.8	-11.10	Hematite (Fe_2O_3)
$\equiv MeOH \overset{K_{a2}^{app}}{\Longleftrightarrow} \equiv MeO^- + H^+$	-4.30	-8.30	Magnetite (Fe_3O_4)
$K_{a2}^{app} = K_{a2}^{int} \cdot e^{\frac{Z \cdot F \cdot \psi}{R \cdot T}}$	1.30	-5.70	Quartz (SiO_2)

pH is the most important factor in the surface chemistry of slurried iron ore. pH defines the surface acidity of the mineral constituents in the slurry. The surface site distributions for these oxide minerals show that the surfaces carry either a positive, negative or neutral charge depending on the pH of the aqueous medium. When the number of positively charged surface sites and the number of negatively charged surface sites are equal, the corresponding pH value is known as the point of zero charge (PZC). When the pH is above the PZC, the surface has a net negative surface charge. When the pH is below the PZC, the surface has a net positive surface charge.

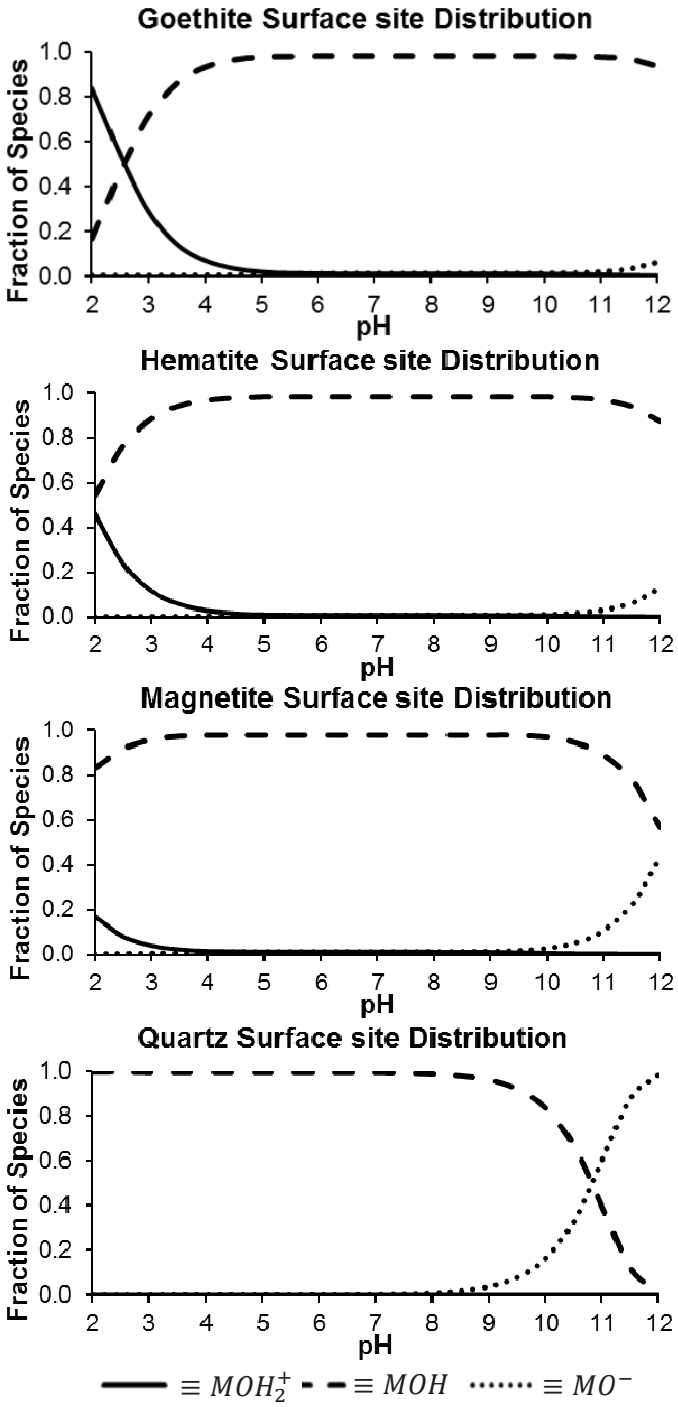

Figure 1.5: Distribution of positively, neutrally and negatively charged surface sites as a function of pH for Goethite, Hematite, Magnetite and Silica. Note: M denotes an atom in the crystal lattice such as iron or silicon.

From Figure 1.5 it can be seen that each different mineral surface has a different distribution of positively, negatively and neutrally charged surface sites at different pHs. Inherently, this causes each surface to carry a different surface potential, ψ, at each pH. Figure 1.6 shows the surface potential of each mineral as a function of pH. The surface potential of the slurry particles attract or repel ions in the process water and is responsible for effective reagent adsorption that drives separation processes such as flotation. The information presented in Figure 1.6 helps explain why certain collectors and surfactants have a narrow effective pH range and why cations and anions are attracted to and bond to surfaces in specific pH ranges.

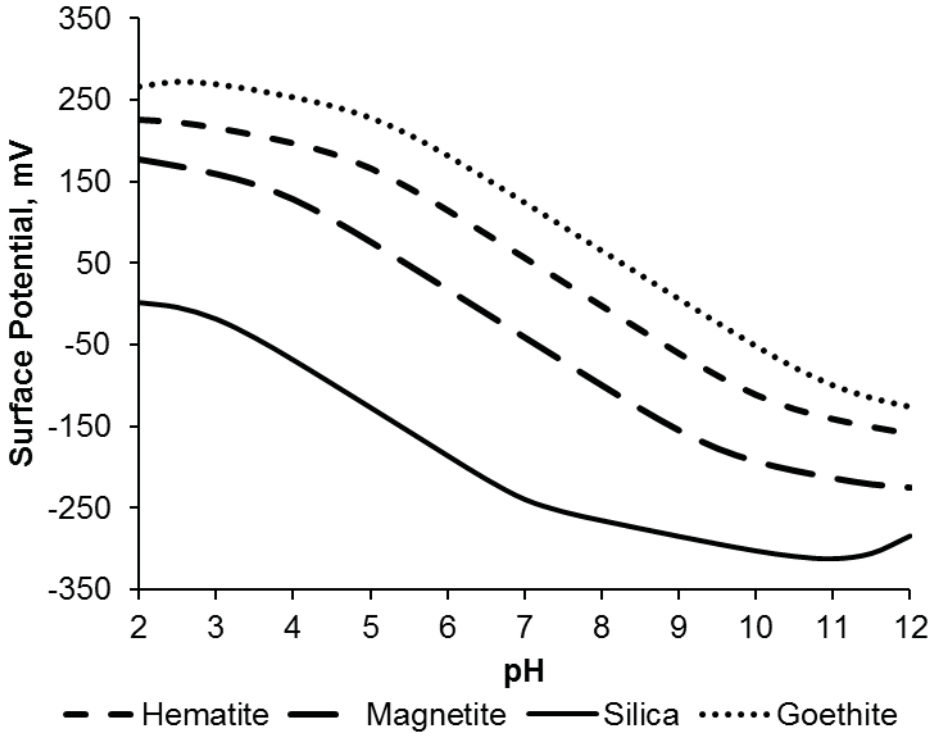

Figure 1.6: Surface potentials as a function of pH for Silica, Magnetite, Hematite and Goethite. Slurry particle characteristics measured from filter feed at hematite ore concentration plant. Site density for mineral surface sites found in literature. (Cornell et al., 1996; Demchuk et al., 2005)

1.3.2 Ion Adsorption Phenomena at Mineral Oxide Surfaces

Like the hydrogen ion, other ions can form physical or chemical bonds with a charged surface and cause changes in the surface potential. Ions that form chemical bonds with the surface, or specifically adsorbing ions, create inner-sphere complexes with the surface. Ions that form physical bonds with the surface via electrostatic interaction create outer-sphere complexes with the surface. Both inner-sphere and outer-sphere complexes have an effect on the selective flocculation and dispersion process.

Inner-sphere complexation can be modeled similarly to the equations discussed above except that equilibrium expressions for ionic interactions with each other must be considered as well. Much data has been compiled on ionic interactions and surface adsorption to iron oxides and silicon oxides in literature (Berka et al., 2001; Dzombak et al., 1990; Kinniburgh et al., 1982; Kinniburgh et al., 1976; Kitamura et al., 1999; Smith et al., 2004). Robust software, such as PHREEQCI, was used to iteratively model ion adsorption and inner-sphere complexation at mineral surfaces while taking ionic equilibrium into account. To use this software, a comprehensive database was created including all surface speciation reactions to be modeled. Some intrinsic adsorption constants for ion adsorption had to be estimated based on those of similar minerals. Using the process water constituents and slurry solid characteristics at an operating hematite concentrator, the speciation of inner-sphere complexes at slurry particle surface sites as a function of pH was developed. This speciation map is shown in Figure 1.7.

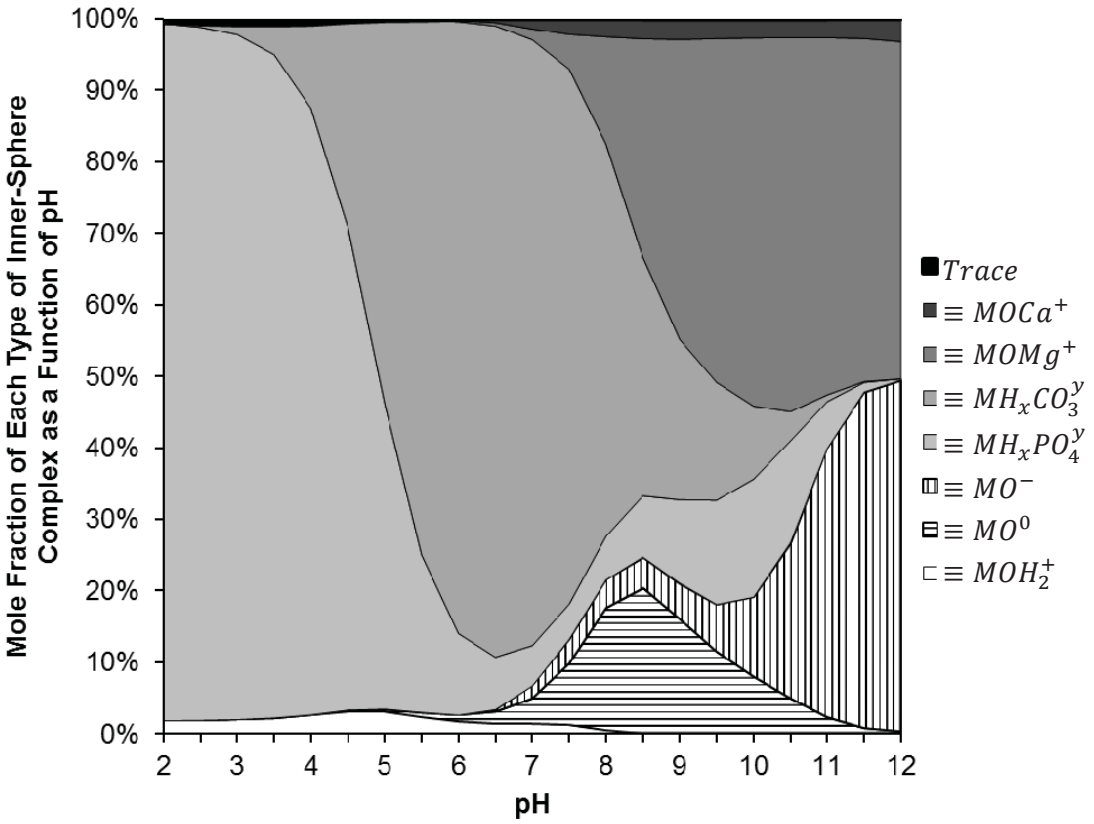

Figure 1.7: Inner-sphere complex speciation at particle surfaces as a function of pH. At a given pH, the percent of a surface covered by a particular surface complex is shaded accordingly. For example, at a pH of 7, most of the surface is covered in carbonate surface complexes. Note: x denotes number of atoms in complex, y denotes charge of complex, trace includes $\equiv MF^0$ ***and*** $\equiv MH_xSO_4^y$.

Figure 1.7 shows, from a theoretical basis, what inner-sphere complexes dominate the surfaces of the iron ore particles. Inner-sphere complexes within Figure 1.7 were grouped according to the ion type; for instance, $[\equiv MH_xPO_4^y]=[\equiv MH_2PO_4^0]+[\equiv MHPO_4^-]+[\equiv MPO_4^{-2}]$. These inner-sphere complexes can be displaced by or hinder adsorption of process reagents depending on the thermodynamics

and chemical equilibrium of the reagent adsorption. These inner-sphere complexes also travel with the surfaces during the process and contribute to the ionic constituents within the final product.

Negatively and neutrally charged phosphate inner-sphere complexes dominate the surface of iron ore particles below a pH of 5, as shown in Figure 1.7. Above pH 5, the surface is dominated by negatively and neutrally charged carbonate inner-sphere complexes until a pH of 8. At a pH of 8 and above, the surface is dominated by positively charged magnesium inner-sphere complexes and un-complexed hydroxyl sites with a negative charge.

Outer-sphere complexes form surrounding the particle near the particle surface and are held to the surface by electrostatic forces. Outer-sphere complexes surrounding particle surfaces remain with the particles during the process due to these electrostatic forces. The total molar quantity of each ion in the diffuse layer can be modeled using PHREEQCI as well. A similar mapping of diffuse layer content as a function of pH is shown in Figure 1.8. These calculations were made assuming the layer of outer-sphere complexes spans to one Debye length beyond the surface using calculations found in Dzombak and Morel (1990).

In acidic conditions, sulfate, chloride and carbonate outer-sphere complexes dominate the surface of hematite ore particles, as shown in Figure 1.8. As the pH approaches neutral, the carbonate outer-sphere complexes diminish allowing for sodium outer-sphere

complexes to dominate. In alkaline conditions, the surface is dominated by sodium and carbonate outer-sphere complexes.

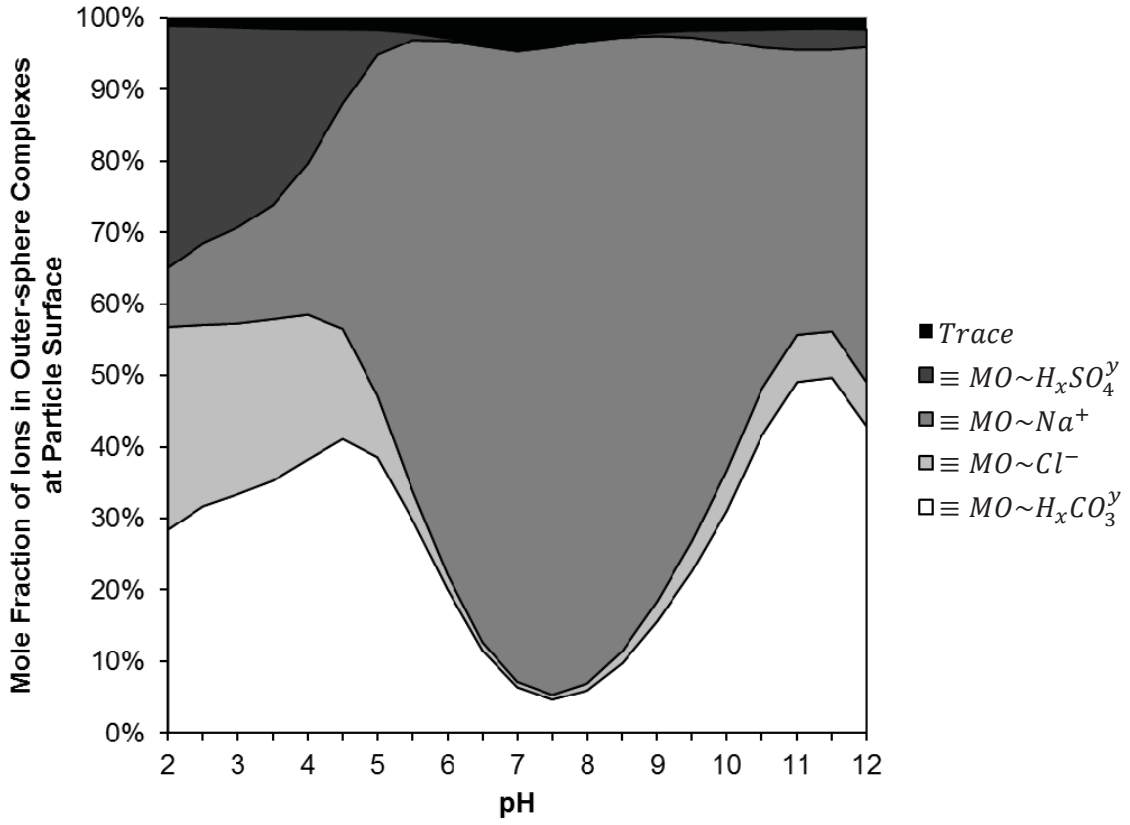

Figure 1.8: Outer-sphere complex speciation at particle surfaces as a function of pH. At a given pH, the percent of a surface covered by a particular outer-sphere complex is shaded accordingly. For example, at a pH of 7, most of the surface is covered in sodium outer-sphere complexes. Note: x denotes number of atoms in complex, y denotes charge of complex, trace includes $\equiv MO{\sim}Ca^{+2}$, $\equiv MO{\sim}F^{-}$, $\equiv MO{\sim}Fe^{y}$, $\equiv MO{\sim}K^{+}$, $\equiv MO{\sim}Mg^{+2}$, $\equiv MO{\sim}NO_x^y$, *and* $\equiv MO{\sim}H_xPO_4^y$.

1.4 References

Arol, A. I., and Iwasaki, I., 2003, "Effect of sodium silicate on flocculation of hematite with starch in the presence of calcium," *Separation Science and Technology,* Vol. 38, No. 3, pp. 647-659.

Bénézeth, P., Dandurand, J. L., and Harrichoury, J. C., 2009, "Solubility product of siderite ($FeCO_3$) as a function of temperature (25–250 °C)," *Chemical Geology*, Vol. 265, No. 1–2, pp. 3-12.

Berka, M., and Bányai, I., 2001, "Surface Complexation Modeling of K^+, NO_3^-, SO_4^{2-}, Ca^{2+}, F^-, Co^{2+}, and Cr^{3+} Ion Adsorption on Silica Gel," *Journal of Colloid and Interface Science*, Vol. 233, No. 1, pp. 131-135.

Choi, H., Cooke, S., and Iwasaki, I., 1961, "Flotation Characteristics of Hematite, Goethite and Activated Quartz with 18-Carbon Aliphatic Acids and Related Compunds," *AIME Transactions,* Vol. 217, pp. 237-244.

Cornell, R. M., and Schwertmann, U., 1996, *The Iron Oxides,* 2nd Edition, John Wiley & Sons, 703 pp.

Davis, J. A., and Hayes, K. F., 1986, *Geochemical Processes at Mineral Surfaces*, American Chemical Society, 683 pp.

Demchuk, E. and Murashov, V. V., 2005, "Surface Sites and Unrelaxed Surface Energies of Tetrahedral Silica Polymorphs and Silicate," *Surface Science,* Vol. 595, pp. 6-19.

Department of Energy, 2001, “Selective Flocculation of Fine Mineral Particles,” Office of Industrial Technologies Energy Efficiency and Renewable Energy, U.S. Department of Energy.

Dzombak, D. A., and Morel, F., 1990, *Surface complexation modeling : hydrous ferric oxide,* Wiley, 393 pp.

Eisele, T. C., Kawatra, S. K., and Ripke, S. J., 2005, "Water Chemistry Effects In Iron Ore Concentrate Agglomeration Feed," *Mineral Processing and Extractive Metallurgy Review*, Vol. 26, No. 3, pp. 295-305.

Engesser, J., 2003, "Effect of water chemistry, water treatment and Blaine on magnetite filtering and magnetite agglomeration with bentonite clay," *Minerals & Metallurgical Processing,* Vol. 20, No. 3, pp. 125-134.

Fuerstenau, M. C., Jameson, G., and Yoon, R.H., 2007, *Froth Flotation: A Century of Innovation,* Society for Mining, Metallurgy, and Exploration, 891 pp.

Green, R. E., and Colombo, A. F., 1984, “Dispersion-Selective Flocculation-Desliming Characteristics of Oxidized Taconites,” US Bureau of Mines, Report of Investigations, RI 8867, 24 pp.

Haselhuhn, H. J., Carlson, J. J., and Kawatra, S. K., 2012, "Water chemistry analysis of an industrial selective flocculation dispersion hematite ore concentrator plant," *International Journal of Mineral Processing,* Vol. 102–103, pp. 99-106.

Iwasaki, I., 1983, "Iron Ore Flotation, Theory and Practice," *Mining Engineering,* Vol. 35, pp. 622-632.

Keranen, C. U., 1986, “Reagent Preparation, Distribution and Feeding Systems at the Tilden Mine,” *Design and Installation of Concentration and Dewatering Circuits,* A. L. Mular and M. A. Anderson eds., Society for Mining, Metallurgy and Exploration, pp. 308-319.

Kinniburgh, D. G., and Jackson, M. L., 1982, "Concentration and pH dependence of calcium and zinc absorption by iron hydrous oxide gel," *Soil Science Society of America Journal*, Vol. 46, No. 1, pp. 56-61.

Kinniburgh, D. G., Jackson, M. L., and Syers, J. K., 1976, "Adsorption of Alkaline Earth, Transition, and Heavy Metal Cations by Hydrous Oxide Gels of Iron and Aluminum," *Soil Science Society of America Journal,* Vol. 40, No. 5, pp. 796-799.

Kitamura, A., Fujiwara, K., Yamamoto, T., Nishikawa, S., and Moriyama, H., 1999, "Analysis of Adsorption Behavior of Cations onto Quartz Surface by Electrical Double-layer Model," *Journal of Nuclear Science and Technology,* Vol. 36, No. 12, pp. 1167-1175.

Laskowski, J. S., and Ralston, J., 1992, *Colloid Chemistry in Mineral Processing,* Elsevier Science, 428 pp.

Mular, A. L., Halbe, D. N., and Barratt, D. J., 2002, *Mineral Processing Plant Design, Practice, and Control,* Society for Mining, Metallurgy, and Exploration, 2500 pp.

Quast, K. B., 2000, "A review of hematite flotation using 12-carbon chain collectors," *Minerals Engineering,* Vol. 13, No. 13, pp. 1361-1376.

Reid, K. L., 1988, "Application of QEM*SEM for Beneficiation Studies of Minnesota Taconite," *Process mineralogy VIII*, D. J. T. Carson Ed., TMS, 391 pp.

Ripke, S. J., and Kawatra, S. K., 2003, "Effect of Cations on Unfired Magnetite Pellet Strength," *Minerals & Metallurgical Processing Journal,* Vol. 20, No. 3, pp. 153-159.

Smith, R. M., Martell, A. E., and Motekaitis, R. J., 2004, "NIST critically selected stability constants of metal complexes database," Version 8.0, National Institute of Standards and Technology, U.S. Department of Commerce.

Sparks, D. L., and Grundl, T. J., 1998, *Mineral-Water Interfacial Reactions,* American Chemical Society, 438 pp.

Stumm, W., Sigg, L., and Sulzberger, B., 1992, *Chemistry of the solid-water interface,* Wiley, 448 pp.

2 Effects of Water Chemistry on Dispersion and Selective Flocculation of Hematite Ore

2.1 Water Chemistry Effects on Zeta Potential of Concentrated Hematite Ore[2]

2.1.1 Abstract

The effectiveness of selective flocculation and dispersion processes for the concentration of hematite ore are strongly dependent on the ionic content of the process water. It has been noticed that magnesium ions are more detrimental to iron recoveries during selective flocculation and dispersion and flotation processes than calcium. This phenomenon was studied by measuring the zeta potential of hematite ore at various concentrations of sodium, magnesium, calcium, strontium and barium at a pH of 11. Results show that zeta potential inverts from negative to positive at very low concentrations of magnesium ions in the solution. It takes a significantly higher concentration of calcium, ions to achieve the same effect. This difference may be attributed to the ability of magnesium ions to adsorb to all surface hydroxyl groups,

[2] The material contained in this chapter has been published in the journal *"Minerals and Metallurgical Processing."* It is included in this dissertation with permission from the journal. This material can be found in the following two publications:

Haselhuhn, H. J., 2012, "Water Chemistry Effects on the Zeta Potential of Concentrated Hematite Ore," *Minerals & Metallurgical Processing,* Vol. 29, No. 2, pp. 135-136.

Haselhuhn, H. J., and Kawatra, S. K., 2015, "The Role of Surface Chemistry in Iron Ore Beneficiation," *Minerals & Metallurgical Proce*ssing, Accepted.

whereas calcium, due to their larger size, can only adsorb to every other hydroxyl group. This hypothesis was confirmed by results similar to those seen with calcium when this test was repeated with strontium and barium ions. The tendency for calcium ions to adsorb to every other surface hydroxyl group causes higher concentrations of calcium to be less detrimental to hematite concentration processes than magnesium.

2.1.2 Introduction

High grade iron ore has been nearly depleted in the United States forcing the mining industry to turn to beneficiation processes to concentrate lower grade ores. Some of these processes exploit the magnetic and electrostatic properties of the iron minerals to separate the valuable iron bearing constituents from impurities. The remainder utilize colloidal interactions as a driving force for their separation processes. A Lake Superior District hematite ore mine has been successfully concentrating 8.0 million tons of hematite ore per year with a process called Selective Flocculation and Dispersion (Cliffs Natural Resources, 2011). This process relies on many different reagents and the surface chemistry of fine colloidal particles to separate hematite from siliceous impurities.

The zeta potential of particle surfaces is extremely important in selective flocculation dispersion processes because it influences particle interactions and the effectiveness of many separation reagents. The zeta potential of the particle surfaces defines the dispersive stability of the particles in solution. Retaining a high dispersive stability is essential for the desliming and flotation processes employed in selective flocculation-dispersion concentrators.

Water softening agents such as sodium polyphosphates, sodium silicate and sodium hydroxide are typically added as dispersants prior to selective flocculation and dispersion of hematite from silica (Keranen, 1986). It has been noticed that magnesium ions have a much more detrimental effect on selective flocculation and dispersion than calcium ions at a local iron concentrator and the reasons behind this are poorly understood (Carlson, 2011).

2.1.3 Background

2.1.3.1 Zeta Potential and Ion Complexation

The pH of the water is the primary factor determining the surface charge of particles in solution. This is well described by the two-pKa model as shown in Equation 2.1 (Laskowski et al., 1992; Stumm et al., 1992). At a low pH the surface is positively charged, whereas, at a high pH, the surface is negatively charged as shown in Figure 1.4. The pH at which the surface bears no charge is referred to as the point of zero charge (PZC).

$$FeOH_2^+ \overset{pK_1}{\longleftrightarrow} FeOH \overset{pK_2}{\longleftrightarrow} FeO^- \qquad \textbf{Equation 2.1}$$

The surface charge determines the charge of ions in solution that will be attracted to the surface. The ions that are attracted to the surface either form inner-sphere or outer-sphere complexes at the surface. An inner-sphere complex consists of a primarily covalent bond between the ion and the surface. An outer sphere complex occurs when the ion approaches the surface through electrostatic forces but is separated from the surface by one or more water molecules, see Figure 1.4 (Stumm et al., 1992).

The electrostatic forces diminish with distance from the surface. As the electrostatic forces diminish, the outer-sphere complexes can no longer be held to the surface and are merely present as diffuse ions in the bulk fluid. The distance at which the electrostatic forces are too weak to hold outer-sphere complexes to the surface is referred to as the shear plane, see Figure 1.4. The potential difference between the shear plane and the bulk solution is referred to as the zeta potential. The zeta potential of particle surfaces is primarily a function of water chemistry and the underlying surface charge of the particle.

2.1.3.2 Hematite Crystal Structure

The hematite crystal structure is nearly identical to that of corundum; a nearly perfect hexagonal close pack (HCP) structure, see Figure 2.1. This crystal structure is composed of layers of iron and oxygen alternating in the [001] direction (Eggleston et al., 1992). The oxygen layers have sets of triangles that are composed of both tightly bound oxygen and loosely bound oxygen. The tightly bound oxygen (O-O) spacing is ~270pm; whereas the loosely bound oxygen spacing is ~300pm, as determined by scanning tunneling microscopy (Eggleston et al., 1992). When this crystal structure is exposed to an alkaline aqueous environment, free iron atoms at the cleavage plane are hydrolyzed. The hydroxyl groups at the surface have been calculated by vector math to be 285pm apart. This value is in agreement with published literature for iron spacing on the surface of un-hydrated hematite (Pradip, 1994; Ravishankar et al., 1995).

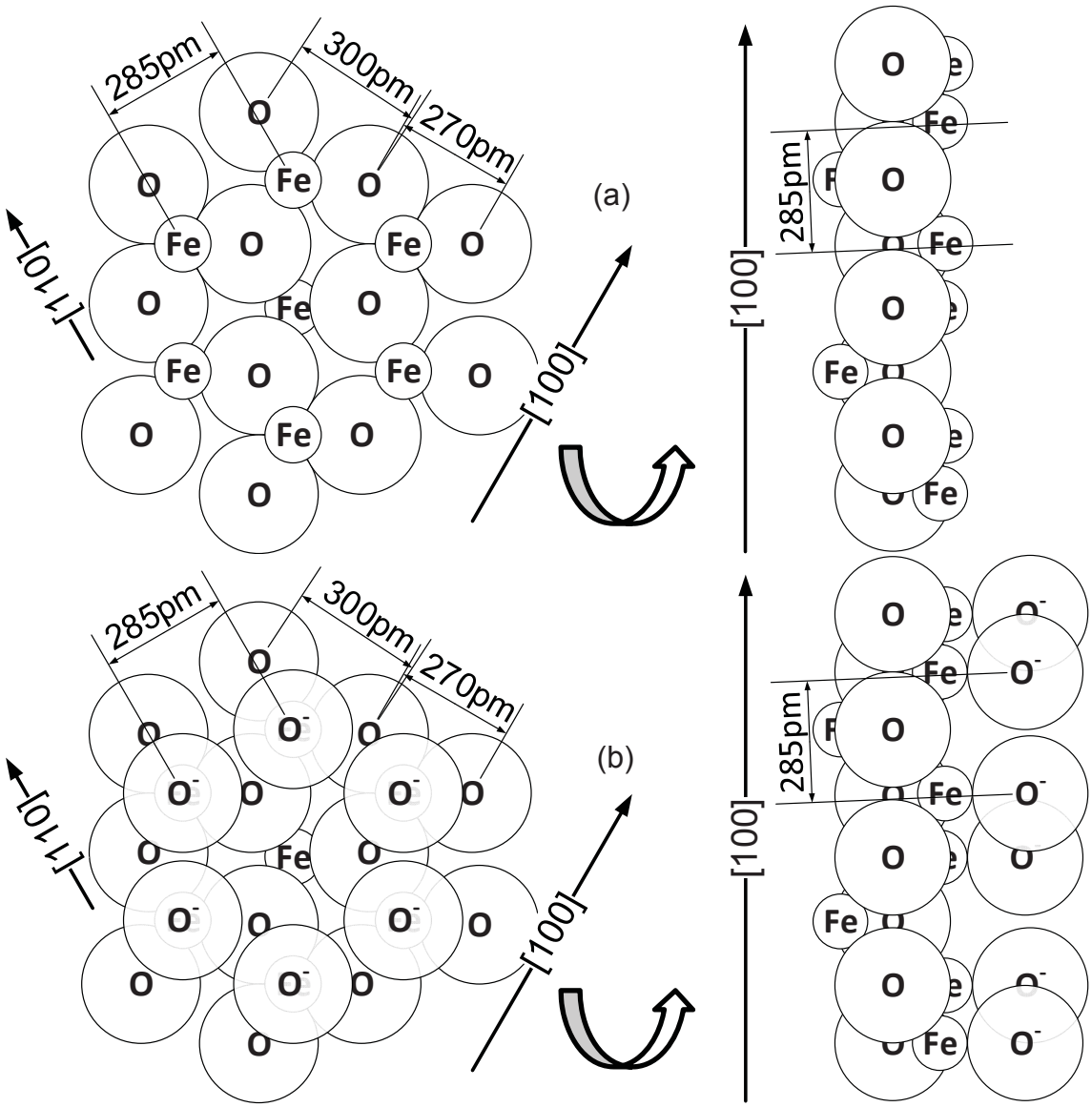

Figure 2.1: (a) Un-hydrated and (b) hydrated hematite surface structure in alkaline conditions; frontal view and side view. Drawn using information from Eggleston et al. (1992), Pradip (1994), and Ravishankar et al. (1995). All dimensions in picometers.

2.1.3.3 *Divalent Cation Adsorption*

Adsorption of divalent cations to the surface hydroxyl groups of iron oxides is strongly dependent upon pH (Dzombak et al., 1990). Adsorption isotherms of calcium,

magnesium, strontium and barium onto an iron oxide surface are shown in Figure 2.2. The surface must have negatively charged hydroxyl groups to attract cations and allow for adsorption. As discussed earlier, a highly alkaline environment maximizes negatively charge hydroxyl groups.

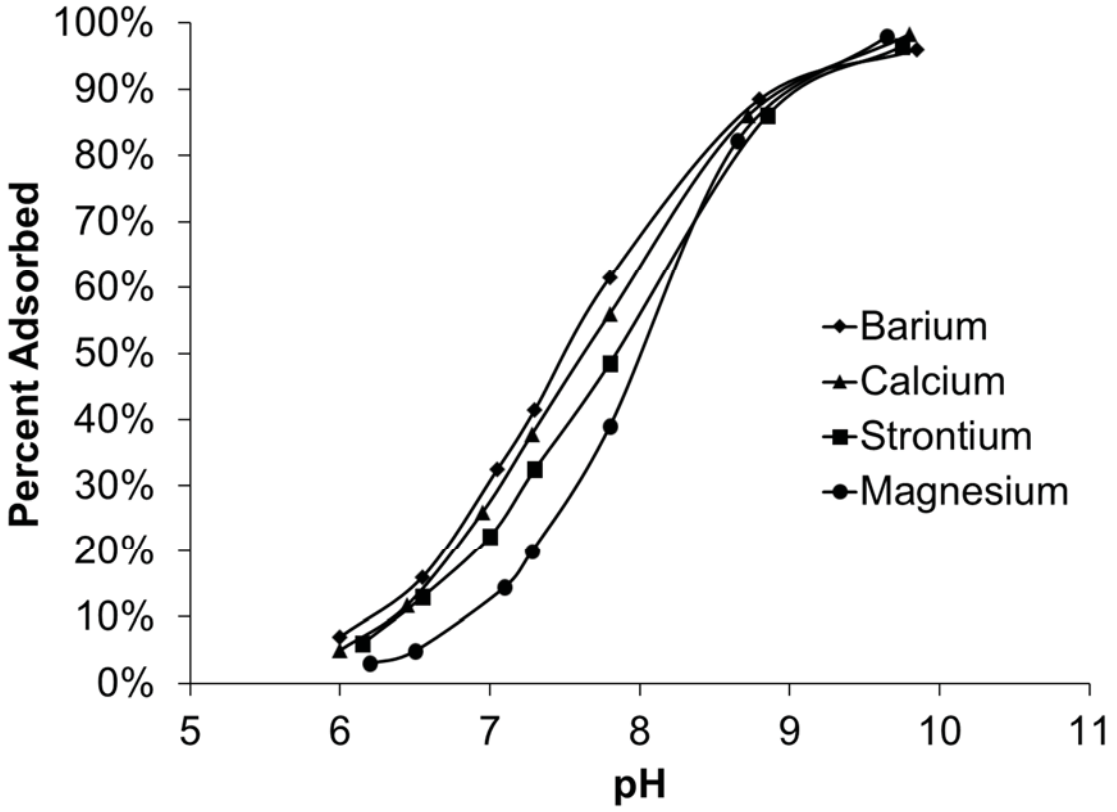

Figure 2.2: Adsorption isotherms for Magnesium (O'Brien et al., 1996), Calcium (Kinniburgh et al., 1982), Strontium and Barium (Kinniburgh et al., 1976) onto a hydrated iron oxide surface.

2.1.4 Materials and Methods

Concentrated iron ore was donated by a hematite ore concentration plant. The concentrated ore was washed with distilled water in a pressure filter in order to remove ions on the surface of the hematite particles. The washed solids were dried in a convection oven at 107°C for 24 hours. A small sample (~50g) of the dried hematite particles were then rehydrated with distilled water in a 300 mL beaker. This slurry was immediately decanted to remove fine particles. This was repeated with 2 liters of 5% HCl, 2 liters of 5% NaOH and 2 liters of distilled water to dissolve and wash away any calcium or magnesium bearing minerals present in the ore that could dissolve during the zeta potential tests. The coarse particles remaining were dried at 107ºC for 24 hours. Once dry, the course particles were split into 1 gram samples with a micro-rotary riffle splitter to ensure a representative sample was obtained for each test. The 1 gram sample was then weighed and hydrated with distilled water for 24 hours prior to use.

An Anton Paar Electrokinetic Analyzer (EKA) with an automatic titrator and a powder cell was used to measure the zeta potential of the coarse hematite particles as a function of titrant dosage. The background solution was one liter of 1mM NaCl brought to a pH of 11 using 1 M NaOH. A pH of 11 was chosen for this study for two reasons. Alkaline environments promote cation adsorption while inhibiting anion adsorption and the slurry pH of a local selective flocculation – dispersion iron ore concentrator is held between 10.5 and 11.5 to maximize dispersion of ground particles (Keranen, 1986).

Titrants were prepared by adding distilled water to reagent grade $MgCl_2 \cdot 6H_2O$, $CaCl_2 \cdot 2H_2O$, $SrCl_2 \cdot 6H_2O$, and $BaCl_2 \cdot 2H_2O$. After the titration was complete, the final background solutions were analyzed for magnesium, calcium, strontium, and barium concentrations. Magnesium and calcium concentrations were measured using an atomic absorption analyzer. Strontium and barium concentrations were measured via Ethylenediamenetetraacetic acid (EDTA) potentiometric titrations using a water hardness ion selective electrode. The concentration of ions at each step in the titration was interpolated from the initial and final concentrations and plotted with their respective zeta potential values. Each zeta potential measurement was repeated in triplicate to show statistical significance in the results.

2.1.5 Results and Discussion

Very small concentrations of magnesium caused the zeta potential to invert from a negative to a positive charge, as shown in Figure 2.3. A much larger concentration of calcium was required to invert the zeta potential from a negative to a positive charge. To determine if atomic size was the cause of this phenomena, larger ions, strontium and barium, were used as titrants in a similar manner.

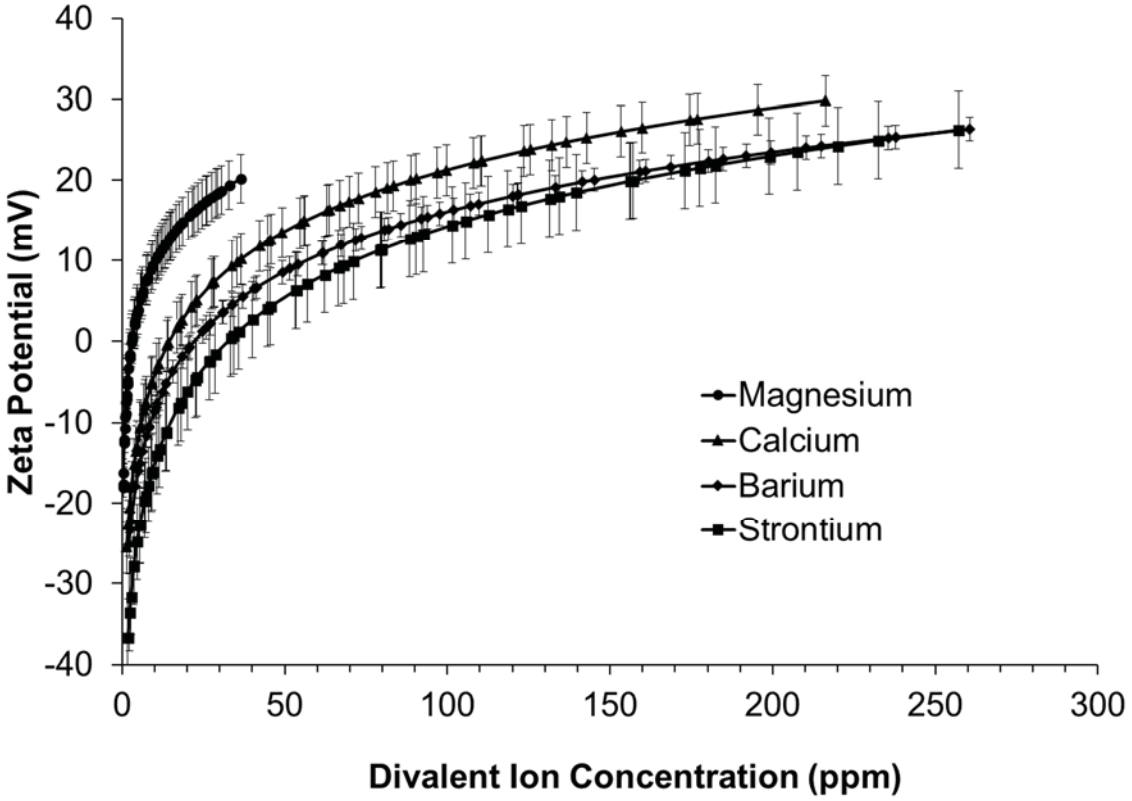

Figure 2.3: Zeta potential of concentrated natural hematite ore as a function of cation concentration at a pH of 11.

The slope of the zeta potential curves is steeper at lower concentrations than at higher concentrations of divalent cations. This shows that these cations may initially form inner-sphere complexes until all available hydroxyl groups have been complexed, as shown in Figure 2.1. Within inner-sphere complexes, the surface hydroxyl groups (-O-) act as lewis bases, donating an electron and increasing the electron density of the coordinated cation (Stumm et al., 1992).

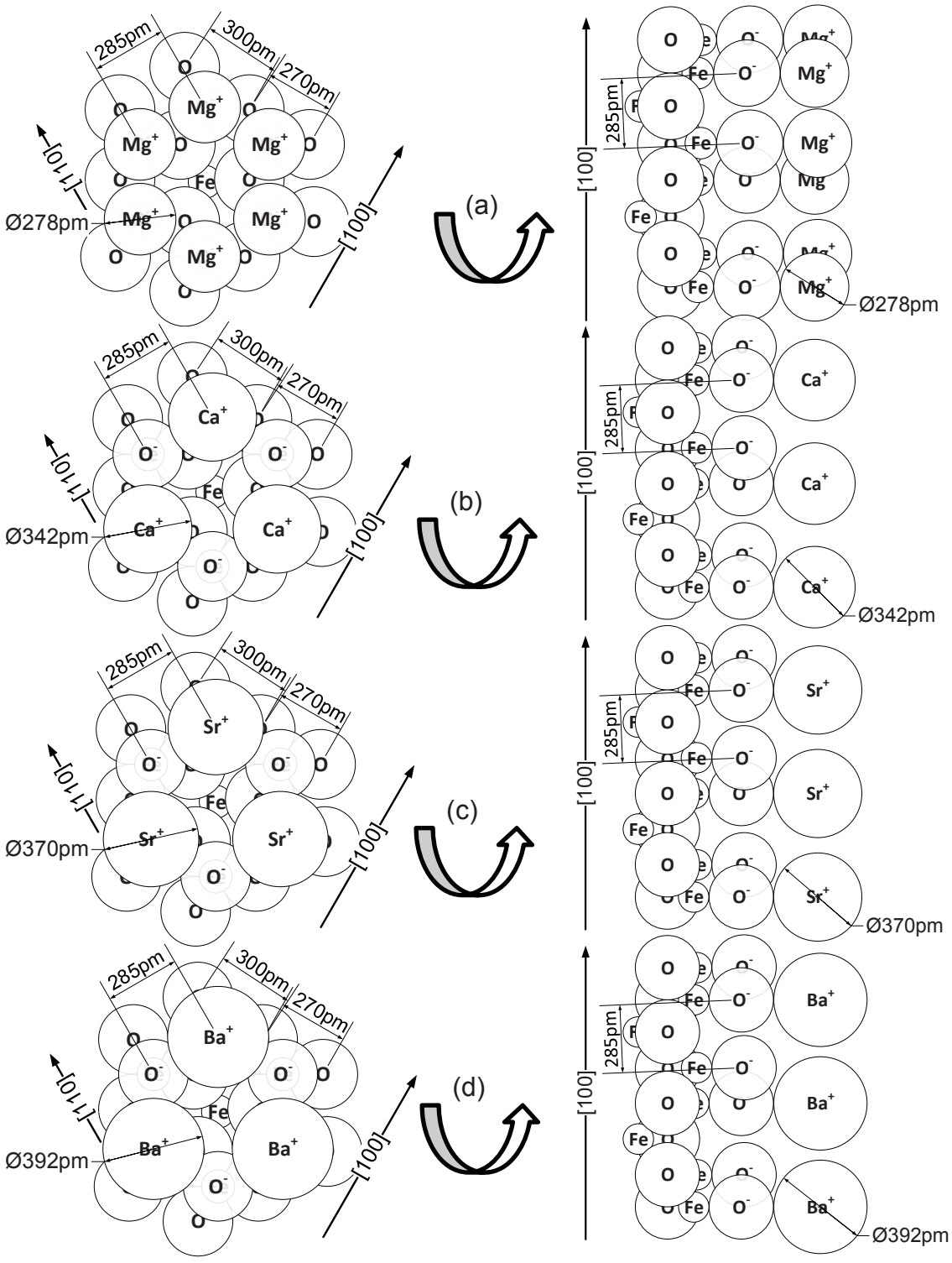

Figure 2.4: Inner-sphere complexes of magnesium, calcium, strontium and barium formed at surface hydroxyl groups in the [100] plane. All measurements in picometers.

At the cleavage plane of the hematite hexagonal close packed crystal structure, the average hydroxyl group spacing was calculated as 285 pm. This spacing is larger than the single covalent diameter of magnesium (278 pm) but smaller than the single covalent diameter of calcium (342 pm), strontium (370 pm), and barium (392 pm) (Pyykkö et al., 2009); see Figure 2.4. Because of this spacing, magnesium inner-sphere complexes can form at every hydroxyl group, however, calcium, strontium and barium inner-sphere complexes can only form at every other hydroxyl group.

2.1.6 Conclusions

In the hematite ore selective flocculation and dispersion process, the zeta potential of the particles is of particular importance because the particles must remain dispersed for effective separation. Magnesium ions have shown a much more detrimental effect on selective flocculation and dispersion than calcium ions at a local hematite concentration plant and the reasons behind this phenomenon are poorly understood. The dependence of the zeta potential of natural hematite concentrate on the concentration of cations at a pH of 11 was studied using an electrokinetic analyzer. Results show that zeta potential inverts from negative to positive at very low concentrations of magnesium ions in the solution. It takes a significantly higher concentration of calcium, strontium and barium ions to achieve the same effect. This difference is attributed to the ability of magnesium ions to form inner-sphere complexes with all surface hydroxyl groups, whereas calcium, strontium and barium, due to their larger atomic size, can only complex with every other hydroxyl group. The tendency for calcium ions to form inner-sphere complexes with

every other surface hydroxyl group causes higher concentrations of calcium to be less detrimental to hematite concentration processes than magnesium.

2.1.7 References

Carlson, J. J., 2011, *Effect of Calcium and Magnesium on Deslime Iron Recovery*, Personal Communication.

Cliffs Natural Resources, 2011, *Steel Starts Here*, Operations Data Fact Sheet, 4 pp.

O'Brien, Robert J., Ajoy Raje, Robert L. Spicer, Liguang Xu, Shiqi Bao, Scott Lambert, and Burtron H. Davis. "Technology Development for Iron Fischer-Tropsch Catalysts." *Proceedings of the First Joint Power & Fuel Systems Contractors Conference,* Pittsburgh, PA. 1996.

Dzombak, D. A., and Morel, F., 1990, *Surface complexation modeling : hydrous ferric oxide,* Wiley, 393 pp.

Eggleston, C. M., and Hochella, M. F., 1992, "The Structure of Hematite (001) Surfaces by Scanning Tunneling Microscopy - Image Interpretation, Surface Relaxation, and Step Structure," *American Mineralogist,* Vol. 77, No. 9-10, pp. 911-922.

Haselhuhn, H. J., 2012, "Water Chemistry Effects on the Zeta Potential of Concentrated Hematite Ore," *Minerals & Metallurgical Processing,* Vol. 29, No. 2, pp. 135-136.

Keranen, C. U., 1986, “Reagent Preparation, Distribution and Feeding Systems at the Tilden Mine,” *Design and Installation of Concentration and Dewatering Circuits,* A. L.

Mular and M. A. Anderson eds., Society for Mining, Metallurgy and Exploration, pp. 308-319.

Kinniburgh, D. G., and Jackson, M. L., 1982, "Concentration and pH dependence of calcium and zinc absorption by iron hydrous oxide gel," *Soil Science Society of America Journal,* Vol. 46, No. 1, pp. 56-61.

Kinniburgh, D. G., Jackson, M. L., and Syers, J. K., 1976, "Adsorption of Alkaline Earth, Transition, and Heavy Metal Cations by Hydrous Oxide Gels of Iron and Aluminum," *Soil Science Society of America Journal,* Vol. 40, No. 5, pp. 796-799.

Laskowski, J. S., and Ralston, J., 1992, *Colloid Chemistry in Mineral Processing,* Elsevier Science, 428 pp.

Pradip, 1994, “Reagents Design and Molecular Recognition at Mineral Surfaces,” *Reagents for Better Metallurgy,* Society for Mining Metallurgy, pp. 245-252.

Pyykkö, P., and Atsumi, M., 2009, "Molecular Single-Bond Covalent Radii for Elements 1–118," *Chemistry – A European Journal,* Vol. 15, No. 1, pp. 186-197.

Ravishankar, S. A., Pradip, and Khosla, N. K., 1995, "Selective flocculation of iron oxide from its synthetic mixtures with clays: a comparison of polyacrylic acid and starch polymers," *International Journal of Mineral Processing,* Vol. 43, No. 3–4, pp. 235-247.

Sparks, D. L., and Grundl, T. J., 1998, *Mineral-Water Interfacial Reactions,* American Chemical Society, 438 pp.

Stumm, W., Sigg, L., and Sulzberger, B., 1992, *Chemistry of the solid-water interface,* Wiley, 448 pp.

2.2 The Role of Water Chemistry in the Selective Flocculation and Dispersion of Iron Ore at a Pilot Scale [3]

2.2.1 Abstract

Fine grained hematite ore can be concentrated by the process of selective flocculation and dispersion. This process relies on proper reagent selection and water chemistry. Many previous studies have been performed that analyze the effects of different reagents on this process in a laboratory environment. This paper focuses on the water chemistry within the process in a pilot scale continuous deslime thickener.

The pH, sodium concentration, calcium concentration, and magnesium concentration were varied to determine their effects on the iron concentrate grade and recovery, and the phosphorus concentrate grade and rejection in the pilot scale selective deslime thickener. It was found that the ideal pH for the iron grade and recovery of the process using a starch selective flocculant is 10.5. Although, phosphorus rejection was increased at lower pH values. Minimization of sodium concentration was shown to improve iron grade, iron recovery and phosphorus rejection. Calcium acted as a nonselective flocculant showing higher iron recovery, lower iron grade and lower phosphorus rejection with increasing

[3] The material contained in this chapter was previously published in the journal *"Minerals and Metallurgical Processing Journal."* It is included in this dissertation with permission from the journal.
Citation:
Haselhuhn, H. J, and Kawatra, S. K., 2015, "The Role of Water Chemistry in the Selective Flocculation and Dispersion of Iron Ore," *Minerals & Metallurgical Processing,* In Press

concentration. Conclusions were unable to be drawn with experiments varying in magnesium concentration.

The zeta potential of the solid-liquid interface of particles in each sample taken was also analyzed to show relationships between zeta potential and process performance. In all cases, a maximization of the magnitude of zeta potential correlated with increased iron grade and recovery. This supports the hypothesis that a higher level of dispersion enhances the selective flocculation separation process.

2.2.2 Introduction

The United States produced 53.2 of the worldwide 3,000 million metric tons of concentrated iron ore in 2012 (Tuck, 2013). With this in mind, there has been a large increase in iron ore processing research (Bolen, 2014; Carlson et al., 2013; Carlson, 2008; Halt, 2014; Halt et al., 2014a; Halt et al., 2014b; Haselhuhn, 2012, 2013; Haselhuhn et al., 2012a; Haselhuhn et al., 2012b; Liu et al., 2014; Manouchehri, 2014; Sandvik et al., 2014; Semberg et al., 2014). Of the 53.2 million metric tons produced, roughly 8 million metric tons of hematite (Fe_2O_3) concentrate were produced using a process known as selective flocculation and dispersion (Cliffs Natural Resources, 2011). This process is the only economically viable method for concentrating low grade (<40% Fe) fine grain (<25μm liberation size) hematite ores. It is scarcely used due to difficulty in controlling the surface chemistry of the ore and high reagent costs (Department of Energy, 2001; Haselhuhn, 2013; Haselhuhn et al., 2012a). The process is highly dependent upon both reagent selection and precise control of the water chemistry during

separation. This study shows the dependence of process performance of a pilot scale deslime thickener on the water chemistry in the feed slurry.

The process used to concentrate hematite ore via selective flocculation and dispersion shown in Figure 1.2 requires two concentration steps. The first and arguably most important step is a selective thickening process known as selective flocculation desliming (Siirak et al., 1988). Selective flocculation desliming is the focus of this research. During this process, a dispersed slurry of liberated ore is treated with a selective flocculant that acts by bridging hematite particles together. These flocs are settled in a thickening vessel while the dispersed gangue minerals leave the process through the overflow. This process requires three reagents to function effectively: Caustic soda, cooked corn starch and sodium polyphosphate.

Caustic Soda (NaOH) is added during primary autogenous grinding as a pH modifier. The caustic soda addition rate is adjusted to deliver a pH of between 10.5 and 11 at the feed of the deslime thickener. This pH is required to both ensure adequate dispersion and to facilitate maximum starch selectivity and adsorption (Green et al., 1984; Haselhuhn et al., 2012a; Weissenborn, 1996).

Cooked acid modified corn starch is used as a selective flocculant for hematite ores. It is added to the finely ground ore immediately following hydrocyclone sizing in the hydrocyclone overflow conditioning tank. It has been speculated that adding starch immediately following grinding is required because of mineral aging effects in the process. Oxidation of freshly cleaved iron oxide surfaces is speculated to diminish starch

adsorption efficiency. This has been observed in laboratory studies though definitive proof of this concept has never been shown.

A 21-member chain sodium polyphosphate is used as a dispersant for hematite ore. This dispersant was chosen due to its ability to reject phosphorus bearing minerals, namely apatite ($Ca_5(PO_4)_3(F,Cl,OH)$), in both selective flocculation desliming and flotation (Siirak et al., 1988). The sodium polyphosphate is added during secondary grinding to ensure the dispersion of fine siliceous minerals that can coat the surfaces of the hematite particles.

The selective flocculation and dispersion process depends upon the surface chemistry of the particles. Because of this, the water used during the process is one of the most important parameters. Even minor changes in water chemistry parameters can cause drastic changes in process performance. In literature, it has been shown that the four primary water quality parameters in the process water that affect the selective flocculation and dispersion process are pH, sodium concentration, magnesium concentration and calcium concentration (Haselhuhn, 2012; Haselhuhn et al., 2012a).

pH control is necessary to maintain dispersion within the process and to promote starch adsorption and selectivity (Haselhuhn et al., 2012a; Weissenborn, 1996). The dispersive quality of the mineral solution is a function of the zeta potential of the particles. The magnitude of the zeta potential of all mineral particles is maximized in highly alkaline conditions as shown in Figure 2.5. Two particles, regardless of mineralogy, with negative zeta potentials of significant magnitude will remain dispersed from one another due to

electrostatic repulsion. Thus, a sufficiently high pH in the process water during selective flocculation and dispersion is required to maintain this electrostatic repulsion.

One important aspect to note is that typical studies involving zeta potential, such as those shown in Figure 2.5, are performed in low conductivity environments with aqueous ion concentrations drastically lower than those seen during beneficiation. The zeta potential of solid-liquid interfaces in mineral beneficiation plants typically do not correlate with those performed in a perfect laboratory environment due to the high concentrations of aqueous ions present and the complex mineralogy of the ores. This study intends to show zeta potentials as they would be seen in an operating hematite beneficiation plant.

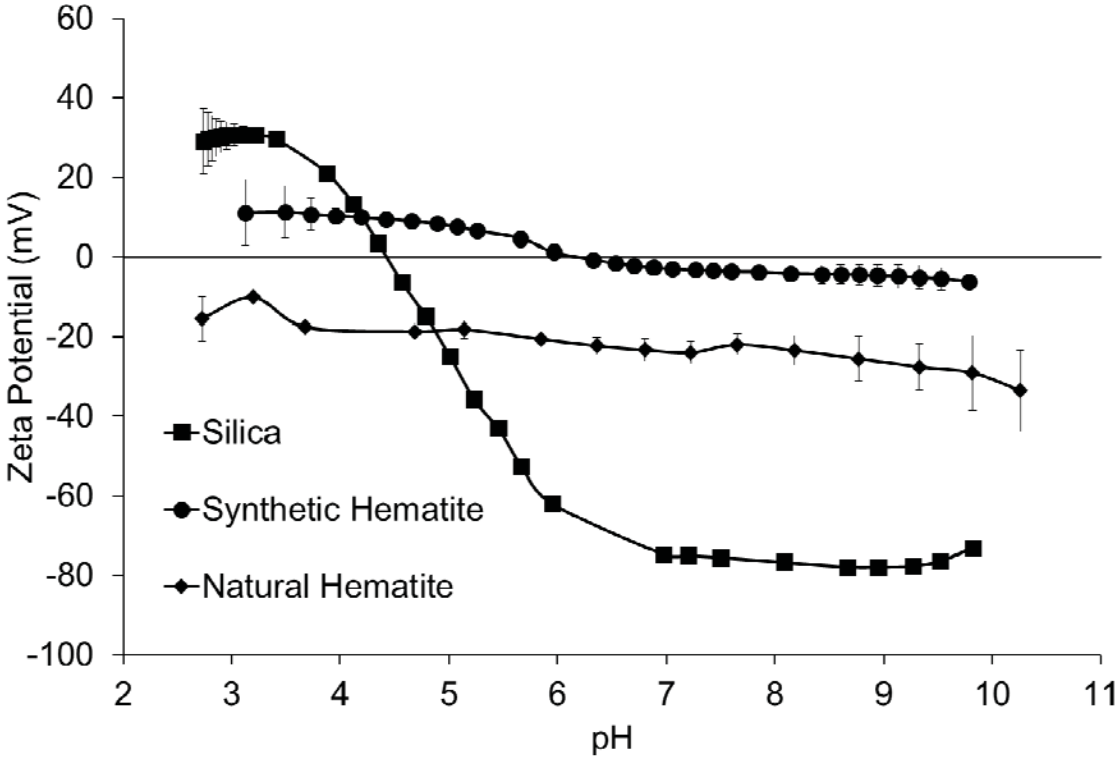

Figure 2.5: Zeta potential of silica, synthetic hematite and natural hematite (Haselhuhn et al., 2012a)

The pH is also important to ensure starch adsorption and selectivity. Several studies have shown maximized iron recovery during both flotation and selective flocculation desliming at a pH of 10.5 (Weissenborn, 1996).

The sodium concentration within a selective flocculation dispersion process is of critical importance because it has the highest concentration within the process and plays a minor role in surface chemistry (Haselhuhn et al., 2012a). These high sodium concentrations, in excess of 500 ppm, typically are the result of caustic use in pH control. Recent efforts to lower the sodium concentration at a hematite selective flocculation and dispersion facility

have shown increases in both iron grade and recovery at the underflow of the deslime thickener.

Calcium and magnesium concentrations within a selective flocculation dispersion process are critical at even low doses due to their ability to non-selectively flocculate mineral particles in alkaline conditions. The ions of these elements form chemical bonds with oxide surfaces in alkaline conditions leaving a free positively charged surface site available for adsorption or electrostatic effects. In significant concentration, the selectivity of the process approaches zero. The polyphosphate dispersants for the process mitigate the effects of calcium and magnesium by forming precipitates with negatively charged surface sites. This can block starch adsorption but regains selectivity (Iwasaki, 1989).

Most published research studies regarding selective flocculation and dispersion have been performed at a laboratory scale in water systems with no competing ions. The water chemistry in an operating hematite beneficiation plant has been reported and reviewed by Haselhuhn et al. (2012a). No previous studies on a pilot scale have been published considering the effects of competing ions in a selective flocculation and dispersion deslime thickener. The purpose of this study was to addresses this research gap.

2.2.3 Materials and Methods

A continuous pilot scale deslime thickener was built to show the dependence of water quality on process performance. The key indications of process performance included iron and phosphorus grade in the deslime thickener underflow, total recovery of iron, and

total phosphorus rejection. These parameters were determined via iron analysis, phosphorus analysis and a mass balance performed at each operating condition.

2.2.3.1 Material Selection and Preparation

Hematite ore was sampled using a cross-flow sampling device at an operating hematite beneficiation plant. The samples were taken after primary comminution but before dispersant addition as shown in Figure 1.2. This location was chosen for three reasons: (1) any location downstream of this location would have a surface active reagent within the process water, (2) sampling after secondary comminution would allow the fresh surface sites to oxidize prior to use in the laboratory thereby reducing starch selectivity as discussed above, (3) a representative ore sample would be very difficult to obtain without at least minimal comminution in the process. The downfall of sampling at this location was that the sample had to be ground in the laboratory to liberation size.

The ore samples from the operating beneficiation plant were dewatered and dried using decantation and a convection oven at 107°C. A particle size analysis of the dried material showed an 80% passing size of 1.41 mm. The particle size required for an effective separation is known to be 82% passing at 25 μm (Siirak et al., 1988). This particle size was achieved through dry grinding in a laboratory ball mill for 130 minutes. To prevent oxidation of the iron oxide surfaces prior to use, the ground samples were immediately split using a rotary riffle splitter and inerted under an argon atmosphere. The ore contained 42.3% iron and 0.0268% phosphorus indicating a higher than average grade ore during the sampling process. An x-ray diffraction of the iron ore used in the study is shown in Figure 2.6.

The water used in the process was created from distilled water mixed with magnesium chloride hexahydrate (to adjust magnesium), calcium chloride dihydrate (to adjust calcium), sodium hydroxide (to adjust pH), potassium chloride (to add potassium), sodium carbonate (to add carbonate), sodium sulfate (to add sulfate) and sodium chloride (to adjust sodium). These reagents were added to create a water profile similar to the actual water chemistry found in the beneficiation process by Haselhuhn et al. (2012a). The total volume of water for each experiment varied to hold a constant 2% solids by weight in the feed slurry. This was necessary due to slight variations in ore mass in each split as a result of the ore splitting process. Throughout the study, the concentration of carbonate, sulfate and potassium ions were held constant at 400 ppm, 400 ppm, and 10 ppm, respectively. Four sets of experiments were carried out: pH modification, sodium concentration modification, calcium concentration modification and magnesium concentration modification. The water quality parameters for these experiments are shown in Table 2.1.

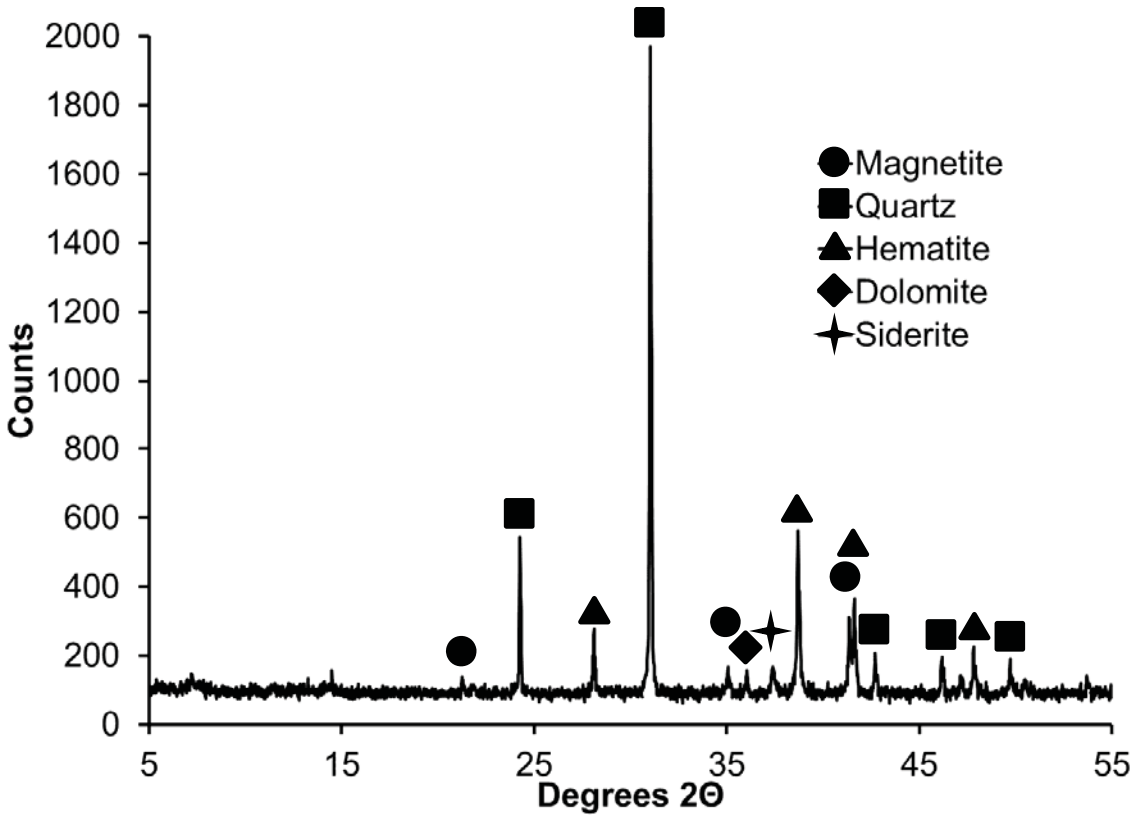

Figure 2.6: X-ray diffraction pattern for iron ore sampled from screen underflow at an operating hematite beneficiation plant

Table 2.1: Water quality parameters for each experiment

Experiment	pH	Ca (ppm)	Mg (ppm)	Na (ppm)
1	9	3	2	600
2	9.5	3	2	600
3	10	3	2	600
4	10.5	3	2	600
5	11	3	2	600
6	11	3	2	600
7	11	3	2	700
8	11	3	2	800
9	11	3	2	900
10	11	3	2	1000
11	11	0	2	600
12	11	3	2	600
13	11	6	2	600
14	11	9	2	600
15	11	12	2	600
16	11	3	0	600
17	11	3	2	600
18	11	3	4	600
19	11	3	6	600
20	11	3	8	600

2.2.3.2 Experimental Setup

The simulated process water and ground hematite ore were mixed in the feed tank of a pilot scale continuous selective deslime thickener. A scaled diagram of the deslime thickener is shown in Figure 2.7. A small mixer controlled by a variac was used to keep the slurry agitated in the feed tank. A Masterflex Easy-Load peristaltic pump was used to pump mixed feed slurry from the feed tank to the feed well of the thickener at a rate of 25 mL/sec. A peristaltic pump, Manostat Veristaltic Pump Jr., was used to remove the underflow slurry from the thickener at a rate of 5 mL/sec. These flow rates were optimized to obtain maximum iron grade and recovery at typical process conditions. The thickener was constructed from 7.62 cm (3 inch) acrylic pipe with a stainless steel conical

bottom at a cone angle of 75°. The total height of the thickening unit was 138.43 cm (54.5 inches). The thickener had a feed-well depth of 21.27 cm (8.375 inches). Under these conditions, a 15 minute and 45 second underflow residence time and a 49 second overflow residence time were achieved.

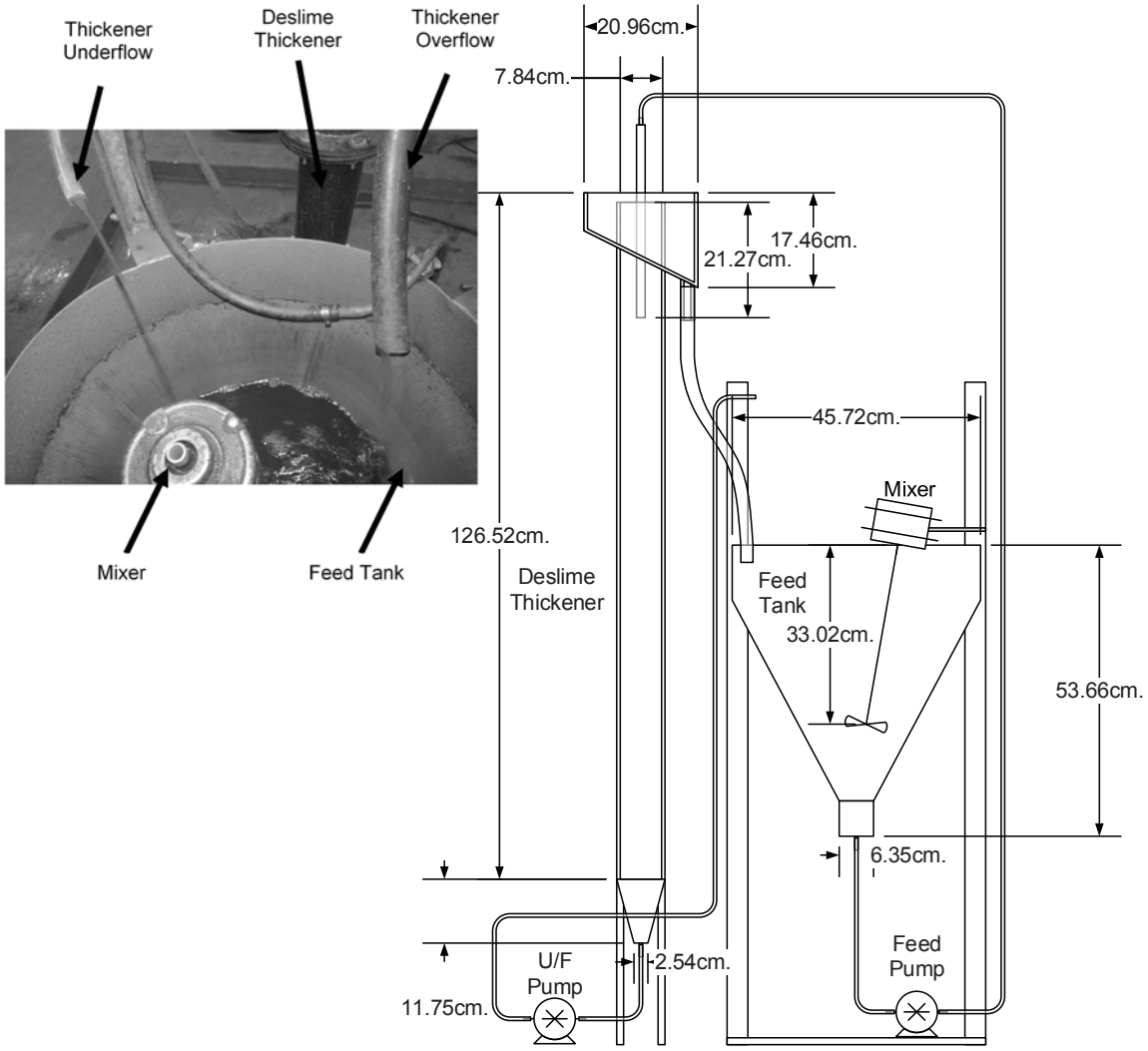

Figure 2.7: Diagram of the continuous pilot scale deslime thickener used in this study

To begin the experiment, the simulated process water was added to the feed tank shown in Figure 2.7. The feed pump was disconnected from the thickener and allowed to recirculate the process water back into the feed tank. Final adjustments in pH were made using hydrochloric acid. Sodium polyphosphate (21-member chain) was added to the process water at a dose of 0.023 g/kg (0.05 lb per metric ton). The ore sample specified for the experiment was then added to the process water. Immediately after the ore was added, cooked corn starch was added at a dose of 0.045 g/kg (0.10 lb per metric ton). This mixture was allowed to recirculate in the feed tank for 5 minutes at which time the feed pump was reconnected to the feed well of the deslime thickener. The underflow pump was then activated to prevent an unmovable buildup of solids in the cone of the thickener. Once the thickener filled and began overflowing, the flow rate of each pump was adjusted to 5 mL/sec for the underflow and 20 mL/sec for the overflow. The system was allowed to equilibrate for 30 minutes prior to sampling.

2.2.3.3 Analysis Methodology

The underflow stream, overflow stream, and feed stream of the thickener was sampled using 500 mL glass sample bottles after the 30 minute equilibration period. These samples were immediately measured for zeta potential using a Malvern Zetasizer. The results from the Malvern Zetasizer reported the average zeta potential of the solid-liquid interfaces within the slurry sample. The overflow and underflow samples were then filtered. The volume of the filtrate was measured in a 500 mL graduated cylinder. The filter cake from each sample was dried in a direct (non-convection) drying oven at 107°C. The dry filter cake was weighed and measured for iron and phosphorus content. The iron

content was measured using a UV-VIS spectrometer via an orthophenanthroline colorimetric reaction. The phosphorus concentration was measured using ASTM Standard E-1070-11 (2011). The data gathered from the filter cake and filtrate analyses were used to construct a mass balance and calculate iron recovery and phosphorus rejection.

2.2.4 Results and Discussion

The results of the experiments confirmed many of the hypotheses found in prior literature (Haselhuhn, 2012; Haselhuhn et al., 2012a; Pradip, 1994; Weissenborn, 1996). Optimal pH conditions and water chemistry during the selective flocculation dispersion desliming process were determined.

2.2.4.1 pH Modification Experiments

The iron grade versus recovery data for the pH modification experiments are shown in Figure 2.8. This data shows that the optimal pH for enhancing both grade and recovery in this process is 10.5. This pH has been shown to optimal in starch adsorption studies performed by Weissenborn (1996). The selectivity of starch is due to the binuclear complexation of un-aged Fe sites with adjacent oxide groups at the ends of the starch polymer. The molecular recognition of starch to these surface sites is due to the matching spacing between Fe surface sites on hematite surfaces (2.852 Å) and oxygen end groups on starch polymers (2.85 Å) (Pradip, 1994). It is important for future studies to determine why the pH of 10.5 is optimal. The enhanced adsorption of cooked corn starch in alkaline conditions is due to the lack of hydrogen available to satisfy anionic oxygen groups at the end monomers of the starch polymer. The downfall of this high pH is phosphorus

rejection. These experiments showed maximum phosphorus rejection at pH values lower than 10. See Figure 2.9.

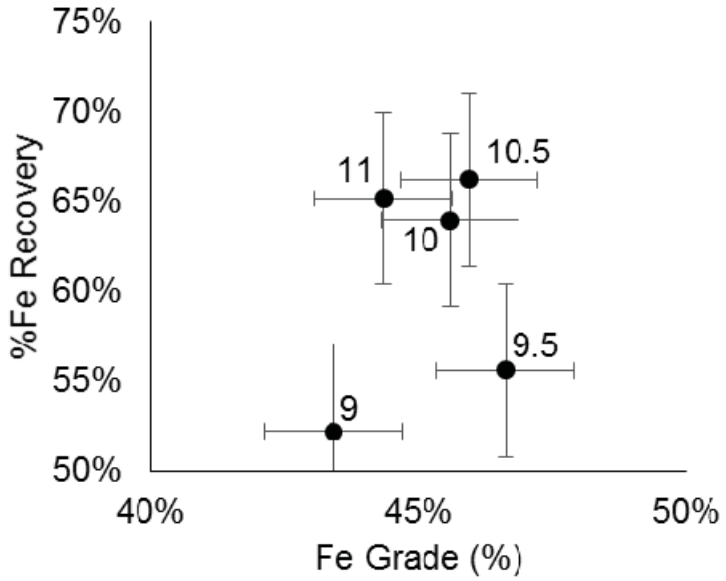

Figure 2.8: Iron grade versus recovery plot for pH experiments. Data labels indicate pH. The best pH for iron grade and recovery was found to be around 10.5.

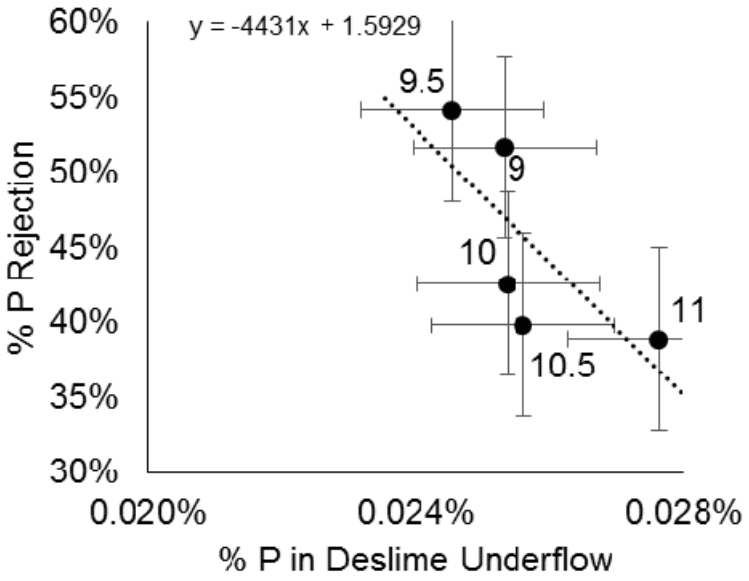

Figure 2.9: Phosphorus grade versus rejection plot for pH modification experiments. Data labels indicate pH. Lower pH values yielded higher phosphorus rejection.

The zeta potential of the solid-liquid interfaces within the slurry is also a function of pH. Figure 2.10 shows the zeta potential of the feed, underflow and overflow samples at varying pH. The maximized magnitude of zeta potential (where zeta potential reaches its highest negative value) of the solid-liquid interfaces in all slurry samples at a pH of 10.5 indicates the highest level of dispersive stability. This correlates well with the grade versus recovery plot in Figure 2.8 showing that the grade and recovery of the deslime thickener is associated with the zeta potential of the solid-water interfaces within the slurry.

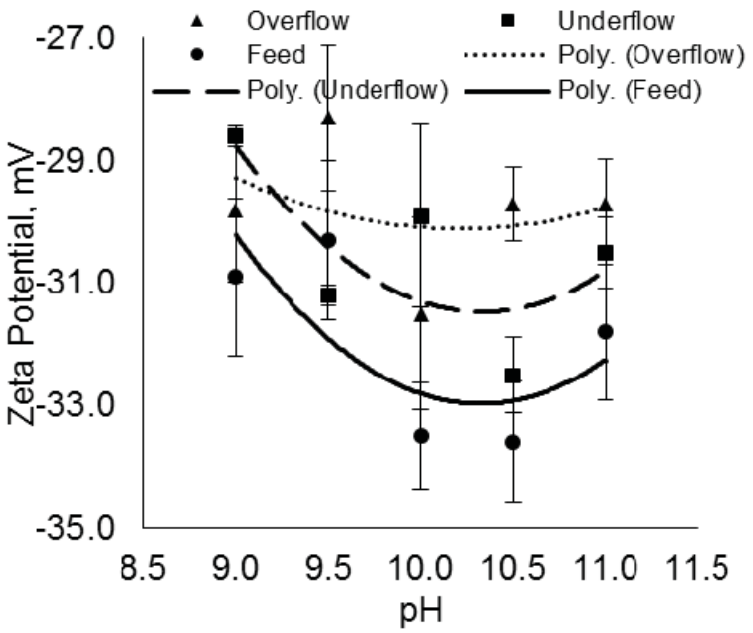

Figure 2.10: The relationship between zeta potential of feed, underflow and overflow samples and pH is shown. A polynomial trend is drawn to show the minimum, most dispersed, state. The 10-10.5 pH range yielded a maximization in the magnitude of zeta potential suggesting higher dispersive stability.

2.2.4.2 Sodium Concentration Modification Experiments

The relationship between sodium concentration and iron grade and recovery is shown in Figure 2.11. These data confirm the plant scale observations that decreased sodium concentrations increase both the grade and the recovery of iron ore. Like the pH modification, the increase in iron grade and recovery is accompanied by a decrease in phosphorus rejection as shown in Figure 2.12. However; the phosphorus grade, under the best iron recovery conditions, is still adequate to meet production goals (~0.04%/wt Phosphorus) (Siirak et al., 1988). Sodium ions within the process water cause double layer compression at the solid-liquid interfaces and ultimately diminish the dispersive

stability and zeta potential of solid-liquid interfaces within the slurry. This hinders starch adsorption and selectivity.

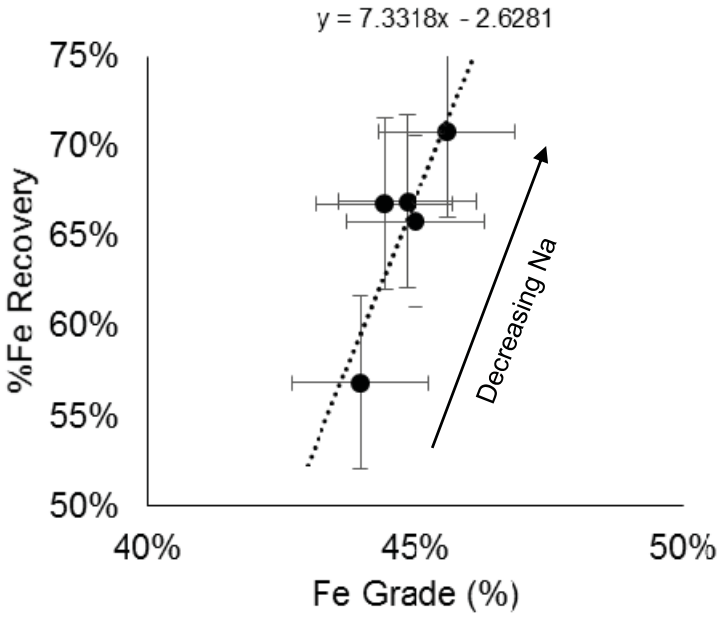

Figure 2.11: Iron grade versus recovery plot for sodium concentration modification experiments. Decreasing sodium yielded both an increase in iron grade and recovery.

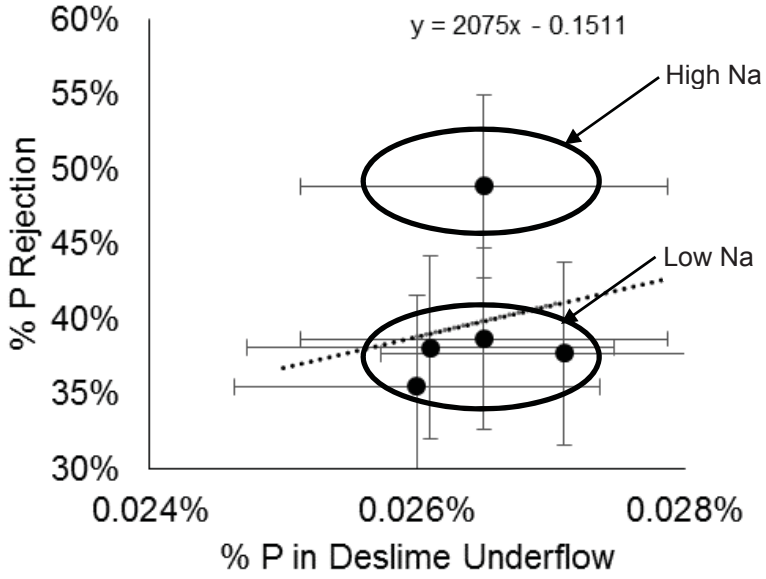

Figure 2.12: Phosphorus grade versus rejection plot for sodium concentration modification experiments. Increasing sodium yielded a phosphorus higher rejection.

The zeta potential of the solid-liquid interfaces within the slurry is dependent not only on the pH of the slurry but also on the ions within the slurry. A plot of the zeta potential of the feed, underflow and overflow samples are shown in Figure 2.13 with a relation to the sodium concentration within the slurry water. As expected, the sample with the highest negative value of zeta potential also had the lowest sodium concentration. The relationship between the zeta potential of solid-liquid interfaces and process performance that was found during pH modification experiments can also be seen in the sodium concentration modification experiments.

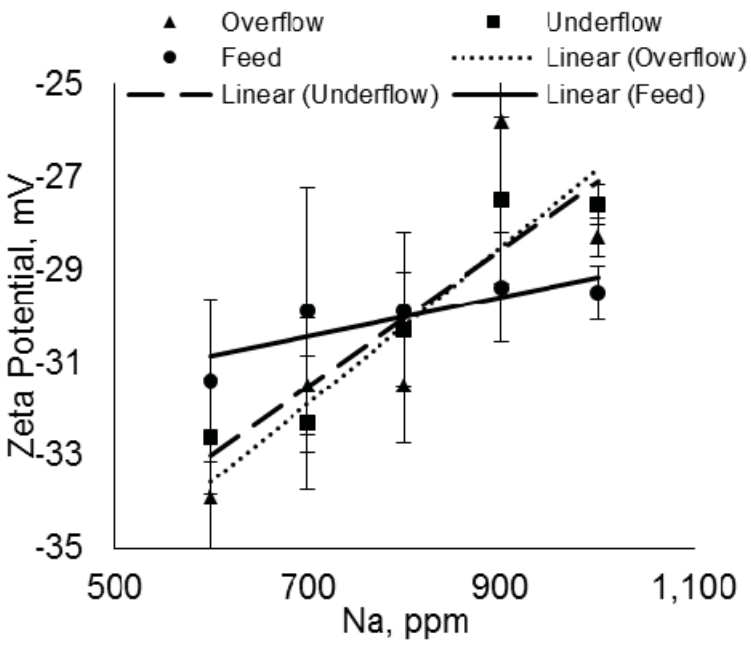

Figure 2.13: The relationship between zeta potential for feed, underflow and overflow samples and sodium concentration. Increases in sodium yielded lower magnitudes of zeta potential suggesting a loss in dispersive stability.

2.2.4.3 *Calcium Concentration Modification Experiments*

Calcium concentration plays a vital role in the selective flocculation and dispersion desliming process. A plot of iron grade versus recovery at varying calcium concentrations is shown in Figure 2.14. Calcium acts as a non-selective flocculant thereby diminishing the selectivity of the process. As calcium concentration increases, more material at a lower grade will fall to the underflow of the thickener. As expected, a higher calcium concentration also causes lower phosphorus rejection as shown in Figure 2.15. This is also due to non-selective flocculation caused by calcium adsorption at the solid-liquid interface. Equation 2.2 and 2.3 show the reactions taking place at the iron oxide and

silicon oxide surface with calcium ions as reported by Dzombak and Morel (1990) and Kitamura et al. (1999). Adsorbed calcium creates a positively charged surface site thereby attracting negatively charged particles non-selectively.

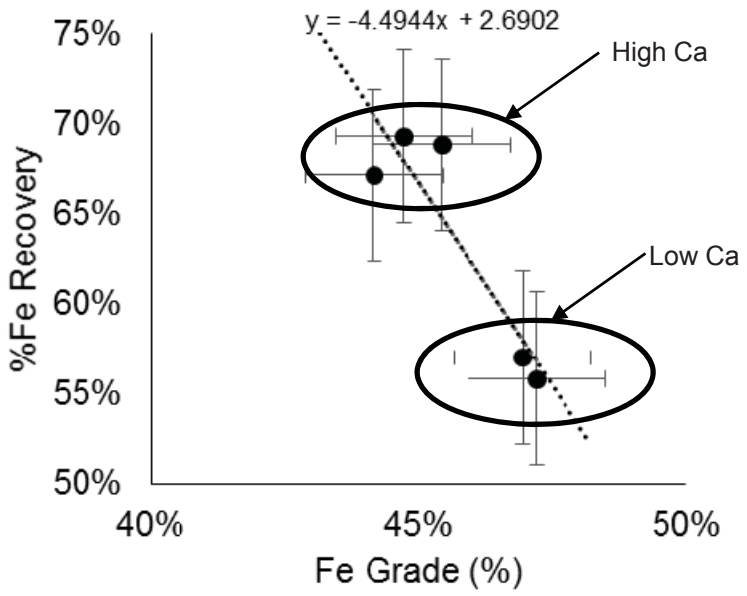

Figure 2.14: Iron grade versus recovery plot for calcium concentration modification experiments. Increasing calcium increased the iron recovery at a lower grade.

Slight changes in calcium concentrations, with no competing ions present, can cause drastic changes in the zeta potential of solid-liquid interfaces (Haselhuhn, 2012). However; this water system has both sulfate and carbonate present thereby diminishing the effects due to aqueous complexation. Ionic competition is occurring between these ions and the charged surfaces as shown in Equation 2.2 - 2.7(Dzombak et al., 1990; Kitamura et al., 1999; Parkhurst et al., 2013).

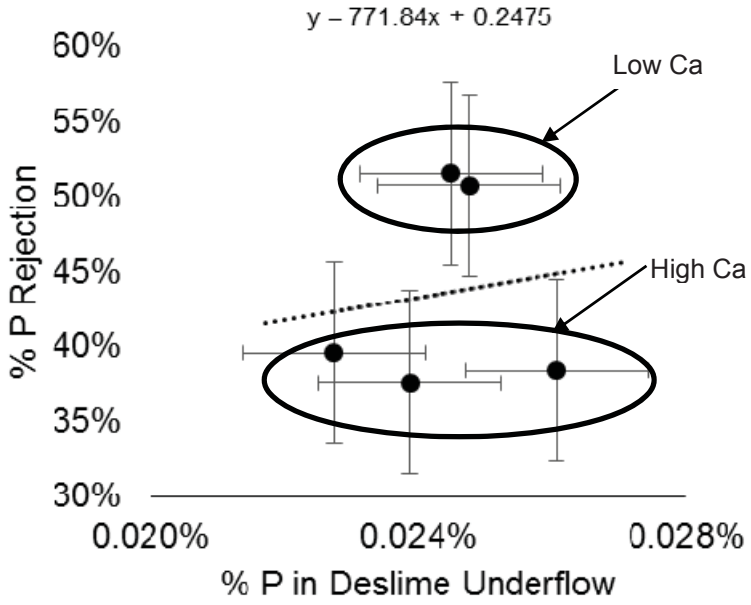

Figure 2.15: Phosphorus grade versus rejection plot for calcium concentration modification experiments. Decreasing calcium yielded an increase in phosphorus rejection.

$$\equiv FeOH + Ca^{2+} \overset{\log(k_{int})=-5.85}{\longleftrightarrow} \equiv FeOCa^{+} + H^{+} \qquad \textit{Equation 2.2}$$

$$\equiv SiOH + Ca^{2+} \overset{\log(k_{int})=-1.54}{\longleftrightarrow} \equiv SiOCa^{+} + H^{+} \qquad \textit{Equation 2.3}$$

$$Ca^{2+} + CO_3^{2-} \overset{\log(k)=3.224}{\longleftrightarrow} CaCO_3 \qquad \textit{Equation 2.4}$$

$$Ca^{2+} + H^{+} + CO_3^{2-} \overset{\log(k)=11.435}{\longleftrightarrow} CaHCO_3^{+} \qquad \textit{Equation 2.5}$$

$$Ca^{2+} + SO_4^{2-} \overset{\log(k)=2.300}{\longleftrightarrow} CaSO_4 \qquad \textit{Equation 2.6}$$

$$Ca^{2+} + HSO_4^{-} \overset{\log(k)=1.08}{\longleftrightarrow} CaHSO_4^{+} \qquad \textit{Equation 2.7}$$

A plot of the zeta potential of the feed, underflow and overflow samples against calcium concentration is shown in Figure 2.16. A slight increasing trend in zeta potential is observed with increasing calcium concentration in all samples.

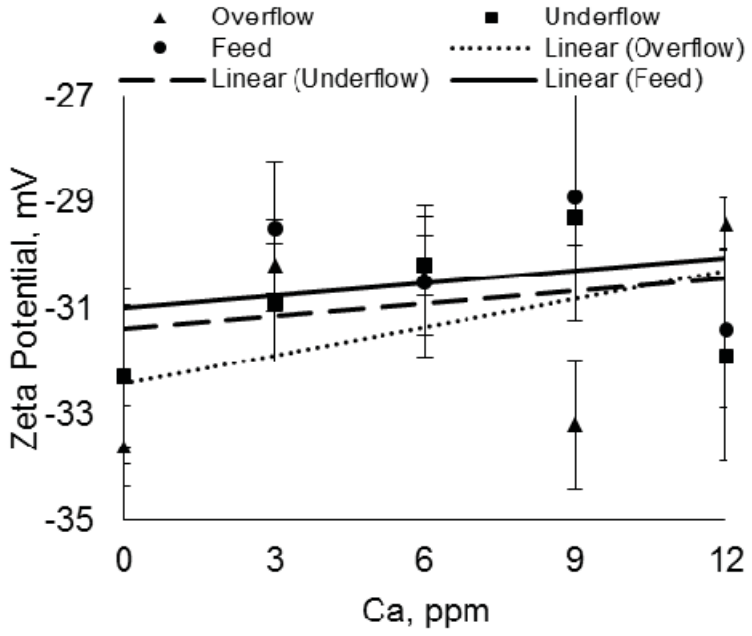

Figure 2.16: The relationship between zeta potential for feed, underflow and overflow samples and calcium concentration. Increases in calcium caused a decrease in the magnitude of the zeta potential.

2.2.4.4 *Magnesium Concentration Modification Experiments*

Magnesium, like calcium, has been speculated during other studies to play a role in the selective flocculation and dispersion and flotation processes (Haselhuhn, 2012; Iwasaki, 1989). This trend was not observed during this study. The plot of grade and recovery of iron is shown in Figure 2.17. Similar to the iron grade and recovery, the phosphorus grade and rejection data showed no trends; see Figure 2.18.

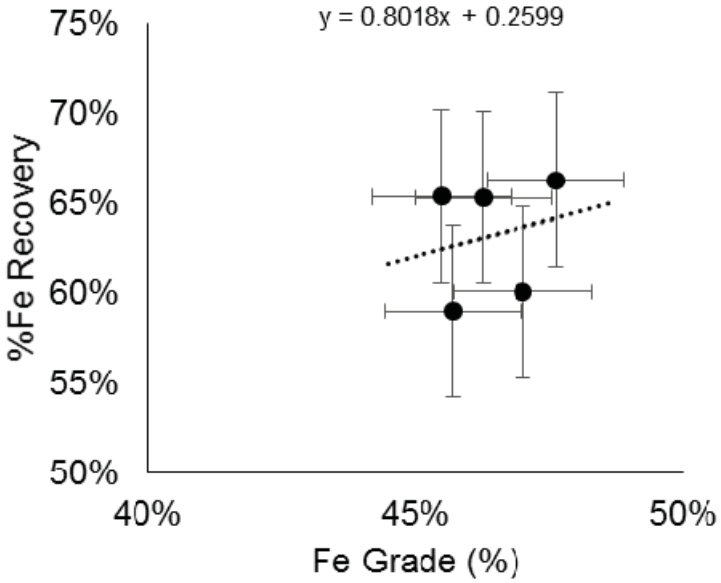

Figure 2.17: Iron grade versus recovery plot for magnesium concentration modification experiments. No conclusions could be drawn from these data.

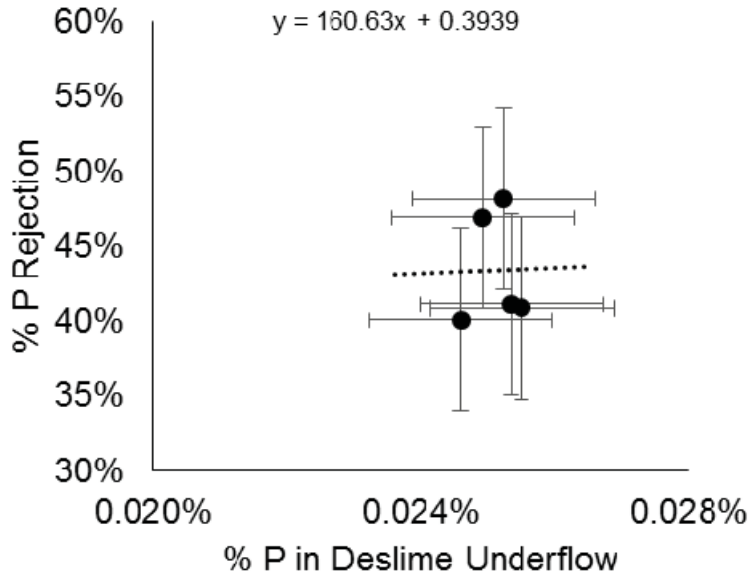

Figure 2.18: Phosphorus grade versus rejection plot for magnesium concentration modification experiments. No conclusions could be drawn from these data.

Changes in magnesium concentration with no competing ions present in the water have shown large changes in zeta potential in other studies (Haselhuhn, 2012). Like calcium, magnesium also participates in aqueous complexation reactions in the presence of sulfate and carbonate ions. Ionic competition is occurring between these ions and the charged surfaces as shown in Equation 2.8-2.12 (Dzombak et al., 1990; Kitamura et al., 1999; Parkhurst et al., 2013).

$$\equiv FeOH + Mg^{2+} \overset{\log(k_{int})=-4.6}{\longleftrightarrow} \equiv FeOMg^{+} + H^{+} \qquad \textbf{Equation 2.8}$$

$$\equiv SiOH + Mg^{2+} \overset{\log(k_{int})=-2.06}{\longleftrightarrow} \equiv SiOMg^{+} + H^{+} \qquad \textbf{Equation 2.9}$$

$$Mg^{2+} + CO_3^{2-} \xleftrightarrow{\log(k)=2.98} MgCO_3 \qquad \textit{Equation 2.10}$$

$$Mg^{2+} + H^{+} + CO_3^{2-} \xleftrightarrow{\log(k)=11.399} MgHCO_3^{+} \qquad \textit{Equation 2.11}$$

$$Mg^{2+} + SO_4^{2-} \xleftrightarrow{\log(k)=2.370} MgSO_4 \qquad \textit{Equation 2.12}$$

This study showed a slight decrease in the magnitude of zeta potential with increasing magnesium concentration. This is due to adsorption of magnesium at the solid-liquid interface of both iron oxide and gangue mineral particles causing charge reversal as seen in Equation 2.8 and 2.9. The plot of zeta potential in relation to magnesium concentration for the feed, underflow and overflow samples is shown in Figure 2.19.

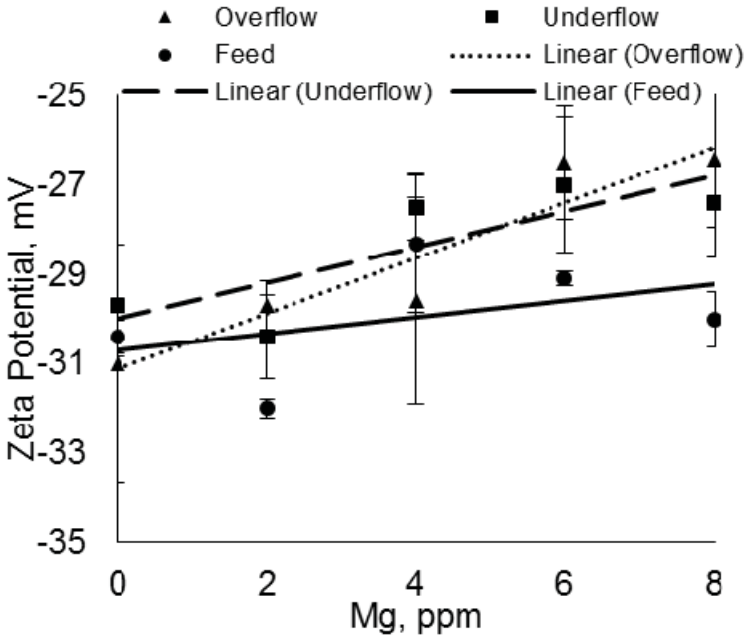

Figure 2.19: The relationship between Zeta potential for feed, underflow and overflow samples and magnesium concentration. Increases in magnesium caused a decrease in the magnitude of the zeta potential.

2.2.5 Discussion, Analysis and Conclusions

This study was performed to show the effects of water chemistry on the selective flocculation and dispersion desliming process for hematite ore. It was conducted in a pilot scale continuous deslime thickener. Finely ground hematite ore was suspended in a solution of simulated process water at varying pH, sodium concentration, calcium concentration and magnesium concentration. Cooked acid modified corn starch was used as a selective hematite flocculant and a 21-member sodium polyphosphate was used as a dispersant.

During the pH modification experiments, pH was varied between 9 and 11. It was found that a pH of 10.5 maximizes iron grade and recovery; though, higher phosphorus rejection was found at lower pH values. The high iron grade and recovery was accompanied by a maximization in the magnitude of zeta potential indicating that the iron grade and recovery is a function of the level of dispersion in the thickener.

Sodium concentration was shown to have a profound effect on the process. The sodium concentration was varied between 600 and 1000 ppm. Unlike traditional grade and recovery curves, in which an increase in grade is associated with a decrease in recovery, decreasing the sodium concentration within the deslime thickener caused an increase in both grade and recovery. Similar to the conclusions found in the pH modification studies, the samples with higher iron grade and recovery also showed a maximization in the magnitude of zeta potential. This suggests that high sodium concentrations can lower the dispersive stability of the slurry yielding lower grades in the product.

Calcium and magnesium have been previously shown to have an effect on the selective flocculation and dispersion process. Both of these ions can adsorb to the oxide particle surfaces causing a charge reversal and non-selective flocculation (Haselhuhn, 2012; Iwasaki, 1989). During this study, calcium was varied from 0 to 12 ppm. The effect of calcium concentration follows a standard grade recovery curve, in which higher grades are accompanied by lower recoveries. As predicted by other studies, the iron recovery increased with increasing calcium; however, the iron grade in the deslime underflow decreased. This suggests non-selective flocculation. Increasing calcium also resulted in a decrease in phosphorus rejection showing that the phosphorus bearing minerals participate in the non-selective flocculation. Magnesium was also studied between 0 and 8 ppm. Changes in the magnesium concentration did not provide any significant correlations to iron recovery or phosphorus rejection. The magnitude of zeta potential during these studies was maximized at lower concentrations of calcium and magnesium. This agrees well with prior studies showing highly negative zeta potentials at low concentrations of calcium and magnesium (Haselhuhn, 2012).

In future studies, the results of this work will be applied directly to a full scale hematite selective flocculation and dispersion beneficiation plant.

2.2.6 References

ASTM, 2011, *E1070-11 Standard Test Method for Determination of Phosphorus in Iron Ores by Phospho-Molybdenum-Blue Spectrophotometry*, ASTM International, Conshohocken, PA.

Bolen, J., 2014, "Modern Air Pollution Control for Iron Ore Induration," *Minerals & Metallurgical Processing,* Vol. 31, No. 2, pp. 103-114.

Carlson, J. J., and Kawatra, S. K., 2013, "Factors Affecting Zeta Potential of Iron Oxides," *Mineral Processing and Extractive Metallurgy Review,* Vol. 34, No. 5, pp. 269-303.

Carlson, J. J. and Kawatra, S. K., 2008, "Effect of Particle Shape on the Filtration Rate in an Industrial Iron Ore Processing Plant," *Minerals & Metallurgical Processing,* Vol. 25, No. 3, pp. 165-168.

Cliffs Natural Resources, 2011, *Steel Starts Here*, Operations Data Fact Sheet, 4 pp.

Department of Energy, 2001. *Selective Flocculation of Fine Mineral Particles*. Office of Industrial Technologies Energy Efficiency and Renewable Energy - U.S. Department of Energy, Washington D.C.

Dzombak, D. A., and Morel, F., 1990, *Surface complexation modeling : hydrous ferric oxide,* Wiley, 393 pp.

Green, R. E., and Colombo, A. F., 1984, “Dispersion-Selective Flocculation-Desliming Characteristics of Oxidized Taconites,” US Bureau of Mines, Report of Investigations, RI 8867, 24 pp.

Halt, J. A., 2014, "Increasing the preheat strength of cornstarch-bonded pellets," *Minerals & Metallurgical Processing,* Vol. 31, No. 3, pp. 179.

Halt, J. A., and Kawatra, S. K., 2014a, "Review of organic binders for iron ore concentrate agglomeration," *Minerals & Metallurgical Processing,* Vol. 31, No. 2, pp. 73-94.

Halt, J. A., Nitz, M. C., Kawatra, S. K., and Dube, M., 2014b. "Iron Ore Pellet Dustiness Part I: Factors Affecting Dust Generation," *Mineral Processing and Extractive Metallurgy Review,* Vol. 36, No. 4, pp. 258-266.

Haselhuhn, H. J., 2012, "Water Chemistry Effects on the Zeta Potential of Concentrated Hematite Ore," *Minerals & Metallurgical Processing,* Vol. 29, No. 2, pp. 135-136.

Haselhuhn, H. J., 2013, "Dispersant Adsorption and Effects on Settling Behavior of Iron Ore," *Minerals & Metallurgical Processing,* Vol. 30, No. 3, pp. 188-189.

Haselhuhn, H. J., Carlson, J. J., and Kawatra, S. K., 2012a, "Water chemistry analysis of an industrial selective flocculation dispersion hematite ore concentrator plant," *International Journal of Mineral Processing,* Vol. 102–103, pp. 99-106.

Haselhuhn, H. J., Swanson, K. P., and Kawatra, S. K., 2012b, "The effect of CO_2 sparging on the flocculation and filtration rate of concentrated hematite slurries," *International Journal of Mineral Processing,* Vol. 112-113, pp. 107-109.

Iwasaki, I., 1989, “Bridging Theory and Practice in Iron Ore Flotation,” *Advances in Coal and Mineral Processing Using Flotation,* Society for Mining, Metallurgy and Exploration, pp. 177-190.

Kitamura, A., Fujiwara, K., Yamamoto, T., Nishikawa, S., and Moriyama, H., 1999, "Analysis of Adsorption Behavior of Cations onto Quartz Surface by Electrical Double-layer Model," *Journal of Nuclear Science and Technology,* Vol. 36, No. 12, pp. 1167-1175.

Liu, S., Zhau, Y., Wang, W., and Wen, S., 2014, "Beneficiation of a Low-grade, Hematite-Magnetite Ore in China," *Minerals & Metallurgical Processing,* Vol. 31, No. 2, pp. 136-142.

Manouchehri, H. R., 2014, "Pyrrhotite Flotation and its Selectivity against Pentlandite in the Beneficiation of Nickeliferous Ores: An Electrochemistry Perspective," *Minerals & Metallurgical Processing,* Vol. 31, No. 2, pp. 115-125.

Parkhurst, D. L., and Appelo, C. A. J., 2013, “Description of input and examples for PHREEQC version 3—A computer program for speciation, batch-reaction, one-dimensional transport, and inverse geochemical calculations: U.S. Geological Survey Techniques and Methods,” US Geological Survey.

Pradip, 1994, “Reagents Design and Molecular Recognition at Mineral Surfaces,” *Reagents for Better Metallurgy,* Society for Mining Metallurgy, pp. 245-252.

Sandvik, K. L., and Larsen, E., 2014, "Iron Ore Flotation with Environmentally Friendly Reagents," *Minerals & Metallurgical Processing,* Vol. 31, No. 2, pp. 95-102.

Semberg, P., Andersson, C., and Bjorkman, B., 2014, "Interaction between Iron Oxides and Olivine in Magnetite Pellets during Reduction at 500°-1,300°C," *Minerals & Metallurgical Processing,* Vol. 31, No. 2, pp. 126-135.

Siirak, J., and Hancock, B. A., 1988, “Progress in Developing a Flotation Phosphorus Reduction Process at the Tilden Iron Ore Mine,” *Proceedings of the XVI International Mineral Processing Congress,* Stockholm, Sweden, pp. 1393-1404.

Tuck, C. A., 2013, “Mineral Commodity Studies - Iron Ore,” US Geological Survey.

Weissenborn, P. K., 1996, "Behaviour of amylopectin and amylose components of starch in the selective flocculation of ultrafine iron ore," *International Journal of Mineral Processing,* Vol. 47, No. 3-4, pp. 197-211.

2.3 Measurement of Zeta Potential and Correlation with Performance throughout an Operating Hematite Beneficiation Plant[4]

2.3.1 Executive Summary

The major separation processes in the operating hematite selective flocculation and dispersion beneficiation plant (desliming, froth flotation, thickening, and filtration) are all dependent on interactions of particles, which are largely controlled by the Zeta potential of the particles. Measurement and control of the Zeta potential is therefore key to controlling the plant operations and preventing process upsets. The objectives of this work are therefore to measure how Zeta potential throughout the plant varies over time, determine how these Zeta potential changes relate to plant performance, and develop methods for estimating Zeta potential from parameters that can be quickly and inexpensively measured on-site at the plant.

During this phase of the project, samples were collected 5 times at 12 locations throughout section 7-9 of the concentrator. Sample locations were strategically chosen to determine zeta potential effects at reagent addition points and zeta potential effects on separation process performance. The following conclusions have been drawn from this study:

[4] Some of the material contained in this chapter was previously submitted to Cliffs Natural Resources as a final report for the project titled *"*Measurement of Zeta Potential and Correlation with Performance Phase 1*"*

1. Zeta potential is largely controlled by pH, ionic content of the process water, conductivity of the process water, silica content, and surface active reagents (starch, Glass-H (sodium henicosapolyphosphate))
2. Conductivity is related to the ionic content of the process water; however, it is most closely associated with the sodium concentration and pH
3. Calcium and magnesium present as minerals in the ore are rejected by the deslime thickener but not by the froth flotation cells.
4. pH has a significant effect on both zeta potential and deslime performance
    4.1. Higher pH causes the surface charge to become more negative.
    4.2. pH has a direct influence on the amount of iron in the deslime underflow.
    4.3. The optimum pH for most calcium and magnesium conditions is near 11. This pH was shown to yield the highest iron recoveries.
    4.4. pH has a significant effect on conductivity.
5. Particle size control is important for influencing deslime weight rejection
6. Water hardness at the cyclone overflow has a large influence on deslime performance. Higher water hardness causes non-selective flocculation of particles; however, it allows for increased starch adsorption onto hematite surfaces
7. Starch does noticeably and reproducibly suppress the surface charge of hematite in both deslime and flotation. The effect of the starch is consistently more prominent in flotation than deslime due to higher iron concentration in particles
8. The addition of CO_2 during dewatering has a significant effect on the pH, conductivity, water hardness, and zeta potential.

9. Flux addition causes the zeta potential to equilibrate at ~-20 mV
10. Deslime recovery is maximized at a lower conductivity, lower water hardness and higher magnitude of zeta potential
11. Flotation recovery is maximized at the opposite conditions: higher conductivity, higher water hardness, and lower magnitude of zeta potential, though flotation recovery is largely dependent on deslime iron recovery and the iron content of the material fed into flotation

Based on these results, it has been found that monitoring the water chemistry and zeta potential at the deslime thickener offers the most potential for increasing iron recovery. It is theorized that pH and water hardness at the deslime thickener can be optimized to yield a higher overall recovery. Another way that could potentially increase overall iron recovery is increasing the water hardness in the flotation feed distributors by adding slaked lime.

2.3.2 Introduction

The major separation processes in the plant (desliming, froth flotation, thickening, and filtration) are all dependent on the interactions of particles, which are largely controlled by the Zeta potential of the particles. Measurement and control of the Zeta potential is therefore key to controlling the plant operations and preventing process upsets. Zeta potential can be controlled by adjusting the water quality, adding flocculants or dispersants, or by adjusting the incoming feed ore.

The objectives of this work were to measure how Zeta potential throughout the plant varies over time, determine how these Zeta potential changes relate to plant performance,

and develop methods for estimating Zeta potential from parameters that can be quickly and inexpensively measured on-site at the plant.

During phase 1 of this project, samples were collected 5 times at 12 locations throughout section 7-9 of the concentrator. Sample locations were strategically chosen to determine zeta potential effects at reagent addition points and zeta potential effects on separation process performance. Samples were tested for water quality parameters including pH, conductivity, water hardness, calcium, magnesium, iron, sodium, potassium, sulfate, carbonate, nitrate and oxidation-reduction potential. The solid content of each sample was analyzed for zeta potential (at process conditions), elemental composition, thermogravimetric degradation, x-ray diffraction, x-ray fluorescence and particle size distribution.

2.3.3 Background

The zeta potential of particle surfaces is extremely important in selective flocculation dispersion processes because it influences particle interactions and the effectiveness of many separation reagents. The zeta potential of the particle surfaces defines the dispersive stability of the particles in solution. Retaining a high dispersive stability is essential for the gravity separation and flotation processes employed in selective flocculation-dispersion concentrators.

2.3.3.1 Zeta Potential and Ionic surface Complexation

The pH of the water is the primary factor determining the surface charge of particles in solution. This is well described by the two-pKa model as shown in Equation 2.13

(Laskowski et al., 1992; Stumm et al., 1992). At a low pH the surface is positively charged, whereas, at a high pH, the surface is negatively charged as shown in Figure 1.4. The pH at which the surface bears no charge is referred to as the point of zero charge (PZC).

$$Fe - OH_2^+ \overset{pK_1}{\longleftrightarrow} Fe - OH \overset{pK_2}{\longleftrightarrow} Fe - O^- \qquad \textbf{Equation 2.13}$$

The surface charge determines the charge of ions in solution that will be attracted to the surface. The ions that are attracted to the surface either form inner-sphere or outer-sphere complexes at the surface. An inner-sphere complex consists of a primarily single covalent bond between the ion and the surface. An outer sphere complex occurs when the ion approaches the surface through coulombic forces but is separated from the surface by one or more water molecules, see Figure 1.4 (Stumm et al., 1992).

The coulombic forces diminish with distance from the surface. As the coulombic forces diminish, the outer-sphere complexes can no longer be held to the surface and are merely present as diffuse ions in the bulk fluid. The distance at which the coulombic forces are too weak to hold outer-sphere complexes to the surface is referred to as the shear plane, see Figure 1.4. The potential difference between the shear plane and the bulk solution is referred to as the zeta potential. The zeta potential of particle surfaces is primarily a function of water chemistry and the underlying surface charge of the particle.

2.3.3.2 Calcium and Magnesium Adsorption

Sorption of both calcium and magnesium ions to the surface hydroxyl groups of iron oxides is strongly dependent upon pH (Dzombak et al., 1990). Sorption isotherms of

calcium and magnesium onto an iron oxide surface are shown in Figure 2.20. The surface must have negatively charged hydroxyl groups to attract cations and allow for adsorption. As discussed earlier, a highly alkaline environment maximizes negatively charge hydroxyl groups thereby maximizing the adsorption capability of the iron oxide.

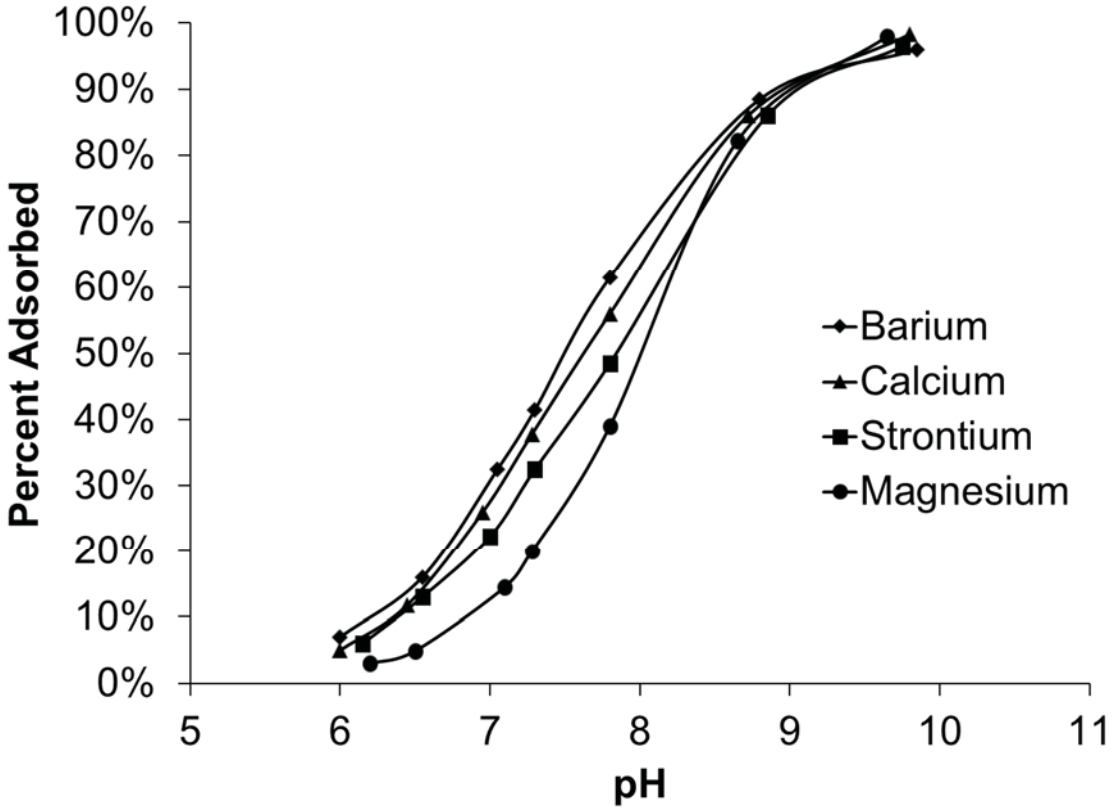

Figure 2.20: Adsorption isotherms for Magnesium (O'Brien et al., 1996), Calcium (Kinniburgh et al., 1982), Strontium and Barium (Kinniburgh et al., 1976) onto a hydrated iron oxide surface.

2.3.3.3 Cation Adsorption and Zeta Potential

Sodium ions slightly decreased the magnitude of zeta potential as concentration increased as shown in Figure 2.21. This is caused by outer-sphere complexation causing the zeta

potential to become more positive. Very small concentrations of magnesium caused the zeta potential to invert from a negative to a positive charge. A much larger concentration of calcium was required to invert the zeta potential from a negative to a positive charge. The slope of the zeta potential curves is steeper at lower concentrations than at higher concentrations of divalent cations. This shows that these cations initially form inner-sphere complexes until all available hydroxyl groups have been complexed.

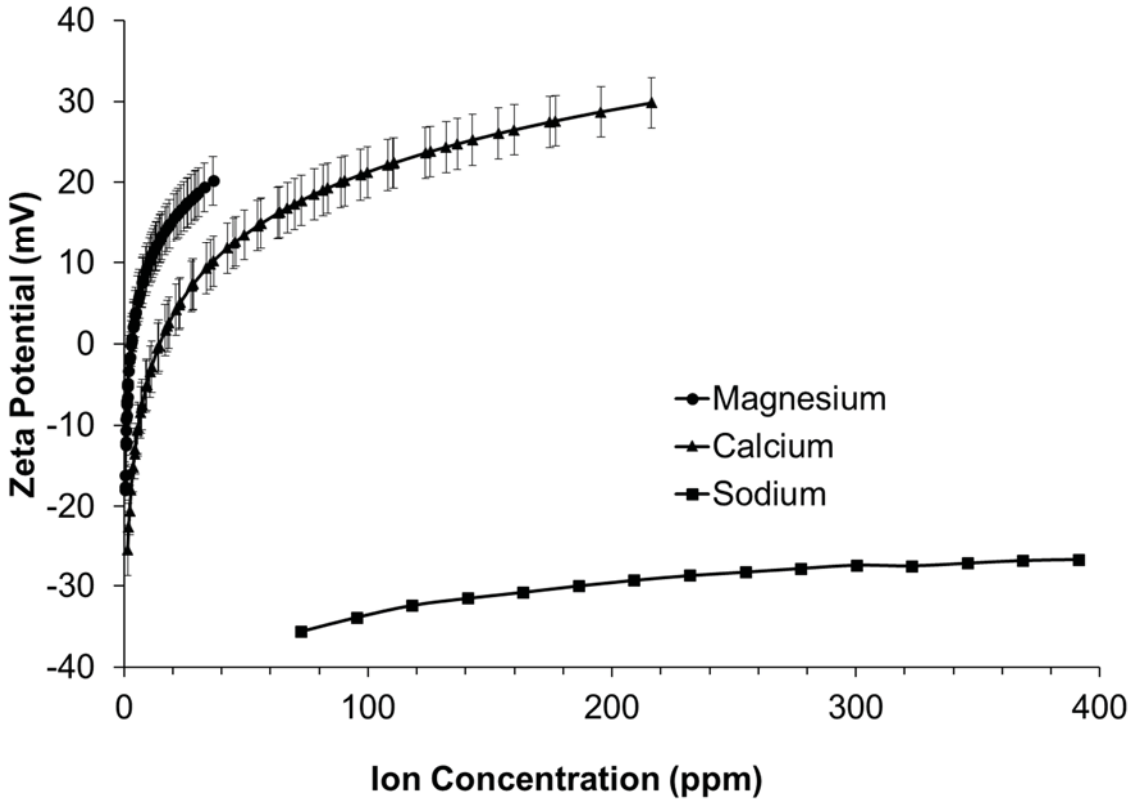

Figure 2.21: Zeta potential of concentrated natural hematite ore as a function of cation concentration at a pH of 11.

Within inner-sphere complexes, the surface hydroxyl groups ($-O^-$) act as lewis bases, donating an electron and increasing the electron density of the coordinated cation. This

causes a single covalent bond to form between the hydroxyl group and the coordinated cation, be it calcium (Ca^{2+}) or magnesium (Mg^{2+}) (Stumm et al., 1992).

The reason for the difference between how Calcium and Magnesium affect zeta potential is unknown; however, it has been suspected that it is due to the size of the ions, magnesium being smaller than calcium. At the cleavage plane of the hematite hexagonal close packed crystal structure, the average hydroxyl group spacing has been reported as being between 285.2 and 291.3 pm (Eggleston et al., 1992; Pradip, 1994). This spacing is larger than the single covalent diameter of magnesium (278 pm) but smaller than the single covalent diameter of calcium (342 pm) (Pyykkö et al., 2009). Because of this spacing, magnesium inner-sphere complexes can form at every hydroxyl group, however, calcium inner-sphere complexes can only form at every third hydroxyl group as shown in Figure 2.22.

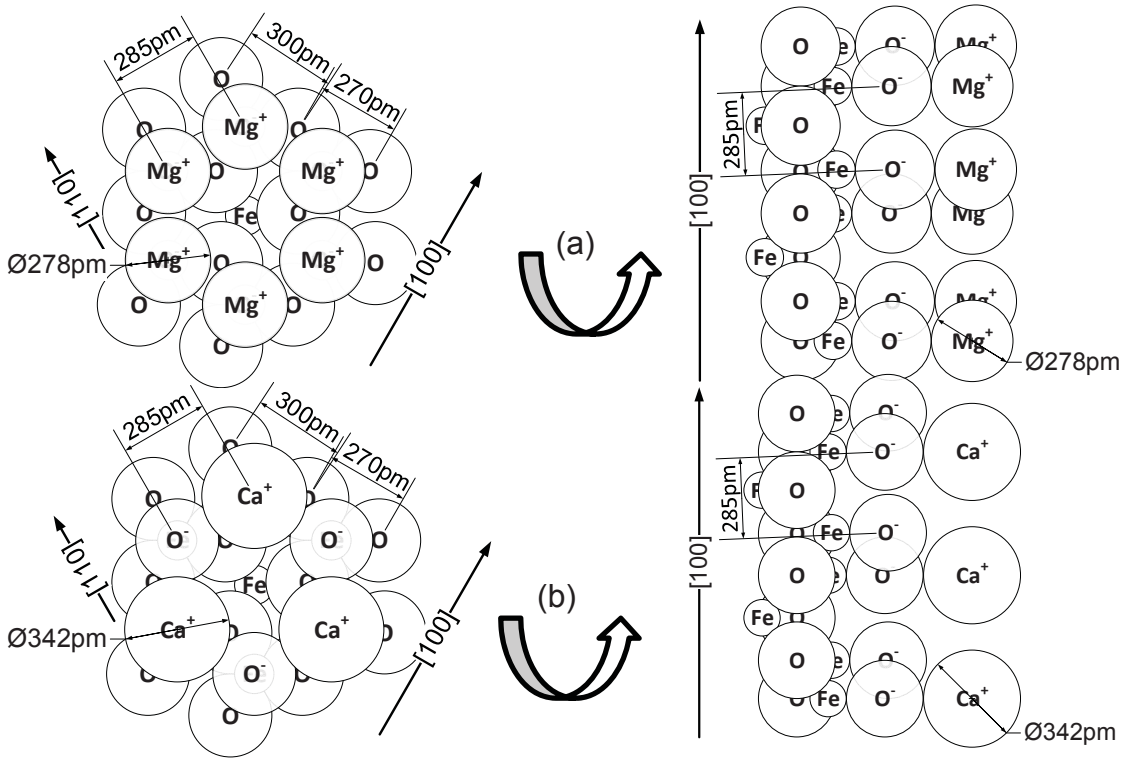

Figure 2.22: Hematite surface structure frontal view and side view. (a) Inner-sphere magnesium complexes formed at surface hydroxyl groups. (b) Inner-sphere calcium complexes formed at surface hydroxyl groups. All dimensions in picometers.

2.3.3.4 Ionic Equilibrium and Water Chemistry

2.3.3.4.1 Ion Pairing

Ions in solution can carry a positive, negative or neutral charge. Positively charged ions, such as sodium (Na^+), are attracted to negatively charged ions, such as carbonate (CO_3^{2-}). Ion pairing can result when electrostatic interactions between cations and anions is large enough to cause the two ions to become one ionic entity. An example of an ion pair is shown in Equation 2.14 below:

$$Na^{+}_{(aq)} + CO^{2-}_{3,(aq)} \overset{k_{assoc}=10^{1.27}}{\longleftrightarrow} NaCO^{-}_{3,(aq)} \qquad \textbf{Equation 2.14}$$

The tendency for an ion pair to form can be determined by its association constant, k_{assoc}. The association constant for monovalent anionic sodium carbonate ($NaCO_3^-$) is defined in Equation 2.15:

$$k_{assoc} = \left(\frac{\left[NaCO^{-}_{3,(aq)} \right]}{\left[Na^{+}_{(aq)} \right] \cdot \left[CO^{2-}_{3,(aq)} \right]} \right)_{eq} \qquad \textbf{Equation 2.15}$$

As can be seen, a higher association constant means the ions are more likely to associate with each other than dissociate from one another.

2.3.3.4.2 Aqueous Complex Formation

Complexes are very similar to ion pairs, however, they involve chemical interactions between the ions and not just electrostatic interactions. A common interaction seen in the concentrator is between iron (Fe^{3+}) and water as shown in Equations 2.16-2.19:

$$Fe^{3+}_{(aq)} + H_2O \overset{k_1=10^{-2.19}}{\longleftrightarrow} FeOH^{2+}_{(aq)} + H^{+}_{(aq)} \qquad \textbf{Equation 2.16}$$

$$Fe^{3+}_{(aq)} + 2H_2O \overset{k_2=10^{-5.67}}{\longleftrightarrow} Fe(OH)^{+}_{2,(aq)} + 2H^{+}_{(aq)} \qquad \textbf{Equation 2.17}$$

$$Fe^{3+}_{(aq)} + 3H_2O \overset{k_3=10^{-12.56}}{\longleftrightarrow} Fe(OH)_{3,(aq)} + 3H^{+}_{(aq)} \qquad \textbf{Equation 2.18}$$

$$Fe^{3+}_{(aq)} + 4H_2O \xleftrightarrow{k_4=10^{-21.6}} Fe(OH)^-_{4,(aq)} + 4H^+_{(aq)} \qquad \textit{Equation 2.19}$$

Based on the equilibrium constants, it can be seen that these reactions become less and less favored as the complex increases in hydroxide groups. The progression of these reactions is highly pH dependent; at a lower pH (higher concentration of H^+), the reaction proceeds backwards towards Fe^{3+}, however at a higher pH (lower concentration of H^+), the reaction proceeds forwards towards $Fe(OH)_4^-$. A graphical distribution of ferric hydroxide ($Fe^{3+}(OH^-)_n$) complexes as a function of pH is shown in Figure 2.23.

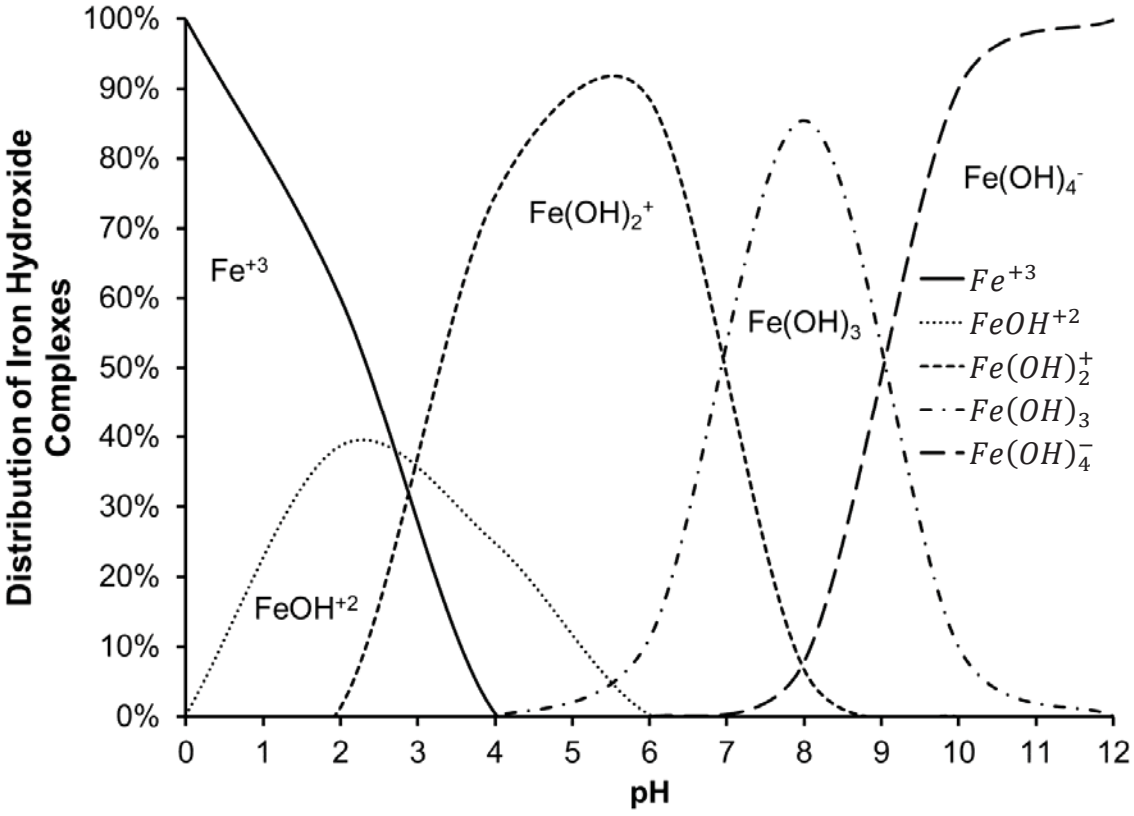

Figure 2.23: Distribution of ferric hydroxide complexes as a function of pH

2.3.3.4.3 Sparingly Soluble Salts

Some salts such as calcium carbonate, $CaCO_3$ (Calcite) do not fully dissolve in water and are called sparingly soluble salts. Several of the reagents added to the process are sparingly soluble salts including calcite and dolomite. Calcite and dolomite can dissolve and release calcium and magnesium ions into the solution. The amount that a sparingly soluble salt dissolves in water is determined by its solubility product:

$$CaCO_{3,(s)} \xleftrightarrow{k_{sp}=4.8\cdot10^{-9}} Ca^{2+}_{(aq)} + CO^{2-}_{3,(aq)} \qquad \textbf{Equation 2.20}$$

$$k_{sp} = \left[Ca^{2+}_{(aq)}\right] \cdot \left[CO^{2-}_{3,(aq)}\right] \qquad \textbf{Equation 2.21}$$

An increase in the concentration of either calcium or carbonate ions in solution causes the formation of aqueous calcium carbonate which can form solid calcite, especially if solid calcite particles are already present for aqueous calcite to precipitate on.

2.3.3.4.4 Calcium and Magnesium Carbonate/Sulfate/Hydroxide Equilibrium

In a solution of calcium, magnesium and carbonate ions, the pH of the solution will dictate which ionic pairs, ionic complexes and salt precipitates will form. An example of this would be the formation of aqueous magnesium carbonate, and magnesium sulfate followed by monovalent magnesium hydroxide ($MgOH^+$) as pH increases as shown in Figure 2.24 (a). A similar equilibrium distribution is seen with calcium; see Figure 2.24 (b).

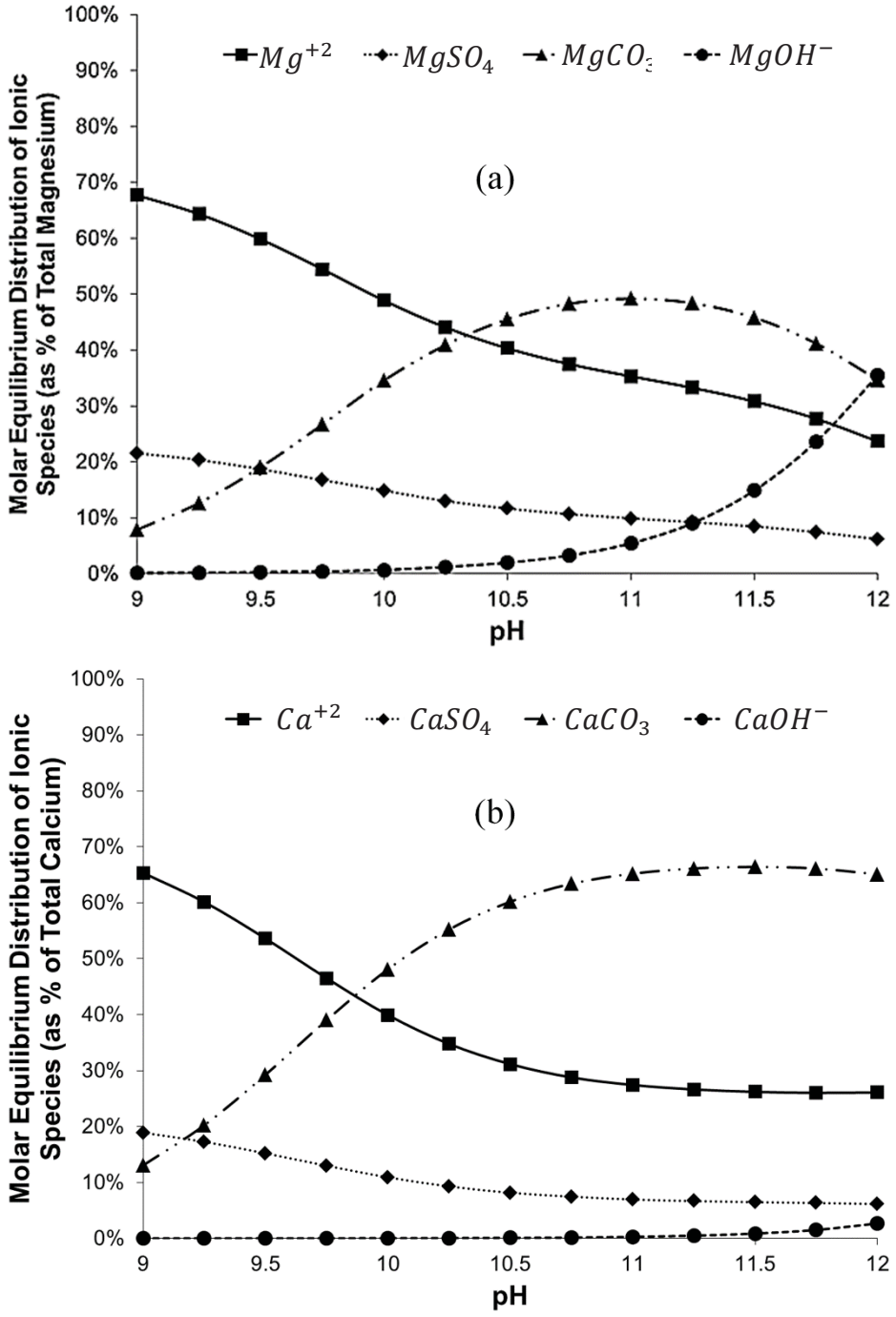

Figure 2.24: (a) Molar equilibrium distribution of magnesium species in process water. (b) Molar equilibrium distribution of calcium species in process water. Cyclone overflow water chemistry data from April 2nd, 2012 was used for this plot.

As discussed previously and shown in Figure 2.21, both calcium and magnesium cations significantly affect zeta potential because they are chemically adsorbed to the surface of particles. These ions cause non-selective flocculation. From the equilibrium distributions of calcium and magnesium shown in Figure 2.24, it can be seen that pH control is necessary to minimize the amount of divalent and monovalent cations present in the process water. The total amount of neutral, monovalent and divalent cations from the calcium and magnesium distributions is shown in Figure 2.25. Maximizing the amount of neutral ions in the water minimizes detrimental ions in the solution. The optimum pH in these process water conditions was found to be 10.99. At this optimum pH, dispersion of particles is maximized allowing for better separation in the deslime thickener.

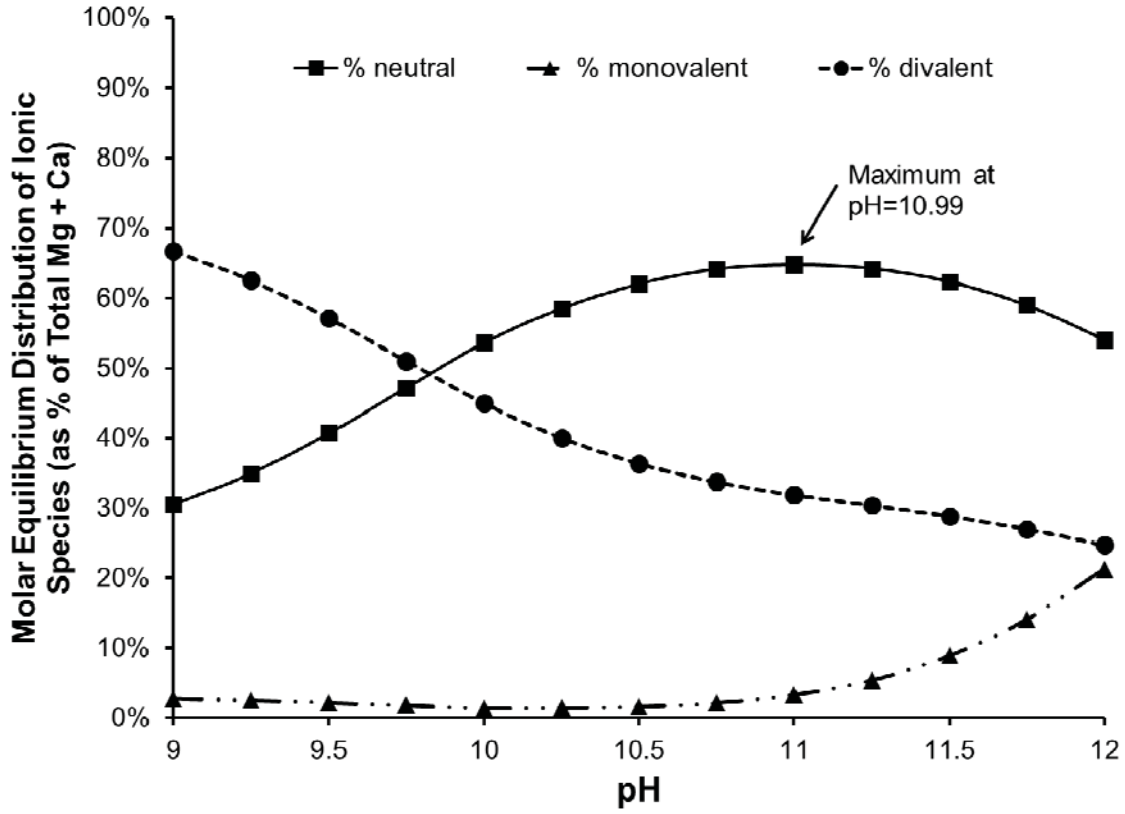

Figure 2.25: Molar distribution of ionic species by valency. Divalent ions include Mg^{2+} and Ca^{2+}. Monovalent ions include $CaHCO_3^+$, $CaOH^+$, $MgHCO_3^+$ and $MgOH^+$. Neutral ions include $CaSO_4$, $CaCO_3$, $MgSO_4$, and $MgCO_3$.

2.3.4 Methods and Materials

2.3.4.1 Sample Collection and Process Locations

The original sampling locations were chosen by Josh Carlson in 2007 based on reagent additions and the process flow sheet. The sampling locations that were originally chosen are shown in Figure 2.26 and Figure 2.27 below and described in Table 2.2. The only change to these locations that has been made was the removal of the cyclone feed sample (location 3). Samples at locations 1 through 7 were taken on sections 7-9 at the

concentrator. Starting at the flotation feed distributor, samples at locations 8 through 11 were taken on sections 7-12 because the float feed from sections 7-12 are mixed at this point. Samples at location 12 and 13 were taken from the concentrate underflow (12) and the polymer addition point (13).

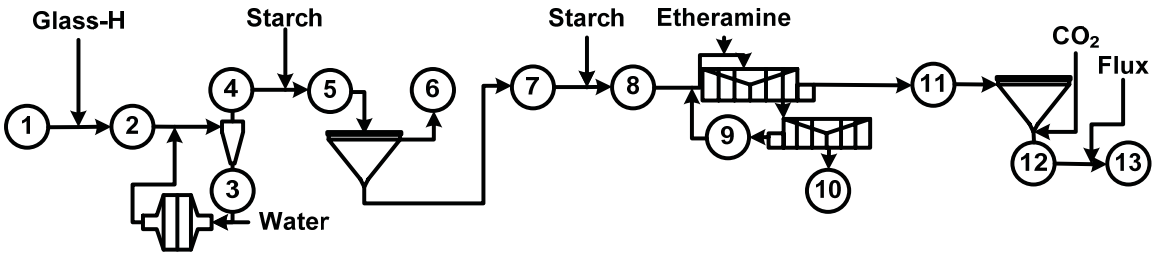

Figure 2.26: Original sampling locations chosen by Dr. Joshua Carlson in 2007

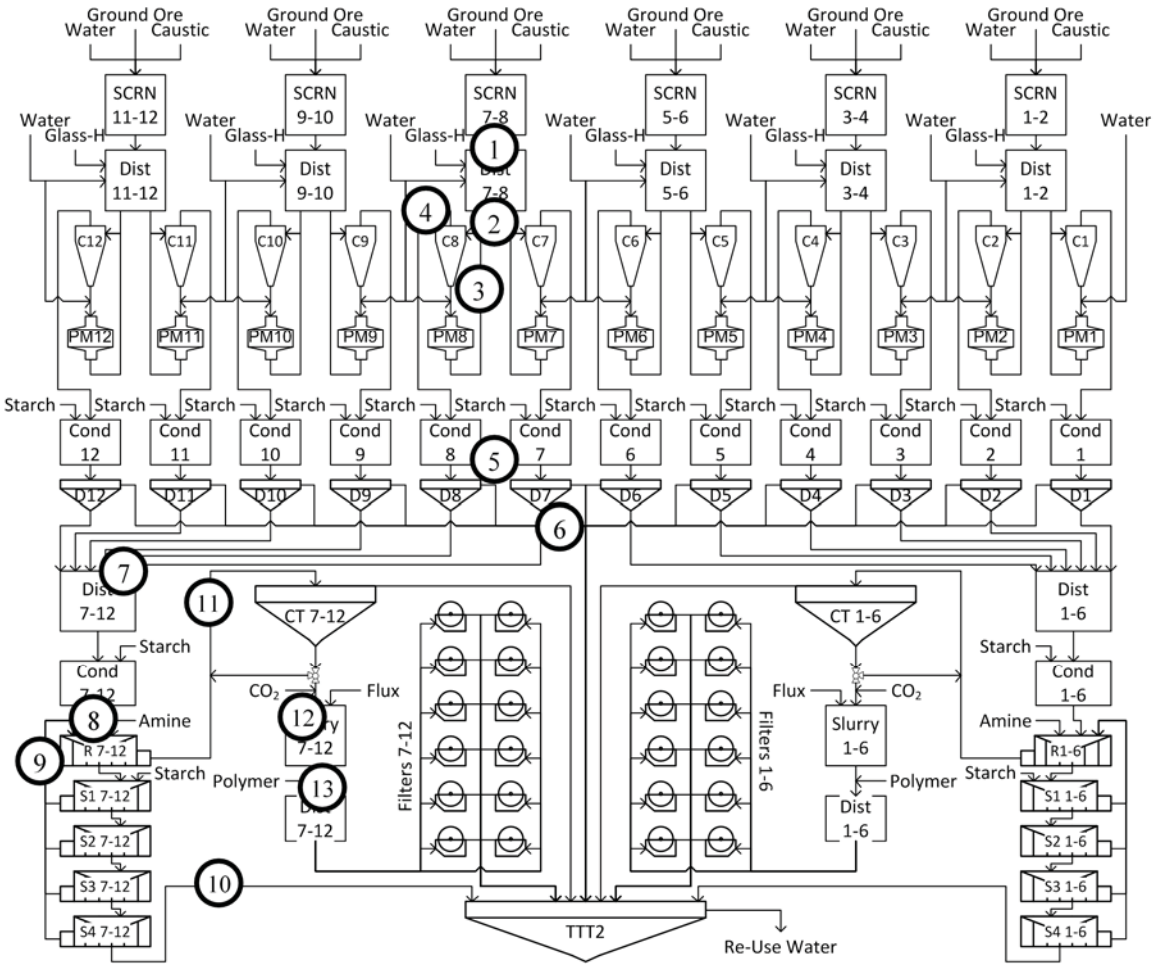

Figure 2.27: Sampling locations in full process flow diagram. Adapted from Keranen (1986).

Table 2.2: Sample location descriptions

Location #	Acronym	Description
1	SUNGH	Screen underflow before dispersant addition
2	SUGH	Screen underflow after dispersant addition
3	-	Cyclone feed
4	CO1	Cyclone overflow before starch addition
5	CO2	Cyclone overflow after starch addition
6	DTO	Deslime thickener overflow
7	DTU	Deslime underflow before starch addition
8	FlF	Flotation circuit feed after starch addition
9	SR	Scavenger return
10	ST	Scavenger tailings
11	RC	Rougher concentrate
12	CTU	Concentrate thickener underflow
13	FiF	Fluxed filter feed

Once the samples were taken, they were immediately transported back to Michigan Tech for analysis. Testing priority was given to the zeta potential analysis of the starched samples because the starch used in the process can degrade over time. When all sample testing was complete, the remaining solids were sent to an external laboratory for XRD/XRF analysis.

2.3.4.2 Solids Analysis Procedure

2.3.4.2.1 Zeta Potential Analysis

Slurry samples were analyzed for zeta potential using an Anton Paar® Electrokinetic Analyzer™ (EKA). To analyze the zeta potential of a slurry, the solid particles and liquid

supernatant must be separated. Settled solids were taken from the bottom of the sample buckets and deslimed in a beaker with distilled water so that only the coarse particles (~ > 25 μm) would be analyzed. This size fraction was chosen due to the particle size limitation of the EKA. The supernatant liquid of the slurry was centrifuged to remove suspended solids prior to use as a background electrolyte in the EKA.

First, the zeta potential of the slurry was analyzed at the process conditions. Then the zeta potential was analyzed as a function of pH by sequential titration using 200 mM HNO_3 down to a pH of < 3.0 in increments of 0.5 pH units. The data from these titrations are plotted in Appendix A.

Samples were not tested in succession by location number but rather by expected concentration of starch from highest to lowest due to the potential degradation of the starch over time. The flotation feed sample (location 8) was the first to be analyzed followed by the deslime thickener feed sample (location 5) as these samples were taken immediately after the starch was added. The rest of the samples were run as expediently as possible following those two samples with the last samples to be tested being locations 1 through 4 because starch had not been introduced at those locations.

2.3.4.2.2 Dry Solids Preparation

Settled solids were re-suspended in distilled water and filtered using a 9 cm Whatman 541 filter medium. The solids were dried in a convection oven at 105°C for 24 hours. The dried solids were then transferred to sealed plastic bags for analysis. Dry solids were analyzed for percent iron, percent calcium, percent magnesium, percent acid insoluble

material (silica), particle size, and XRD/XRF. A thermogravimetric analysis (TGA) was also conducted on each sample.

2.3.4.2.3 Elemental Analysis (%Fe, %Ca, %Mg, % Acid Insolubles)

Dried solid samples were split using a micro rotary riffle splitter down to a ~1 g sample. The split sample was then digested in a beaker according to ASTM standards using 50 mL of concentrated HCL on a stir plate at 200°C for 20 minutes (ASTM, 2006). The digested solution was diluted to 200 mL with distilled water in a class-A volumetric flask, shaken, and allowed to settle for 2 hours. This solution was then diluted into the appropriate background solutions for iron, calcium and magnesium analysis by atomic absorption spectroscopy (AAS). AAS results were used to back-calculate the percent iron, percent calcium, and percent magnesium in the samples. Percent aluminum was attempted; however, the data was not consistent due to overwhelming AAS interference by the iron in solution.

The remaining digested solution was filtered using a weighed Gooch crucible and Whatman 42 filter media. The Gooch crucible was dried at 105°C for 24 hours and weighed to determine the percent acid insoluble material in the digested solution.

2.3.4.2.4 Thermogravimetric Analysis

Dried solid samples were split by the four-corners grab sample method and analyzed in a LECO TGA701 thermogravimetric analyzer. The method ramped temperature up to 107°C at 8°C/min and held until constant weight was achieved. The final mass at constancy was reported as the moisture content of the sample. The next step was a ramp

from 107°C to 207°C at a rate of 8°C/min and held until constant weight was achieved. The final mass at constancy was reported as the volatile organics content of the sample. The final step was a ramp from 207°C to 1000°C at a ramp rate of 1°C per minute. During this time period, many decompositions occur in each sample depending on the mineralogy. The decompositions most noted are as follows:

$$2FeO(OH) \xrightarrow{225-325^{\circ}C} Fe_2O_3 + H_2O \qquad \textbf{Equation 2.22}$$

$$4Fe_3O_4 + O_2 \xrightarrow{325-415^{\circ}C} 6Fe_2O_3 \qquad \textbf{Equation 2.23}$$

$$FeCO_3 \xrightarrow{325-1000^{\circ}C} FeO + CO_2 \qquad \textbf{Equation 2.24}$$

$$CaCO_3 \xrightarrow{325-1000^{\circ}C} CaO + CO_2 \qquad \textbf{Equation 2.25}$$

$$CaMg(CO_3)_2 \xrightarrow{325-1000^{\circ}C} MgO + CaO + CO_2 \qquad \textbf{Equation 2.26}$$

To distinguish between the decomposition of siderite ($FeCO_3$), calcite ($CaCO_3$), and dolomite ($CaMg(CO_3)_2$), the TGA data was compared to the elemental analysis to isolate decompositions due to calcium, and magnesium. The remainder of the carbonate decomposition was assumed to be due to iron in siderite. All thermolysis graphs can be found in Appendix B.

2.3.4.2.5 Particle Size Analysis

Dried solid samples were split by the four-corners grab sample method and analyzed for particle size using a MicroTrac™ SRA9200 laser scattering particle size analyzer. The raw particle size data for all samples can be found in Appendix C.

2.3.4.2.6 XRD/XRF

X-ray Diffraction and X-ray Fluorescence was conducted on the dried solid samples by Thomas Campbell at Cliffs Natural Resources.

2.3.4.3 Water Chemistry Analysis Procedure

2.3.4.3.1 Sample Preparation

The liquid samples were prepared by centrifugation followed by filtration using 9 cm Whatman 42® 2 µm filter media. Samples were then diluted with a background solution for analysis by either atomic absorption spectroscopy (AAS), direct measurement via an ion selective electrode (ISE), or gravimetric precipitation followed by thermogravimetric analysis (TGA). Background solutions were prepared according to ASTM standards and recommendations found in the Agilent Technologies AAS Analytical Methods Manual.

2.3.4.3.2 pH and Conductivity

pH and conductivity were measured both at the mine during sample collection and in the laboratory at Michigan Technological University. Laboratory pH and conductivity are reported here because the portable measurement devices can be less accurate than the stationary laboratory devices. pH and conductivity were measured in the laboratory using

the Electrokinetic Analyzer (EKA). The laboratory pH and conductivity meters were calibrated within 24 hours of sample collection.

2.3.4.3.3 Calcium and Total Water Hardness

Calcium and total hardness were tested by the mine on each sample. The test entails a colorimetric EDTA (ethylene-diamine-tetraacetic acid) titration. The indicator for this type of titration is typically Eriochrome Black T which turns red in the presence of metal ions. The addition of EDTA (a stronger complexing reagent) causes the indicator to turn blue when all of the metal ions have been complexed.

2.3.4.3.4 Sodium Concentration

Sodium concentration was determined on the 11/30/2011 samples and the two sets of 4/2/2012 samples. The 11/30/2011 samples were analyzed directly using a calibrated Sodium ISE. The results from this electrode are given as the activity of the ion, which, for sodium is very close to the total concentration. Upon further development of reliable laboratory procedures, the total concentration of sodium was measured using AAS with an air-acetylene flame for the 4/2/2012 samples. The background solution was (1+99) HCL + 2000 ppm KCl.

2.3.4.3.5 Potassium Concentration

Potassium concentrations were measured on the final sample set to verify that they were consistent with levels previously reported (Haselhuhn et al., 2012a). Potassium is also a small contributor to conductivity. Total potassium concentration was measured by AAS

with an air-acetylene flame for the 4/2/2012 samples (ASTM, 2010d). The background solution was (1+99) HCl + 2000 ppm NaCl.

2.3.4.3.6 Calcium Concentration

Calcium concentration was inferred from calcium water hardness for all samples except the 4/2/2012 samples. The calcium concentrations of these samples were measure using AAS with a nitrous oxide-acetylene flame (ASTM, 2010a). The background solution was (1+99) HCl + 2000 ppm KCl. The AAS results were comparable to the calcium hardness results reported by the mine.

2.3.4.3.7 Magnesium Concentration

Magnesium concentration was measured by AAS using an air-acetylene flame on the 11/30/2011 and the 4/2/2012 samples (ASTM, 2010a). The background solution was (1+99) HCl + 2000 ppm KCl. Magnesium concentrations did not match well with the total hardness measurements reported by the mine.

2.3.4.3.8 Soluble Iron Concentration

Soluble iron concentration was measured by AAS using an air-acetylene flame on the 4/2/2012 samples (ASTM, 2010c). The background solution was (3+99) HCl. Iron was measured to determine if trends in iron levels were consistent with those found in a previous study (Haselhuhn et al., 2012a).

2.3.4.3.9 Chloride Concentration

Chloride is a small contributor to conductivity, which can be easily be measured online and may aid in increasing iron recovery. Chloride concentration was measured using a chloride ISE on the 11/30/2011 and 4/2/2012 samples (ASTM, 2010b).

2.3.4.3.10 Nitrate Concentration

Nitrate concentration, though very minimal, is a small contributor to conductivity as well. Nitrate was measured using a nitrate ISE on the 4/2/2012 samples mostly to compare with trends found in a previous study (Haselhuhn et al., 2012a).

2.3.4.3.11 Carbonate and Sulfate Concentration

Total carbonate and sulfate concentration was measured simultaneously by gravimetric precipitation with strontium chloride followed by thermogravimetric analysis. Aqueous strontium precipitates readily with both sulfate and carbonate in solution to form a white particle suspension by the following reactions (Knovel, 2003).

$$Sr^{2+}_{(aq)} + CO^{2-}_{3,(aq)} \xrightarrow{K_{sp}=10^{-8.8}} SrCO_{3,(s)} \qquad \textbf{Equation 2.27}$$

$$Sr^{2+}_{(aq)} + SO^{2-}_{4,(aq)} + 2.7H_2O \xrightarrow{K_{sp}=10^{-6.55}} SrSO_4 \cdot 2.7H_2O_{(s)} \qquad \textbf{Equation 2.28}$$

After precipitation, the solids were filtered and weighed to determine the total amount of $SrSO_4 \cdot 2.7H_2O$ and $SrCO_3$ present. The amount of CO_3^{2-} and SO_4^{2-} was determined

quantitatively by the amount of thermal decomposition during thermogravimetric analysis. Thermal decomposition of a mixture of $SrSO_4 \cdot 2.7H_2O$ and $SrCO_3$ proceeds as follows.

$$SrSO_4 \cdot 2.7H_2O_{(s)} + SrCO_{3,(s)} \xrightarrow{260-400°C} SrSO_{4,(s)} + SrCO_{3,(s)} + 2.7H_2O_{(g)} \quad \textbf{Equation 2.29}$$

$$SrSO_{4,(s)} + SrCO_{3,(s)} \xrightarrow{850-1000°C} SrSO_{4,(s)} + SrO_{(s)} + CO_{2,(g)} \quad \textbf{Equation 2.30}$$

This method has not been reported in literature, however, has been proven to be accurate to ±0.87% using synthetic carbonate and sulfate reagents.

2.3.4.3.12 Oxidation-Reduction Potential

Oxidation-Reduction Potential (ORP) was measured electrochemically with an ORP electrode. ORP was measured to give an indication of whether the process water was an oxidizing environment or a reducing environment. This is an important factor for surface chemistry as it predicts the propensity of free iron sites to oxidize.

2.3.4.3.13 Total Dissolved Solids

Total dissolved solids (TDS) were measured on the April 2nd, 2012 sample sets by an external laboratory. 500 mL samples were prepared by centrifugation and filtration.

2.3.4.3.14 Equilibrium Distribution Modeling

The equilibrium distribution of ionic species in complex solutions can be modeled using many different software packages such as PHREEQC, which is freeware created and

distributed by USGS. Equilibrium distributions for this report have been assembled using this software.

2.3.5 Results and Discussion

2.3.5.1 Overfrothing – May 5th, 2011

2.3.5.1.1 Introduction

The goal of this work was to determine what water chemistry factors play a significant role in the magnitude of the zeta potential and if there is an inexpensive method for monitoring zeta potential (or inferring it from other measurements) at any point within the plant. The May 5th, 2011 sample date was chosen due to poor operating conditions at the concentrator. The flotation tailings was said to be "overfrothing". This phenomenon was attributed to humic acid buildup in the reuse water due to melting snow and runoff. Although this hypothesis could not be confirmed, this sample set was successful in delivering a base set of data that the rest of the project could build on.

2.3.5.1.2 pH

pH was recorded both at the plant and during the zeta potential measurements as shown in Figure 2.28. The pH of the plant water slowly decreased throughout the concentrator from ~11 post-comminution down to ~10.7 at the concentrate thickener. The pH did not drift much between the time when the samples were taken and when they were analyzed at Michigan Technological University except for the concentrate thickener underflow sample at location 12, see Figure 2.28. The concentrate thickener underflow sample rose

in pH from 8.85 to 9.45. This was probably due to the slow dissolution of flux in the recycled concentrate added to the concentrate thickener.

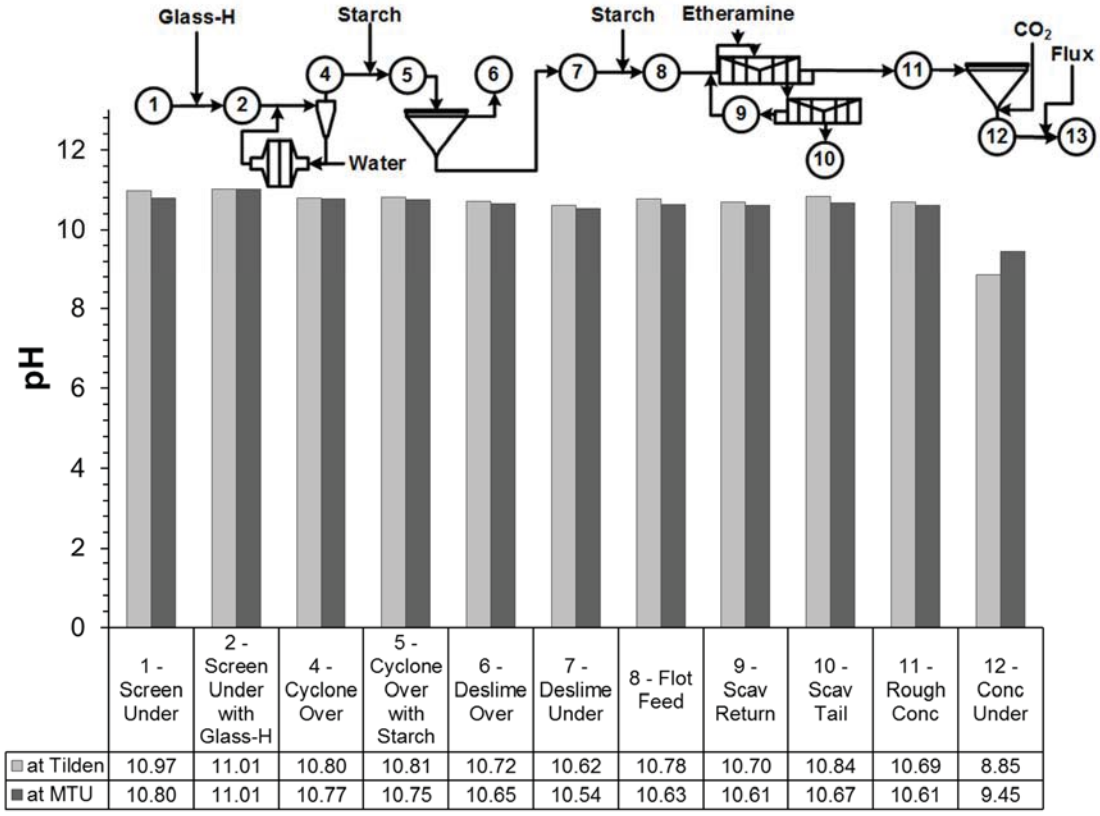

	1 - Screen Under	2 - Screen Under with Glass-H	4 - Cyclone Over	5 - Cyclone Over with Starch	6 - Deslime Over	7 - Deslime Under	8 - Flot Feed	9 - Scav Return	10 - Scav Tail	11 - Rough Conc	12 - Conc Under
at Tilden	10.97	11.01	10.80	10.81	10.72	10.62	10.78	10.70	10.84	10.69	8.85
at MTU	10.80	11.01	10.77	10.75	10.65	10.54	10.63	10.61	10.67	10.61	9.45

Figure 2.28: pH of each sample by location on May 5th, 2011

2.3.5.1.3 Conductivity

Conductivity was recorded at the plant using a portable conductivity meter and during the EKA zeta potential measurements. This was done to ensure that any conductivity drift between sampling and testing was recorded. The results of conductivity testing are shown in Figure 2.29. Conductivity slowly decreased throughout the plant from ~3000 µS/cm post-comminution down to ~240 µS/cm at the rougher concentrate.

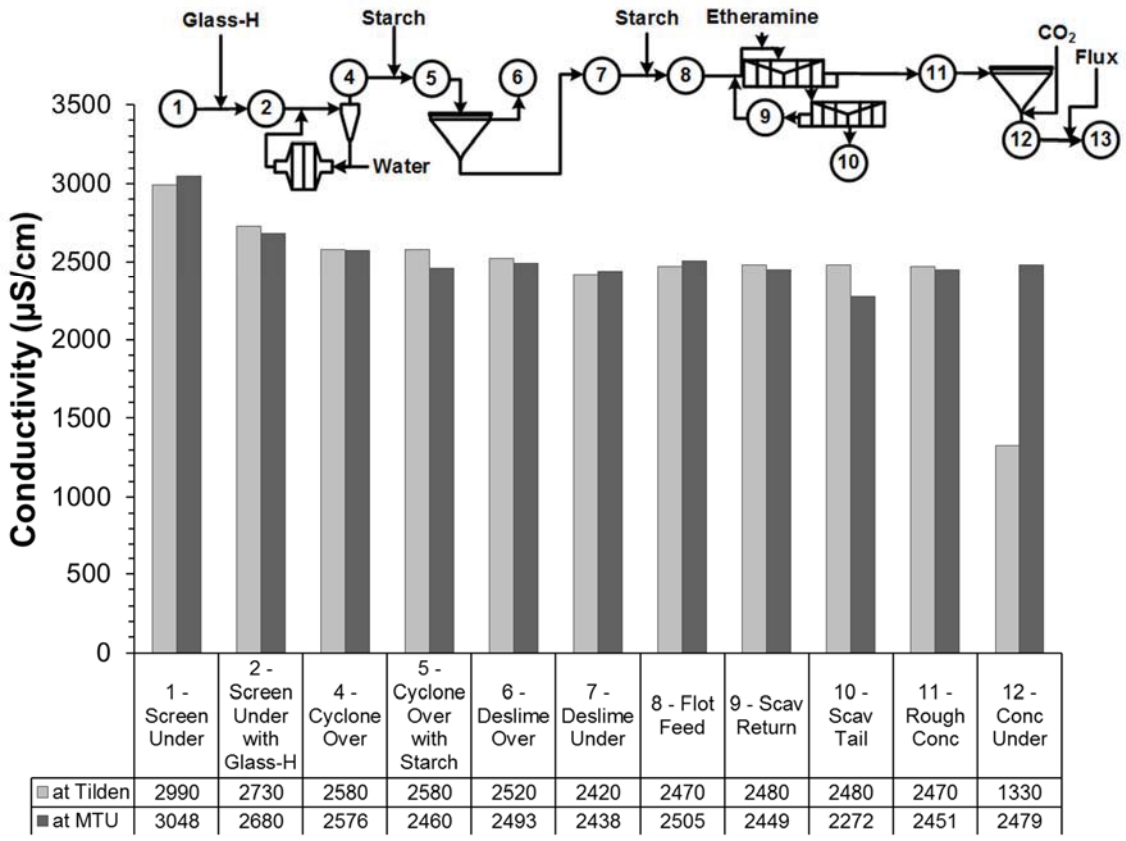

Figure 2.29: Conductivity of each sample by location on May 5th, 2011

2.3.5.1.4 Calcium and Total Hardness

Calcium hardness and total hardness tests were conducted by the plant personnel and the results are shown in Figure 2.30. The water hardness was at or below 30 ppm except for at the deslime underflow (location 7), the scavenger returns (location 9), and the concentrate underflow (location 12). The reason for the high calcium and total hardness seen at the deslime underflow and scavenger returns was unknown but could be a result of sampling error or testing error. The concentrate underflow water hardness was strongly affected by the addition of recycled fluxed concentrate. As the flux dissolved at the lower pH, the water hardness was increased substantially.

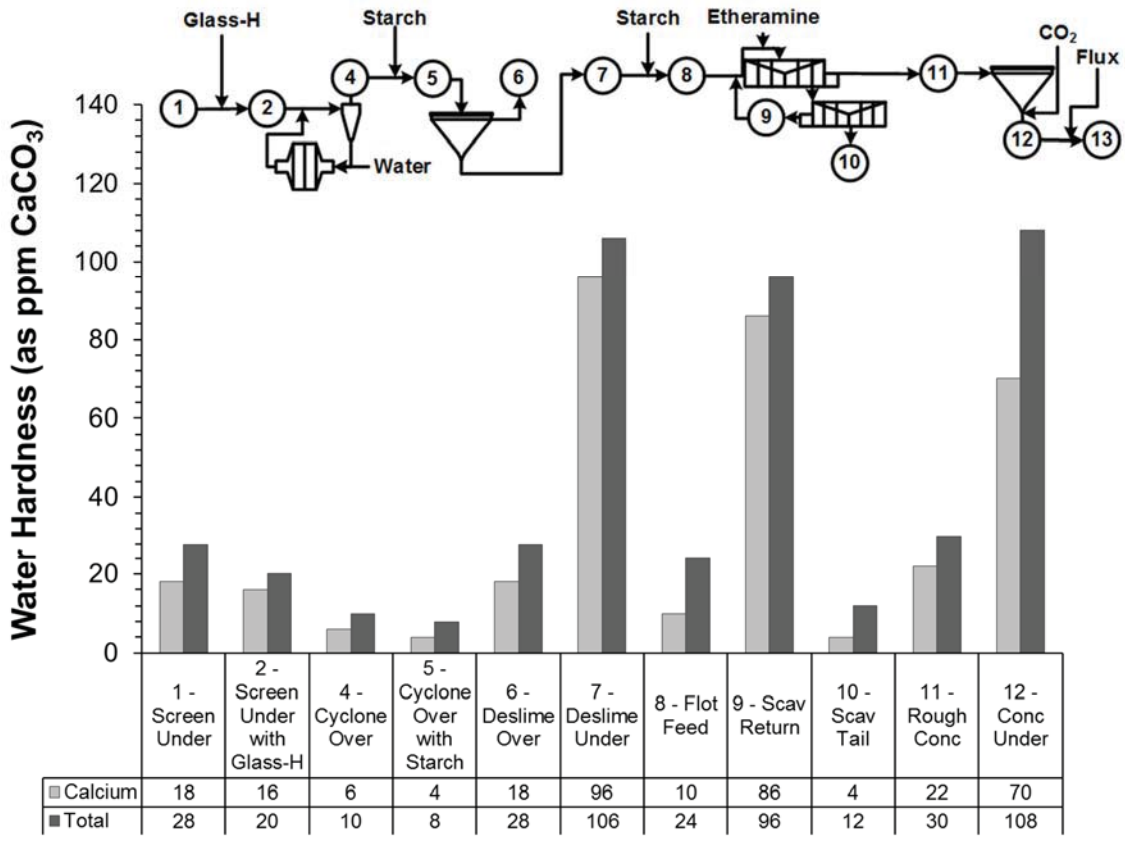

Figure 2.30: Calcium hardness and total hardness for each sample by location on May 5th, 2011

2.3.5.1.5 Zeta Potential

The zeta potential at process conditions (pH, conductivity) are shown in Figure 2.31. It was very apparent that the starch suppressed the surface charge of the hematite particles by comparing sample locations 4 and 5 (cyclone overflow before and after starch addition) and sample locations 7 and 8 (deslime underflow before and after starch addition). Zeta potential versus pH plots of these samples are included in Appendix A. The starch addition at the cyclone overflow and deslime underflow showed depressions in surface charge by 6 mV and 14 mV, respectively.

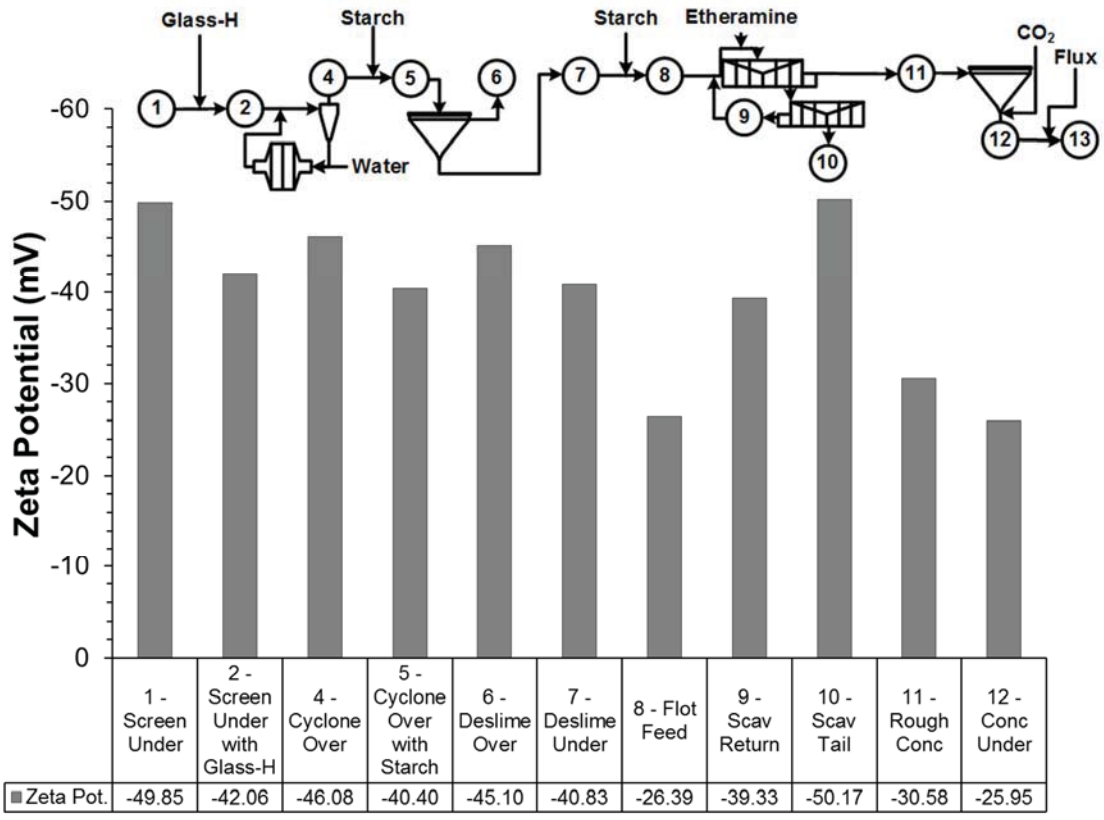

Figure 2.31: Zeta potential of each sample at process conditions by location on May 5th, 2011.

Other notable findings with zeta potential included a more negative deslime overflow zeta potential than deslime underflow zeta potential. This suggested that silica was being removed in the deslime thickener because silica has much more negative zeta potential than hematite at the pH of the deslime thickener (pH=~10.7). The elemental analysis confirmed this observation by showing that the deslime overflow silica content (67.94% acid insol.) was much higher than the deslime underflow silica content (19.21% acid insol.). This observation was also seen at the scavenger tails sample. The zeta potential of

the scavenger tails was the most negative showing that the abundance of silica (64.88% acid insol.) in the sample has a direct effect on the zeta potential.

A plot of zeta potential versus silica content can be seen in Figure 2.32. The general trend was that higher silica content yielded higher zeta potentials. The trend line was not a perfect match due to the use of many surface active reagents in the process including starch (hematite depressant/selective flocculant), glass-H (dispersant), etheramine (cationic collector and frother), and recycled fluxed hematite concentrate (general flocculant).

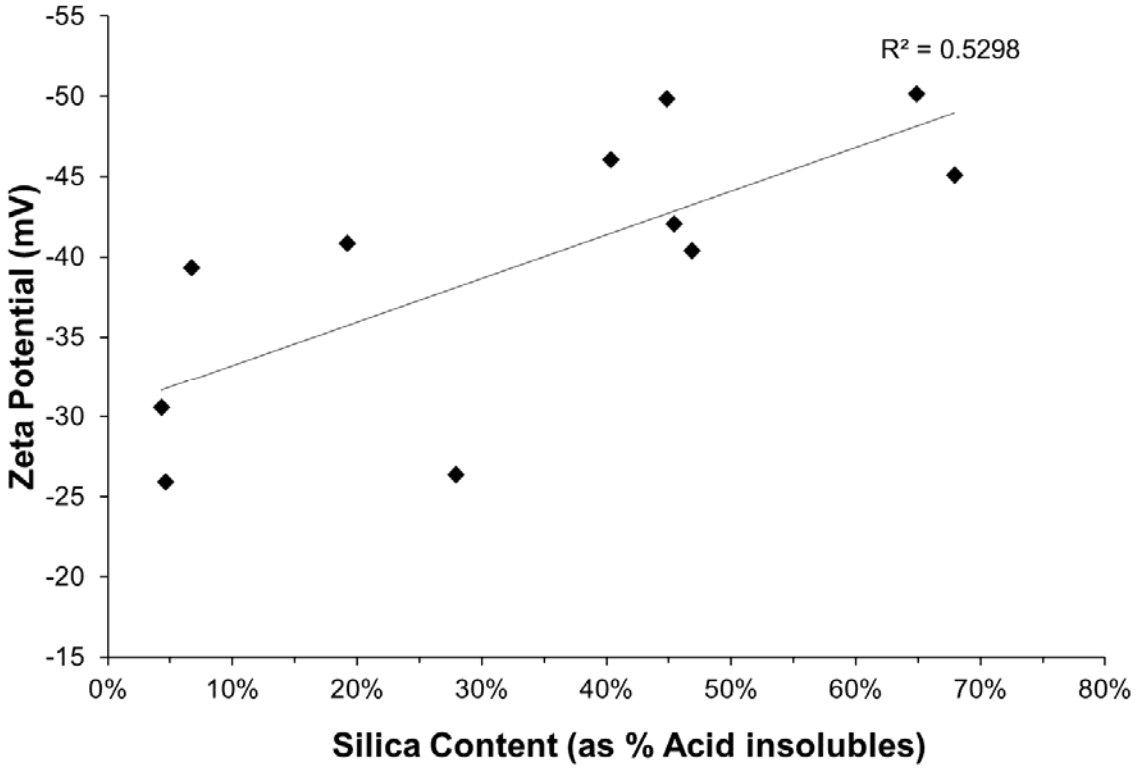

Figure 2.32: The Effect of silica content on zeta potential of hematite ore. Most outliers are due to the addition of surface altering flocculants throughout the process.

2.3.5.1.6 Process Data

Process data for May 5th, 2011 can be seen in Table 2.3. The sample set taken on May 5th, had calcium hardness values between 4 and 18 ppm (as $CaCO_3$) throughout deslime and flotation accompanied by a 67.6% overall recovery (deslime overflow (DTO) at 16.2% Fe and scavenger tails (ST) at 22.3% Fe). The high iron content of the scavenger tailings sample on May 5th was accompanied by high water hardness values at the flotation feed.

Table 2.3: Process data for May 5th, 2011.

Date: 5/5/11 Time: 7:00 AM												
Section 7-9									Tilden 2 Average			
	%Fe	%Wt.	Fe Units	Fe Dist.	pH Lab	Glass-H Rate	Total Recovery Weight	Iron Unit		%Fe	%Wt.	Caustic Rate
CYC O/F	34.9	100	34.9	100.0	11.0	lbs/ton			CYC O/F	35.3	100	Crude lbs/ton
DTU	48.6	57.7	28.1	80.4	pH Plant	0.175	37.7	67.6	DTU	47.8	60.5	1.85
DTO	16.2	42.3	6.8	19.6	11.0				DTO	16.3	39.5	
									Flot Tail	22.3	22.2	
					%Passing at 500 Mesh		83.2		Flot Conc	62.5	38.3	
Date: 5/5/11 Time: 1:00 PM												
Section 7-9									Tilden 2 Average			
	%Fe	%Wt.	Fe Units	Fe Dist.	pH Lab	Glass-H Rate	Total Recovery Weight	Iron Unit		%Fe	%Wt.	Caustic Rate
CYC O/F	34.9	100	34.9	100.0	10.8	lbs/ton			CYC O/F	35.3	100	Crude lbs/ton
DTU	51.5	53.8	27.7	79.3	pH Plant	0.175	39.1	70.0	DTU	49.3	59.6	1.85
DTO	15.6	46.2	7.2	20.7	11.0				DTO	14.5	40.4	
									Flot Tail	22.1	19.5	
					%Passing at 500 Mesh		83.4		Flot Conc	62.5	40.1	

2.3.5.1.7 Conclusions

The zeta potential of the slurry particles seemed to be the product of several process conditions. pH and conductivity are always factors in the zeta potential of any colloidal system. Other likely factors in the determination of zeta potential are charge suppressants such as starch, ionic collectors and flocculants, and the concentration of siliceous particle species.

Several conclusions were made about the zeta potential at the concentrator including:

1. Starch did noticeably and reproducibly suppress the surface charge of hematite in both deslime and flotation
2. The effect of the starch was more prominent in flotation
3. The addition of CO_2 had a significant effect on the pH, conductivity, water hardness, and zeta potential. These additions resulted in a
    3.1. Decrease in pH
    3.2. Increase in water hardness
    3.3. Increase in zeta potential

2.3.5.2 Normal Operations – July 13th, 2011

2.3.5.2.1 Introduction

The goal of this work was to determine what water chemistry factors play a significant role in the magnitude of the zeta potential and if there is an inexpensive method for monitoring zeta potential (or inferring it from other measurements) at any point within the plant. The July 13th, 2011 sample set was taken when sections 7-9 were running well. This was the first set of data taken on a normal processing day and provided a basis that can be used for comparing data from abnormal processing days.

2.3.5.2.2 pH

The pH of the process on May 5th, 2011 remained between 10.5 and 10.8 until dewatering as shown in Figure 2.28. On July 13th, the pH was held above 11 throughout much of the process as shown in Figure 2.33. A higher pH typically caused a higher

magnitude of zeta potential of the iron and silica particles resulting in greater dispersion. In both sample sets, the pH dropped considerably upon the addition of CO_2. This was to be expected as CO_2 dissolves in water as carbonic acid (H_2CO_3) and immediately loses protons (H^+) to free hydroxide ions (OH^-) thereby lowering the pH. Depending on the equilibrium pH, the carbonate ions in solution will either be in the form of bicarbonate (HCO_3^-) or carbonate (CO_3^{2-}) ions:

$$CO_{2(g)} + H_2O_{(aq)} \rightarrow H_2CO_{3(aq)} \xrightarrow{pH\sim6.2} HCO^-_{3(aq)} + H^+_{(aq)} \xrightarrow{pH\sim10.5} CO^{2-}_{3(aq)} + 2H^+_{(aq)}$$

Equation 2.31

The filter feed sample (location 13) of the May 5th sample set was taken too close to the polymer mixing point. This caused the sample to be extremely viscous and testing was stopped for fear of equipment damage. The July 13th filter feed sample was taken when the process was stabilized and the results showed an increase in pH. The dissolution of calcium and magnesium from flux (calcium/magnesium carbonates) can neutralize some of the carbonic acid resulting in the increase in pH shown at the filter feed.

For the July 13th sample set, the deslimed solids from the deslime thickener overflow were extremely fine (80% passing at 18.45 μm) and could not be measured with the electrokinetic analyzer (EKA). The pH readings in Figure 2.33 were taken using the EKA explaining the loss of the location 6 data point in Figure 2.33. This can be considered a good thing, in that, the deslime thickener was removing slimes and fine particles with little loss of larger hematite particles that day.

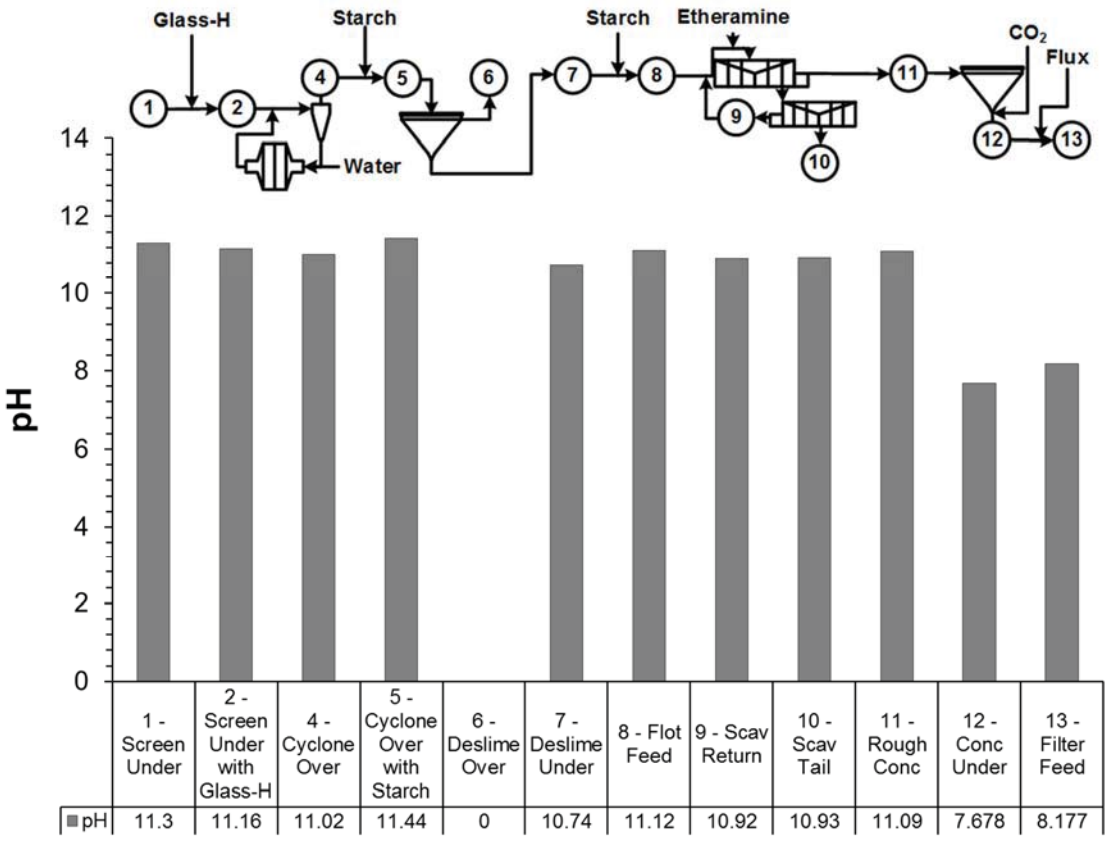

Figure 2.33: pH of each sample by location on July 13th, 2011

2.3.5.2.3 Conductivity

The conductivity of the May and July sample sets exhibited the same decreasing trend throughout the process, however, the July post-comminution samples were significantly higher in conductivity than the May samples. See Figure 2.34. This indicated a difference in ore mineralogy, makeup water contents, and/or caustic/dispersant (Glass-H) addition rates. In both cases, the conductivity stabilized in the mid 2000's after deslime thickening.

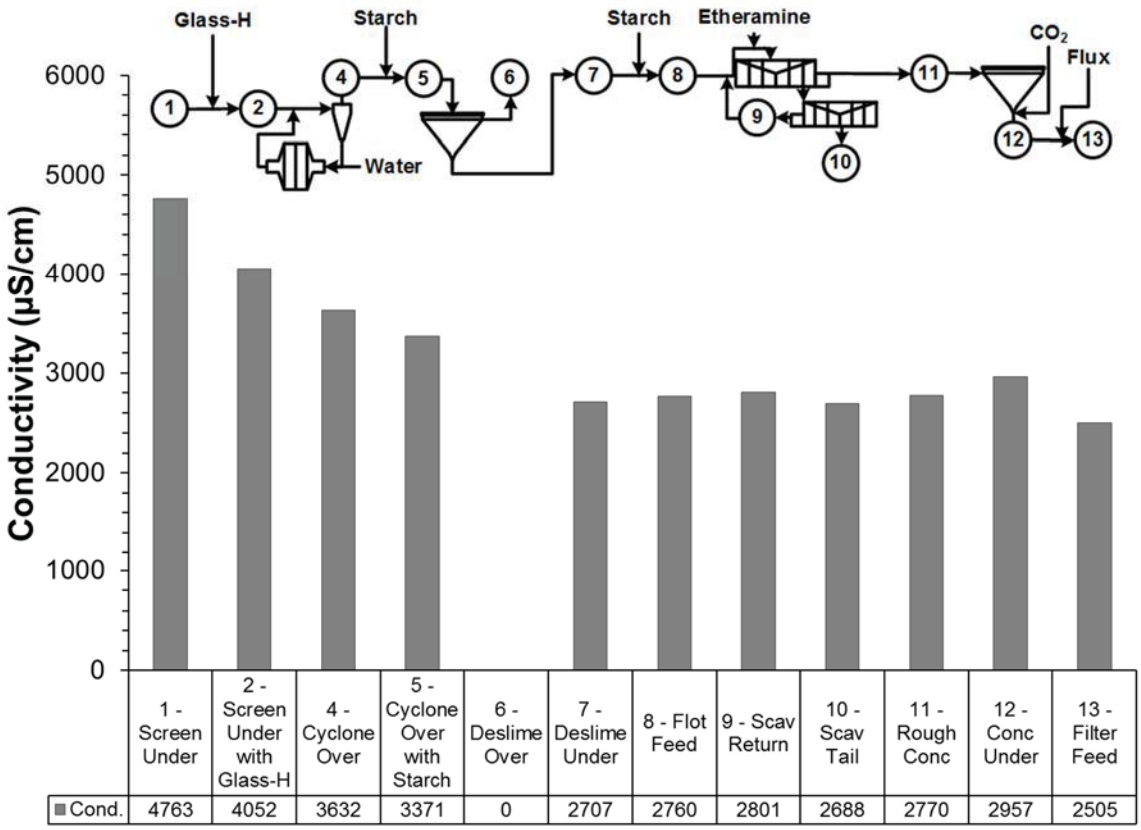

Figure 2.34: Conductivity of each sample by location on July 13th, 2011

2.3.5.2.4 Calcium and Total Hardness

The water hardness tests were somewhat erratic between sampling dates as shown in Figure 2.35.There are several commonalities between the two sample sets: the deslime starch addition at locations 4 and 5 did not significantly affect hardness, and the addition of CO_2 drastically increased the water hardness. Based on the idea that starch does not affect hardness, the dramatic decrease present in the May 5th samples at the amine and starch addition (locations 7-8) must be attributed to an error in sampling/testing, an effect caused by the amine, or the reason behind the over-frothing in the flotation cells seen that

day. These fluctuations may be attributed to the higher calcium content of the ore during the May 5th samples (0.49% Ca on May 5th, 0.24% Ca on July 13th).

Another notable phenomenon occurred in the concentrate thickener underflow upon the addition of CO_2. The hardness data suggest that the addition of CO_2 dissolves the flux in the recycled fluxed concentrate. This is most likely due to the dramatic increase in solubility of calcite and dolomite at the decreased pH.

Increasing the hydrogen content of the water (lowering the pH) causes calcite (and dolomite) to dissolve because the hydrogen will displace calcium in calcite and form a bicarbonate ion (or carbonic acid at low pH) and a free calcium ion. This is the source for increased water hardness upon addition of CO_2 to the slurry.

The addition of flux was accompanied with a decrease in water hardness as well as an increase in pH. This showed that a new equilibrium was being established with the increased concentration of flux in the slurry.

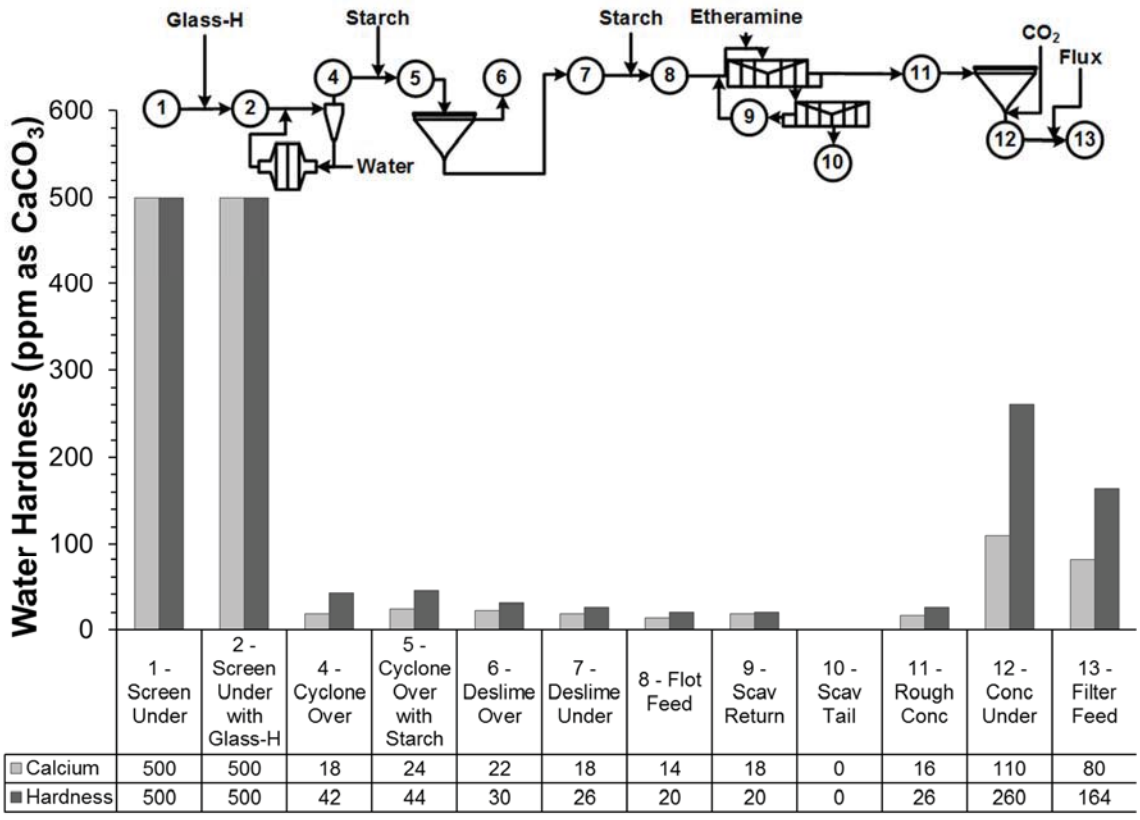

Figure 2.35: Calcium hardness and total hardness for each sample by location on July 13th, 2011

2.3.5.2.5 Zeta Potential

The zeta potentials at the process conditions (pH, conductivity) are shown in Figure 2.36. The first noticeable trend was the increase in zeta potential with the addition of Glass-H. This appeared on both sampling dates. This phenomenon was postulated to be a result of phosphate ion adsorption onto un-hydrated hematite and silica surfaces.

It was very apparent that the starch suppresses the surface charge of the hematite particles by comparing samples 4 and 5 (cyclone overs before and after starch addition) and samples 7 and 8 (flotation feed before and after starch addition). This observation was

consistent in both sample sets with a more pronounced effect at the flotation starch addition. Zeta potential versus pH plots of these samples are included in Appendix A.

Both sample sets also showed a consistent 5mV increase in zeta potential upon the addition of CO_2. This is to be expected with the pH change and has been shown to increase filtration rates (Haselhuhn et al., 2012b). In the July sample, the flux addition caused a decrease in zeta potential which may have been negating the effects of the CO_2 on filtration.

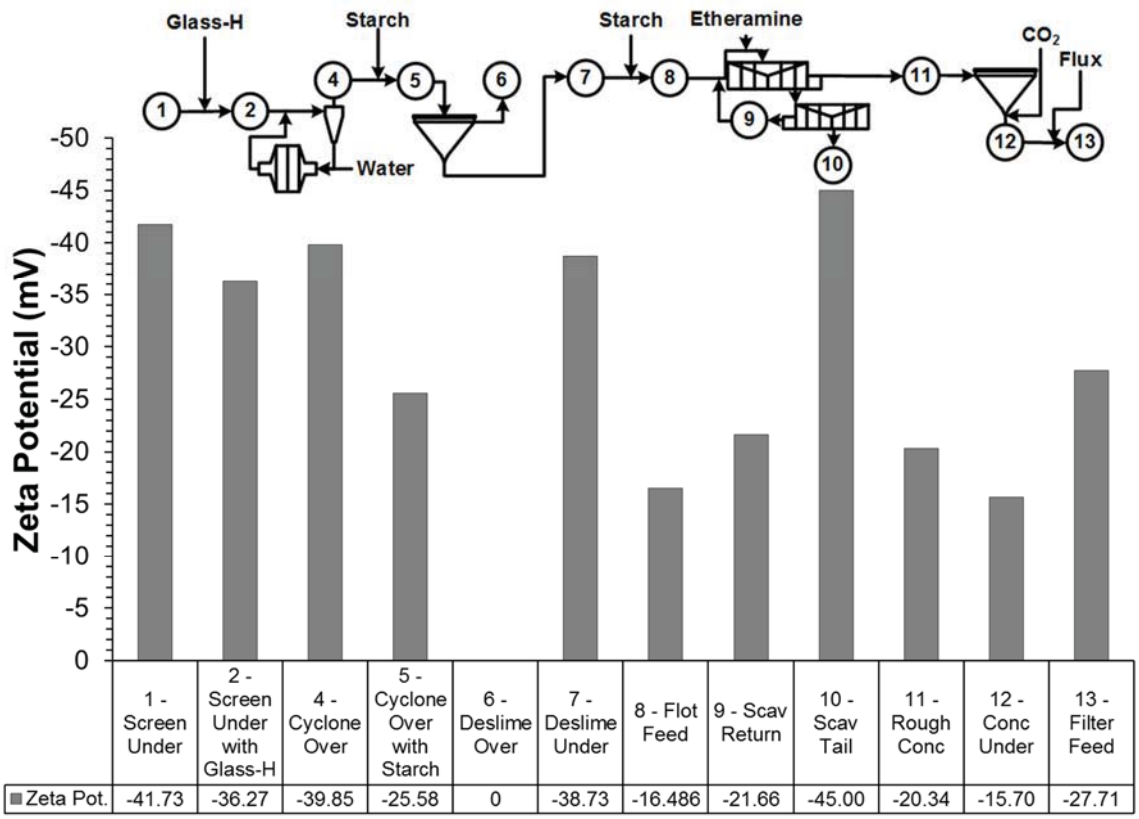

Figure 2.36: Zeta potential of each sample at process conditions by location on July 13th, 2011.

Other notable findings with zeta potential included a more negative scavenger tails zeta potential than flotation feed zeta potential. A similar trend between silica content and zeta potential was observed for this sample set as well. This suggested that silica is being effectively removed during flotation because silica has a much more negative zeta potential than hematite at the pH of flotation (pH=~10.7).

2.3.5.2.6 Process Data

Iron recovery, metallurgical balance, and reagent addition rates can be found in Table 2.4. The recovery on May 5th was 4.4% lower than on July 13th. 1.3% of this decrease in recovery is due to extra losses in deslime. Water chemistry differences between these two days included a lower pH, lower water hardness and a diminished effectiveness of starch adsorption on May 5th. The latter water chemistry properties may play a significant role in the selectivity and effectiveness of the starch. A diminished selectivity of starch would cause losses of iron to the deslime overflow.

The sample set taken on July 13th had calcium hardness values between 15 and 24 ppm (as $CaCO_3$) throughout deslime and flotation accompanied by a maximum overall recovery of 72.0% (deslime overflow (DTO) at 14.9% Fe and scavenger tails (ST) at 18.4% Fe). The low flotation tailings iron content on July 13th was accompanied by low water hardness at the flotation feed. This consistency shows a need to monitor water hardness and pH levels at the float feed distributor as there may be a connection between iron rejection, water hardness, and pH in flotation.

Table 2.4: Process Data on July 13th, 2011

Date: 7/13/2011 Time: 7:00 AM												
Section 7-9									Tilden 2 Average			
	%Fe	%Wt.	Fe Units	Fe Dist.	pH Lab	Glass-H Rate	Total Recovery Weight	Total Recovery Iron Unit		%Fe	%Wt.	Caustic Rate
CYC O/F	34.7	100.0	34.7	100.0	11.1	lbs/ton			CYC O/F	34.5	100.0	Crude lbs/ton
DTU	47.0	61.7	29.0	83.5	pH Plant	0.16	39.9	72	DTU	45.6	65.5	1.85
DTO	14.9	38.3	5.7	16.5	11.1				DTO	13.6	34.5	
									Flot Tail	18.4	25.2	
						%Passing at 500 Mesh	78.9		Flot Conc	62.6	40.3	
Date: 7/13/2011 Time: 1:00 PM												
Section 7-9									Tilden 2 Average			
	%Fe	%Wt.	Fe Units	Fe Dist.	pH Lab	Glass-H Rate	Total Recovery Weight	Total Recovery Iron Unit		%Fe	%Wt.	Caustic Rate
CYC O/F	34.2	100.0	34.2	100.0	11.2	lbs/ton			CYC O/F	34.1	100.0	Crude lbs/ton
DTU	47.6	59.1	28.2	82.3	pH Plant	0.14	38.5	70.5	DTU	46.4	62.2	1.85
DTO	14.8	40.9	6.0	17.7	11.1				DTO	13.9	37.8	
									Flot Tail	19.6	23.4	
						%Passing at 500 Mesh	80.9		Flot Conc	62.6	38.8	

2.3.5.2.7 Conclusions

The July 13th sample set confirmed several theories made about how the zeta potential is affected by process conditions. The following are the conclusions drawn from this sample set:

1. Starch did noticeably and reproducibly suppress the surface charge of hematite in both deslime and flotation
2. The effect of the starch was consistently more prominent in flotation
3. Starch did not significantly change the water hardness
4. The addition of CO_2 had a significant effect on the pH, conductivity, water hardness, and zeta potential. These additions resulted in a
   4.1. Decrease in pH
   4.2. Increase in conductivity
   4.3. Increase in water hardness

4.4. Increase in zeta potential

2.3.5.3 Crushers Shut Down – November 30th, 2011

2.3.5.3.1 Introduction

The goal of this work was to determine what water chemistry factors play a significant role in the magnitude of the zeta potential and if there is an method for monitoring zeta potential (or inferring it from other measurements) at any point within the plant. The November sample set was taken when the deslime and flotation processes had a very high iron rejection and the crushers were shut down for maintenance.

Several process conditions were noticeably different on this day:

1. Flotation and deslime had a very high weight rejection with high iron concentration in tailings
2. Water hardness values were extraordinarily low throughout the plant (<10 ppm)
3. Flotation overflow appeared stagnant in some areas
4. Crushers were shut down for maintenance
5. Plant flow-rates were turned down
6. Low flow rates caused inadequate distribution of slurry between roughers

2.3.5.3.2 pH

The pH of the process water was reported at 11.0 from the plant labs. This matched well with the pH at the screen underflow sample however it was not representative of the entire process during this sampling campaign as shown in Figure 2.37. The pH tended to decrease throughout the process and hit a low point at 10.28 at the flotation feed. This can

cause the zeta potential to increase therefore hindering collector performance and overall particle dispersion. On May 5th, the same trend in pH occurred, but not to such an extent. This was also accompanied with higher than normal loss of iron in flotation.

The pH decreases substantially upon the addition of CO_2 at the concentrate underflow followed by a slight increase when flux is added. This is to be expected because dolomite dissolves and establishes equilibrium at a pH between 8 and 9. This effect at the dewatering stage has been seen in all sample sets taken.

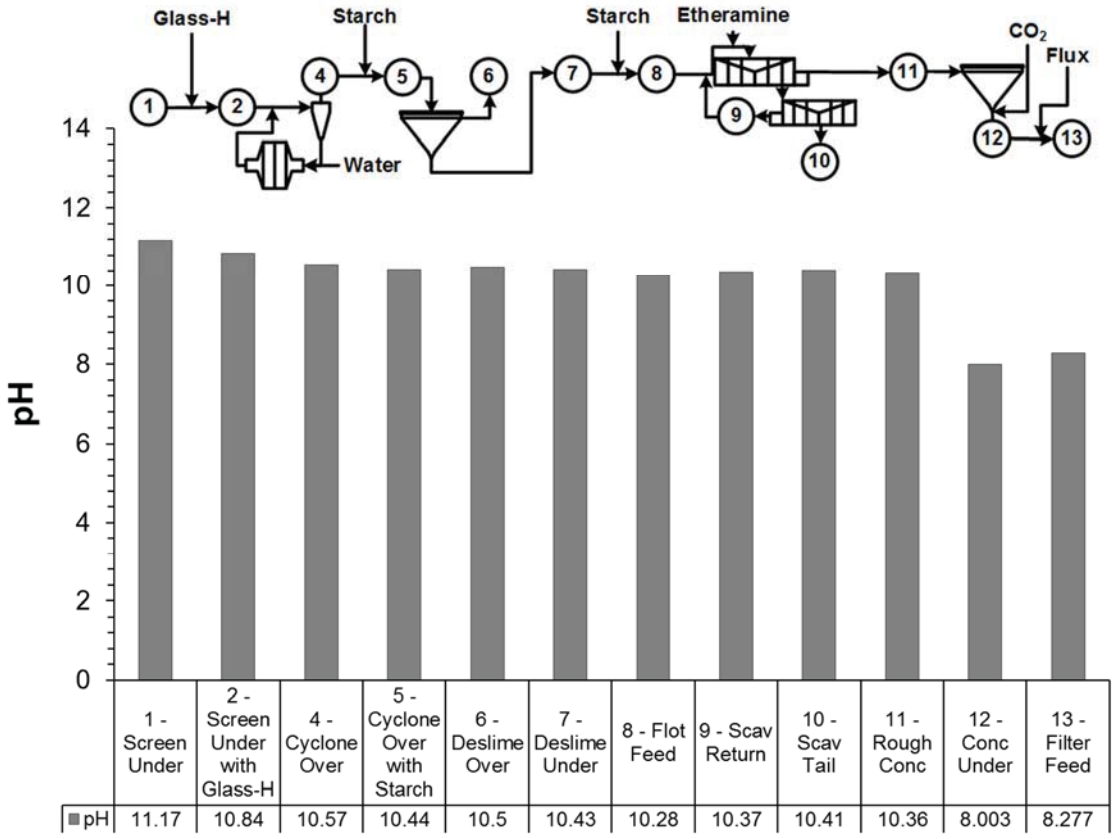

Figure 2.37: pH of each sample by location on November 30th, 2011

2.3.5.3.3 Conductivity

The conductivity throughout the process followed the same trends as in previous sample sets: starts high and decreases throughout until CO_2 and dolomite are added; see Figure 2.38.

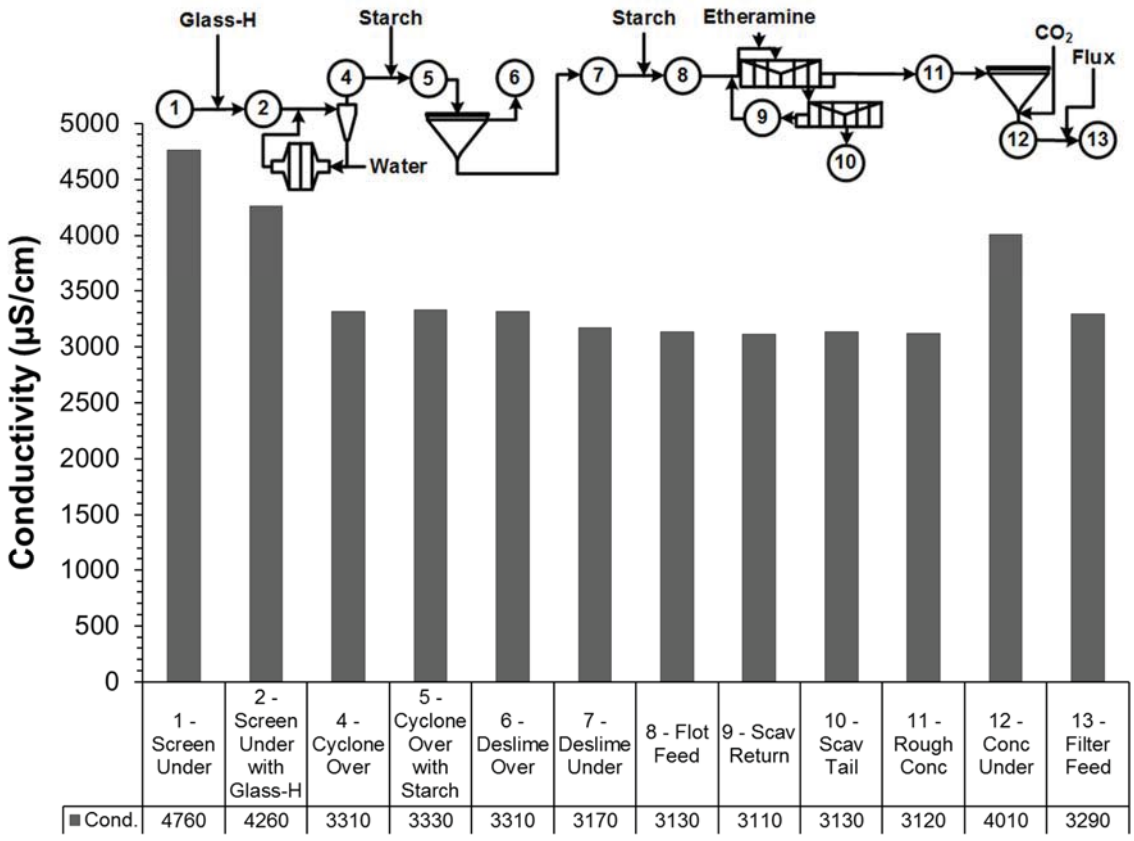

Figure 2.38: Conductivity of each sample by location on November 30th, 2011

2.3.5.3.4 Sodium and Chloride

The sodium and chloride content of the process water, shown in Figure 2.39, were measured using ion selective electrodes (ISEs). The chloride concentration remained fairly steady between 375 and 475 ppm throughout. The sodium concentration throughout the plant followed very closely with the conductivity of the process water, varying

between 750 and 1050 ppm. In this sample set, the conductivity correlated linearly very well with the sodium concentration of each sample with a correlation coefficient of 0.986 as shown in Figure 2.40. This is a very good finding because sodium ions decrease the magnitude of zeta potential as shown in Figure 2.21.

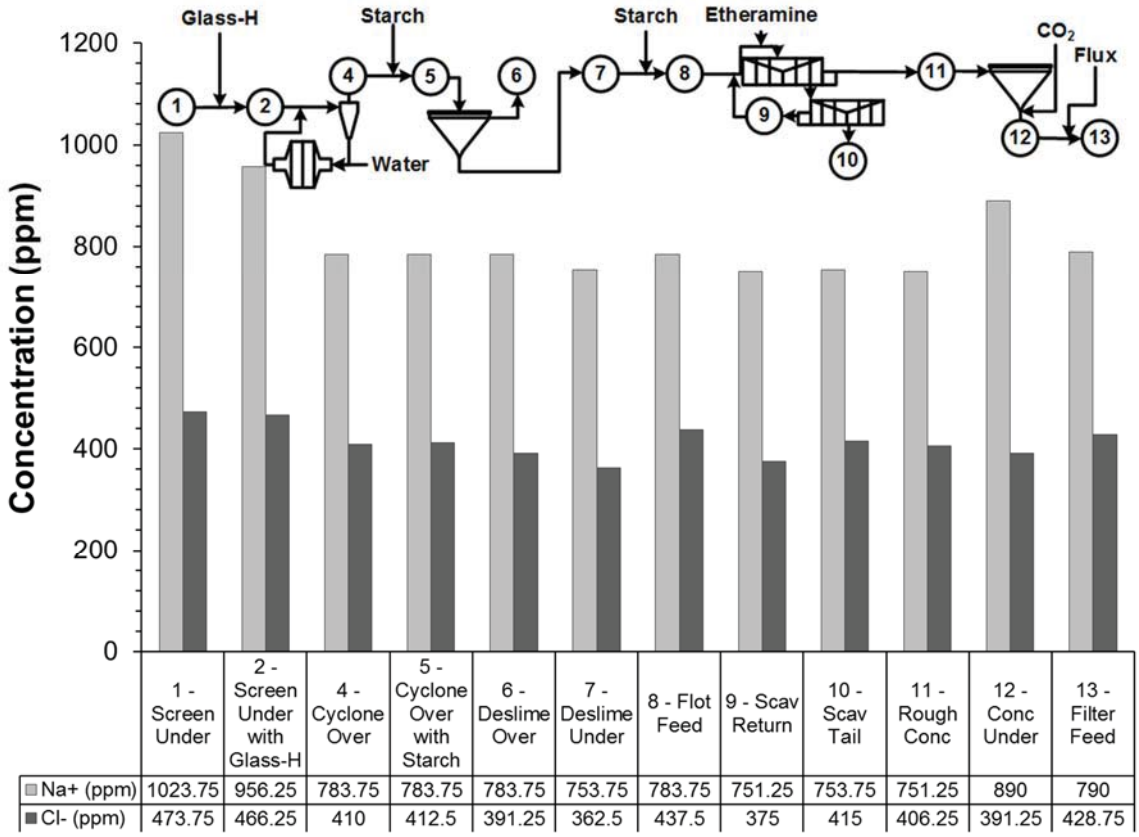

	1 - Screen Under	2 - Screen Under with Glass-H	4 - Cyclone Over	5 - Cyclone Over with Starch	6 - Deslime Over	7 - Deslime Under	8 - Flot Feed	9 - Scav Return	10 - Scav Tail	11 - Rough Conc	12 - Conc Under	13 - Filter Feed
Na+ (ppm)	1023.75	956.25	783.75	783.75	783.75	753.75	783.75	751.25	753.75	751.25	890	790
Cl- (ppm)	473.75	466.25	410	412.5	391.25	362.5	437.5	375	415	406.25	391.25	428.75

Figure 2.39: Sodium and chloride concentrations of each sample by location on November 30th, 2011

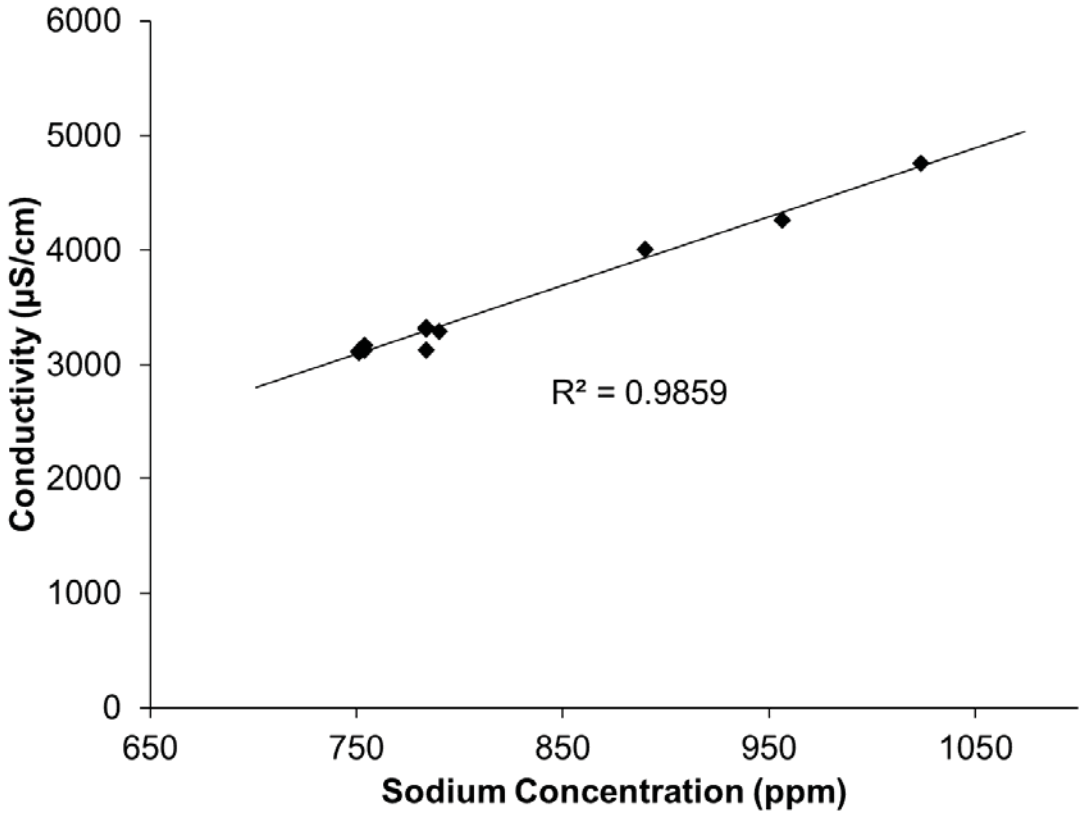

Figure 2.40: Correlation between sodium and conductivity of the November 30th, 2011 sample set

Sodium ions enter the solution via one of five routes. Some sodium is naturally brought in from the ore and re-use water. Sodium is also added to the process from caustic (NaOH), Glass-H ($(NaPO_3)_{21}*Na_2O$), and sodium silicate (Na_2SiO_3).

2.3.5.3.5 Calcium, Magnesium and Water Hardness

Common alkaline earth metals (Magnesium and Calcium) are the primary contributors to water hardness. Control of Mg^{2+} and Ca^{2+} ions is essential to maintaining high iron recoveries in deslime and flotation. Previous studies and ongoing research have shown a strong link between the concentrations of calcium, magnesium, water hardness, zeta

potential and iron recovery. The calcium, magnesium, and total hardness concentrations of the each location in the process are shown in Figure 2.41.

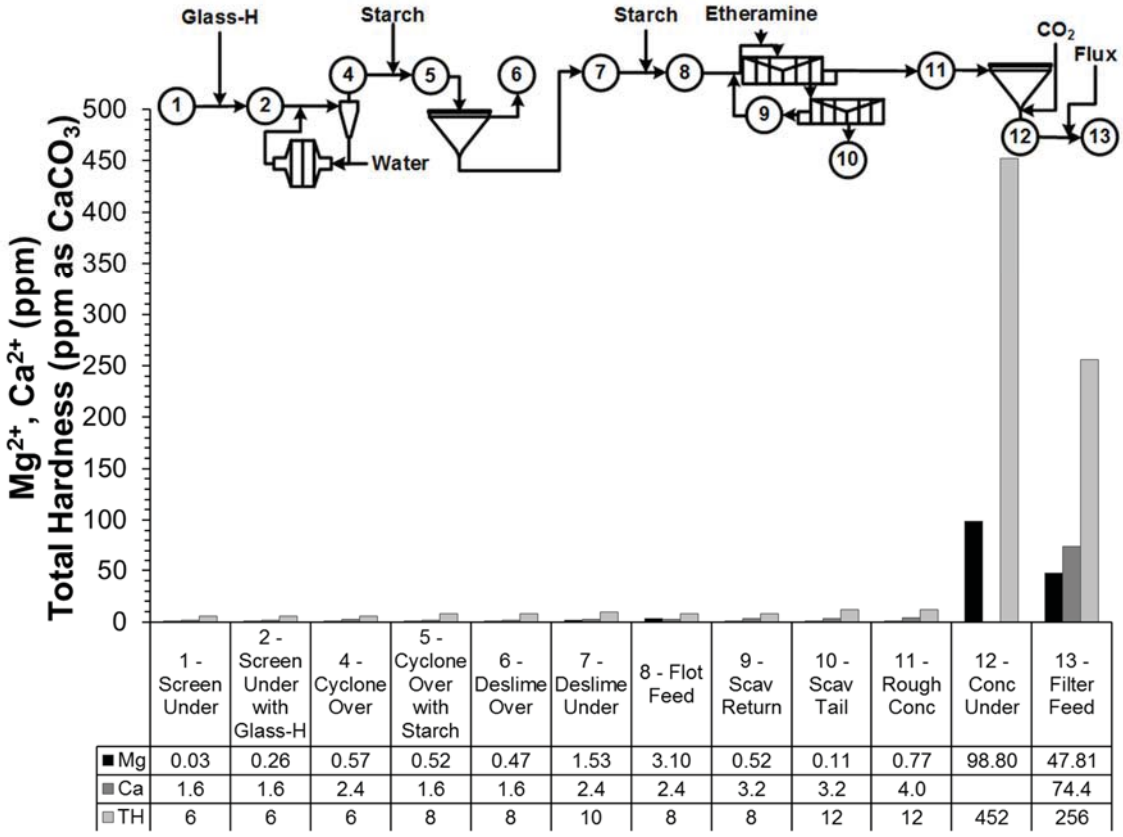

Figure 2.41: Magnesium, calcium and total hardness concentrations of each sample by location on November 30th, 2011

This sample set had very low concentrations of calcium and magnesium content compared to previous sample sets. These values were accompanied by the lowest total iron recoveries so far at 59.1% (7:00 AM) - 59.2% (1:00 PM); see Table 2.5. Soon after the calcium concentrations were determined (~ 10 AM), the Glass-H (dispersant) rate was lowered from 0.06 to 0.03 lb/ton which yielded an immediate improvement in

deslime recovery. The deslime overflow iron content was 16.2% Fe at 7:00 AM and was lowered to 11.1% Fe by 1:00 PM.

The flotation iron rejection increased between these two times. There were several factors affecting this:

1. Overgrinding causing overabundance of fines that are easily rejected by flotation
2. Change in Glass-H rate did not affect 1:00PM mass balance at flotation because of high residence time in pebble mill and deslime

The large concentration of magnesium (1.5 and 3.1) between deslime and flotation caused magnesium to specifically adsorb to surface sites on hematite particles, lowering zeta potential, see Figure 2.21. This high magnesium concentration was most likely due to the low pH (10.3) at the flotation feed.

2.3.5.3.6 Zeta Potential

The zeta potential at process conditions (pH, conductivity) are shown in Figure 2.42. The first noticeable trend was the minimal change in zeta potential with the addition of Glass-H (dispersant). In previous sample sets Glass-H increased the zeta potential more substantially, as seen in Figure 2.31 and Figure 2.36.

It is very apparent that the starch suppressed the surface charge of the hematite particles by comparing samples 4 and 5 (cyclone overflow before and after starch addition) and samples 7 and 8 (flotation feed before and after starch addition). This observation was

consistent in all sample sets with a more pronounced effect at the flotation starch addition. Zeta potential curves of these samples are included in the Appendix A.

All sample sets have shown an increase by 5 – 9 mV in zeta potential upon the addition of CO_2. The addition of flux decreases the zeta potential to ~20 mV. This may cause negative effects on filtration performance.

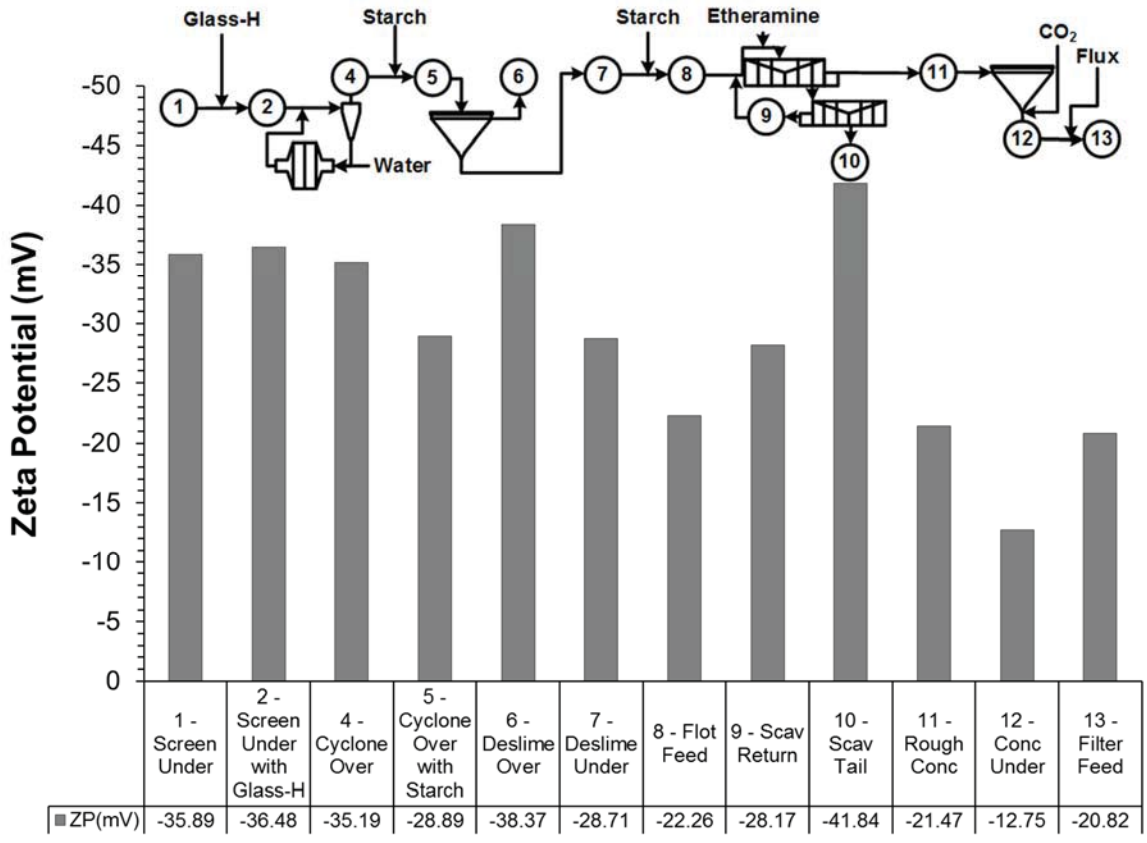

Figure 2.42: Zeta potential of each sample by location on November 30th, 2011

2.3.5.3.7 Process Data

Iron recovery, metallurgical balance, and reagent addition rates can be found in Table 2.5. The total wt% recovery on section 7-9 was 32.1% and 31.8% at 7:00 AM and 1:00

PM, respectively, with a target recovery of 42.5 wt%. This was significantly lower than on any previous sample dates due to high weight rejection in the deslime thickener. This high rejection is caused by abundance of fines due to overgrinding and lower than normal water hardness. Flotation had a high iron rejection due to the lower than normal pH and high magnesium content in the float feed. Overgrinding on section 7-9 caused an 81.7 % and 86.3% passing at 500 mesh at 7:00 AM and 1:00 PM, respectively. This was higher than any other section.

Table 2.5: Process data for November 30th, 2011

Date: 11/30/11 Time: 7:00 AM												
Section 7-9									Tilden 2 Average			
	%Fe	%Wt.	Fe Units	Fe Dist.	pH Lab	Glass-H Rate	Total Recovery Weight	Iron Unit		%Fe	%Wt.	Caustic Rate
CYC O/F	34	100	34.0	100.0	11.0	lbs/ton			CYC O/F	34	100	Crude lbs/ton
DTU	46.8	58.2	27.2	80.1	pH Plant	0.06	32.1	59.1	DTU	46.8	58.2	1.87
DTO	16.2	41.8	6.8	19.9	11.0				DTO	16.2	41.8	Conc lbs/ton
									Flot Tail	27.3	26.3	5.27
					%Passing at 500 Mesh		81.7		Flot Conc	62.7	32.1	
Date: 11/30/11 Time: 1:00 PM												
Section 7-9									Tilden 2 Average			
	%Fe	%Wt.	Fe Units	Fe Dist.	pH Lab	Glass-H Rate	Total Recovery Weight	Iron Unit		%Fe	%Wt.	Caustic Rate
CYC O/F	33.6	100	33.6	100.0	10.9	lbs/ton			CYC O/F	34	100	Crude lbs/ton
DTU	47	62.7	29.5	87.7	pH Plant	0.03	31.8	59.2	DTU	46.1	66.1	1.96
DTO	11.1	37.3	4.1	12.3	11.0				DTO	10.4	33.9	Conc lbs/ton
									Flot Tail	30.9	34.4	5.45
					%Passing at 500 Mesh		86.3		Flot Conc	62.7	31.7	

2.3.5.3.8 Elemental Analysis

The concentration of calcium, magnesium, and iron (Fe^{2+} and Fe^{3+}) was measured by acid leaching followed by atomic absorption spectroscopy (ASTM, 2006); see Figure 2.43 and Figure 2.44. The calcium and magnesium content of the solids were very similar to each other throughout the process signifying some dolomite present in the ore. Upon flux addition, the concentration of calcium rose more than magnesium suggesting the use of a

calcite-rich flux. Some notable trends include calcite/dolomite rejection during deslime followed by a high level calcium/magnesium concentration at the flotation feed. The source of this higher than expected concentration of calcium and magnesium prior to flotation was most likely due to the merging of section 7-9 and section 10-12 in the float feed distributor. Section 10-12 may have contained more calcium and magnesium than section 7-9.

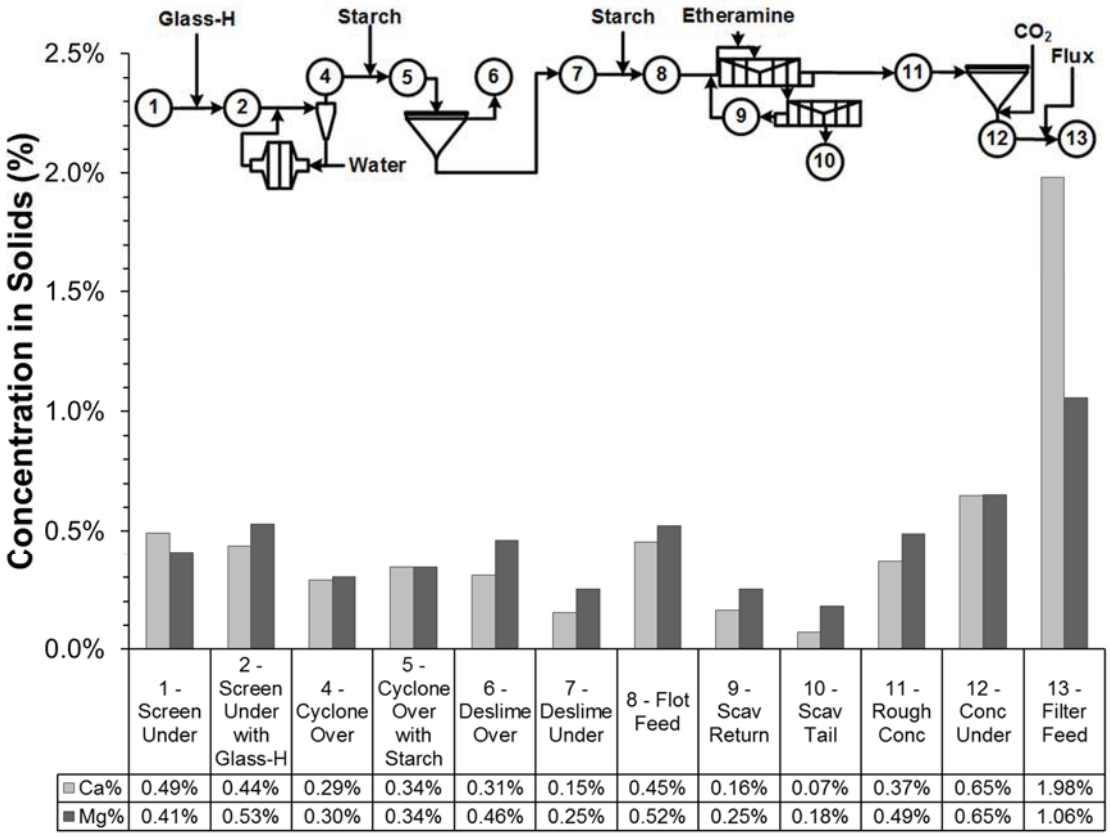

	1 - Screen Under	2 - Screen Under with Glass-H	4 - Cyclone Over	5 - Cyclone Over with Starch	6 - Deslime Over	7 - Deslime Under	8 - Flot Feed	9 - Scav Return	10 - Scav Tail	11 - Rough Conc	12 - Conc Under	13 - Filter Feed
Ca%	0.49%	0.44%	0.29%	0.34%	0.31%	0.15%	0.45%	0.16%	0.07%	0.37%	0.65%	1.98%
Mg%	0.41%	0.53%	0.30%	0.34%	0.46%	0.25%	0.52%	0.25%	0.18%	0.49%	0.65%	1.06%

Figure 2.43: Calcium and magnesium content of the solids of each sample by location on November 30th, 2011

The iron content and acid insoluble material content of the slurry solids are shown in Figure 2.44. Acid insolubles are typically silica and any phosphate minerals that are not

dissolved in hot concentrated hydrochloric acid. As expected, there was a large acid insolubles rejection during deslime and flotation where silica and other gangue minerals were removed. The iron was concentrated by both the deslime and flotation, however, there were high iron losses in the tailings (14.85% in deslime and 31.6% in flotation). The inconsistency between the deslime underflow and the flotation feed was caused by the merging of process sections 10-12 with sections 7-9 at that point. There seems to have been a higher silica concentration in the other sections.

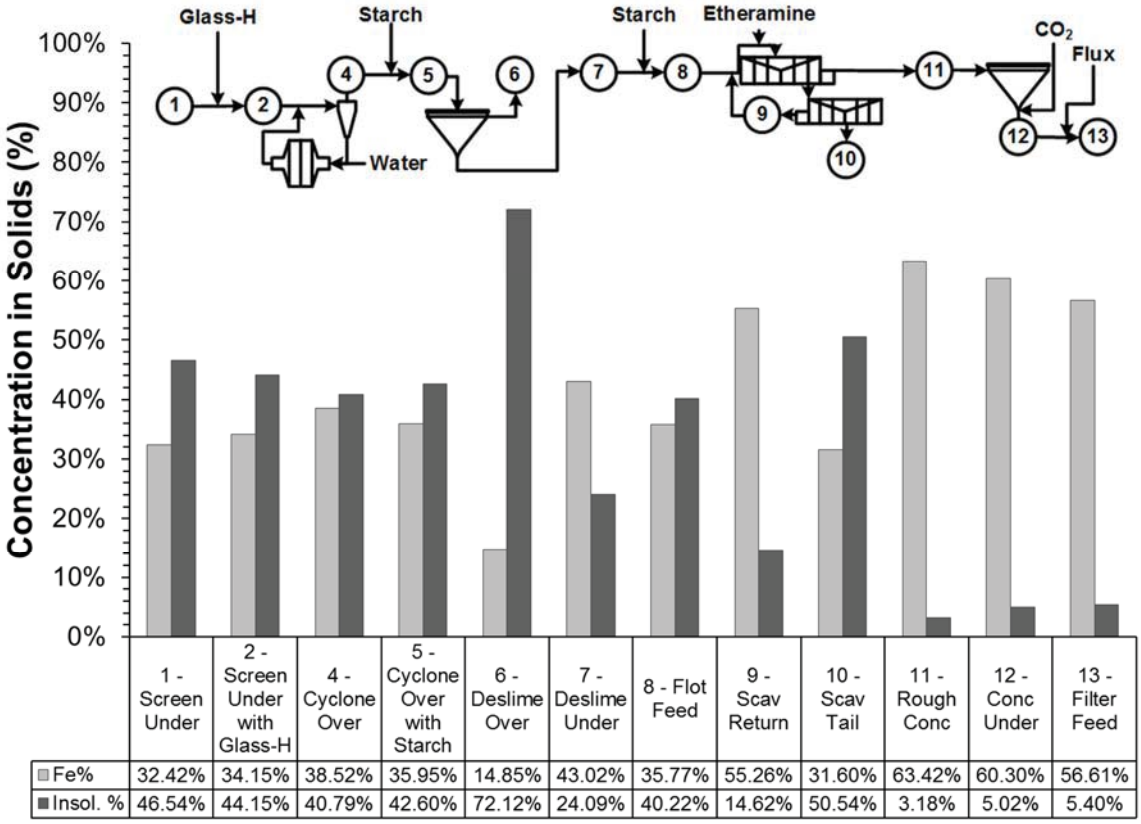

	1 - Screen Under	2 - Screen Under with Glass-H	4 - Cyclone Over	5 - Cyclone Over with Starch	6 - Deslime Over	7 - Deslime Under	8 - Flot Feed	9 - Scav Return	10 - Scav Tail	11 - Rough Conc	12 - Conc Under	13 - Filter Feed
Fe%	32.42%	34.15%	38.52%	35.95%	14.85%	43.02%	35.77%	55.26%	31.60%	63.42%	60.30%	56.61%
Insol. %	46.54%	44.15%	40.79%	42.60%	72.12%	24.09%	40.22%	14.62%	50.54%	3.18%	5.02%	5.40%

Figure 2.44: Iron and acid insolubles content of the solids of each sample by location on November 30th, 2011

2.3.5.3.9 Conclusions

This 'emergency' sampling was performed because of low iron recoveries; especially on sections 7-9. Several process conditions were noticeably different on this day:

1. Flotation and deslime had a very high weight rejection with high iron concentration in tailings
2. Water hardness values were extraordinarily low throughout the plant (<10 ppm)
3. Flotation overflow appeared stagnant in some areas
4. Crushers were shut down for maintenance
5. Plant flow-rates were turned down
6. Low flow rates caused inadequate distribution of slurry between roughers

Overgrinding due to inadequate crushing of critical size material yielded an abundance of fine material that contributed to the high weight rejection in both deslime and flotation. Low water hardness at deslime caused over-dispersion of the abundant fines and contributed to the high weight rejection in the deslime thickener.

The pH of the process water was initially ~11.17 at the screen underflow. The pH decreased progressively until it reached a low point of about 10.3 at the flotation feed. This caused an overabundance of dissolved magnesium possibly causing poor starch selectivity, poor etheramine collector selectivity, and decreased zeta potential. The combination of these three factors led to the high iron loss in the flotation tailings.

The conductivity of the process water was found to be directly proportional to the sodium concentration in this sample set. This important finding will allow for online

determination of monovalent cations based on conductivity measurements from the new online conductivity meter that became operational in early April, 2012.

This dataset also solidified theories made from the May 5th and July 13th datasets. The following are the conclusions drawn from this sample set and from the project thus far:

1. Starch did noticeably and reproducibly suppress the surface charge of hematite in both deslime and flotation
2. The effect of the starch was consistently more prominent in flotation
3. Starch did not significantly change the water hardness
4. The addition of CO_2 had a significant effect on the pH, conductivity, water hardness, and zeta potential. These additions resulted in a
    4.1. Decrease in pH
    4.2. Increase in conductivity
    4.3. Increase in water hardness
    4.4. Increase in zeta potential

2.3.5.4 Caustic Adjustment Study – April 2nd, 2012

2.3.5.4.1 Introduction

The goal of this work is to determine what water chemistry factors play a significant role in the magnitude of the zeta potential and if there is an method for monitoring zeta potential (or inferring it from other measurements) at any point within the plant. The April 2nd, 2012 sample sets were taken to determine the effects of a pH change on the water chemistry, zeta potential and iron recovery. The first sample set was gathered

between 8 AM and 12 PM on 4/2/2012 when the pH was 10.9 with a caustic rate of 1.48 lb/ton (crude). After this sample set was taken, the caustic rate was increased to 2.03 lb/ton and the process was given time to allow this change to take effect. The second sample set was taken between 8 PM and 12 PM on 4/2/2012 when the pH had reached 11.0.

There were several observations on April 2nd that also had an effect on process:

1. Very low water hardness
2. Low glass-H rates compared to previous sample sets (0.04 – 0.07 lb/ton)
3. The plant pH meter was giving pH values ~ 0.4 pH units higher than the calibrated laboratory pH meter

2.3.5.4.2 Process Data

The process data for sections 7-9 on April 2nd, 2012 is shown in Table 2.6. The process had been running consistently well for several days prior to these sample sets. At the start of the first sample set, the pH was at 10.9 with a fairly low caustic rate and Glass-H (sodium henicosapolyphosphate) rate (1.48 and 0.04 lbs/ton, respectively). The weight % recovery was average compared to other samples (39.0%) with a higher than average iron recovery (72.3%). After the first sample set, the caustic rate was increased to 2.03 lbs/ton causing a pH increase up to 11.0. This caused the deslime thickener to have a lower weight rejection. The lower weight rejection was accompanied by a smaller amount of iron lost in the deslime overflow (Fe distribution dropped from 11.2 down to 7.0 in the DTO). Though there was less iron lost in deslime, the grade of the ore at the deslime

underflow was lower forcing more of the separation requirement onto flotation. Overall, the increase in caustic rate led to less iron loss in deslime, more iron loss in flotation, and a lower overall recovery.

Table 2.6: Process data for sections 7-9 on April 2nd, 2012

Date: 4/2/12 Time: 7:00 AM												
Section 7-9									Tilden 2 Average			
	%Fe	%Wt.	Fe Units	Fe Dist.	pH Lab	Glass-H Rate	Total Recovery Weight	Iron Unit		%Fe	%Wt.	Caustic Rate
CYC O/F	34.4	100	34.3	100.0	10.8	lbs/ton			CYC O/F	34.9	100	Crude lbs/ton
DTU	48.1	63.3	30.4	88.8	pH Plant	0.04	39	72.3	DTU	48	63.4	1.48
DTO	10.5	36.7	3.9	11.2	10.9				DTO	12.1	36.6	Conc lbs/ton
									Flot Tail	23.2	24.5	3.86
					%Passing at 500 Mesh		83.5		Flot Conc	63.6	38.9	
Date: 4/2/12 Time: 7:00 PM												
Section 7-9									Tilden 2 Average			
	%Fe	%Wt.	Fe Units	Fe Dist.	pH Lab	Glass-H Rate	Total Recovery Weight	Iron Unit		%Fe	%Wt.	Caustic Rate
CYC O/F	34.4	100	34.7	100.0	10.9	lbs/ton			CYC O/F	34.6	100	Crude lbs/ton
DTU	45	69.3	32.3	93.0	pH Plant	0.07	37.4	69.2	DTU	45.4	70.1	2.03
DTO	10.5	30.7	2.4	7.0	11.0				DTO	9.2	29.9	Conc lbs/ton
									Flot Tail	23.1	31.5	5.38
					%Passing at 500 Mesh		82.8		Flot Conc	63.7	38.6	

2.3.5.4.3 pH

The pH of each sample before and after caustic addition is shown in Figure 2.45. As stated earlier, the pH readings taken in the lab were consistently lower than the pH given by the online meter. The pH was consistently higher at every sample location after the addition of caustic except for the concentrate thickener underflow sample. It was unlikely that the change in caustic would have affected the concentrate thickener because of its large residence time. The average increase in pH was 0.18 pH units with the most significant changes seen at the screen underflow.

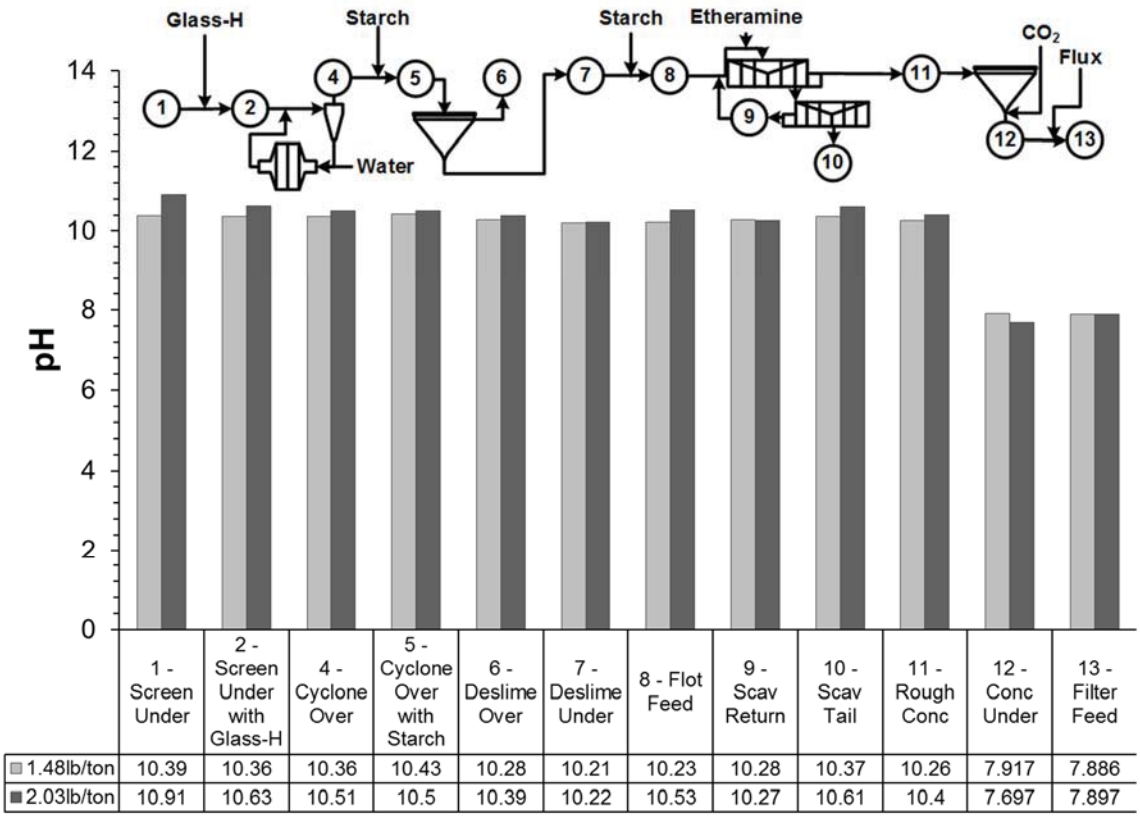

	1 - Screen Under	2 - Screen Under with Glass-H	4 - Cyclone Over	5 - Cyclone Over with Starch	6 - Deslime Over	7 - Deslime Under	8 - Flot Feed	9 - Scav Return	10 - Scav Tail	11 - Rough Conc	12 - Conc Under	13 - Filter Feed
1.48lb/ton	10.39	10.36	10.36	10.43	10.28	10.21	10.23	10.28	10.37	10.26	7.917	7.886
2.03lb/ton	10.91	10.63	10.51	10.5	10.39	10.22	10.53	10.27	10.61	10.4	7.697	7.897

Figure 2.45: pH of each sample before and after caustic addition on April 2nd, 2012

2.3.5.4.4 Conductivity

The conductivity of each sample before and after caustic addition is shown in Figure 2.46. For each sample set, the same decreasing trend that was seen in previous samples occurred throughout the process. At the lower pH, the conductivity started at 2932 µS/cm and stabilized at around 2500 µS/cm. After caustic addition, the initial conductivity was very high at 3692 µS/cm and diminished to around 2600 µS/cm. The addition of caustic increased the overall conductivity by an average of 200 µS/cm with a larger difference seen closer to the screen underflow.

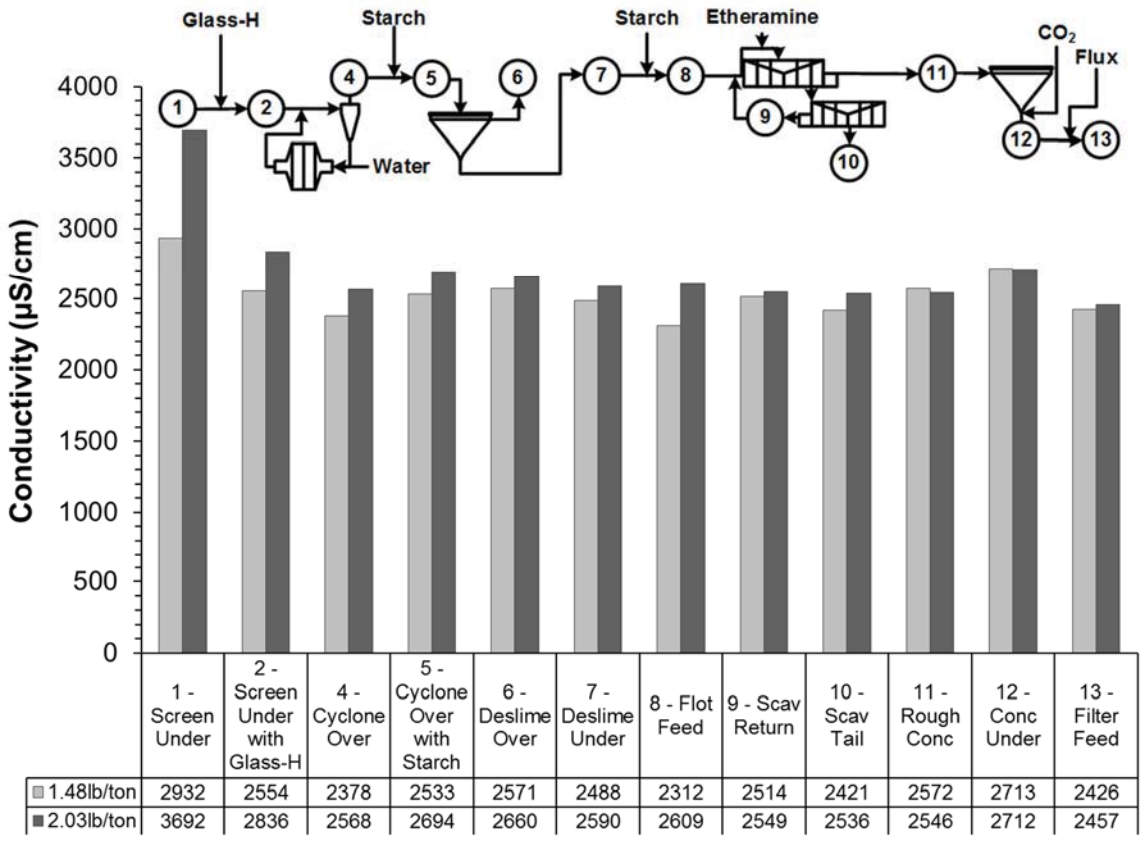

Figure 2.46: Conductivity of each sample before and after caustic addition on April 2nd, 2012

2.3.5.4.5 Sodium and Potassium (monovalent cations)

The sodium concentration before and after the increase in caustic rate are shown in Figure 2.47. Upon increase in caustic rate, the sodium levels immediately increased from 238 to 280 ppm. This was to be expected because caustic (NaOH) will dissociate into sodium and hydroxide ions when dissolved. The sodium concentration did not remain higher at the increased pH however. A possible explanation for this is that the increased pH caused a decrease in the surface potential of the particles in solution causing an

increased attraction of cations to the particle surfaces. This would cause the sodium to decrease as it did.

The overall sodium levels were ~750 ppm lower on April 2nd, 2012 than in the November 30th, 2011 sample set. This could be due to the change in the incoming water supply or due to a limited use of caustic over the winter months. In these sample sets, the conductivity related well to the sodium concentration as seen in the November 30th, sample set; see Figure 2.48. The trend-line was shifted upwards after the addition of caustic suggesting that pH has a large influence on the conductivity as well.

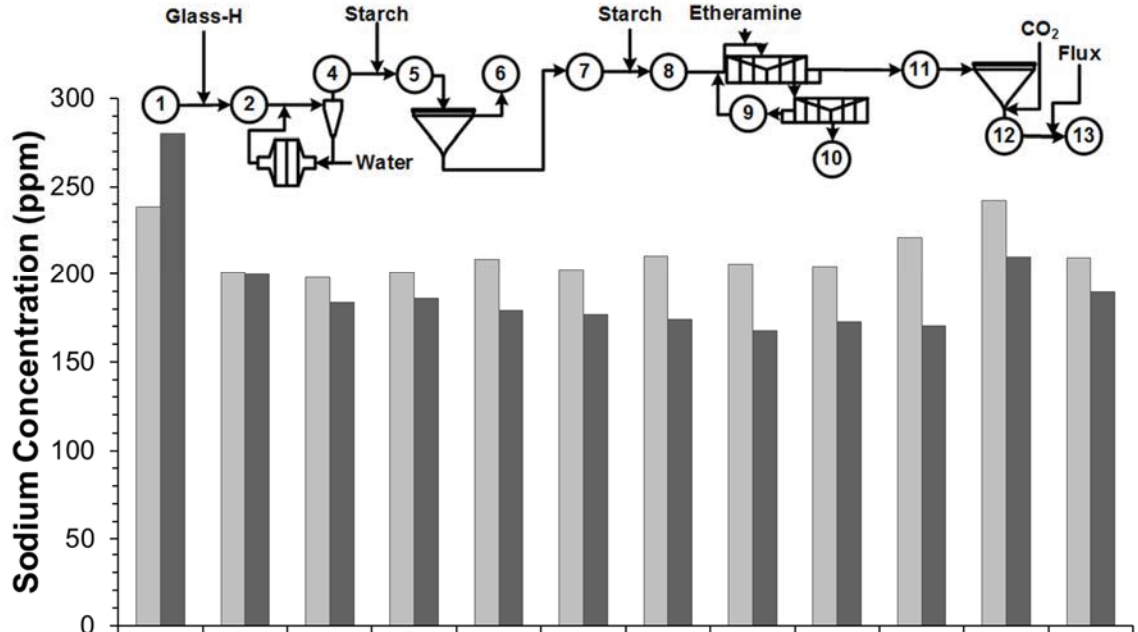

	1 - Screen Under	2 - Screen Under with Glass-H	4 - Cyclone Over	5 - Cyclone Over with Starch	6 - Deslime Over	7 - Deslime Under	8 - Flot Feed	9 - Scav Return	10 - Scav Tail	11 - Rough Conc	12 - Conc Under	13 - Filter Feed
1.48lb/ton	238.53	200.65	198.2	200.61	208.73	202.43	210.57	205.76	204.43	220.81	242.33	209.5
2.03lb/ton	280.06	199.91	183.65	185.86	178.95	176.7	174.34	167.58	172.76	170.4	209.94	189.66

Figure 2.47: Sodium concentration of each sample before and after caustic addition on April 2nd, 2012

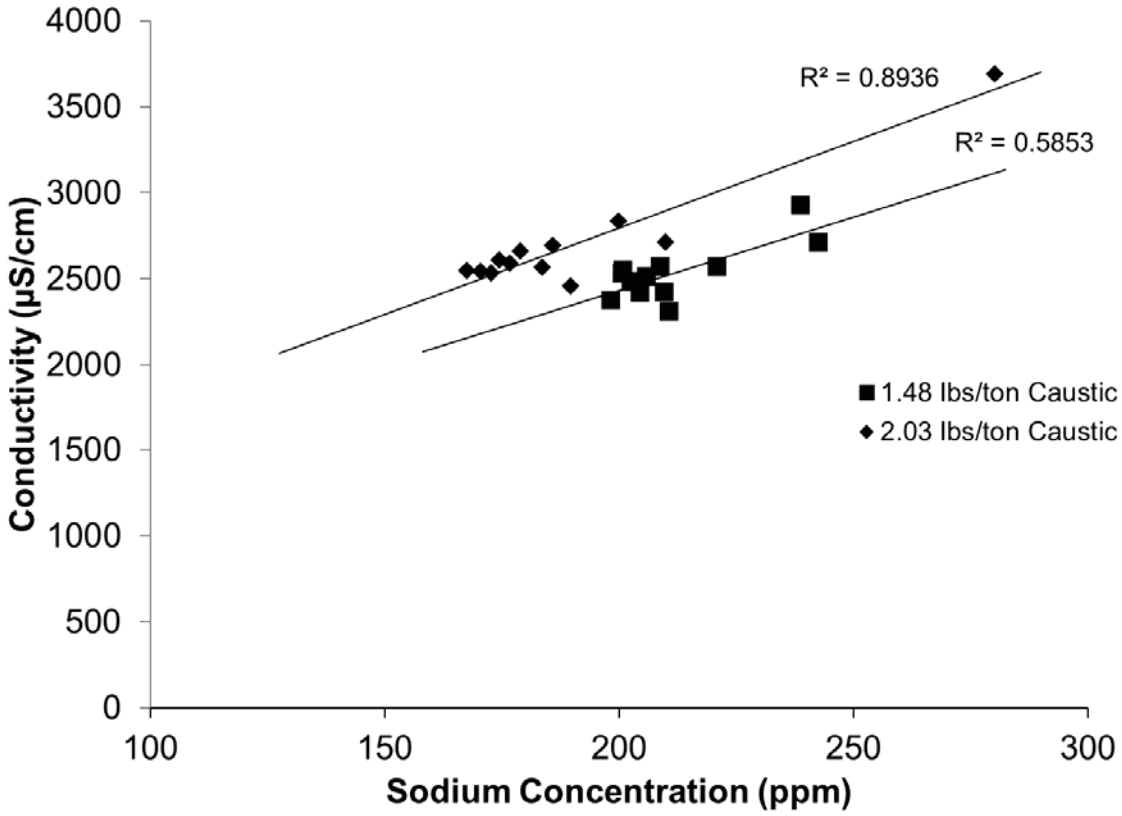

Figure 2.48: Correlation between sodium and conductivity of the April 2nd, 2012 sample sets

The potassium levels were measured in this sample set primarily to compare to a previous water chemistry study in which samples were taken at these addition points and sent to a certified laboratory for analysis (Haselhuhn et al., 2012a). The potassium concentrations before and after the caustic addition rate increase are shown in Figure 2.49. Upon the addition of caustic, the potassium levels decreased. This supports the theory proposed above regarding the decrease in sodium levels due to surface chemistry.

In the previous study, the potassium ranged from 10 to 15 ppm until the concentrate thickener, where the potassium concentration increased to 20 ppm (Haselhuhn et al.,

2012a). This same trend was found with both of the April 2nd sample sets; however, the overall potassium levels were slightly lower.

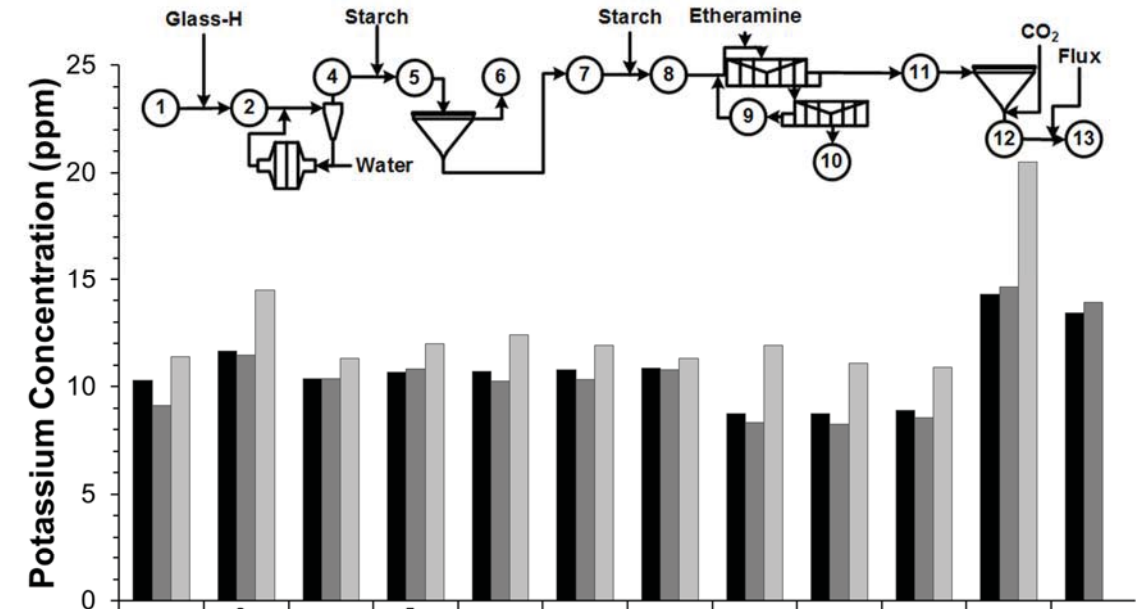

	1 - Screen Under	2 - Screen Under with Glass-H	4 - Cyclone Over	5 - Cyclone Over with Starch	6 - Deslime Over	7 - Deslime Under	8 - Flot Feed	9 - Scav Return	10 - Scav Tail	11 - Rough Conc	12 - Conc Under	13 - Filter Feed
1.48lb/ton	10.31	11.65	10.37	10.67	10.7	10.78	10.87	8.73	8.74	8.88	14.28	13.42
2.03lb/ton	9.13	11.48	10.36	10.81	10.27	10.35	10.78	8.34	8.27	8.55	14.62	13.91
Oct. 2010	11.4	14.5	11.3	12	12.4	11.9	11.3	11.9	11.1	10.9	20.5	

Figure 2.49: Potassium concentration of each sample before and after caustic addition on April 2nd, 2012

2.3.5.4.6 Calcium, Magnesium and Water Hardness

Common alkaline earth metals (Magnesium and Calcium) are the primary contributors to water hardness. Control of Mg^{2+} and Ca^{2+} ions is essential to maintaining high iron recoveries in deslime and flotation. Previous studies and ongoing research have shown a strong link between the concentrations of calcium, magnesium, water hardness, zeta

potential and iron recovery. The calcium, magnesium, and total hardness concentrations of the each location in the process are shown in Figure 2.50, 2.51, and 2.52.

On April 2nd, it was requested that the Glass-H rate remain constant throughout the day; however, it was increased from 0.04 to 0.07 lbs/ton between 7 AM and 7 PM. The increased caustic rate and Glass-H rate consistently lowered the calcium, magnesium and total water hardness of the sample, but it cannot be inferred whether this loss in calcium was due to the additional caustic or Glass-H.

The overall calcium concentration on April 2nd, 2012 was very similar throughout the process compared to the November 30th, sample set; however, the magnesium concentration on April 2nd was nearly twice that of November 30th. The total hardness did not reflect the increased magnesium concentration suggesting that total hardness is not a good indicator of magnesium concentration.

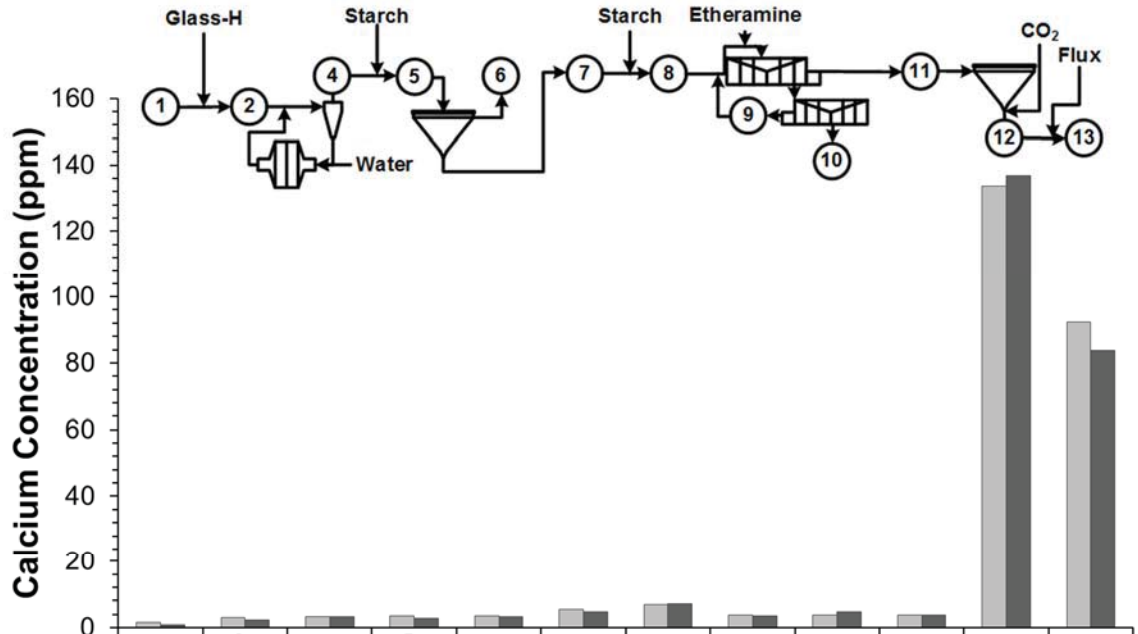

	1 - Screen Under	2 - Screen Under with Glass-H	4 - Cyclone Over	5 - Cyclone Over with Starch	6 - Deslime Over	7 - Deslime Under	8 - Flot Feed	9 - Scav Return	10 - Scav Tail	11 - Rough Conc	12 - Conc Under	13 - Filter Feed
1.48lb/ton	1.51	3.11	3.25	3.64	3.54	5.46	7	3.84	3.76	3.82	133.75	92.25
2.03lb/ton	0.83	2.42	3.18	2.85	3.34	4.8	7.28	3.65	4.81	3.75	136.75	83.75

Figure 2.50: Calcium concentration of each sample before and after caustic addition on April 2nd, 2012

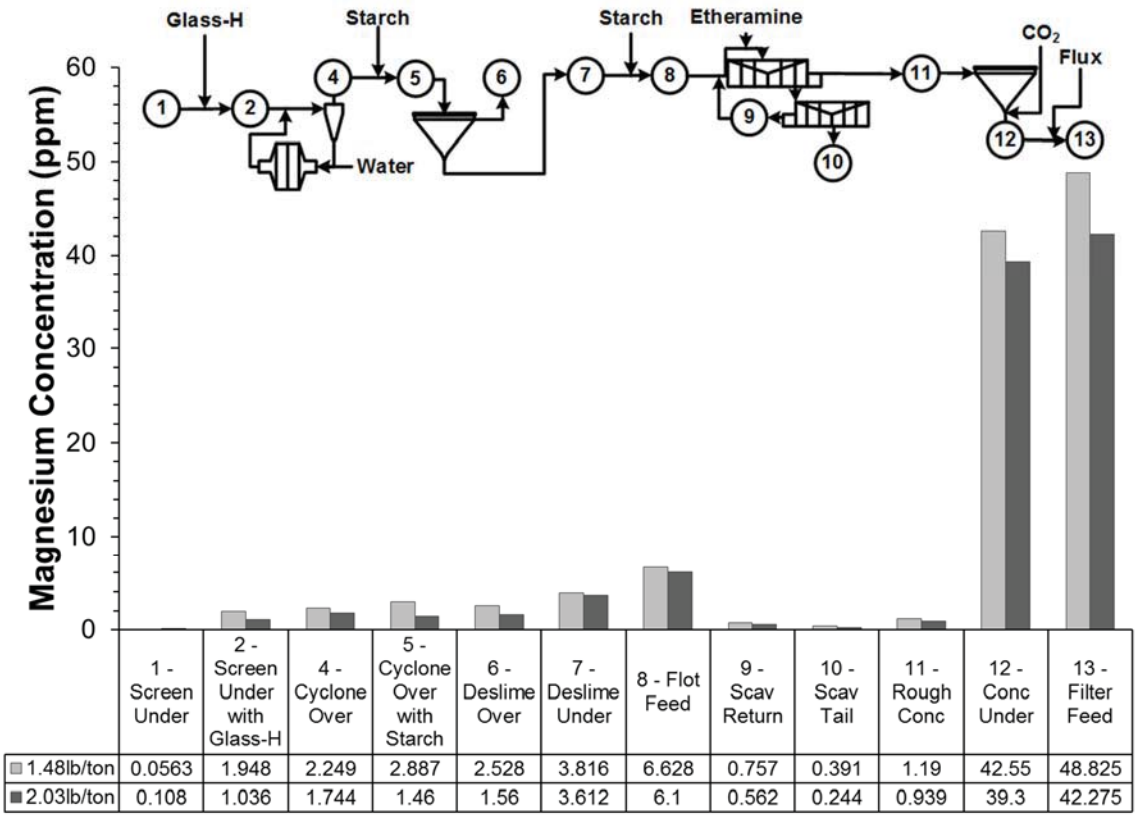

	1 - Screen Under	2 - Screen Under with Glass-H	4 - Cyclone Over	5 - Cyclone Over with Starch	6 - Deslime Over	7 - Deslime Under	8 - Flot Feed	9 - Scav Return	10 - Scav Tail	11 - Rough Conc	12 - Conc Under	13 - Filter Feed
1.48lb/ton	0.0563	1.948	2.249	2.887	2.528	3.816	6.628	0.757	0.391	1.19	42.55	48.825
2.03lb/ton	0.108	1.036	1.744	1.46	1.56	3.612	6.1	0.562	0.244	0.939	39.3	42.275

Figure 2.51: Magnesium concentration of each sample before and after caustic addition on April 2nd, 2012

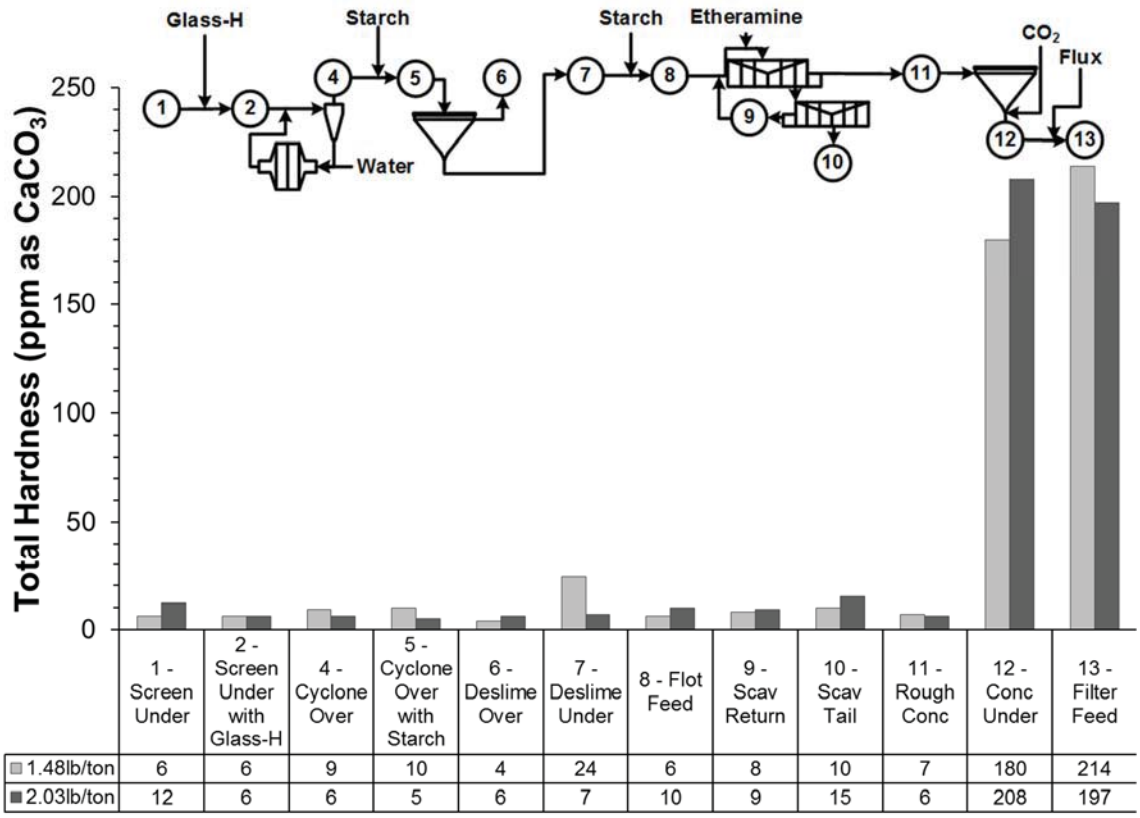

	1 - Screen Under	2 - Screen Under with Glass-H	4 - Cyclone Over	5 - Cyclone Over with Starch	6 - Deslime Over	7 - Deslime Under	8 - Flot Feed	9 - Scav Return	10 - Scav Tail	11 - Rough Conc	12 - Conc Under	13 - Filter Feed
1.48lb/ton	6	6	9	10	4	24	6	8	10	7	180	214
2.03lb/ton	12	6	6	5	6	7	10	9	15	6	208	197

Figure 2.52: Total Hardness of each sample before and after caustic addition on April 2nd, 2012

2.3.5.4.7 Soluble Iron

Soluble iron was measured to compare with trends found in a previous study performed by Haselhuhn et al. (2012a). Soluble iron, in alkaline conditions, is mostly in the form of $Fe(OH)_4^-$ as shown in Figure 2.23 and is a contributor to water hardness when measured by the EDTA titration method. The soluble iron concentrations of samples before and after the increased caustic addition rate are shown in Figure 2.53. The increase in caustic rate caused an increase in soluble iron concentration throughout the plant.

A previous study in October, 2010 performed by Haselhuhn et al. (2012a) showed a progressive increase in soluble iron concentration ending at the flotation feed sample. This trend was observed again in the April 2nd, 2012 samples except the end of the trend occurred after the flotation feed sample. This difference was due to a change in sampling location between studies. The October, 2010 flotation feed sample was taken from the rougher feed box where etheramine was being added, whereas the April 2nd, 2012 flotation feed sample was taken from the output of the flotation feed distributor where amine had not been added. This observation proved the hypothesis proposed during the October 2010 study stating that the etheramine caused the reduction in soluble iron concentration.

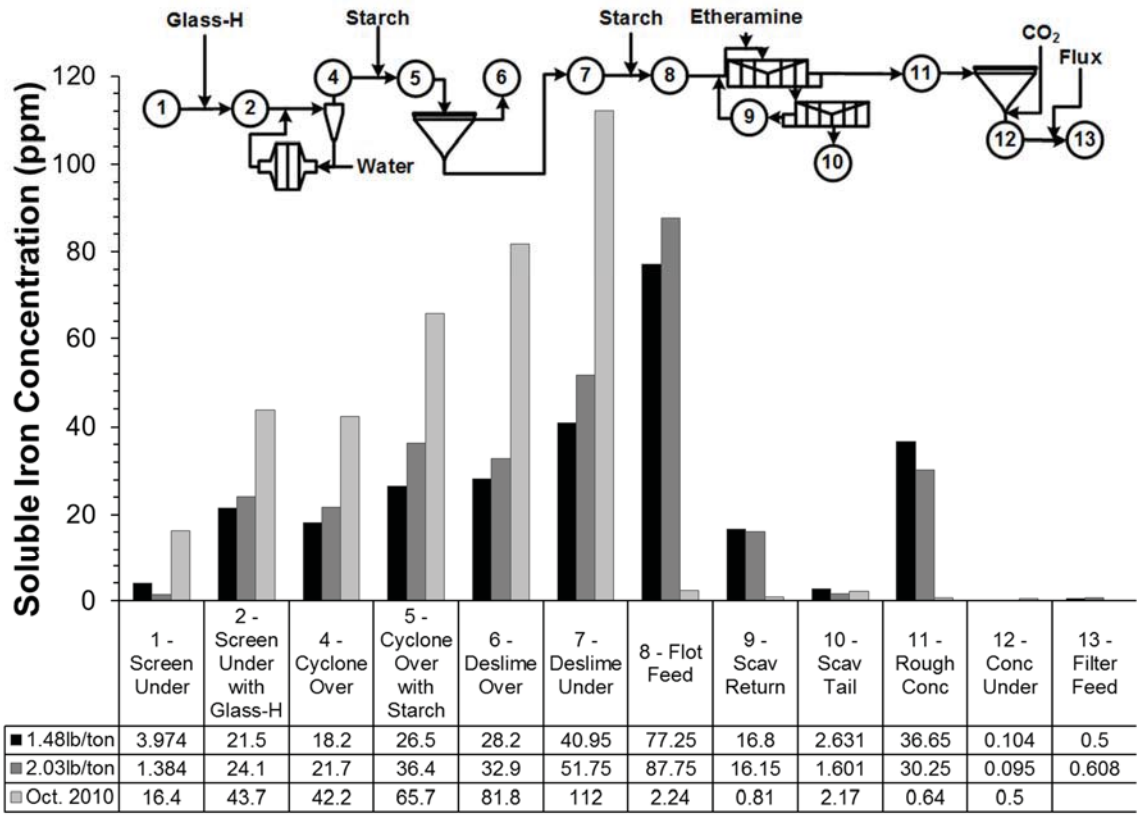

	1 - Screen Under	2 - Screen Under with Glass-H	4 - Cyclone Over	5 - Cyclone Over with Starch	6 - Deslime Over	7 - Deslime Under	8 - Flot Feed	9 - Scav Return	10 - Scav Tail	11 - Rough Conc	12 - Conc Under	13 - Filter Feed
1.48lb/ton	3.974	21.5	18.2	26.5	28.2	40.95	77.25	16.8	2.631	36.65	0.104	0.5
2.03lb/ton	1.384	24.1	21.7	36.4	32.9	51.75	87.75	16.15	1.601	30.25	0.095	0.608
Oct. 2010	16.4	43.7	42.2	65.7	81.8	112	2.24	0.81	2.17	0.64	0.5	

Figure 2.53: Soluble iron concentration of each sample before and after caustic addition on April 2nd, 2012

2.3.5.4.8 Chloride and Nitrate (monovalent anions)

The chloride and nitrate concentrations before and after the increase in caustic addition rate are shown in Figure 2.54 and Figure 2.55. The chloride concentration remained between 220 and 320 ppm throughout the process and the change in caustic addition rate seemed to have little effect on their respective concentrations. The deslime underflow sample showed a significant decrease in chloride concentration for an unknown reason.

The nitrate concentration remained very low until the addition of recycled flux concentrate and CO_2. The nitrate concentration increased substantially when any flux was

added to the process making it apparent that there were small amounts nitrate salts within the flux.

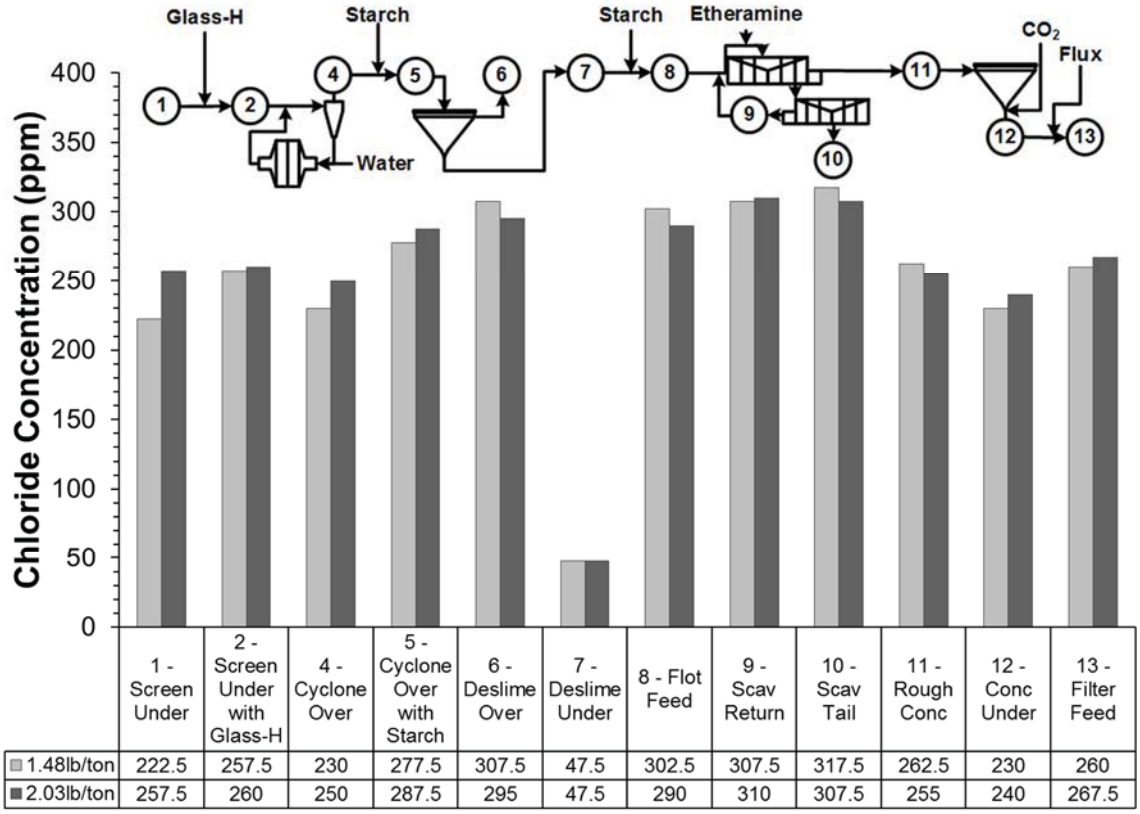

	1 - Screen Under	2 - Screen Under with Glass-H	4 - Cyclone Over	5 - Cyclone Over with Starch	6 - Deslime Over	7 - Deslime Under	8 - Flot Feed	9 - Scav Return	10 - Scav Tail	11 - Rough Conc	12 - Conc Under	13 - Filter Feed
1.48lb/ton	222.5	257.5	230	277.5	307.5	47.5	302.5	307.5	317.5	262.5	230	260
2.03lb/ton	257.5	260	250	287.5	295	47.5	290	310	307.5	255	240	267.5

Figure 2.54: Chloride concentration of each sample before and after caustic addition on April 2nd, 2012

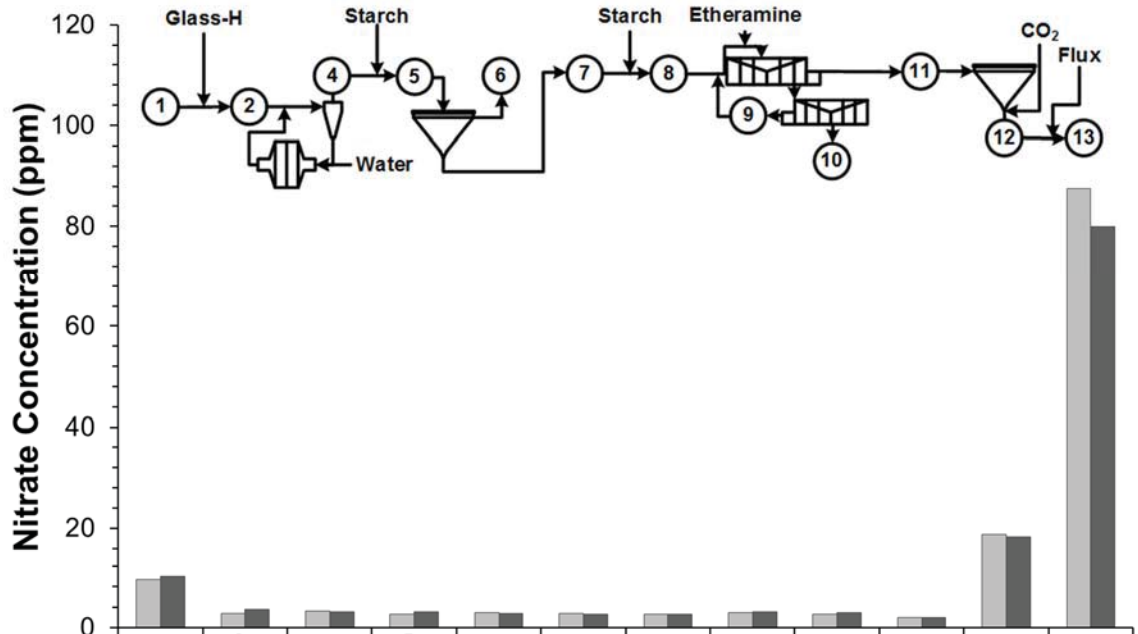

	1 - Screen Under	2 - Screen Under with Glass-H	4 - Cyclone Over	5 - Cyclone Over with Starch	6 - Deslime Over	7 - Deslime Under	8 - Flot Feed	9 - Scav Return	10 - Scav Tail	11 - Rough Conc	12 - Conc Under	13 - Filter Feed
1.48lb/ton	9.4	2.8	3.3	2.7	3	2.8	2.7	2.9	2.7	2	18.7	87.5
2.03lb/ton	10	3.6	3.1	3.2	2.8	2.7	2.7	3.2	3	2	18.2	80

Figure 2.55: Nitrate concentration of each sample before and after caustic addition on April 2nd, 2012

2.3.5.4.9 Carbonates

The total carbonate concentration before and after the increase in caustic addition rate is shown in Figure 2.56. The carbonate concentrations measured included both carbonate (CO_3^{2-}) and bicarbonate (HCO_3^-) forms. Carbonate concentration is an extremely important factor because carbonate ions in solution tend to precipitate with metal cations such as calcium and magnesium. As shown, the carbonate concentration remained fairly stable until the addition of CO_2. CO_2 addition, as expected, increased the carbonate

concentration drastically. The change in caustic addition rate seemed to have very little effect on the carbonate concentration.

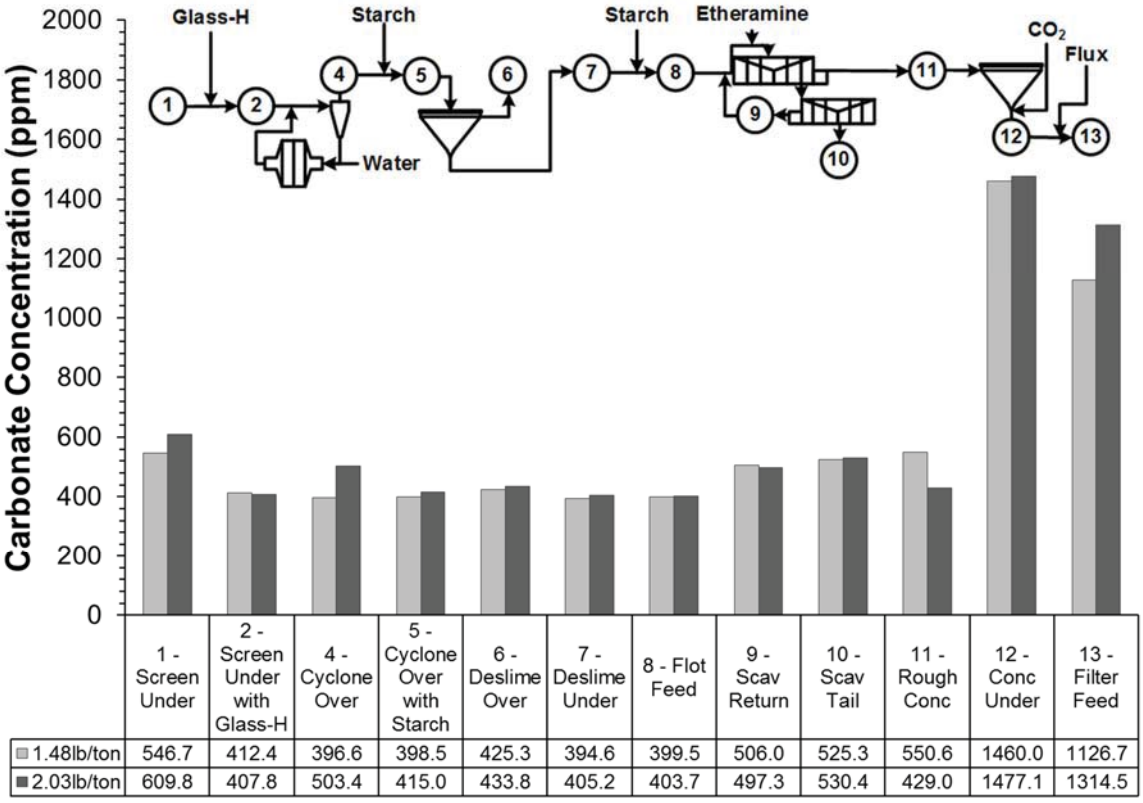

	1 - Screen Under	2 - Screen Under with Glass-H	4 - Cyclone Over	5 - Cyclone Over with Starch	6 - Deslime Over	7 - Deslime Under	8 - Flot Feed	9 - Scav Return	10 - Scav Tail	11 - Rough Conc	12 - Conc Under	13 - Filter Feed
1.48lb/ton	546.7	412.4	396.6	398.5	425.3	394.6	399.5	506.0	525.3	550.6	1460.0	1126.7
2.03lb/ton	609.8	407.8	503.4	415.0	433.8	405.2	403.7	497.3	530.4	429.0	1477.1	1314.5

Figure 2.56: Total carbonate concentration of each sample before and after caustic addition on April 2nd, 2012

2.3.5.4.10 Sulfate

The sulfate concentration of each sample before and after the increase in caustic addition rate is shown in Figure 2.57. The change in caustic addition rate seemed to have very little effect on the sulfate concentration; however, the sulfate concentration seemed to follow the same trend as soluble iron throughout the process; see Figure 2.58. Iron sulfates are slightly soluble in water and could be could be a constituent of the incoming

ore in the form of natrojarosite mineral ($NaFe_3(OH)_6(SO4)_2$) which has been found at the Chicagon mine in Menominee, MI (Ralph et al., 2014). Slow dissolution of natrojarosite would fully explain the phenomenon seen in both the soluble iron and the sulfate concentrations.

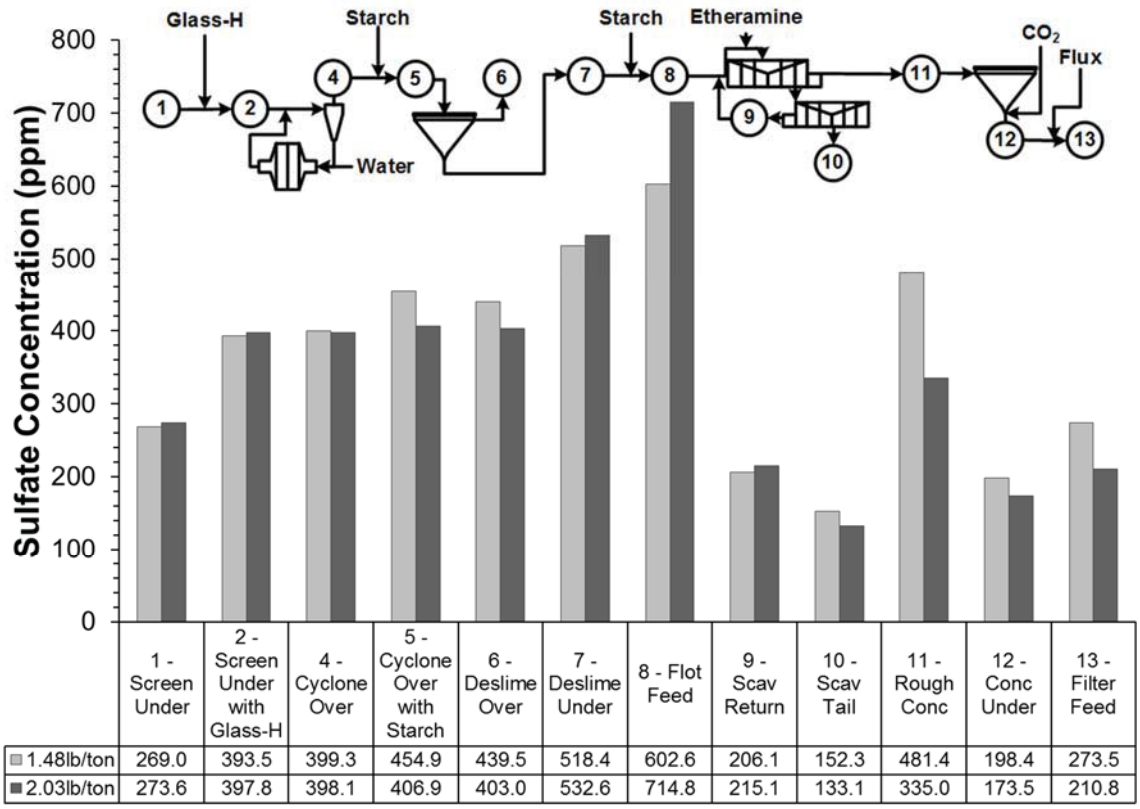

	1 - Screen Under	2 - Screen Under with Glass-H	4 - Cyclone Over	5 - Cyclone Over with Starch	6 - Deslime Over	7 - Deslime Under	8 - Flot Feed	9 - Scav Return	10 - Scav Tail	11 - Rough Conc	12 - Conc Under	13 - Filter Feed
1.48lb/ton	269.0	393.5	399.3	454.9	439.5	518.4	602.6	206.1	152.3	481.4	198.4	273.5
2.03lb/ton	273.6	397.8	398.1	406.9	403.0	532.6	714.8	215.1	133.1	335.0	173.5	210.8

Figure 2.57: Sulfate concentration of each sample before and after caustic addition on April 2nd, 2012

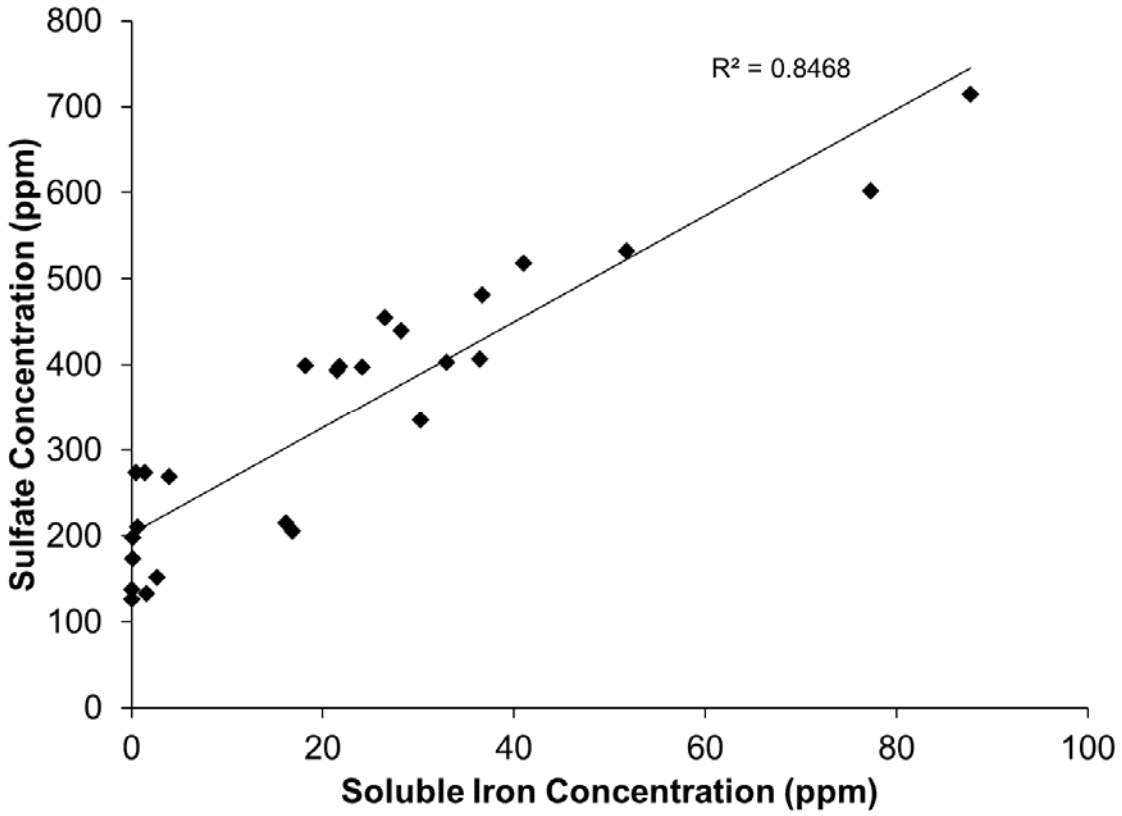

Figure 2.58: Correlation between soluble iron and sulfate of the April 2nd, 2012 sample sets

2.3.5.4.11 Total Dissolved Solids

The total dissolved solids (TDS) of each sample before and after the increase in caustic addition rate is shown Figure 2.59. TDS is a measure of the total quantity (by mass) of ions in a solution. As expected, the addition of caustic resulted in an overall increase in TDS throughout the plant.

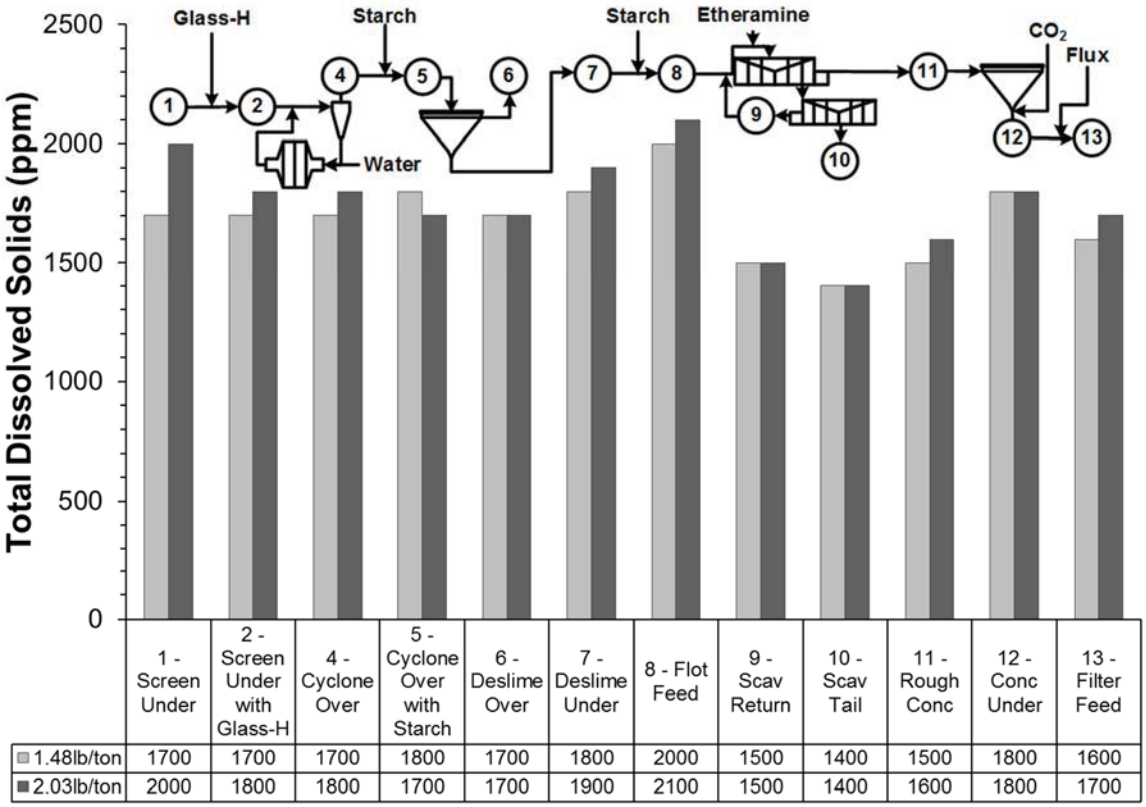

	1 - Screen Under	2 - Screen Under with Glass-H	4 - Cyclone Over	5 - Cyclone Over with Starch	6 - Deslime Over	7 - Deslime Under	8 - Flot Feed	9 - Scav Return	10 - Scav Tail	11 - Rough Conc	12 - Conc Under	13 - Filter Feed
1.48lb/ton	1700	1700	1700	1800	1700	1800	2000	1500	1400	1500	1800	1600
2.03lb/ton	2000	1800	1800	1700	1700	1900	2100	1500	1400	1600	1800	1700

Figure 2.59: Total dissolved solids (TDS) of each sample before and after caustic addition on April 2nd, 2012

2.3.5.4.12 Zeta Potential

The zeta potential at process conditions before and after the increase in caustic addition rate is shown in Figure 2.60. The first noticeable trend was the increase in zeta potential with the addition of Glass-H (sodium henicosapolyphosphate dispersant). This trend was seen in all sample sets except for the November 30th, 2011 sample set. The average increase in zeta potential was 6 mV.

Suppression of the surface charge was not seen at the cyclone overflow at the lower caustic addition rate; however, it was seen at the flotation feed. The increase in caustic

addition rate caused an increase in surface charge suppression by starch at the cyclone overflow but did not affect charge suppression at the flotation feed. Zeta potential curves of these samples are included in the Appendix A.

All sample sets have shown an increase by 5 – 14 mV in zeta potential upon the addition of CO_2. The addition of flux decreased the zeta potential consistently to ~20 mV. This could cause negative effects on filtration performance.

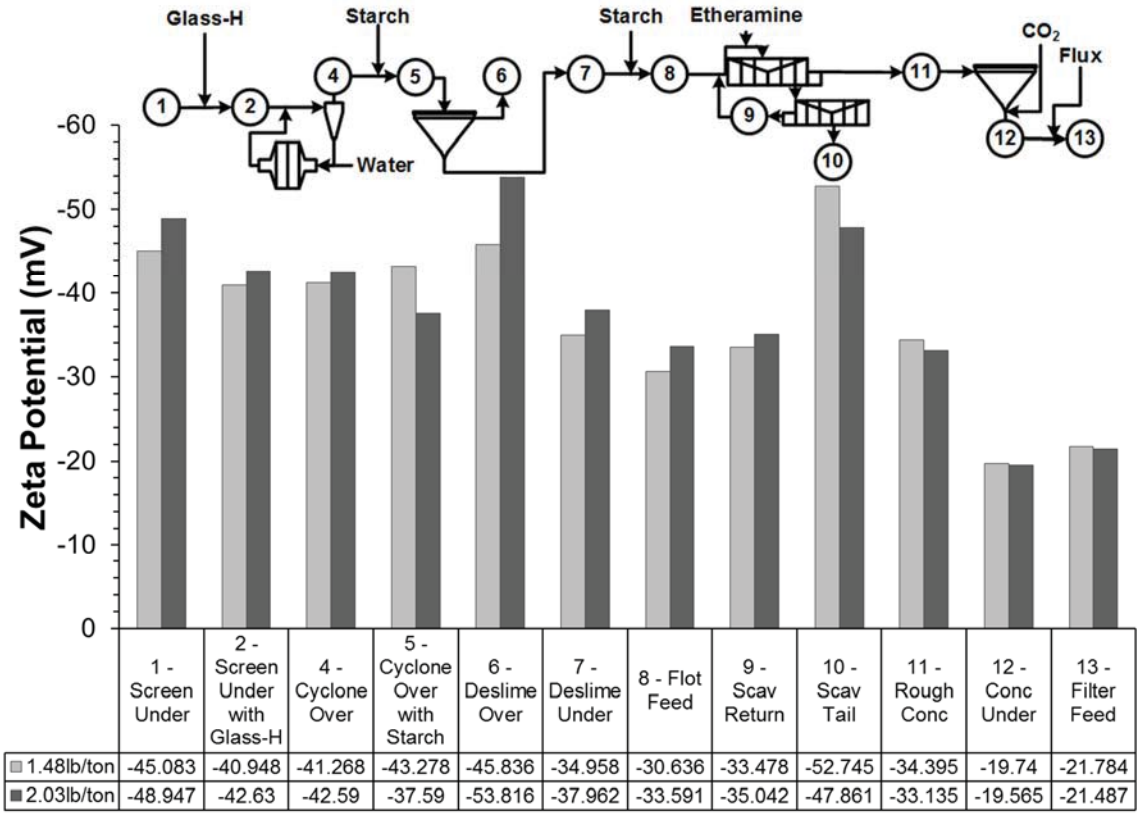

	1 - Screen Under	2 - Screen Under with Glass-H	4 - Cyclone Over	5 - Cyclone Over with Starch	6 - Deslime Over	7 - Deslime Under	8 - Flot Feed	9 - Scav Return	10 - Scav Tail	11 - Rough Conc	12 - Conc Under	13 - Filter Feed
1.48lb/ton	-45.083	-40.948	-41.268	-43.278	-45.836	-34.958	-30.636	-33.478	-52.745	-34.395	-19.74	-21.784
2.03lb/ton	-48.947	-42.63	-42.59	-37.59	-53.816	-37.962	-33.591	-35.042	-47.861	-33.135	-19.565	-21.487

Figure 2.60: Zeta potential of each sample before and after caustic addition on April 2nd, 2012

2.3.5.4.13 Elemental Analysis

The concentration of calcium, magnesium, iron (Fe^{2+} and Fe^{3+}), and acid insoluble material was measured by acid leaching followed by atomic absorption spectroscopy and gravimetry; see Figure 2.61, 2.62, 2.63 and 2.64. The magnesium content of the solids was consistently higher than the calcium content. This was consistent with the increased dissolved magnesium concentration in the water. Upon flux addition, the concentration of calcium rose more than magnesium suggesting the use of a calcite-rich flux. As with previous sample sets, calcite/dolomite rejection occurred during deslime but not during flotation.

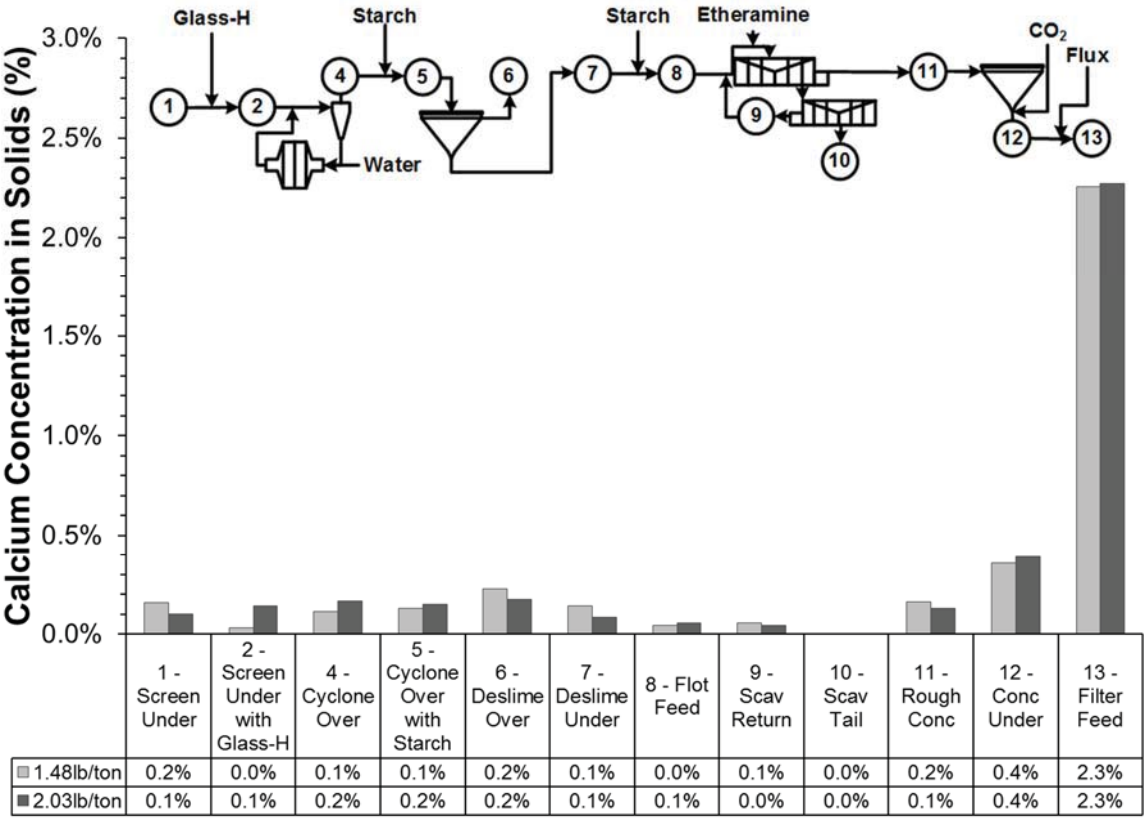

	1 - Screen Under	2 - Screen Under with Glass-H	4 - Cyclone Over	5 - Cyclone Over with Starch	6 - Deslime Over	7 - Deslime Under	8 - Flot Feed	9 - Scav Return	10 - Scav Tail	11 - Rough Conc	12 - Conc Under	13 - Filter Feed
1.48lb/ton	0.2%	0.0%	0.1%	0.1%	0.2%	0.1%	0.0%	0.1%	0.0%	0.2%	0.4%	2.3%
2.03lb/ton	0.1%	0.1%	0.2%	0.2%	0.2%	0.1%	0.1%	0.0%	0.0%	0.1%	0.4%	2.3%

Figure 2.61: Calcium concentration in solids of each sample before and after caustic addition on April 2nd, 2012

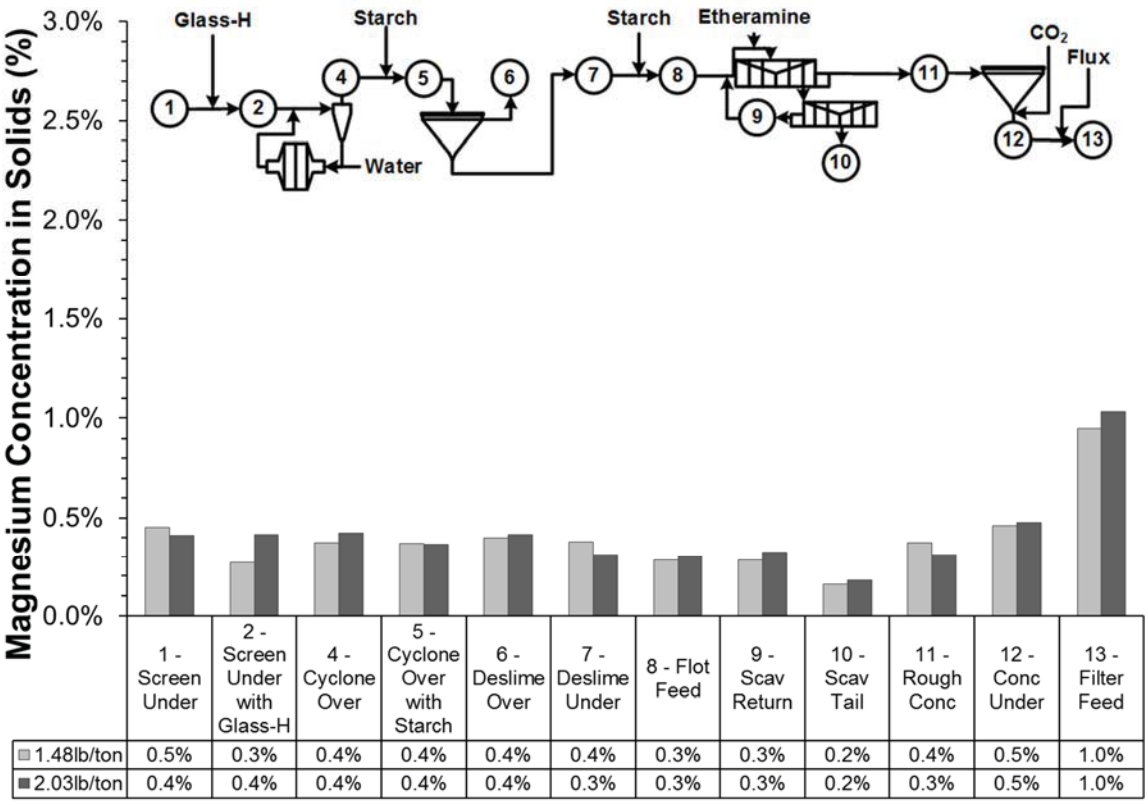

	1 - Screen Under	2 - Screen Under with Glass-H	4 - Cyclone Over	5 - Cyclone Over with Starch	6 - Deslime Over	7 - Deslime Under	8 - Flot Feed	9 - Scav Return	10 - Scav Tail	11 - Rough Conc	12 - Conc Under	13 - Filter Feed
1.48lb/ton	0.5%	0.3%	0.4%	0.4%	0.4%	0.4%	0.3%	0.3%	0.2%	0.4%	0.5%	1.0%
2.03lb/ton	0.4%	0.4%	0.4%	0.4%	0.4%	0.3%	0.3%	0.3%	0.2%	0.3%	0.5%	1.0%

Figure 2.62: Magnesium concentration in solids of each sample before and after caustic addition on April 2nd, 2012

The iron content and acid insoluble material content of the slurry solids are shown in Figure 2.63 and 2.64. As expected, there was a large acid insolubles rejection during deslime and flotation where silica and other gangue minerals were removed. The iron was concentrated by both the deslime and flotation. The inconsistency between the deslime underflow and the flotation feed was caused by the merging of section10-12 with section 7-9 at that point.

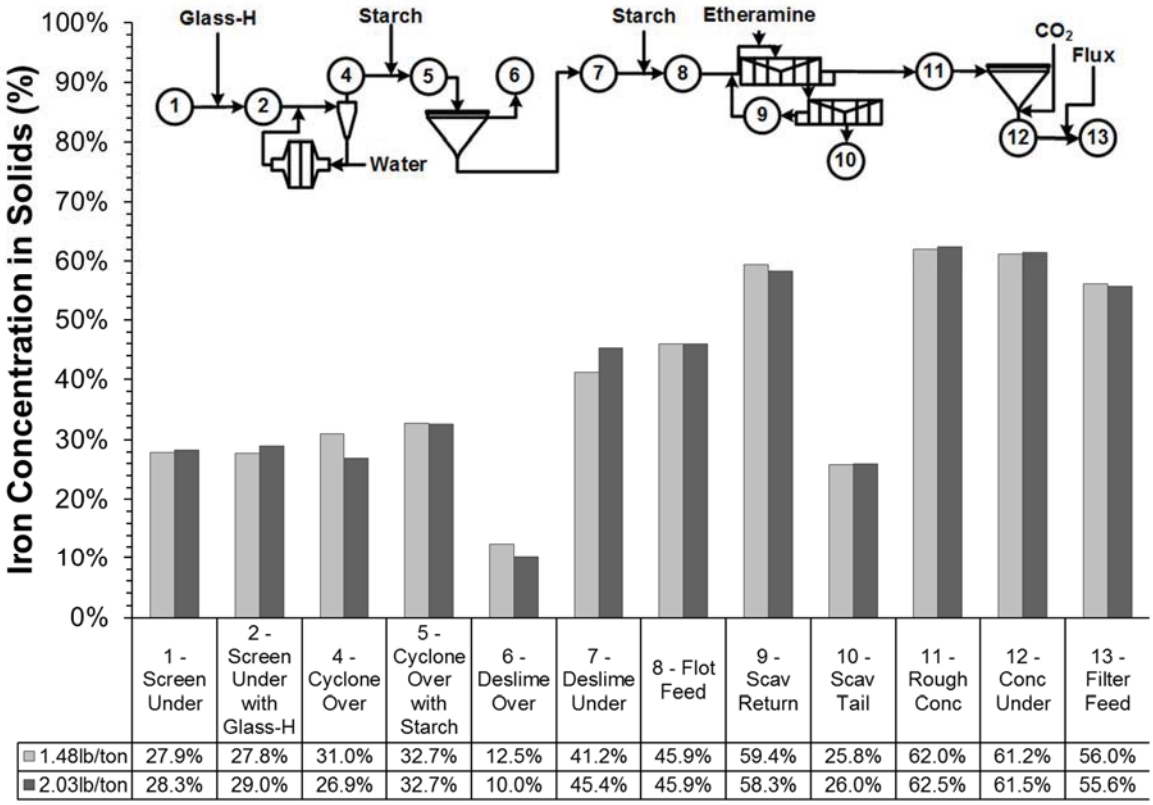

Figure 2.63: Iron concentration in solids of each sample before and after caustic addition on April 2nd, 2012

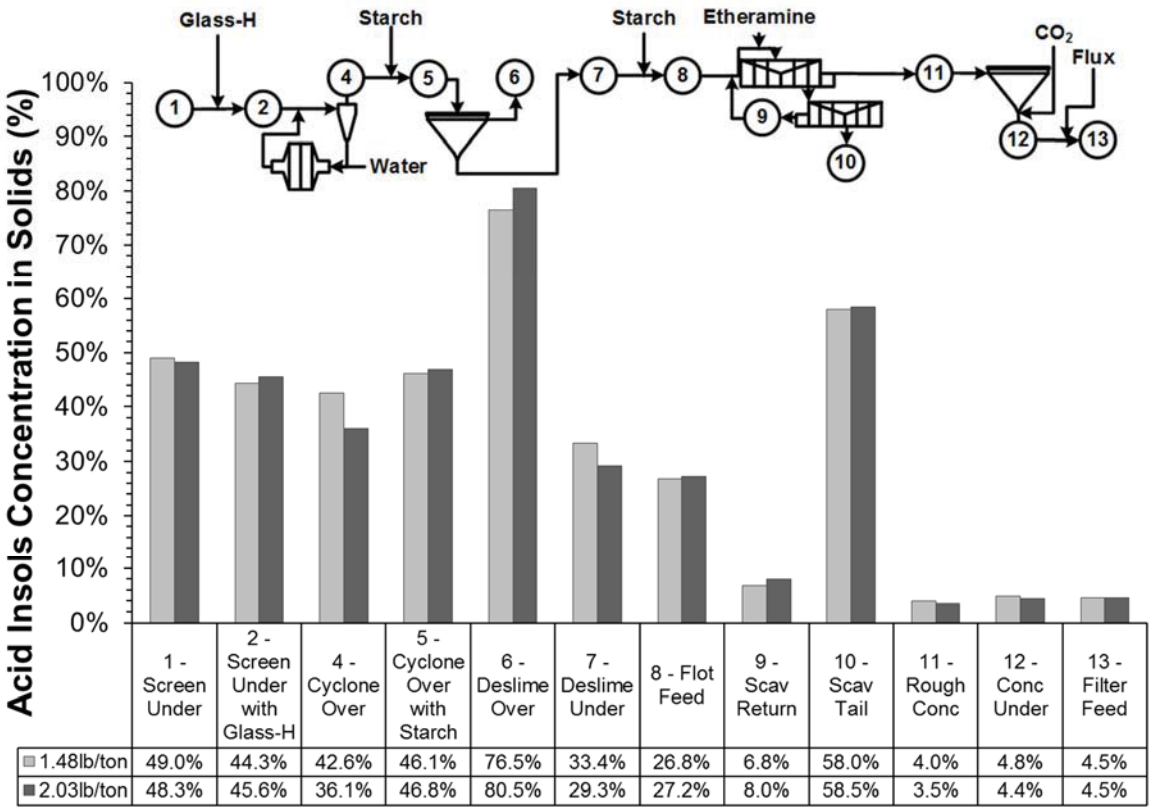

Figure 2.64: Acid insoluble concentration in solids of each sample before and after caustic addition on April 2nd, 2012

2.3.5.4.14 Conclusions

These sample sets provided a substantial amount of additional correlations between water chemistry, zeta potential and process performance. Overall, the increase in caustic rate led to less iron loss in deslime, more iron loss in flotation, an increase in soluble iron concentration, and a lower overall recovery. The overall loss in recovery was primarily due to the increased load on the flotation circuit caused by a lower total weight rejection in deslime.

A previous study hypothesized that etheramine caused a reduction in soluble iron concentration when added during flotation. This theory was solidified with this dataset and also showed a correlation between soluble iron and sulfate concentration. The association between iron and sulfate suggests the presence of natrojarosite minerals ($NaFe_3(OH)_6(SO_4)_2$) in the ore. This finding was not verified by XRD.

This dataset also solidifies theories made from all previous datasets. The following are the conclusions drawn from all sample sets:

1. Starch does noticeably and reproducibly suppress the surface charge of hematite in both deslime and flotation
2. The effect of the starch is consistently more prominent in flotation
3. Starch does not significantly change the water hardness
4. The addition of CO_2 has a significant effect on the pH, conductivity, water hardness, and zeta potential. These additions result in a
    4.1. Decrease in pH
    4.2. Increase in conductivity
    4.3. Increase in water hardness
    4.4. Increase in zeta potential
5. Conductivity is directly proportional to the sodium concentration of the process water
6. Flux addition causes the zeta potential to equilibrate at ~-20 mV
7. Calcium and magnesium are rejected by the deslime thickener but not during flotation

2.3.5.5 *Plant-wide Overall Trends Observed*

2.3.5.5.1 *Glass-H Addition*

Glass-H addition caused a significant decrease in the magnitude of zeta potential (5-14 mV) in all sample sets except for the November 30th, 2011 sample set as shown in Figure 2.65. Glass-H ($(NaPO_4)_{21}*Na_2O$, sodium henicosapolyphosphate) is a surface modifying reagent that is typically used for its dispersive qualities. Glass-H requires positively charged surface sites (un-hydrated iron or covalently bonded calcium/magnesium) for a chemical bond to form causing dispersion.

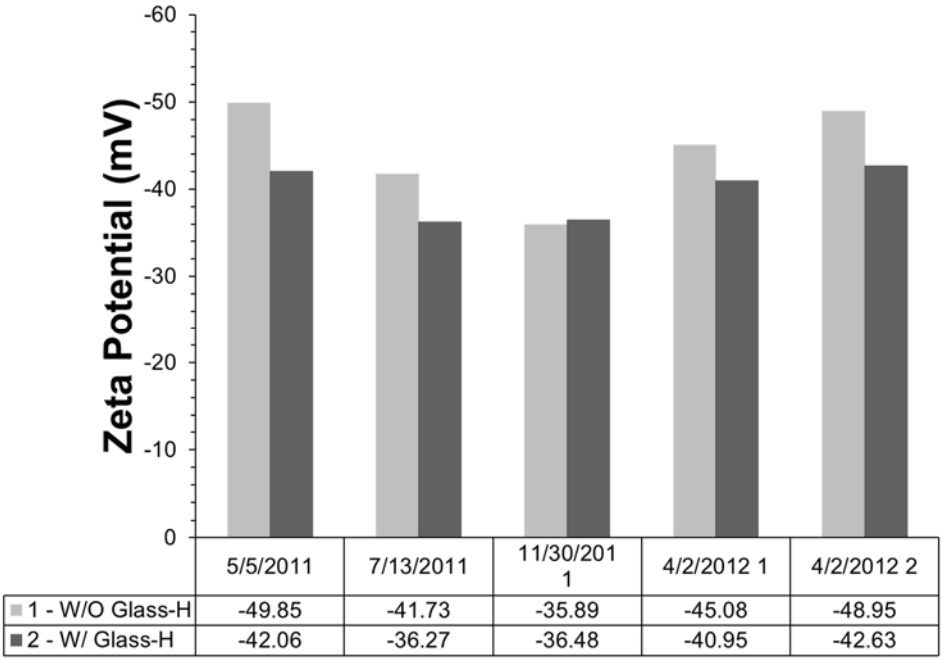

	5/5/2011	7/13/2011	11/30/2011	4/2/2012 1	4/2/2012 2
1 - W/O Glass-H	-49.85	-41.73	-35.89	-45.08	-48.95
2 - W/ Glass-H	-42.06	-36.27	-36.48	-40.95	-42.63

Figure 2.65: Effects of Glass-H on Zeta Potential

2.3.5.5.2 Cyclone Overflow Starch Addition

Starch caused a significant decrease in the magnitude of zeta potential in all sample sets except for the April 2nd, 2012 set at low caustic rate as shown in Figure 2.66. Starch has been shown in literature to be a selective flocculent for hematite (Balajee et al., 1969). Starch adsorption occurs at the surface of hematite due structural compatibility The average distance between iron atoms at the surface of un-hydrated hematite particles is 2.852 A° (angstroms (A°) = 10^{-10} m), whereas the spacing between oxygen atoms at the end of a starch chain is 2.85 A°. According to literature, a bond forms between these oxygen atoms in starch and un-hydrated Fe surface sites (Pradip, 1994).

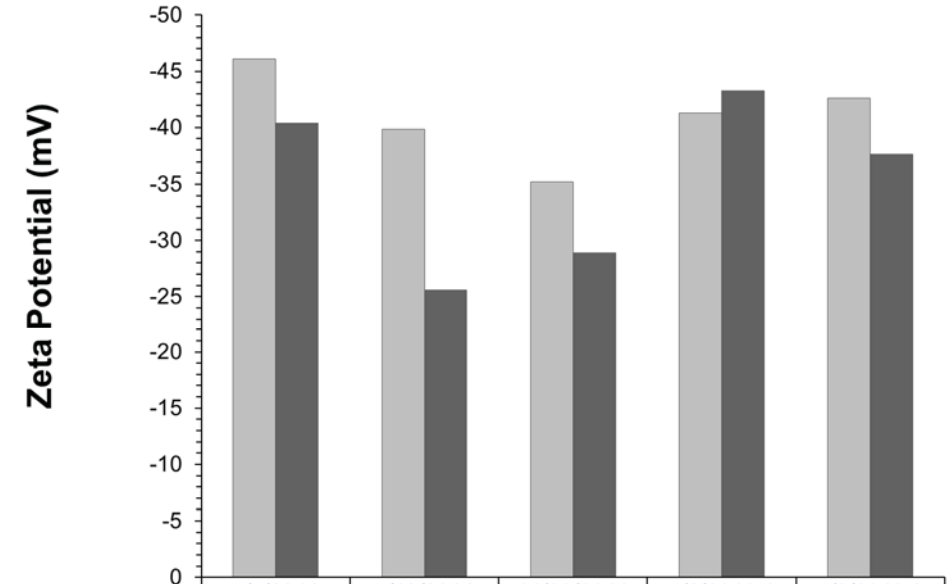

	5/5/2011	7/13/2011	11/30/2011	4/2/2012 1	4/2/2012 2
4 - Before Starch	-46.08	-39.85	-35.19	-41.27	-42.59
5 - After Starch	-40.40	-25.58	-28.89	-43.28	-37.59

Figure 2.66: Cyclone overflow starch effects on zeta potential

The starch coats the hematite particles causing the magnitude of the surface charge to decrease, thereby lowering the magnitude of the zeta potential. The amount that the

magnitude of zeta potential decreases is relative to the amount of starch adsorbed to the hematite particle surfaces. As shown in Figure 2.67, the decrease in the magnitude of zeta potential due to starch adsorption seemed to be dependent on the water hardness in the sample. This suggested a certain degree of water hardness is required for starch adsorption, and calcium/magnesium ions acted as an activator for starch adsorption on hematite surfaces. However, it is common knowledge that too much calcium can cause a loss in selectivity of the starch.

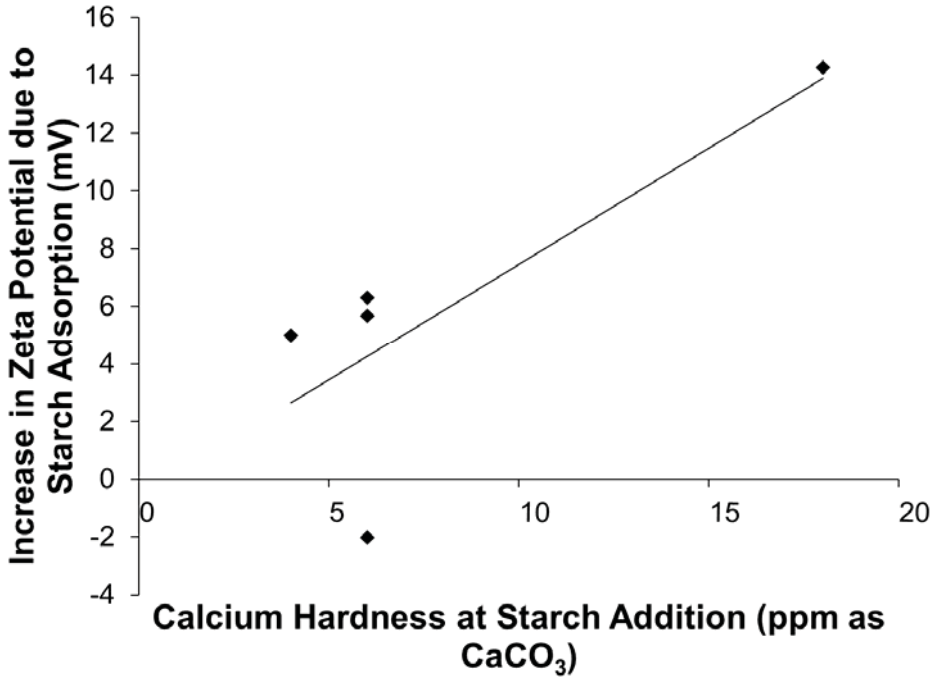

Figure 2.67: Starch effectiveness as a function of calcium hardness at cyclone overflow

2.3.5.5.3 Deslime Thickener

An important finding of this project was the correlation of zeta potential to the iron concentration in the deslime overflow sample. Silica tended to have a much higher magnitude of zeta potential (~-100 mV) in alkaline conditions than hematite (~15 mV),

therefore, the zeta potential of a hematite/silica mixture should be dependent upon the amount of hematite in the mixture. As shown in Figure 2.68, this was indeed the case; as the hematite concentration increased, the zeta potential decreased. Variations in this behavior can be attributed to changes in water chemistry.

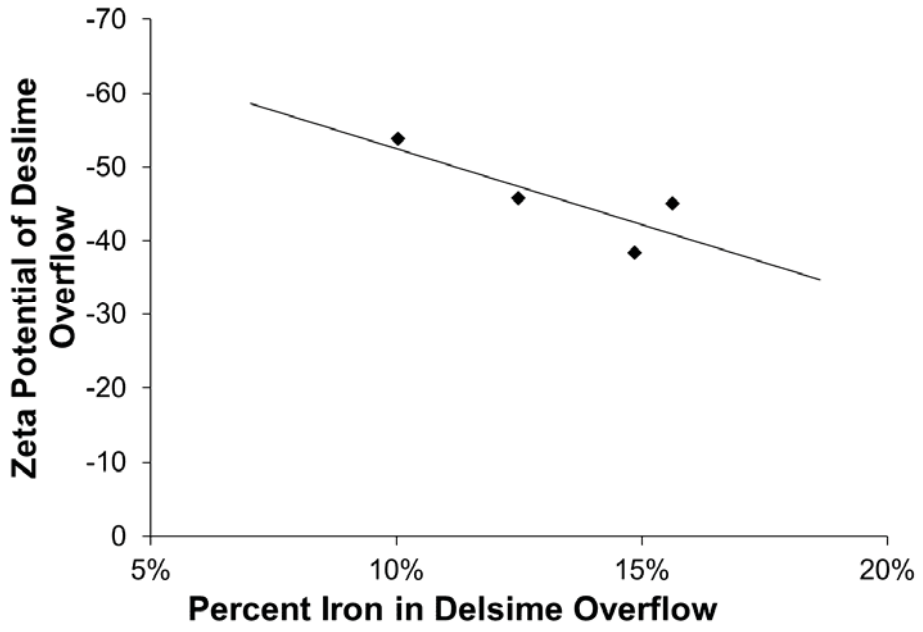

Figure 2.68: Dependence of iron concentration on zeta potential in deslime overflow samples

The zeta potential at the deslime feed had a large effect on the iron recovery of the deslime thickener as seen in Figure 2.69. Zeta potential is a direct indicator of dispersive stability; a higher magnitude of zeta potential indicates the slurry is highly dispersed; a low magnitude of zeta potential indicates that the slurry particles can non-selectively flocculate. In the deslime thickener, a highly dispersed slurry is required to maximize the separation of iron oxides from gangue minerals.

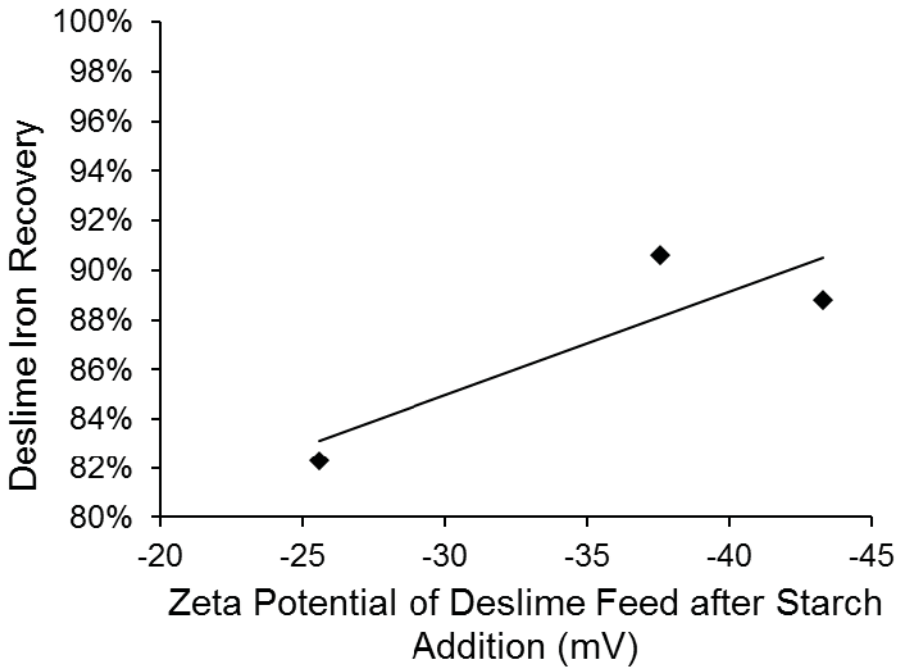

Figure 2.69: Correlation between zeta potential at the deslime feed and the iron recovery within the deslime thickener.

Water hardness played a vital role in the effectiveness of the deslime thickener. There were two ways in which the calcium/magnesium concentration played a major role in the deslime thickener:

1. Calcium and magnesium activated iron oxide surfaces for starch adsorption
2. Calcium and magnesium caused flocculation of fine particles

Low water hardness at the deslime thickener feed caused higher dispersion and increased selectivity of starch adsorption; see Figure 2.70. This scenario yielded the highest iron recovery. Higher water hardness both decreased the selectivity of starch and lowered dispersion. Overall, a higher water hardness yielded a lower deslime recovery.

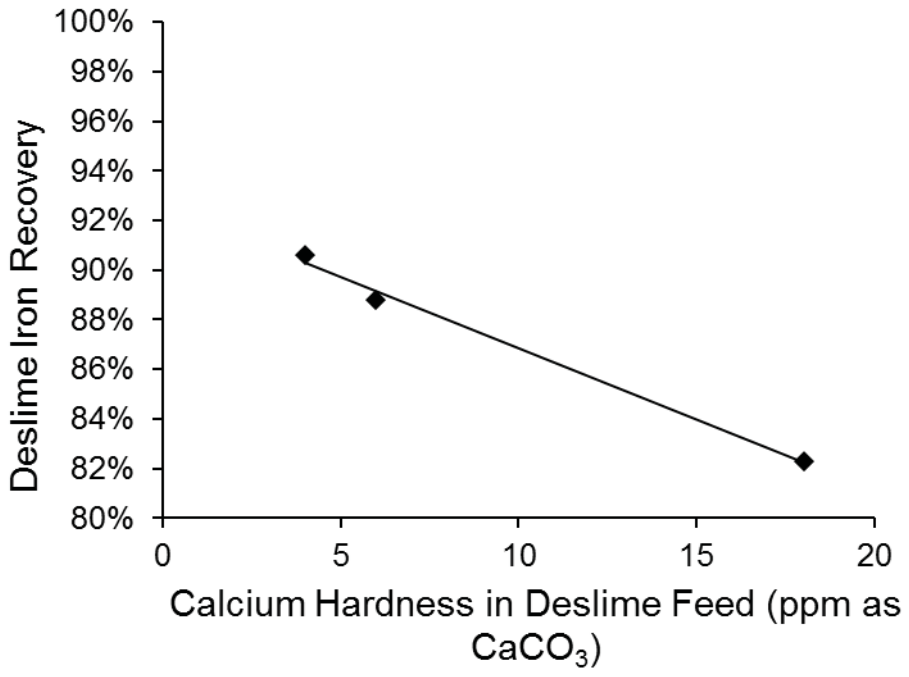

Figure 2.70: Correlations between calcium hardness and process performance. Both 11/30/11 and 5/5/11 samples were not included because they were taken during a process upset.

Conductivity is a significant factor in water chemistry because it relates to the total ionic content of the slurry. Each type of ion (OH^-, Na^+, Cl^-, Ca^{2+}, etc.) contributes to the conductivity based on its concentration and a constant specific to that ion called the limiting ion conductivity. Although conductivity is not related directly to zeta potential, it can be assumed that a higher conductivity in alkaline conditions will result in a decrease in the magnitude of zeta potential.

Conductivity can be used as a predictor of process performance because of its relationship to the ionic content of the process water. A higher conductivity is associated with a large abundance of ions in the water. These ions are electrostatically attracted to

the particles and cause a phenomenon called ‘double layer compression’. This phenomenon reduces the net charge of the particles resulting in non-selective flocculation. Non-selective flocculation, as seen with increased water hardness, causes a lower iron recovery in the deslime thickener; see Figure 2.71. In contrast, a lower conductivity is associated with increased repulsive charges of particles, thereby increasing the dispersive stability and iron recovery.

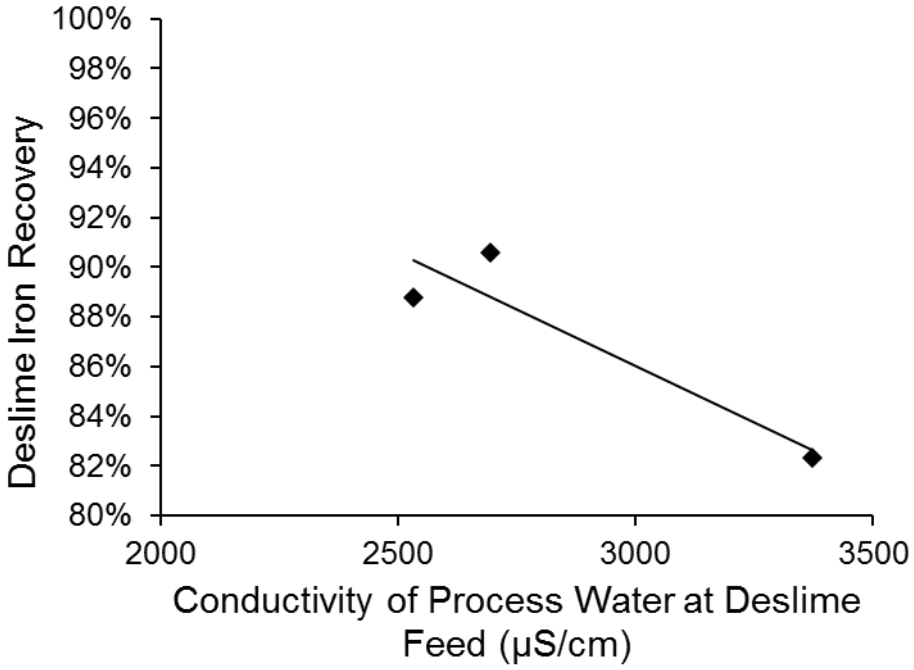

Figure 2.71: Correlation between deslime iron recovery and conductivity of deslime feed. Both 11/30/11 and 5/5/11 samples were not included because they were taken during a process upset.

2.3.5.5.4 Flotation Feed Starch Addition

The flotation feed showed a significant decrease in the magnitude of zeta potential (increase in zeta potential) upon starch addition as shown in Figure 2.72. This signified

selectivity of starch towards iron oxides because of the increased iron oxide content at this point as opposed to the cyclone overflow. The large increases in zeta potential seen on 5/5/2011 and 7/13/2011 were both accompanied by higher water hardness values. As with the cyclone overflow samples, water hardness had a significant effect on starch adsorption, as shown in Figure 2.73. By comparing the slope of the linear trend-line at the cyclone overflow in Figure 2.67 to the slope of the linear trend-line at the flotation feed in Figure 2.73, starch adsorption at the flotation feed was three times as sensitive to water hardness.

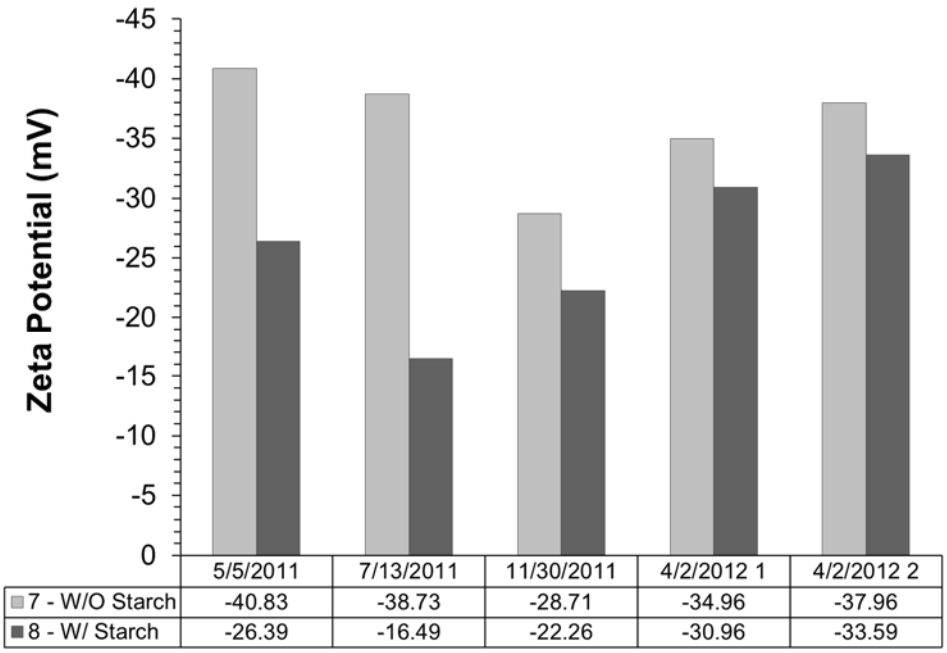

	5/5/2011	7/13/2011	11/30/2011	4/2/2012 1	4/2/2012 2
7 - W/O Starch	-40.83	-38.73	-28.71	-34.96	-37.96
8 - W/ Starch	-26.39	-16.49	-22.26	-30.96	-33.59

Figure 2.72: Flotation feed starch effects on zeta potential

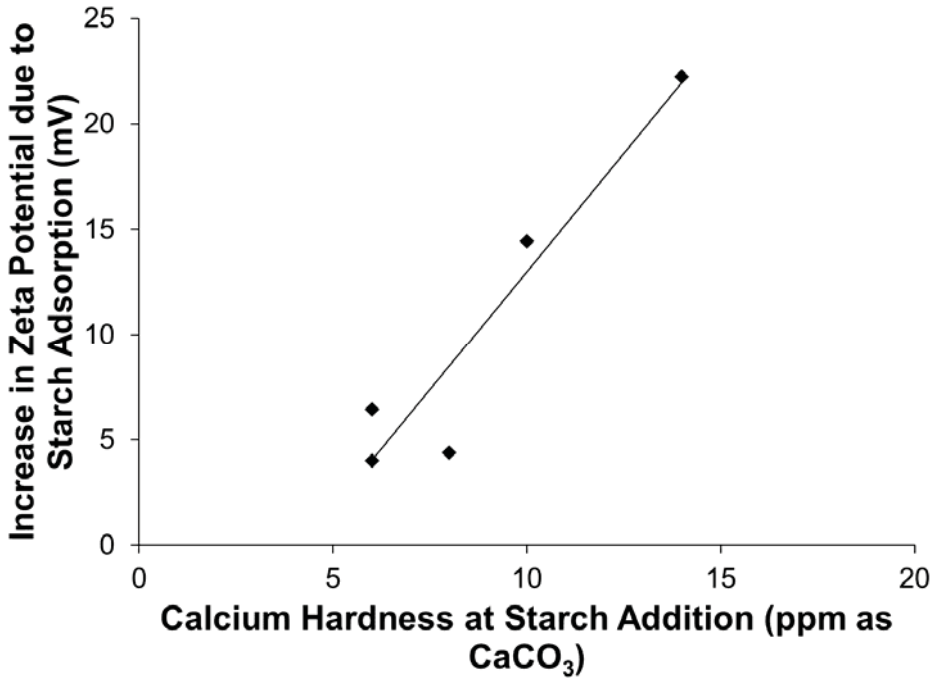

Figure 2.73: Starch effectiveness as a function of calcium hardness at flotation feed

2.3.5.5.5 Flotation Circuit

The zeta potential throughout flotation is extremely important because it affects both starch and etheramine adsorption. In the alkaline environment, both silica and iron oxides carry a negative surface charge. The surface charge of the iron oxides must be suppressed to allow for selective adsorption of the cationic collector (etheramine) onto silica surfaces. The flotation feed sample typically had a lower magnitude of zeta potential due to the suppression of the surface charge of iron oxides by starch, as shown in Figure 2.74. The silica retained its high magnitude zeta potential, and was floated to the tailings. The rougher concentrate, primarily hematite, retained a low magnitude zeta potential.

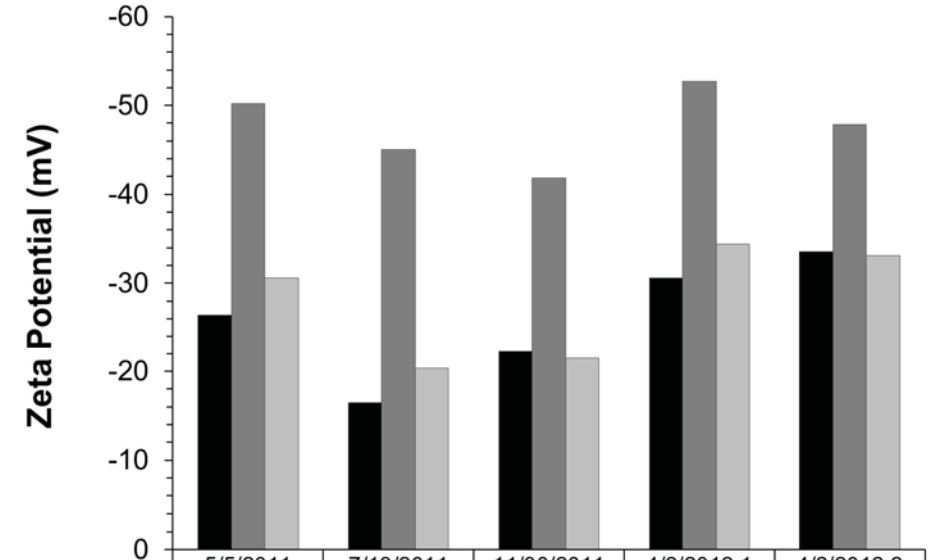

	5/5/2011	7/13/2011	11/30/2011	4/2/2012 1	4/2/2012 2
8 - Flot Feed	-26.39	-16.49	-22.26	-30.64	-33.59
10 - Flot Tails	-50.17	-45.00	-41.84	-52.75	-47.86
11 - Flot Conc	-30.58	-20.34	-21.47	-34.39	-33.14

Figure 2.74: Zeta potential throughout flotation cells during each sampling campaign

The zeta potential of the flotation feed has a large effect on the concentration of iron in the flotation tailings as shown in Figure 2.75. Lower magnitude zeta potentials at the flotation feed were caused by more complete coverage by starch, allowing for higher selectivity in etheramine adsorption and therefore increased iron recovery. Higher magnitude zeta potentials indicated a high level of dispersion and incomplete coverage by

starch. This reduced etheramine selectivity and ultimately caused a decrease in iron recovery during flotation. This trend is opposite to that seen in the deslime thickener.

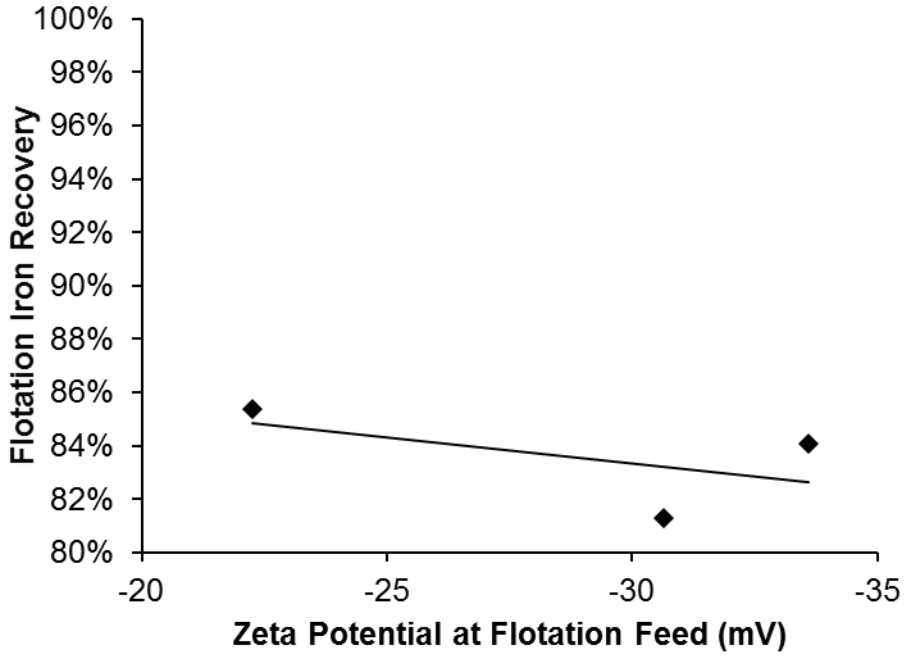

Figure 2.75: Effect of zeta potential of flotation feed on iron recovery. Both 11/30/11 and 5/5/11 samples were not included because they were taken during a process upset.

As stated previously, starch adsorption was affected by water hardness. Water hardness was therefore directly related to the iron recovery during flotation, as shown in Figure 2.76. Prior to flotation, the iron oxide particles have completely hydrated, yielding no positive surface sites for starch adsorption that aren't created by adsorbed calcium/magnesium. When the water hardness is low, the fully hydrated hematite could be coated in starch. This limited etheramine selectivity and ultimately lowered iron recovery. When water hardness is high (>10 ppm), positive surface sites formed on the

iron oxide surface allowing for starch adsorption. The calcium and magnesium ions can also form positive surface sites on gangue mineral particles and reduce starch selectivity. This indicates that there was an ideal water hardness to yield the highest flotation recovery. Due to lack of data at water hardness values above 8 ppm, the only conclusion that can be made is that the optimum water hardness was above 8 ppm.

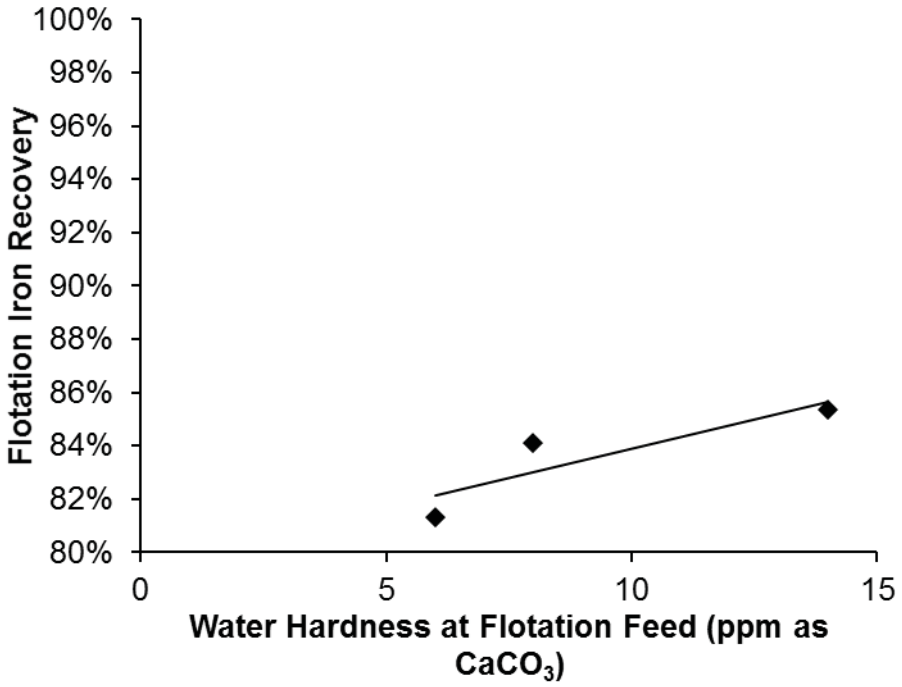

Figure 2.76: Effect of calcium hardness in flotation on the iron recovery. Both 11/30/11 and 5/5/11 samples were not included because they were taken during a process upset.

The conductivity during flotation, through its relationship to zeta potential and the surface chemistry of the particles, was a good predictor of flotation performance. Higher conductivity was associated with lower dispersion and a higher iron recovery during flotation as shown in Figure 2.77.

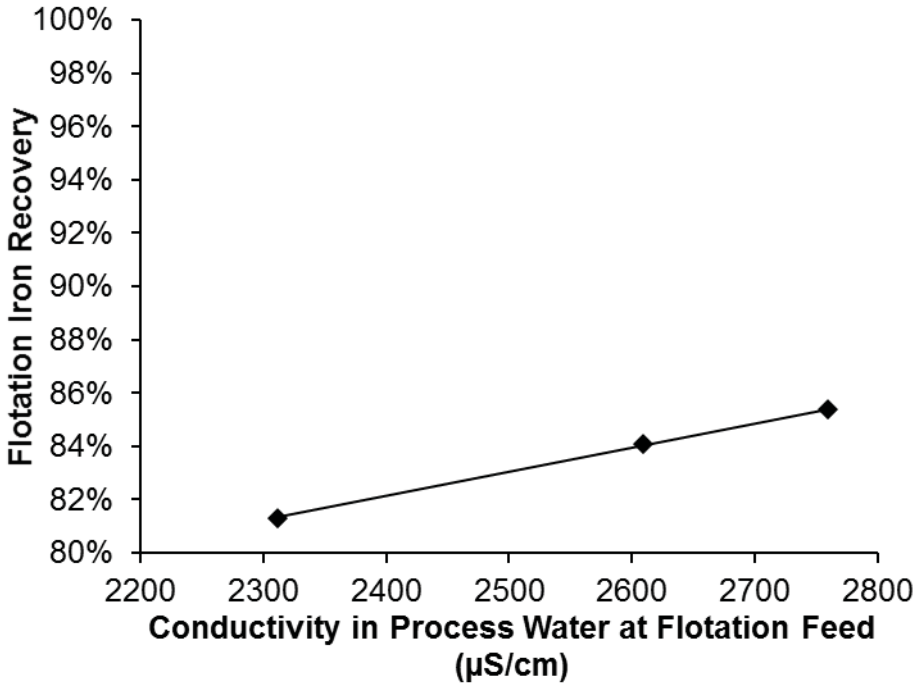

Figure 2.77: Effect of conductivity in flotation on the iron recovery. Both 11/30/11 and 5/5/11 samples were not included because they were taken during a process upset.

The effectiveness of the deslime thickener had a large bearing on how much iron was lost during flotation. As shown in Figure 2.78, if the total weight rejected by the deslime thickener was minimal, flotation rejected more iron. Although calcium hardness and zeta potential did show an effect on the iron recovery, both of those parameters also affected deslime performance in the opposite manner, thereby cancelling each other out. This suggests that flotation was primarily capacity limited and depended on the desliming process to be effective. Focusing the study on deslime thickening provides the most potential for overall increases in iron recovery.

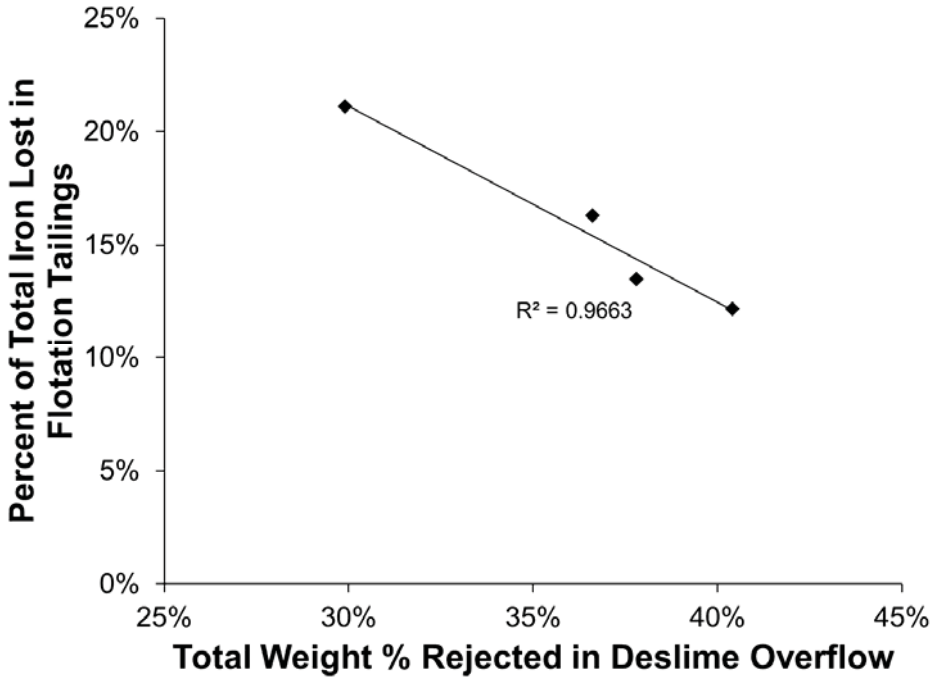

Figure 2.78: The effect of deslime weight rejection on iron loss during flotation. 11/30/11 sample excluded due to overgrind

Ultimately, from these samples, it was shown that the separation processes required different processing conditions to be optimized; see Figure 2.79. Water hardness was critical to effective separation in both deslime and flotation. At low water hardness values, iron recovery was high in deslime and low in flotation. At high water hardness values, iron recovery was low in deslime and high in flotation. From the data gathered, there seemed to be little variability in the overall recovery, but these data sets were missing processing conditions in which the water hardness was in the range of 6 and 18 ppm at the deslime feed.

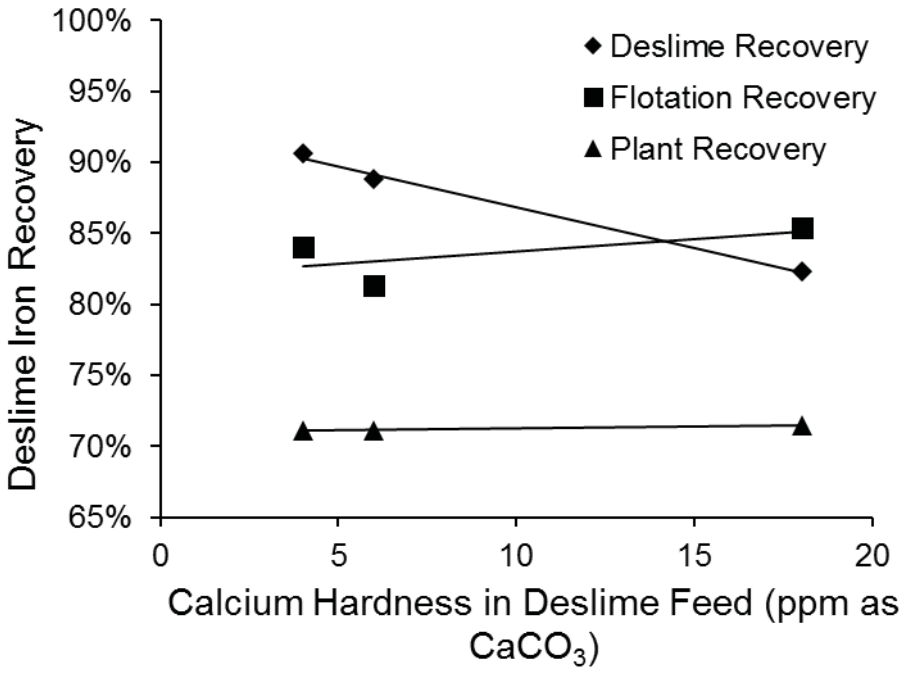

Figure 2.79: The effect of water hardness on deslime, flotation and overall recovery. Both 11/30/11 and 5/5/11 samples were not included because they were taken during a process upset.

2.3.5.5.6 Dewatering

During dewatering, there were many water chemistry changes that accompanied the addition of flux (calcite/dolomite), CO_2, and dewatering aids/polymers. The addition of CO_2 to decrease the pH caused changes in the equilibrium distribution of carbonate ions as shown in Figure 2.80. Carbonate ions (CO_3^{2-}) form bicarbonate ions (HCO_3^-) at the lower pH. Some of the sodium carbonate ($NaCO_3^-$) ions can also hydrolyze to form aqueous sodium bicarbonate ($NaHCO_3$).

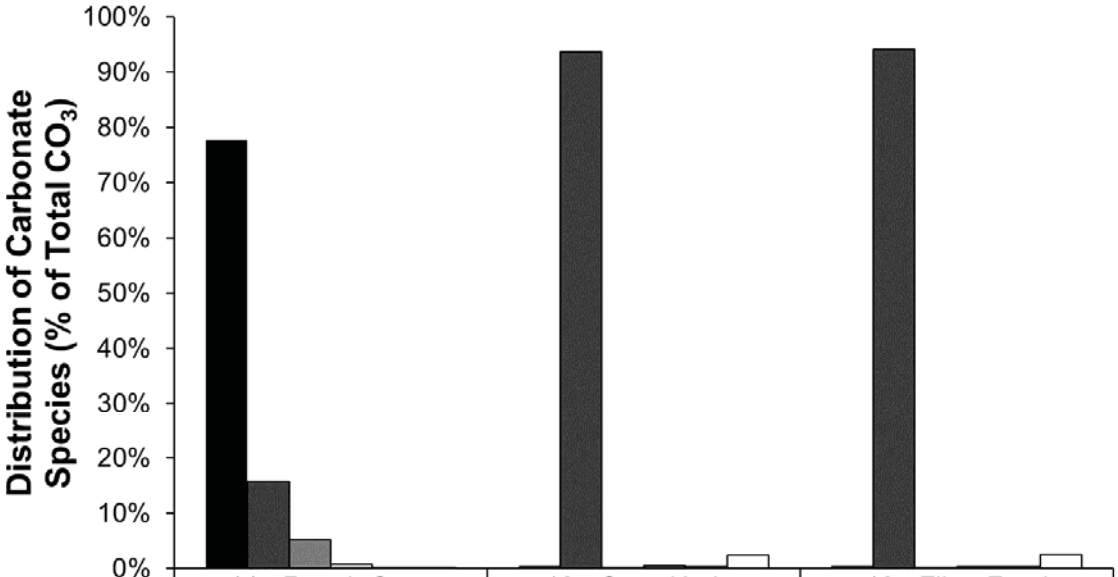

	11 - Rough Conc	12 - Conc Under	13 - Filter Feed
CO3-2	77.83%	0.51%	0.49%
HCO3-	15.86%	93.65%	94.06%
NaCO3-	5.21%	0.04%	0.03%
CaCO3	0.74%	0.57%	0.38%
NaHCO3	0.06%	0.39%	0.34%
MgCO3	0.00%	2.35%	2.51%

Figure 2.80: Carbonate equilibrium distribution changes during dewatering. Note: only 1st 4/2/2012 sample shown.

The decrease in pH caused some of the flux and possibly some of the calcium and magnesium minerals present in the ore to dissolve into calcium and magnesium ions, as shown in Figure 2.81 and Figure 2.82. At the higher pH of the rougher concentrate, most of the aqueous calcium and magnesium was present in a carbonate form ($CaCO_3$, $MgCO_3$). After the pH was lowered with CO_2, the presence of aqueous carbonated calcium and magnesium was diminished. This was accompanied by a rise in free calcium/magnesium ions (Ca^{2+}, Mg^{2+}) and calcium/magnesium bicarbonate ions

($CaHCO_3^-$, $MgHCO_3^-$). There was little change in the concentration of aqueous metal sulfate ions ($CaSO_4$, $MgSO_4$).

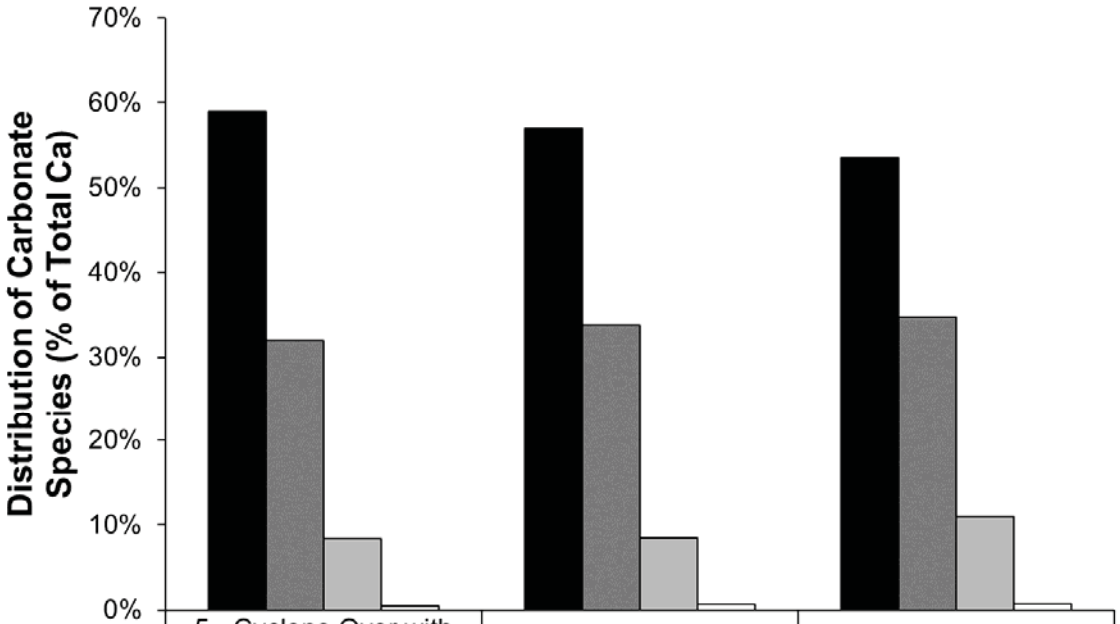

	5 - Cyclone Over with Starch	6 - Deslime Over	7 - Deslime Under
CaCO3	59.01%	56.96%	53.56%
Ca+2	32.01%	33.81%	34.72%
CaSO4	8.43%	8.52%	10.97%
CaHCO3+	0.46%	0.64%	0.69%

Figure 2.81: Calcium equilibrium distribution changes during dewatering. Note: only 1st 4/2/2012 sample shown.

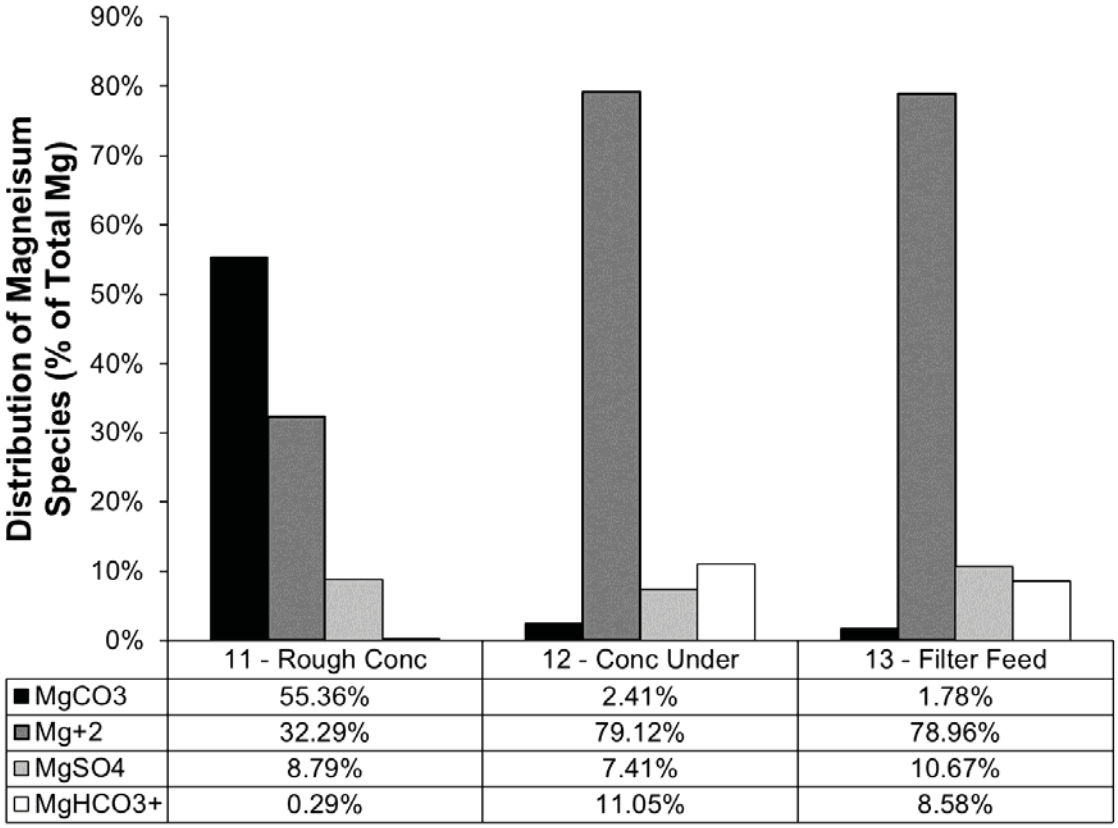

	11 - Rough Conc	12 - Conc Under	13 - Filter Feed
MgCO3	55.36%	2.41%	1.78%
Mg+2	32.29%	79.12%	78.96%
MgSO4	8.79%	7.41%	10.67%
MgHCO3+	0.29%	11.05%	8.58%

Figure 2.82: Magnesium equilibrium distribution changes during dewatering. Note: only 1st 4/2/2012 sample shown.

These water chemistry changes had a significant impact on zeta potential as shown in Figure 2.83. The introduction of CO_2 between the rougher concentrate and concentrate thickener underflow decreased the magnitude of zeta potential for two reasons: it caused higher concentrations of aqueous divalent cations which formed inner-sphere complexed at hematite surface thereby increasing surface charge, and it caused a decrease in pH causing hematite to approach its isoelectric point. The addition of flux at the filter feed established a shifted equilibrium between calcium, magnesium and carbonate. This

shifted equilibrium was also associated with an increase in pH. The increase in pH caused the zeta potential to decrease slightly to ~-20mV.

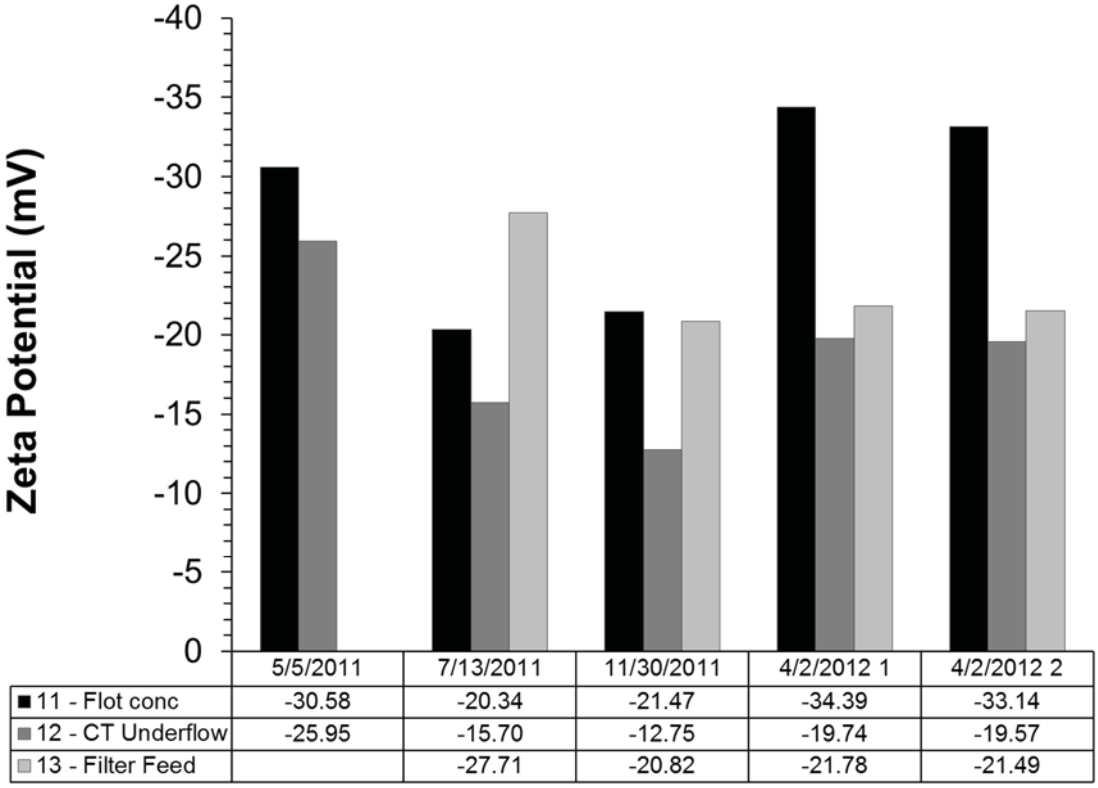

	5/5/2011	7/13/2011	11/30/2011	4/2/2012 1	4/2/2012 2
11 - Flot conc	-30.58	-20.34	-21.47	-34.39	-33.14
12 - CT Underflow	-25.95	-15.70	-12.75	-19.74	-19.57
13 - Filter Feed		-27.71	-20.82	-21.78	-21.49

Figure 2.83: Zeta potential of sample during dewatering steps

2.3.5.6 Conclusions

During this phase of this project, samples were collected 5 times at 12 locations throughout section 7-9 of the hematite ore concentrator. Sample locations were strategically chosen to determine zeta potential effects at reagent addition points and zeta potential effects on separation process performance. Samples were tested for water quality parameters including pH, conductivity, water hardness, calcium, magnesium, iron, sodium, potassium, sulfate, carbonate, nitrate and oxidation-reduction potential. The

solid content of each sample was analyzed for zeta potential (at process conditions), elemental composition, thermogravimetric degradation, x-ray diffraction, x-ray fluorescence and particle size distribution.

The following conclusions have been drawn from this study thus far:

1. The zeta potential of the slurry was largely controlled by 6 main factors: pH, water hardness, conductivity, mineralogy, Glass-H adsorption and starch adsorption.
    1.1. Increases in pH tended to cause a more negative zeta potential.
    1.2. Higher water hardness caused inner-sphere complexation at all oxide surfaces which yielded a less negative zeta potential.
    1.3. Higher conductivity, due to metal cations in solution, caused both inner-sphere and outer-sphere complexation with metal cations which created a phenomenon called double-layer compression. Double layer compression caused a less negative zeta potential.
    1.4. The mineralogy, silica in particular, had a drastic effect on zeta potential. Different minerals have different zeta potentials at any given pH. Silica has a very negative zeta potential. A higher concentration of silica caused the overall zeta potential of the slurry to be more negative.
    1.5. Starch selectively coated hematite due to structural compatibility (Pradip, 1994). Modified corn starch created a non-ionic coating around hematite thereby suppressing its surface charge. This caused the zeta potential to become more positive.

2. Conductivity was a function of many water chemistry parameters including pH, sodium, potassium, chloride, calcium, and magnesium.
    2.1. On most days, sodium levels throughout the plant varied drastically compared to other ions due to the addition of caustic (NaOH) and glass-H ($(NaPO_3)_{21}*Na_2O$). This caused the conductivity to be nearly directly proportional to the sodium concentration in the process water.
3. Calcium and magnesium present as minerals in the ore were rejected by the deslime thickener but not by the froth flotation cells.
4. pH had a significant effect on both zeta potential and deslime performance.
    4.1. Higher pH caused the surface charge to become more negative. It also caused significant changes in ion types and concentrations in the water.
    For instance, a high pH (>11) caused much of the calcium to be present as aqueous $CaCO_3$ but caused magnesium to be present as $MgOH^+$. The magnesium hydroxide caused unselective flocculation. At a low pH (~10.6), calcium was present as both Ca^{2+} and $CaCO_3$ whereas magnesium was present primarily as aqueous $MgCO_3$. The divalent calcium caused unselective flocculation as well. Depending on the concentrations of magnesium and calcium, there was an ideal pH to maximize overall dispersion.
    4.2. pH had a direct influence on the amount of iron in the deslime underflow. An ideal pH that maximizes overall dispersion will maximize the iron in the underflow while minimizing the iron in the overflow.

4.3. The optimum pH for most calcium and magnesium conditions was near 11. This pH was shown to yield the highest iron recoveries.

4.4. pH had a significant effect on conductivity. As stated previously, pH affected the types of ions present in the water.

5. Particle size control was important for influencing deslime weight rejection. Finer particles tended to be more liberated allowing for easier separation; however, fine particles without adequate flocculation were easily lost in the deslime overflow. This was witnessed on 11/30/2011 when the crushers were shutdown causing overgrinding.
6. Water hardness at the cyclone overflow had a large influence on deslime performance. Higher water hardness caused non-selective flocculation of particles which lead to:

   6.1. Lower deslime recovery

   6.2. Lower magnitude zeta potential
7. Starch did noticeably and reproducibly suppress the surface charge of hematite during both deslime and flotation. This was seen as a decrease in the magnitude of zeta potential upon starch addition. The degree to which starch suppressed zeta potential was dependent upon the water hardness at the time of starch addition. The effect of the starch was consistently more prominent in flotation than desliming due to a higher iron concentration in particles.
8. The addition of CO_2 during dewatering had a significant effect on the pH, conductivity, water hardness, and zeta potential. CO_2 addition causes the initial

formation of carbonic acid (H_2CO_3) which then dissociates to carbonate (CO_3^{2-}) and bicarbonate (HCO_3^-) ions, lowering the pH. The increased ionic content caused an increase in conductivity. The decrease in pH caused calcite and dolomite in the ore to dissolve which yielded an increased water hardness. Both the decrease in pH and the increase in water hardness caused the zeta potential to become less negative.

9. Flux addition caused the zeta potential to equilibrate at ~-20 mV.
10. Maximized deslime iron grade was associated with
    - 10.1. Lower water hardness
    - 10.2. Lower conductivity
    - 10.3. Higher magnitude of deslime feed zeta potential
11. Maximized flotation iron grade was associated with
    - 11.1. Higher water hardness (>8 ppm)
    - 11.2. Higher conductivity
    - 11.3. Lower magnitude of flotation feed zeta potential
12. Flotation iron recovery was largely dependent on deslime iron recovery; therefore, flotation seemed to be capacity limited. An ore of lower grade entering flotation caused higher iron losses; therefore, separation at the deslime thickener is critical to preventing excessive iron loss during flotation.

Based on these results, it has been found that monitoring the water chemistry and zeta potential at the deslime thickener offers the most potential for increasing iron recovery. It was theorized that pH and water hardness at the deslime thickener can be optimized to yield a higher overall recovery. Another way that could potentially increase overall iron

recovery is increasing the water hardness in the flotation feed distributors by adding slaked lime.

2.3.6 Extended Deslime Thickener Analysis

2.3.6.1 Introduction

The major separation processes in the beneficiation plant (desliming, froth flotation, thickening, and filtration) are all dependent on the interactions of particles, which are largely controlled by the Zeta potential of the particles. Measurement and control of the Zeta potential is therefore key to controlling the plant operations and preventing process upsets. Zeta potential can be controlled by adjusting the water quality, adding flocculants or dispersants, or by adjusting the incoming feed ore.

The objectives of this work were to measure process water quality and zeta potential onsite at the mine to determine what process parameters were important for optimizing the iron grade and recovery during deslime thickening. Samples were taken at the feed, overflow, and underflow of the section 7-9 deslime thickeners over the course of one week (5 days). It was important to analyze these samples as soon as possible because it was hypothesized in earlier in the project that the surfaces change over time.

Samples were collected 3 times per day at 3 locations surrounding the deslime thickeners of section 7-9. Samples were tested for water quality parameters including pH, conductivity, calcium, magnesium, sodium, potassium, and oxidation-reduction potential. The solid content of each sample was analyzed for zeta potential (at process conditions), x-ray diffraction, and x-ray fluorescence.

2.3.6.2 Materials and Methods

During the study, process samples were taken and analyzed both onsite at the mine and offsite at Michigan Technological University and an external laboratory. The analyses were used to determine what process parameters were important for optimizing the deslime thickener operation.

2.3.6.2.1 Plant Sampling

Slurry samples were taken on sections 7-9 at 7 AM, 1 PM, and 7 PM between March 17th and March 21st, 2014. The samples were taken at 3 locations: deslime feed (Figure 2.26 location 5), deslime overflow (Figure 2.26 location 6), and deslime underflow (Figure 2.26 location 7). Each sample was obtained in a 500 mL plastic bottle and transported to the analysis laboratory at the mine. The samples were analyzed for zeta potential immediately after collection using a Malvern Zetasizer Nano ZS. The pH, conductivity, calcium hardness ISE value, sodium ISE value, chloride ISE value, and ORP were also measured onsite.

After onsite measurement, the samples were centrifuged and filtered to separate the liquid and solid fractions. The liquid was analyzed for calcium, magnesium, potassium and sodium concentration using inductively coupled plasma optical emission spectroscopy (ICP-OES). The solids were dried and sent an external laboratory for X-Ray diffraction and X-ray fluorescence spectroscopy. Plant process data was collected by mine employees for analysis.

2.3.6.3 Results and Discussion

Due to the enormous amount of data generated during this week-long study, it was important to decide what the most important factors were. As with any mineral processing plant, the product grade and the mineralogical recovery are typically the most important pieces of information. Determining what process parameters have significant influence on product grade and recovery is of utmost importance. This data analysis begins with all of the iron grade and recovery data, see Figure 2.84, and seeks to determine the cause of fluctuations in the grade versus recovery curve.

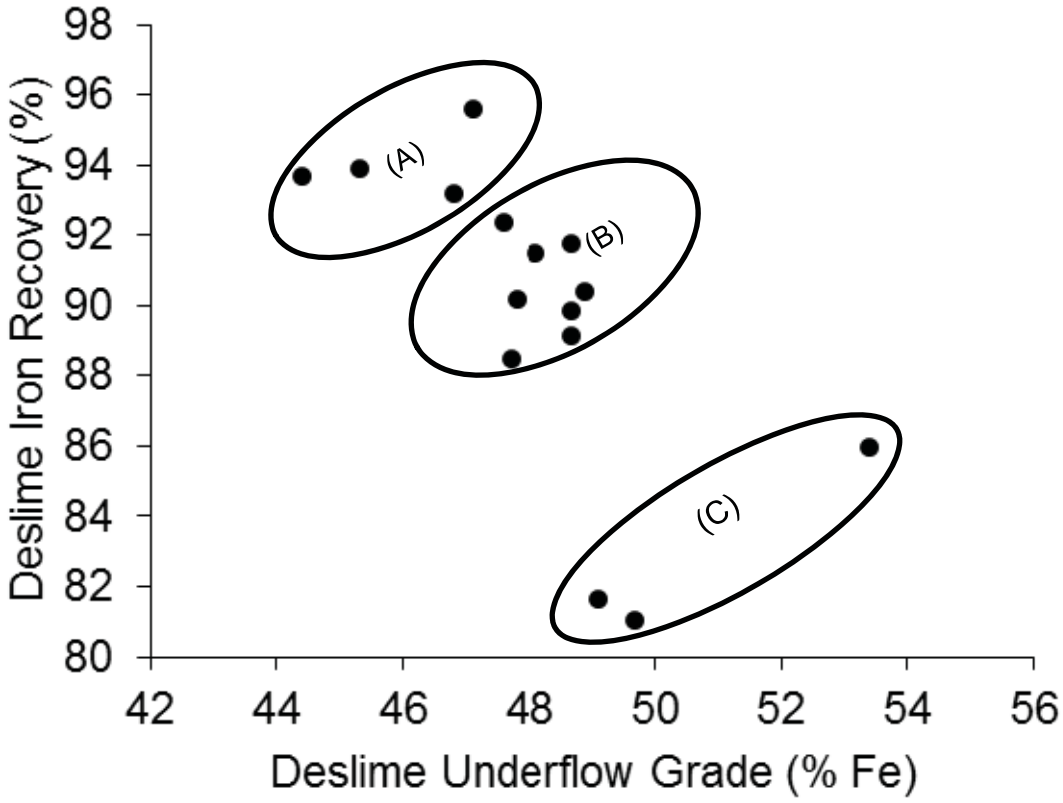

Figure 2.84: Grade versus recovery curve for the deslime thickener during the week of March 17th through March 21st, 2014. Ellipses represent groups of data falling in different operational ranges: (A) Low Fe grade and high Fe recovery, (B) Average Fe grade and recovery, (C) High Fe grade and low Fe recovery.

Strictly targeting either a higher Fe grade or a higher Fe recovery in the deslime thickener is not as important as determining what range of grades and recoveries are conducive to a higher Fe recovery in the entire plant. For example, compare a point in the ellipse labeled (A) in Figure 2.84 and a point in the ellipse labeled (C) in Figure 2.84. Running the deslime thickener in ellipse A will recover more iron at the expense of grade and cause higher iron losses in the flotation circuit, as shown in phase 1. On the other hand, running

the deslime thickener in ellipse C will lose more iron during deslime but less iron will be lost in the flotation circuit. The question is: where is the point on the deslime grade versus recovery curve that is good for the entire plant?

With a continuously changing feed, it may be a better metric to look at an enrichment ratio versus recovery plot to eliminate the effects of changing feed conditions. Enrichment ratio is calculated as follows:

$$enrichment\ ratio = \frac{\%Fe\ in\ Concentrate}{\%Fe\ in\ Feed} \qquad \textbf{\textit{Equation 2.32}}$$

Obviously, if you start with a material with a higher Fe content, you expect to see a higher Fe content in the concentrate. The enrichment ratio versus recovery, as shown in Figure 2.85, essentially shows, essentially, the separation versus the recovery. Just like with the grade versus recovery, higher enrichment ratios are typically accompanied by lower recoveries. However; for these data, it shows that the high grade versus low recovery (ellipse C) was really a combination of high feed grade with low separation efficiency. This can be seen by comparing the horizontal translations of the data points in ellipse C in Figure 2.86. The data points tend to translate left showing a lower than expected enrichment ratio for that grade. The low grade versus high recovery data (ellipse A), when comparing it by enrichment ratio, shows the same trend. This implies that these outliers (points in ellipse A and C) were due to low separation efficiency.

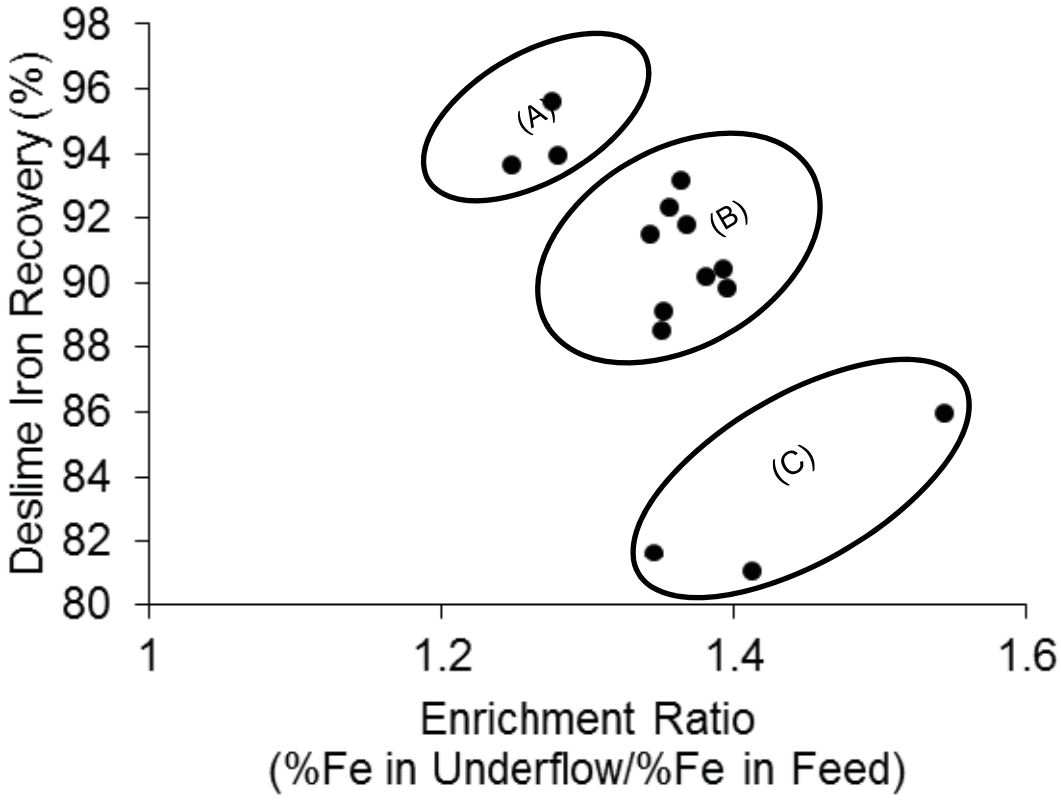

Figure 2.85: Enrichment ratio versus recovery curve for the deslime thickener during the week of March 17th through March 21st, 2014. Ellipses represent groups of data falling in different operational ranges: (A) Low Fe enrichment ratio and high Fe recovery, (B) Average Fe enrichment ratio and recovery, (C) High Fe enrichment ratio and low Fe recovery.

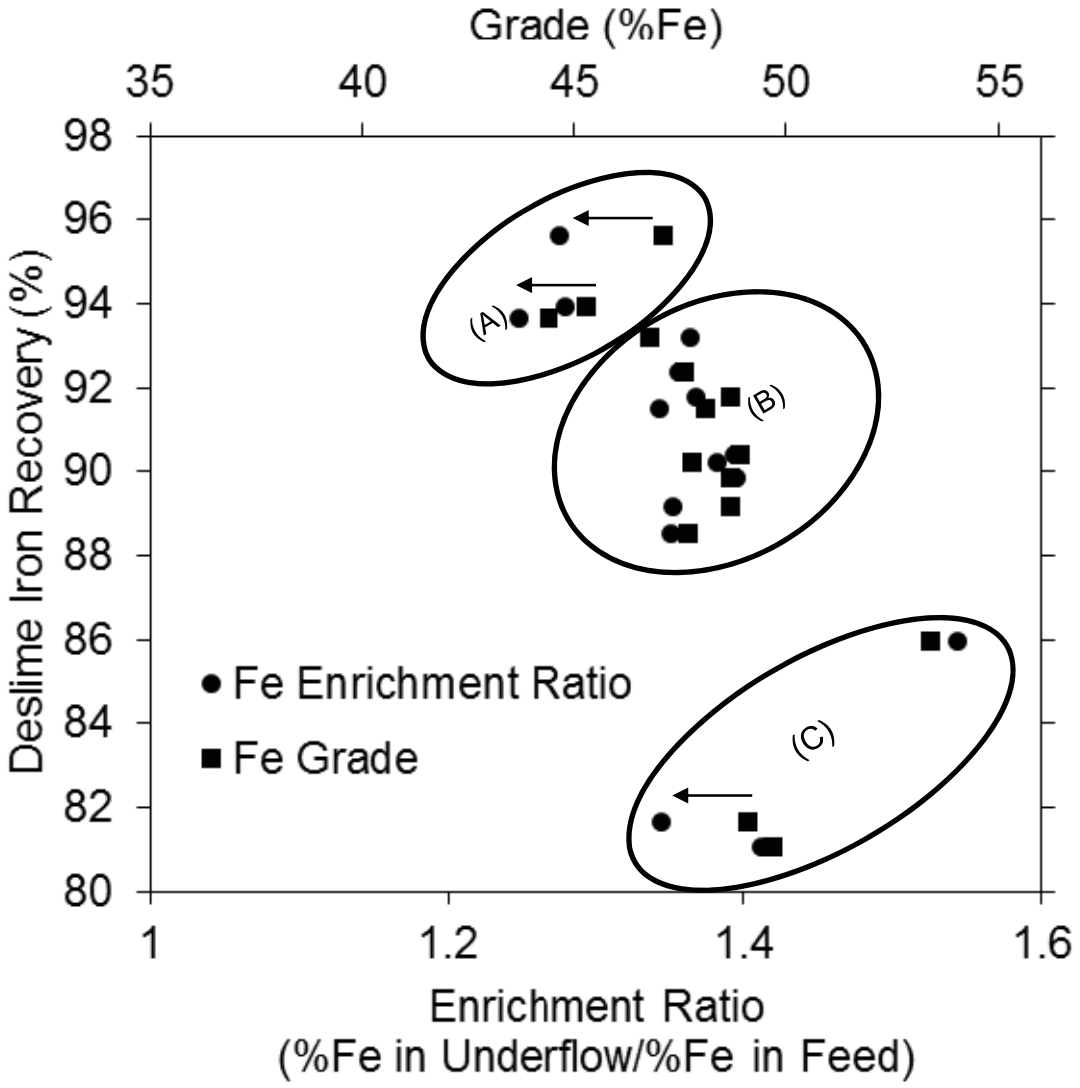

Figure 2.86: Enrichment ratio and grade versus recovery curve for the deslime thickener during the week of March 17th through March 21st, 2014. Ellipses represent groups of data falling in different operational ranges: (A) Low Fe enrichment ratio and grade with high Fe recovery, (B) Average Fe enrichment ratio, grade, and recovery, (C) High Fe enrichment ratio and grade with low Fe recovery. Horizontal arrows indicate instances during which the grade was superficially high compared to the enrichment ratio due to high Fe grade in the feed.

Going back to the proposed fundamental question; the data points in ellipse B have very little translation when comparing concentrate grade and enrichment ratio. This means that the operational parameters seen during these times are the most conducive to higher overall plant recoveries. The next question is: what are these operational parameters and what needs to be done to maintain them? To answer that question, it is necessary to look at the differences between operations in ellipses A, B and C.

2.3.6.3.1 Ideal Process Parameters Targeting Recovery

As seen in phase one of this project, there are many factors that can influence Fe recovery in the deslime thickener. The key parameters from a water and surface chemistry standpoint are the zeta potential, pH, water hardness (Ca +Mg), and the conductivity. These parameters are summarized in Table 2.7.

Table 2.7: Operational parameters found to be important during phase 2 of the project relating to the iron recovery during deslime thickening. The operational parameter values were averaged for each recovery range.

	Deslime Feed Conditions						Underflow % Solids
Deslime Fe Recovery	**Zeta Potential (mV)**	**pH**	**Ca (ppm)**	**Mg (ppm)**	**Na (ppm)**	**Conductivity (mS/cm)**	
High (>93%, ellipse A in Figure 2.84)	-37.3	10.88	5.0	1.8	567.6	2.69	54.94
Mid (86-93%, ellipse B in Figure 2.84)	-36.2	10.95	3.2	1.6	559.1	2.68	54.70
Low (<86%, ellipse C in Figure 2.84)	-36.9	10.88	3.6	2.1	562.8	2.68	52.99

It was found that lower values of zeta potential (magnitude) typically caused destabilization of the slurry. On a theoretical basis, this should result in a higher recovery with a less selective separation. The zeta potentials reported in Table 2.7 are the feed zeta potentials after starch addition. From the conclusions in phase 1, low zeta potential magnitudes occurred because calcium adsorbed to all surfaces causing non-selective flocculation when starch was added. This can be counteracted by higher dispersant

addition. From the data shown in Table 2.7, the lowest magnitudes of zeta potential resulted in the points seen in ellipse B in Figure 2.84. From a recovery standpoint, having a low feed zeta potential is conducive to better recoveries without a loss in enrichment ratio.

The pH is a very important parameter for three reasons: (1) high pH results in a higher dispersive stability. This results in a higher level of dispersion between gangue minerals and iron oxides causing a higher chance that iron oxides will flocculate selectively. (2) It has been reported that starch is more effective in a particular pH range. Results from a study performed by Weissenborn (1996) are shown in Figure 2.87 depicting this range. This study reported that as pH was increased above 10, the recovery declined; however, the grade increased. And (3), as depicted in Figure 2.24 a and b, the pH range between 10.8 and 11.1 was ideal to allow free calcium and magnesium ions to complex with carbonate and sulfate ions which limits their surface interactions. To recap, high pH was good for dispersive stability, a pH higher than 10 limited starch activity, and a pH between 10.8 and 11.1 was ideal to limit calcium and magnesium ionic effects on surfaces. According to the data presented in Table 2.7, higher pH values put the process in the mid-range for recovery at an acceptable grade (ellipse B in Figure 2.84).

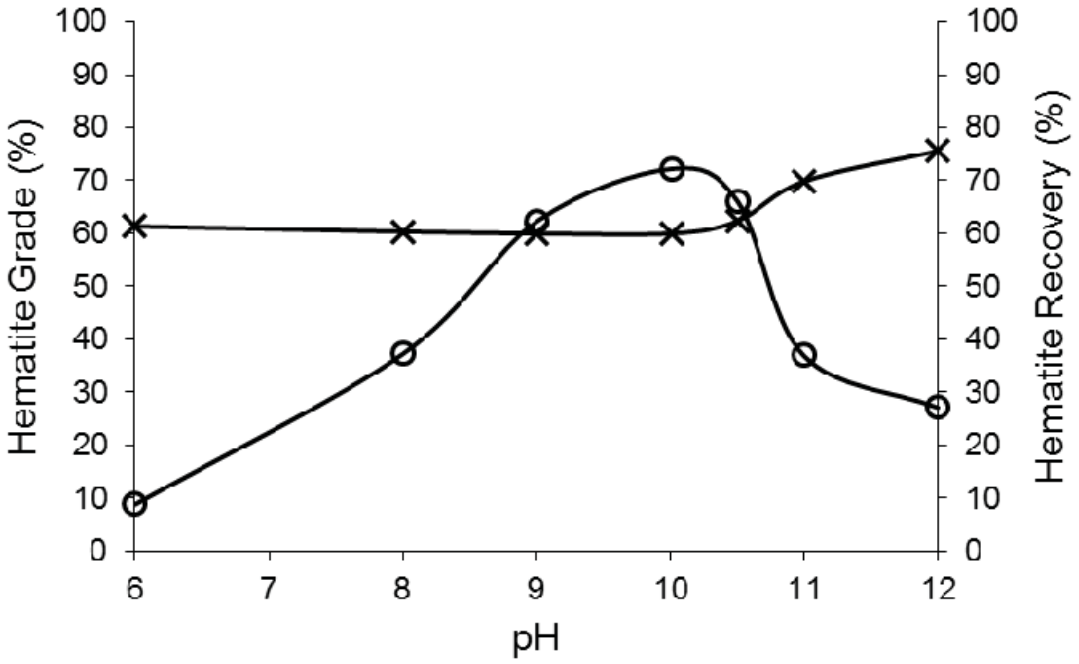

Figure 2.87: Iron grade and recovery during selective flocculation and dispersion of an ultrafine (9-% passing at 13.8µm) iron ore. Feed hematite grade was 53.2%. Starch with a 74% amylopectin and 26% amylose content was used at 50 mg/L as a selective flocculant. Adapted from Weissenborn (1996).

Another important parameter is the water hardness. This is typically a function of the calcium and magnesium concentration within the process water. Water hardness contributes to non-selective flocculation. This is good for iron recovery but detrimental to the separation. As seen in Table 2.7, the higher recoveries seen in ellipse A in Figure 2.84 were associated with high calcium concentration. The recoveries in the 91% (Figure 2.84, ellipse B) range were associated with the lowest calcium and magnesium concentrations. The recoveries in the 83% (Figure 2.84, ellipse C) range had moderately low calcium and

magnesium concentrations but other process parameters were found to be the cause of these low recoveries.

Finally, the last two parameters presented in Table 2.7 are sodium concentration and conductivity. In phase 1, a strong correlation was found between sodium concentration and conductivity. The sodium concentration in this plant varies drastically due to the use of caustic for pH adjustment. Sodium causes double-layer compression at the surfaces of the mineral particles. This can diminish zeta potential (as seen in Figure 2.21) and result in less effective reagent adsorption. At a pilot scale (discussed later) it was found that sodium concentration was a key parameter for increasing both the grade and recovery of the process. Lower sodium concentrations correlated to better grades and recoveries. This is also shown in Table 2.7 for the plant data. The values of sodium in ellipse B of Figure 2.84 were lower than those in ellipse A and C.

One of the key process parameters that was found during this study was the deslime underflow density. The deslime underflow density averaged around 55% solids except for the Figure 2.84 ellipse C data. These points of low recovery were associated with low underflow densities at around 50% solids. This could have been due to low solids concentration in the feed, too high of an underflow flow rate or over-dispersion of the pulp. In any case, the underflow density was the biggest outlier in the data set at these times of low recovery.

2.3.6.3.2 Ideal Process Parameters Targeting Grade

Targeting a particular grade is another way to evaluate process performance. Table 2.8 shows the same process parameters for high (>49% Fe), low (<47% Fe) and mid-level deslime underflow grades. Just as with recovery, a higher grade is not necessarily a good thing because it is typically accompanied by a lower recovery. The best plant performances were found when the grade was in the mid-range because these times also had mid-range recoveries. By comparing Table 2.8 to Table 2.7, it is apparent that the best operational parameters to achieve these mid-range grade values are similar to those when pursuing the mid-range recoveries. These include:

- Low magnitude of zeta potential
- High pH
- Low calcium
- Low magnesium
- Low sodium
- Low conductivity

Table 2.8: Operational parameters found to be important during phase 1 of the project relating to the deslime underflow iron grade. The operational parameter values were averaged for each grade range.

	Deslime Feed Conditions					
Deslime Underflow Fe Grade	**Zeta Potential (mV)**	**pH**	**Ca (ppm)**	**Mg (ppm)**	**Na (ppm)**	**Conductivity (mS/cm)**
High (>49% Fe)	-36.9	10.88	3.6	2.1	562.8	2.68
Mid (47-49% Fe)	-36.0	10.96	3.2	1.6	558.0	2.68
Low (<47% Fe)	-38.0	10.86	5.1	1.9	570.8	2.70

2.3.6.3.3 Ideal Process Parameters Targeting Enrichment Ratio

Targeting a high enrichment ratio is a better way to evaluate process performance than targeting grade, at least in the deslime thickener. Enrichment ratio allows the removal of feed ore inconsistencies from the evaluation, and, since flotation is used to reach the final grade, having the highest grade at the deslime underflow is not as critical as reducing iron loss. Table 2.9 shows the same process parameters for high (>1.4), low (<1.3) and mid-level deslime enrichment ratios. Just as with grade and recovery, a higher enrichment ratio is not necessarily a good thing because it is typically accompanied by a lower recovery. The best plant performances were found when the enrichment ratio was in the mid-range because these times also had mid-range recoveries. By comparing Table 2.9 to Table 2.7 and Table 2.8 it is apparent that the best operational parameters to achieve these mid-range enrichment ratios are similar to those when pursuing the mid-range recoveries. An exception to this is the zeta potential. When targeting enrichment ratio, the

zeta potential did not seem to have a large effect. The targets for the process parameters outlined in Table 2.9 include:

- High pH
- Low calcium
- Low magnesium
- Low sodium
- Low conductivity

Table 2.9: Operational parameters found to be important during phase 1 of the project relating to the iron enrichment ratio. The operational parameter values were averaged for each enrichment ratio range.

	Deslime Feed Conditions					
Deslime Enrichment Ratio	**Zeta Potential (mV)**	**pH**	**Ca (ppm)**	**Mg (ppm)**	**Na (ppm)**	**Conductivity (mS/cm)**
High (>1.4)	-36.1	10.91	3.7	2.1	574.7	2.73
Mid (1.3-1.4)	-36.5	10.95	3.2	1.6	555.2	2.66
Low (<1.3)	-37.3	10.88	5.0	1.8	567.6	2.69

2.3.6.4 Conclusions

The objectives of this work were to measure process water quality and zeta potential onsite at the mine to determine what process parameters were important for optimizing the iron grade and recovery during deslime thickening. It was determined that the best

conditions for optimizing both iron grade and recovery during the deslime thickening process include:

1. Low magnitude of zeta potential
2. High pH
3. Low calcium concentration in process water
4. Low magnesium concentration in process water
5. Low sodium concentration in process water
6. Low conductivity in process water

These conditions, when present in the plant, were effective at increasing the grade, recovery and enrichment ratio of iron in the process. To verify these findings, a pilot scale study was performed that assessed the effects of calcium concentration, magnesium concentration, sodium concentration and pH on the zeta potential, iron grade obtainable and iron recovery during deslime thickening.

Finely ground hematite ore was suspended in a solution of simulated process water at varying pH, sodium concentration, calcium concentration and magnesium concentration. Cooked acid modified corn starch was used as a selective hematite flocculant and a Glass-H was used as a dispersant. The following conclusions were drawn from this study:

1. A pH between 10 and 11 yields the highest iron grade and recovery. At lower pH values, the recovery drops significantly.

2. Lower sodium concentrations yielded both a higher grade and a higher recovery of iron. Decreasing sodium in the process water could substantially affect the process performance.
3. Calcium acts as a nonselective flocculant. Higher calcium concentrations decrease grade but improve recovery while lower calcium concentrations increase grade but decrease recovery.

Another set of experiments was performed in the pilot scale thickener assessing six different types of dispersants. The six dispersants tested included sodium silicate, Glass-H (21-member sodium polyphosphate), a mixture of both sodium silicate and Glass-H, 2,000 MW polyacrylic acid, 4,000 MW polyacrylic acid, and 7,000 MW polyacrylic acid. The dosages of the dispersants were selected based upon operational data from the mine and from manufacturer recommendations.

Of the inorganic dispersants tested, Glass-H yielded the best grade/recovery curve for iron and was able to reject the most phosphorus during desliming. Sodium silicate and a mixture of the two dispersants did not yield grade/recovery curves comparable to that of Glass-H alone. The sodium silicate seemed to lessen the dispersive ability of the Glass-H.

All three polyacrylic acids, varying in molecular weight from 2,000 to 7,000 Da, performed nearly identically in the process for both iron recovery and phosphorus rejection. It was found that Glass-H, at 0.05 lb/ton of ore, yielded the best grade/recovery curve for iron; however, 0.25 lb/ton 4000 MW PAA was able to reject up to 40% more

phosphorus with concentrate phosphorus concentrations as low as 0.022%. The iron grade/recovery curve for the Glass-H was only slightly better than the 4000 MW PAA.

The following recommendations can be made from this study:

1. Lowering sodium concentration within the plant should increase both the grade and recovery of iron. This can be accomplished by switching from caustic to calcium hydroxide as a pH modifier. This will require a higher dispersant dose to account for the excess calcium in the process water.
2. Maintaining a high pH (10.9 – 11.0) during desliming seemed to produce the highest iron grade and recovery.
3. Switching from Glass-H to a low molecular weight (2000-7000 DA) polyacrylic acid at the proper dose may increase phosphorus rejection. A study should be performed to determine if PAA can be used economically in the plant. If an economical dose is achieved, nearly all liberated phosphorus can be rejected during deslime thickening.
4. Monitoring conductivity will be more important if caustic is replaced with calcium hydroxide as a pH modifier. Conductivity is a good measure of sodium concentration and seen in previously in this project.

2.3.7 References

ASTM, 2006, *D1971-02 Standard Practices for Digestion of Water Samples for Determination of Metals by Flame Atomic Absorption, Graphite Furnace Atomic*

Absroption, Plasma Emission Spectroscopy, or Plasma Mass Spectroscopy, Water and Environmental Technology, ASTM International, Pennsylvania.

ASTM, 2010a, *D511-09 Standard Test Methods for Calcium and Magnesium in Water,* Water and Environmental Technology, ASTM International, Pennsylvania.

ASTM, 2010b, *D512-04 Standard Test Methods for Chloride Ion in Water,* Water and Environmental Technology, ASTM International, Pennsylvania.

ASTM, 2010c, *D1068-05 Standard Test Methods for Iron in Water,* Water and Environmental Technology, ASTM International, Pennsylvania.

ASTM, 2010d, *D4192-08 Standard Test Method for Potassium in Water by Atomic Absorption Spectrophotometry,* Water and Environmental Technology, ASTM International, Pennsylvania.

Balajee, S. R., and Iwasaki, I., 1969, "Adsorption Mechanism of Starches in Flotation and Flocculation of Iron Ores," *AIME Transactions,* Vol. 244, pp. 401-406.

O'Brien, Robert J., Ajoy Raje, Robert L. Spicer, Liguang Xu, Shiqi Bao, Scott Lambert, and Burtron H. Davis. "Technology Development for Iron Fischer-Tropsch Catalysts." *Proceedings of the First Joint Power & Fuel Systems Contractors Conference,* Pittsburgh, PA. 1996.

Dzombak, D. A., and Morel, F., 1990, *Surface complexation modeling : hydrous ferric oxide,* Wiley, 393 pp.

Eggleston, C. M., and Hochella, M. F., 1992, "The Structure of Hematite (001) Surfaces by Scanning Tunneling Microscopy - Image Interpretation, Surface Relaxation, and Step Structure," *American Mineralogist,* Vol. 77, No. 9-10, pp. 911-922.

Haselhuhn, H. J., Carlson, J. J., and Kawatra, S. K., 2012a, "Water chemistry analysis of an industrial selective flocculation dispersion hematite ore concentrator plant," *International Journal of Mineral Processing,* Vol. 102–103, pp. 99-106.

Haselhuhn, H. J., Swanson, K. P., and Kawatra, S. K., 2012b, "The effect of CO_2 sparging on the flocculation and filtration rate of concentrated hematite slurries," *International Journal of Mineral Processing,* Vol. 112-113, pp. 107-109.

Keranen, C. U., 1986, “Reagent Preparation, Distribution and Feeding Systems at the Tilden Mine,” *Design and Installation of Concentration and Dewatering Circuits,* A. L. Mular and M. A. Anderson eds., Society for Mining, Metallurgy and Exploration, pp. 308-319.

Kinniburgh, D. G., and Jackson, M. L., 1982, "Concentration and pH dependence of calcium and zinc absorption by iron hydrous oxide gel," *Soil Science Society of America Journal,* Vol. 46, No. 1, pp. 56-61.

Kinniburgh, D. G., Jackson, M. L., and Syers, J. K., 1976, "Adsorption of Alkaline Earth, Transition, and Heavy Metal Cations by Hydrous Oxide Gels of Iron and Aluminum," *Soil Science Society of America Journal,* Vol. 40, No. 5, pp. 796-799.

Knovel, 2003, *Knovel Critical Tables (2nd Edition),* Knovel.

Laskowski, J. S., and Ralston, J., 1992, *Colloid Chemistry in Mineral Processing,* Elsevier Science, 428 pp.

Pradip, 1994, "Reagents Design and Molecular Recognition at Mineral Surfaces," *Reagents for Better Metallurgy,* Society for Mining Metallurgy, pp. 245-252.

Pyykkö, P., and Atsumi, M., 2009, "Molecular Single-Bond Covalent Radii for Elements 1–118," *Chemistry – A European Journal,* Vol. 15, No. 1, pp. 186-197.

Ralph, J., and Chau, I., 2014, "Chicagon mine, Menominee iron range, Iron Co., Michigan, USA," Mindat.org, http://www.mindat.org/loc-3840.html, Accessed: 12/16/2014

Sparks, D. L., and Grundl, T. J., 1998, *Mineral-Water Interfacial Reactions,* American Chemical Society, 438 pp.

Stumm, W., Sigg, L., and Sulzberger, B., 1992, *Chemistry of the solid-water interface,* Wiley, 448 pp.

Weissenborn, P. K., 1996, "Behaviour of amylopectin and amylose components of starch in the selective flocculation of ultrafine iron ore," *International Journal of Mineral Processing,* Vol. 47, No. 3-4, pp. 197-211.

3 Effects of Reagent Selection on Dispersion and Selective Flocculation of Hematite Ore

3.1 Effects of Dispersant Adsorption on Settling Behavior of Iron Ore [5]

3.1.1 Abstract

The settling behavior of ground hematite-rich iron ore at a pH of 11 was assessed in the presence of aqueous calcium; sodium silicate, sodium tripolyphosphate (STPP), sodium hexametaphosphate (SHMP) and sodium henicosapolyphosphate (Glass-H) inorganic dispersants; and Ethylenediaminetetraacetic acid (EDTA). Without calcium, the inorganic dispersants had no effect on the dispersive stability of the ore. This suggests that the inorganic dispersants do not adsorb to the oxide surfaces at a pH of 11 due to their inability to displace the negatively charged hydroxyl groups at the oxide-water interface. In the absence of calcium, EDTA was found to increase the dispersion of the ore, suggesting EDTA adsorption to hydrated iron oxide without the presence of positively charged surface sites. Calcium was found to lower the dispersive stability of the ore by flocculating fine particles.

[5] Some of the material contained in this chapter was previously published in the journal *"Minerals and Metallurgical Processing."* It is included in this dissertation with permission from the journal.
Citation:
Haselhuhn, H. J., 2013, "Dispersant Adsorption and Effects on Settling Behavior of Iron Ore," *Minerals & Metallurgical Processing,* Vol. 30, No. 3, pp. 188-189.

In the presence of 20 ppm of aqueous calcium, each dispersant affected the dispersive stability of the iron ore differently. Sodium silicate caused little to no dispersion in the presence of 20 ppm calcium. All of the phosphate based dispersants effectively re-dispersed the ore in the presence of 20 ppm calcium. EDTA caused further flocculation of the ore in the presence of 20 ppm calcium. It has been concluded that inorganic dispersants require positively charged surface sites, such as calcium inner-sphere complexes, to adsorb and cause dispersion of an iron ore pulp at a pH of 11. EDTA only causes dispersion without positively charged surface site. The order of dispersant effectiveness from lowest to highest in the presence of 20 ppm calcium at a pH of 11 was found to be Ethylenediamenetetraacetic acid (EDTA) < sodium silicate < sodium tripolyphosphate (STPP) < sodium henicosapolyphosphate (Glass-H) < sodium hexametaphosphate(SHMP).

3.1.2 Introduction

Many reagents are added to enhance the separation of iron oxide from its impurities in iron ore concentration processes. While processing fine (< 50 μm liberation size) non-magnetic ores, such as hematite, the process relies on selective flocculation and dispersion followed by reverse flotation to produce a concentrated iron oxide product (Green et al., 1984). Selective flocculation and dispersion relies on several reagents to effectively separate iron ore particles based on mineralogy. These reagents adsorb to the particle surfaces causing a change in surface chemistry that either flocculates or disperses the ore particles. An overall dispersant, such as those shown in Table 3.1, is used to disperse iron ore particles from the gangue minerals present in the ore (Green et al., 1984;

Potapova et al., 2011). A selective flocculant, such as corn starch or a polyacrylamide, is used to selectively flocculate iron oxide particles (Green et al., 1984; Iwasaki, 1989). The flocs of iron oxide particles sink while the dispersed gangue minerals are rejected in the overflow. The effectiveness of reagent adsorption onto particle surfaces is critical during desliming to promote effective selective flocculation and dispersion.

Table 3.1: Chemical names and structures of common dispersants used in iron ore concentration processes.

Chemical Name	Trade Name	Chemical Formula	Structure
Sodium Silicate	Water Glass	Na_2SiO_3	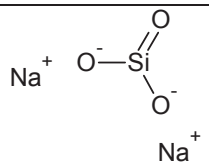
Sodium Tripoly-phosphate	STPP	$Na_5P_3O_{10}$	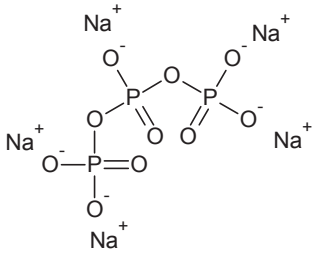
Sodium Hexameta-phosphate	SHMP	$Na_6P_6O_{18}$	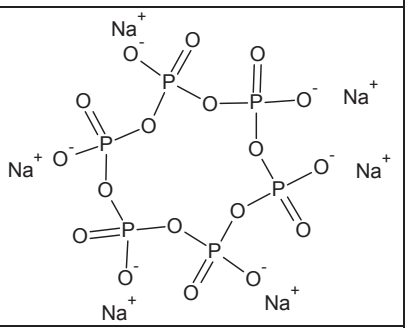
Sodium Henicosa-polyphosphate	Glass-H	$Na_{23}P_{21}O_{64}$	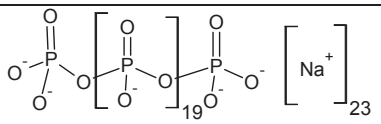
Ethylene-diamine-tetraacetic Acid	EDTA	$Na_4C_{10}H_{12}N_2O_8$	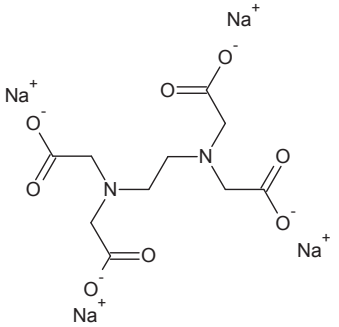

The mechanisms of ion adsorption to iron oxide and silica surfaces have been widely established. An ion will adsorb to a hydrated metal oxide surface via either an outer-

sphere complex or an inner-sphere complex as shown in Figure 3.1. An outer-sphere complex is an ion drawn to an oppositely charged surface by electrostatic attraction. The ion does not form a bond with the surface and is surrounded by one or more water molecules. An inner-sphere complex is an ion that is chemically adsorbed to the surface. Inner-sphere complexes can drastically alter the surface charge and zeta potential of the metal oxide (Potapova et al., 2011).

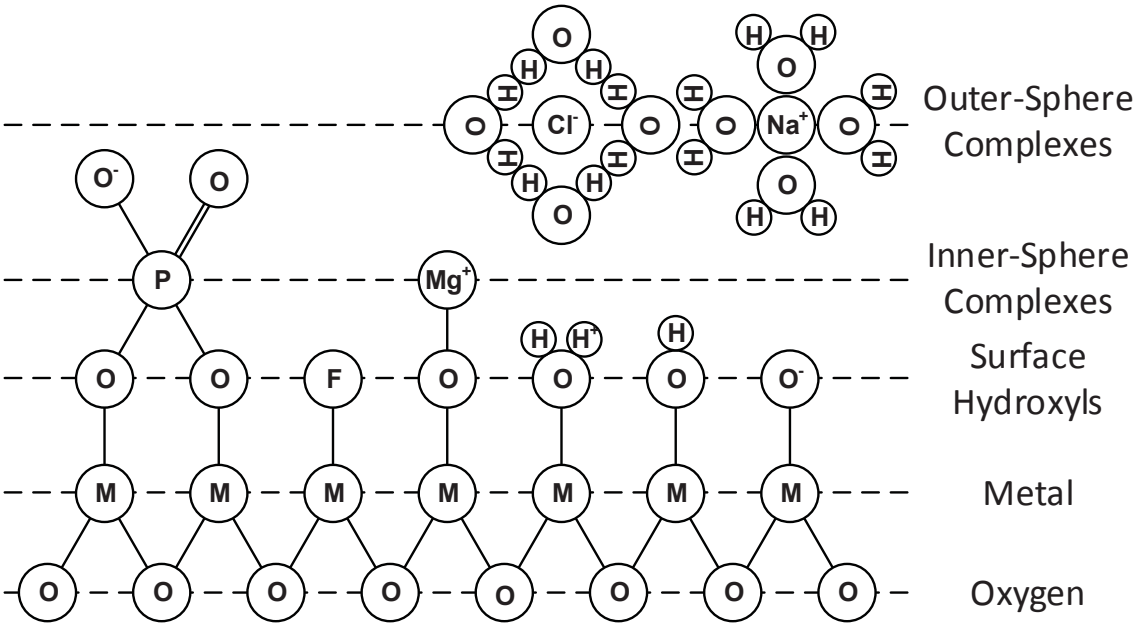

Figure 3.1: Surface complex formation at the metal-oxide/water interface. Adapted from (Stumm et al., 1992).

Adsorption of both anions and cations to hydrated iron oxide surfaces are a function of pH as shown in Figure 3.2. At any given pH, certain ions are adsorbed more readily than others. For instance, at a pH of 6.5, the extent of adsorption of anions on hydrated iron oxide decreases as follows: $H_3SiO_4^- > H_2PO_4^- > MoO_4^{2-} > SO_4^{2-} > Cl^- = NO_3^-$ (Ryden et

al., 1987; Stumm et al., 1992). In general, at a low pH, the surface is positively charged and attracts anions that can either form inner-sphere or outer-sphere complexes. At a higher pH, the surface carries a negative charge and attracts cations that can form inner-sphere or outer-sphere complexes.

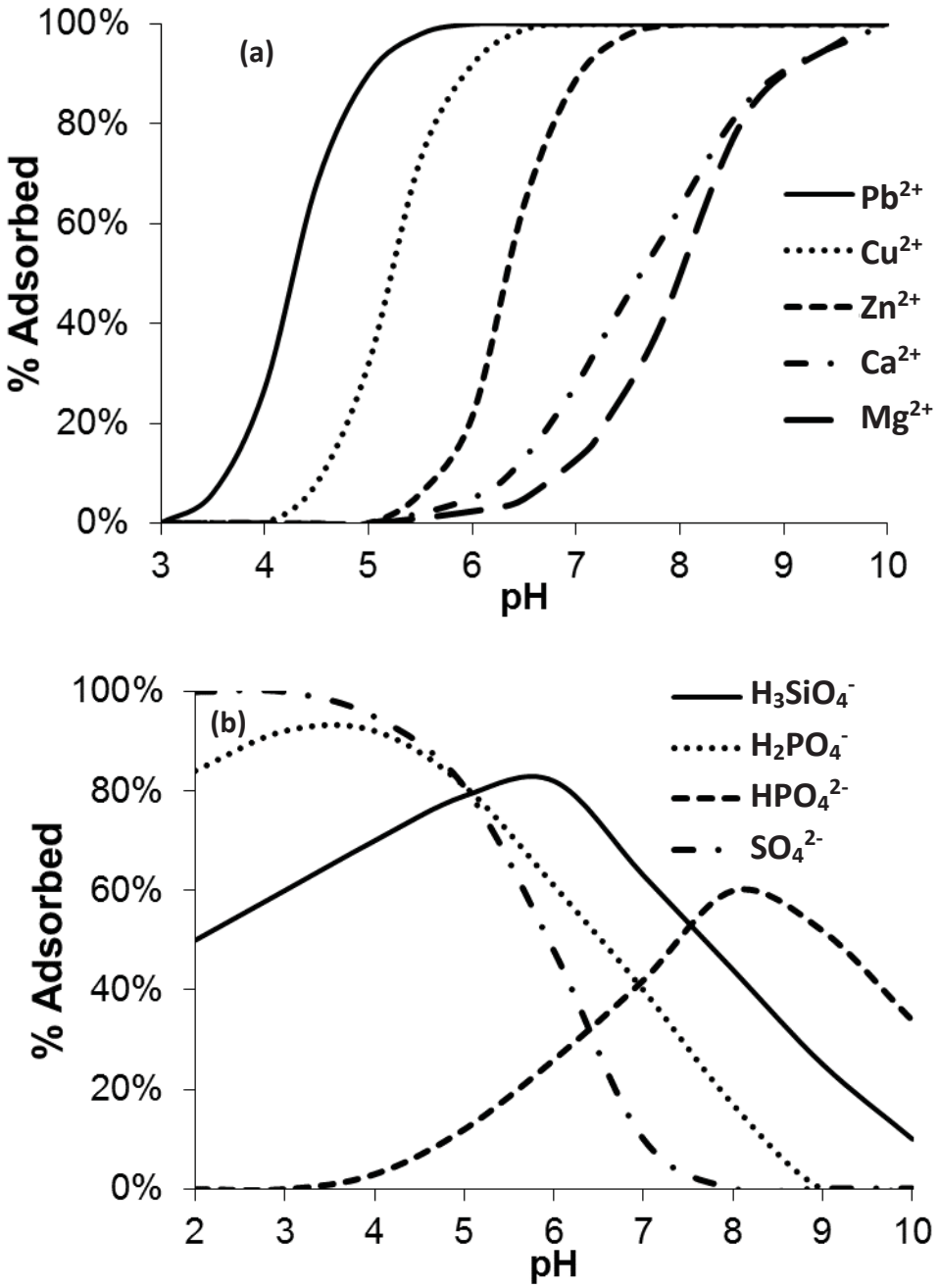

Figure 3.2: pH dependance of cation (a) and anion (b) adsorption (inner-sphere complexation) on hydrated iron oxide surfaces (Dzombak et al., 1990; Kinniburgh et al., 1976; Stumm et al., 1992)

Concentration processes that separate hematite, goethite and/or magnetite from siliceous gangue minerals typically use reverse cationic flotation as their primary means of separation. To maximize dispersion in these processes, sodium hydroxide is used to adjust their pH to between 10.5 and 11 (Benner et al., 1994). In an alkaline environment such as this, adsorption of dispersive anions (silicates and polyphosphates) to hydrated oxide surfaces can be limited due to the highly negative charge of the hydrated oxide surfaces. Even in these highly alkaline process conditions, dispersion is still accomplished with the aforementioned dispersants. There are three possible reasons for this phenomenon:

- The dispersive anions coat surfaces with inner-sphere complexes, displace hydroxyl groups at the surface, and decrease the surface charge of all particles
- The anions form stable complexes with calcium and magnesium in solution, withdrawing them from the particle surfaces, thereby decreasing the surface charge of all particles (Ding et al., 2007)
- The anions form stable surface complexes with positively charged calcium and magnesium inner-sphere complexes at the surface. This neutralizes calcium and magnesium surface complexes and decreases the surface charge causing dispersion of particles (Green et al., 1984)

Illustrations for these methods of dispersion in alkaline conditions using a polyphosphate as an example are shown in Figure 3.3.

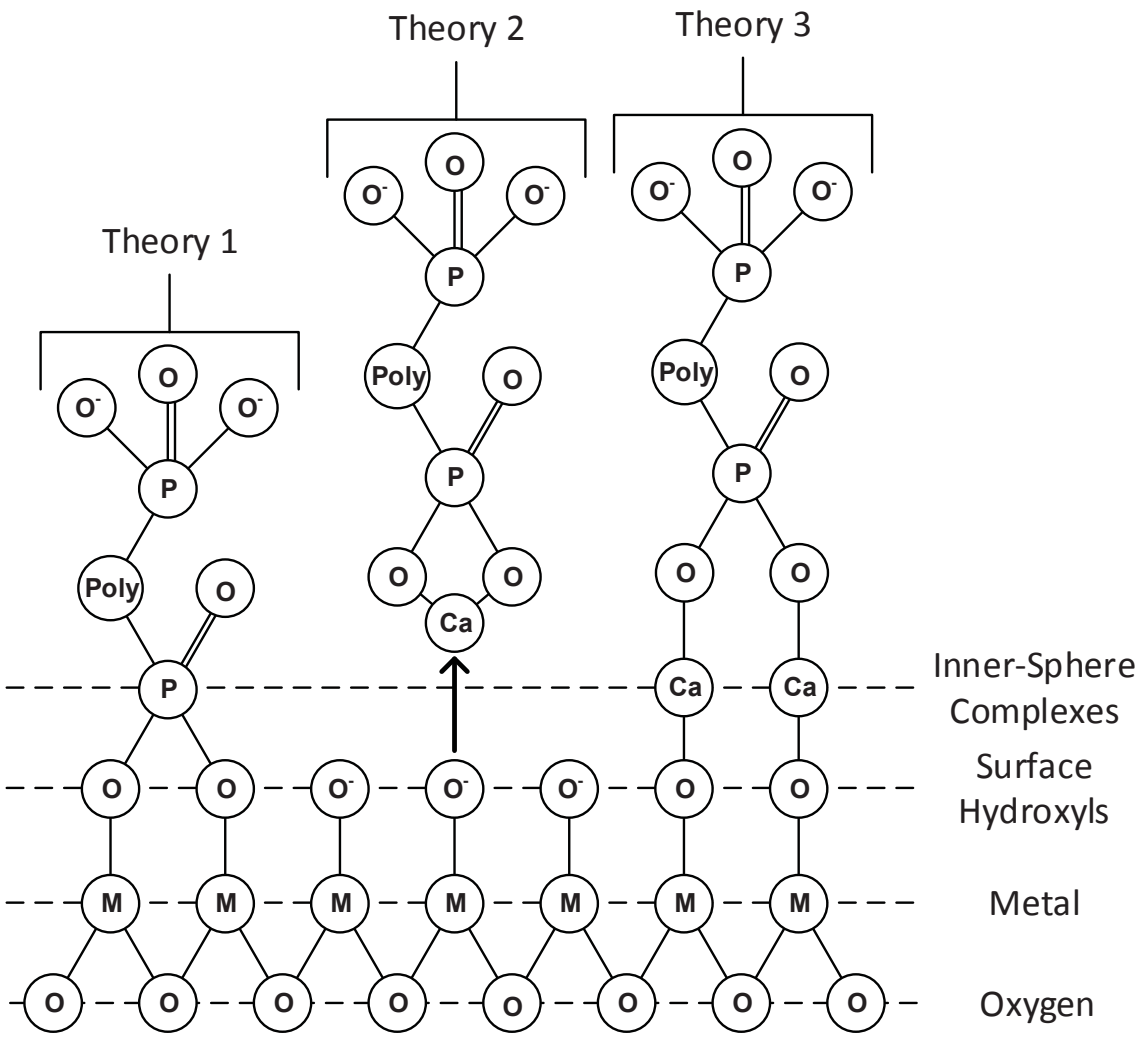

Figure 3.3: Illustrations of the 3 theories behind dispersant action at metal oxide surfaces.

Settling behavior is a good indication of the dispersive stability of a slurry of charged particles. Particles that are highly dispersed will settle very slowly, if at all. Particles that are flocculated will settle quickly. Settling rate can be determined by monitoring the total suspended solids concentration over time. As solids settle, the totals suspended solids concentration will decrease. Total suspended solids concentration can be measured by

UV/VIS spectroscopy at 810 nm with an appropriate linear calibration (Hach, 2010; Krawczyk et al., 1959).

3.1.3 Materials and Methods

The iron ore that was used was sampled at a local hematite concentrator at a location between the grinding circuit and the deslime thickeners. X-ray diffraction patterns show the presence of quartz (SiO_2), magnetite (Fe_3O_4), hematite (Fe_2O_3), as well as trace amounts of siderite ($FeCO_3$) and dolomite ($CaMg(CO_3)_2$), as shown in Figure 3.4. Elemental analysis on the dried solid particles was conducted by acid digestion and atomic absorption spectroscopy (ASTM, 2006). The results of the elemental analysis are shown in Table 3.2. Particle size analysis using a Microtrac™ laser scattering particle size analyzer yielded an 80% passing size of 30.99 μm.

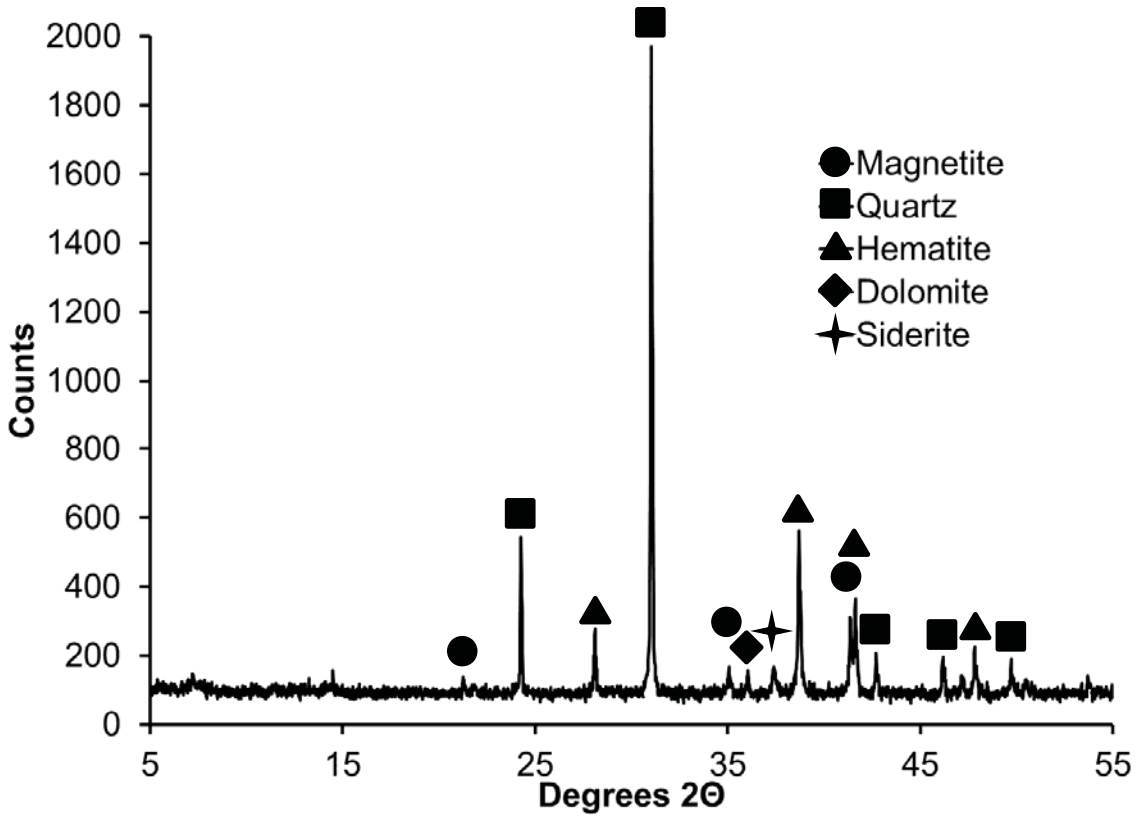

Figure 3.4: XRD patterns of iron ore used for dispersant study with major peaks identified.

Table 3.2: Elemental analysis of iron ore used in this study

Constituent	Assay
Iron	38.52%
Calcium	0.29%
Magnesium	0.30%
Acid Insolubles	40.79%

Samples of filtered, dried iron ore were split using a micro-rotary riffle splitter into representative 1 gram splits. The 1 gram splits were then hydrated and sealed for 24 hours

with distilled water adjusted to a pH of 11 with NaOH. Upon hydration, a 1 gram sample was added to a 250 mL plastic beaker with 200 mL of distilled water that was adjusted previously to a pH of 11 with NaOH. A small laboratory stand mixer with a plastic impeller and shaft was used to keep the particles in solution suspended. Plastic laboratory equipment was used to prevent any surface adsorption to laboratory instruments. During experiments requiring the use of calcium, a 4.5 g/L (as Ca^{2+}) solution of calcium chloride was added using an adjustable pipette. Dispersants were added in a similar manner using 1 g/L solutions of their solid anhydrous sodium salts. The dispersant dosage (0.1 lb/ton and 0.2 lb/ton) was chosen to be a comparable value that has been used in the local iron ore concentrator that provided the iron ore sample.

The effectiveness of dispersants was determined by measuring total suspended solids concentration in a 3 mL sample of the mixed slurry using a 5 minute time lapse UV/VIS measurement at 810 nm. A Hach DR5000™ UV/VIS spectrophotometer was used in a time-lapse mode with 10mm light path cuvettes for this test. Each measurement was made in triplicate to ensure accuracy and statistical significance of data. The raw data was normalized linearly to a distilled water trial in order to make direct comparisons between trials. The absorbance at 810 nm was calibrated by comparison to gravimetric total suspended solids measurements using various concentrations of the iron ore in distilled water at a pH of 11.

3.1.4 Results and Discussion

Each dispersant showed differing levels of dispersive ability for the ground iron ore at a pH of 11. Settling behavior evaluations for varying doses of sodium silicate (Na_2SiO_3)

are shown in Figure 3.5. Without calcium in the slurry, the dispersive stability remains constant at the same level as distilled water regardless of sodium silicate dose. This shows that the adsorption theory in which the anion displaces the hydroxyl groups does not apply (theory 1 described above) in these conditions. When calcium is added at 20 ppm, the dispersive stability is lowered drastically. This is due to the addition of positively charged calcium inner-sphere complexes to the negatively charged hydroxyl groups causing flocculation of once-suspended particles. When sodium silicate is added as a dispersant to the calcium-rich slurry, the dispersive stability is unchanged. This shows that sodium silicate is not an effective dispersant at these doses for a slurry containing 20 ppm calcium.

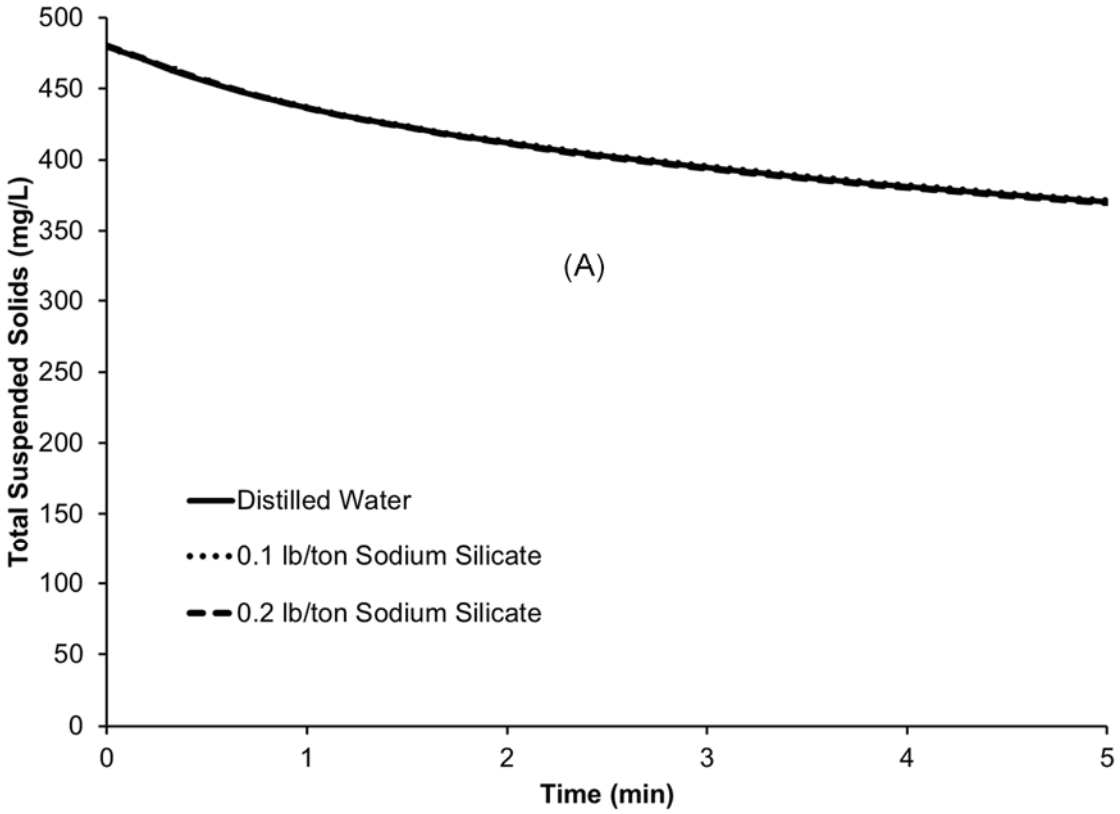

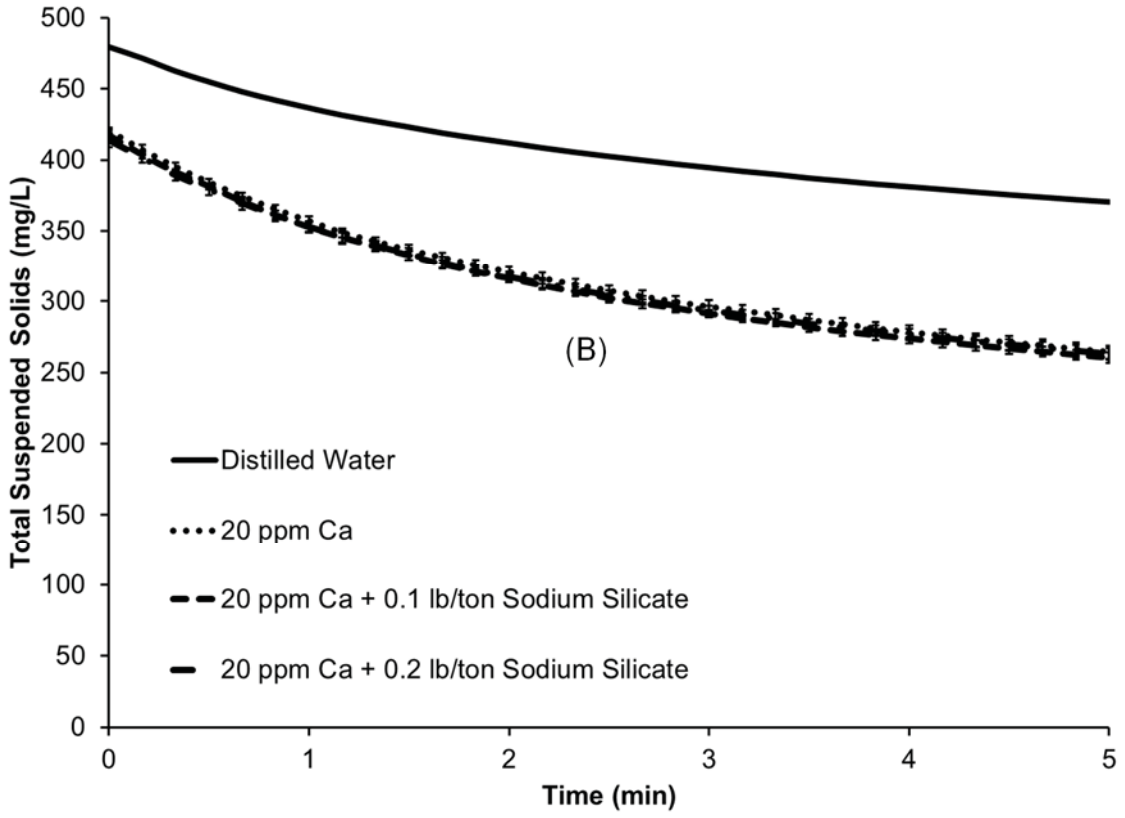

Figure 3.5: Sodium silicate effectiveness as a dispersant. Total suspended solids over time of hematite ore in a distilled water solution at a pH of 11. Sodium silicate dispersant added without calcium present (a) and after calcium had been added (b).

The settling behavior for varying doses of sodium tripolyphosphate ($Na_5P_3O_{10}$, STPP) is shown in Figure 3.6. Without calcium in the slurry, the dispersive stability remains constant at the same level as distilled water regardless of the amount of STPP added. This is the same phenomenon seen when adding sodium silicate. When calcium is added at 20 ppm, the dispersive stability is again lowered drastically. When STPP is added as a

dispersant to the calcium-rich slurry, the dispersive stability increased slightly. When STPP was added at 0.1 lb/ton and 0.2 lb/ton, the final total suspended solids increased by 14 mg/L and 16 mg/L, respectively. This shows that STPP will re-disperse the ore in the presence of calcium with diminishing returns on dispersant dose. This also shows that STPP does not conform to theory 2 described above in which the dispersant removes calcium inn-sphere complexes from the surface of the particles.

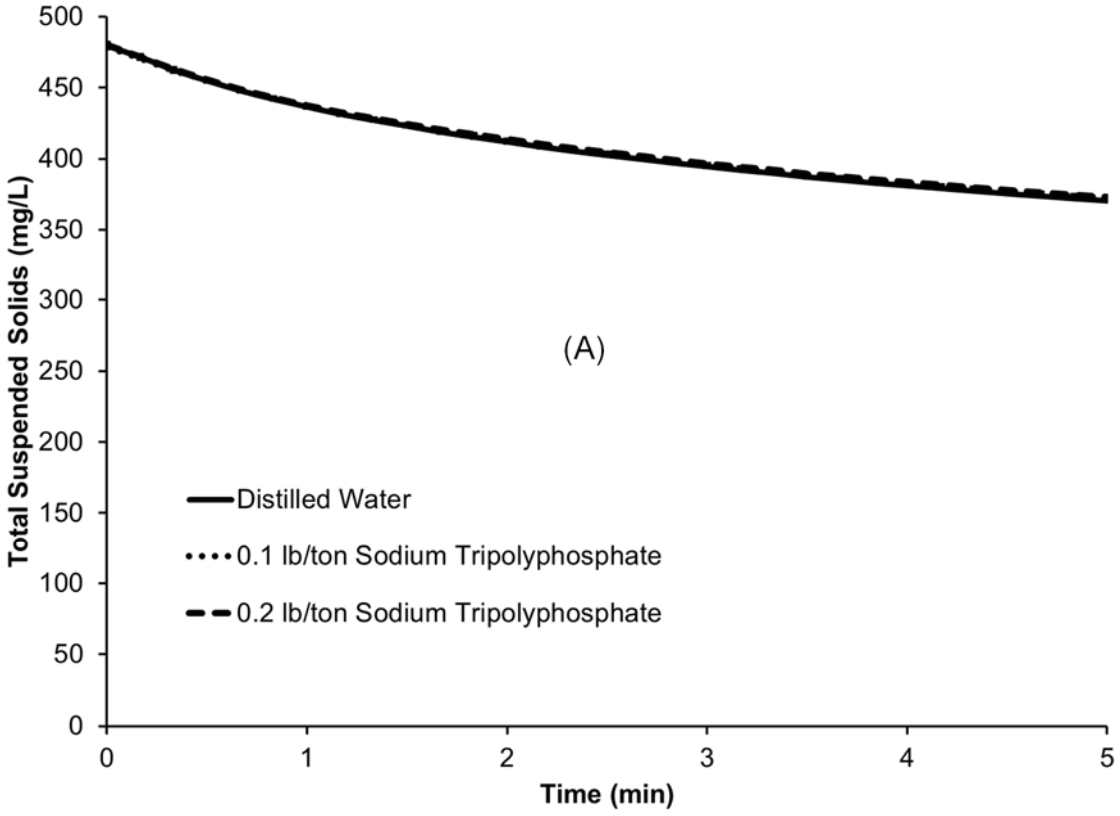

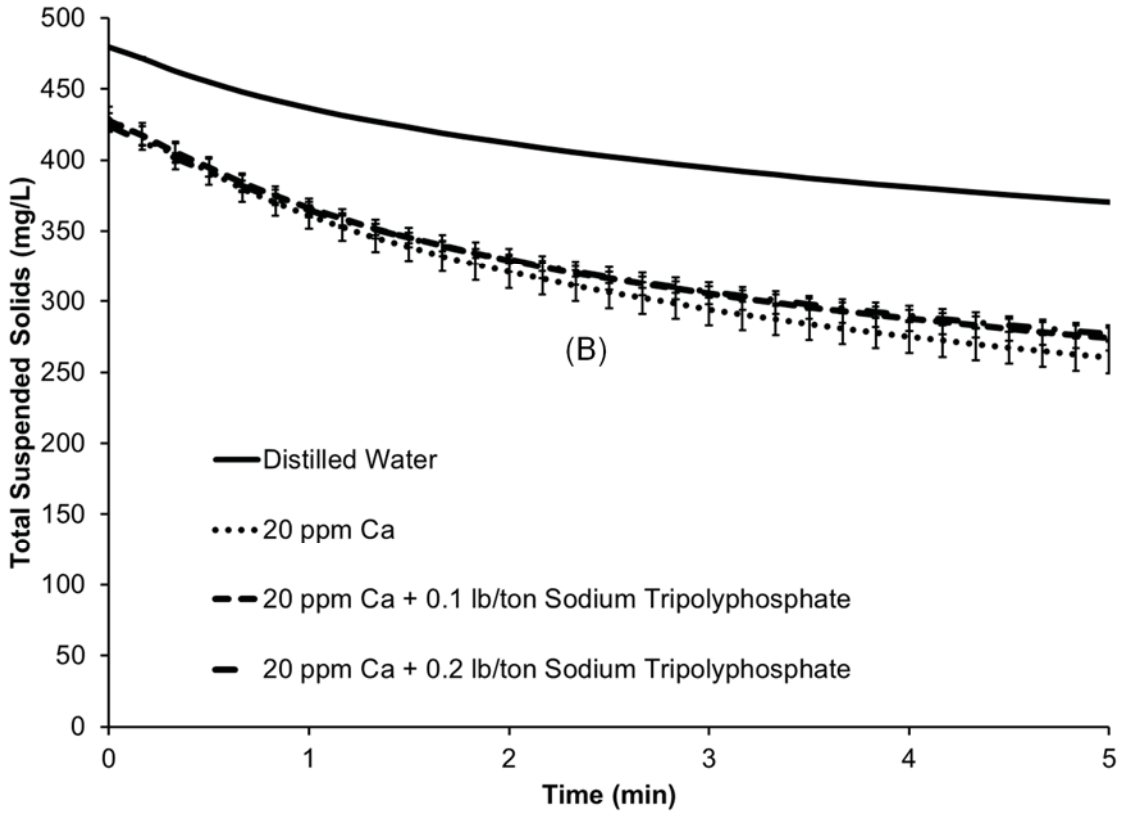

Figure 3.6: Sodium tripolyphosphate effectiveness as a dispersant. Total suspended solids over time of hematite ore in a distilled water solution at a pH of 11. Sodium tripolyphosphate (STPP) dispersant added without calcium present (a) and after calcium had been added (b).

The settling behavior for varying doses of sodium hexametaphosphate ($Na_6P_6O_{18}$, SHMP) is shown in Figure 3.7. Without calcium in the slurry, the dispersive stability remains constant at the same level as distilled water regardless of the amount of SHMP added. This is the same phenomenon seen when adding sodium silicate and STPP. When calcium is added at 20 ppm, the dispersive stability is again lowered drastically. When SHMP is added as a dispersant to the calcium-rich slurry, the dispersive stability

increased substantially. When SHMP was added at 0.1 lb/ton and 0.2 lb/ton, the final total suspended solids increased by 18 mg/L and 30 mg/L, respectively. This shows that SHMP will re-disperse the ore in the presence of calcium with little diminish in returns upon increased dosages. SHMP may conform to theory 2, theory 3 or both because the dispersive effect of the SHMP changed progressively with increased dispersant dose.

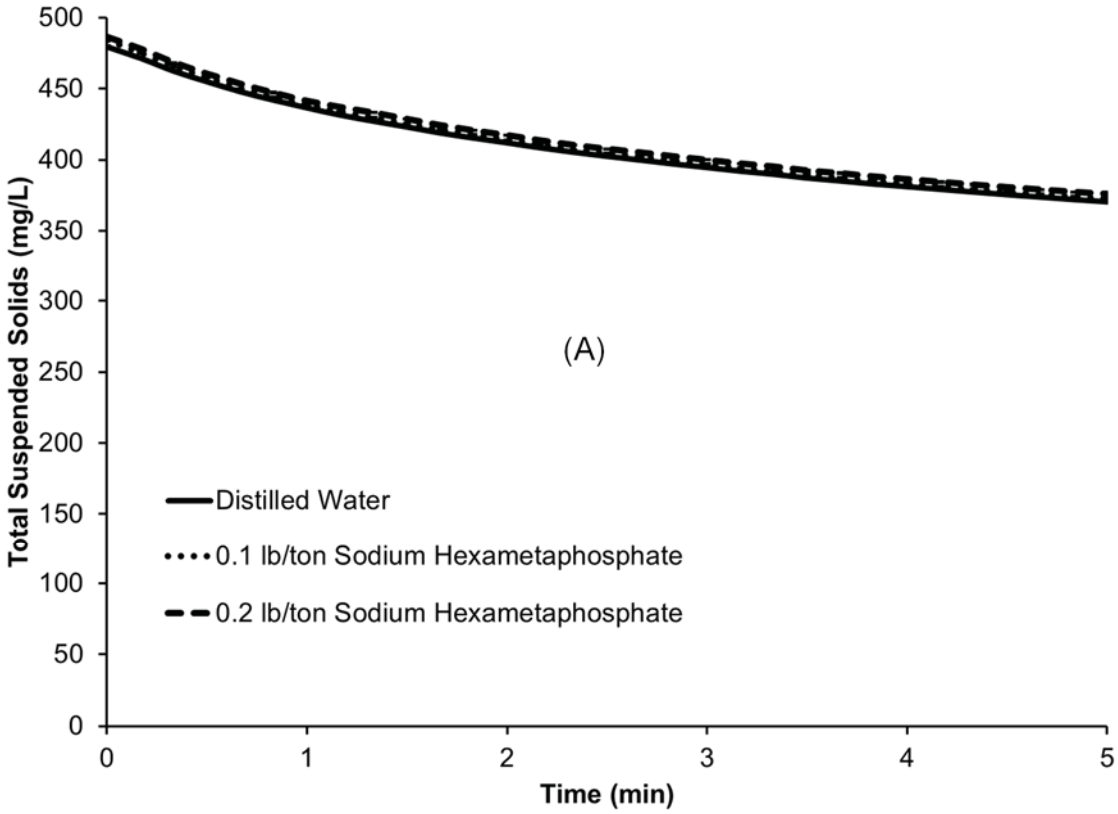

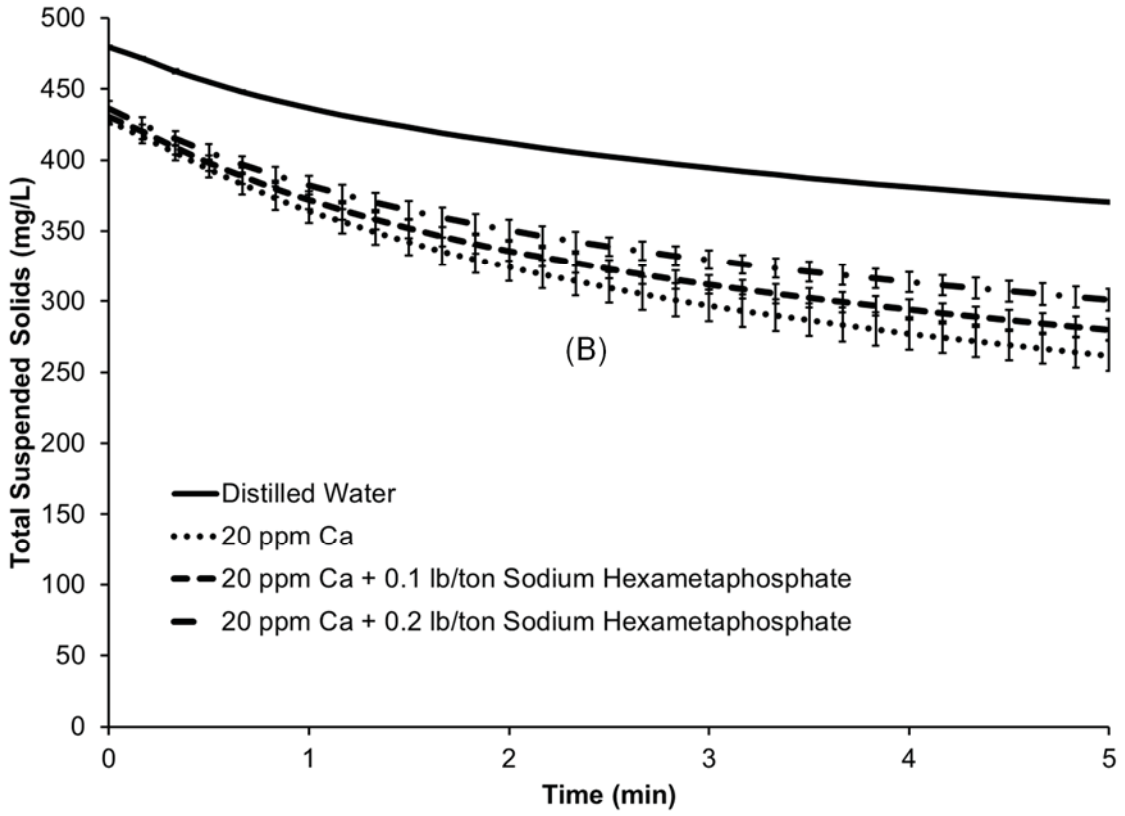

Figure 3.7: Sodium hexametaphosphate effectiveness as a dispersant. Total suspended solids over time of hematite ore in a distilled water solution at a pH of 11. Sodium hexametaphosphate (SHMP) dispersant added without calcium present (a) and after calcium had been added (b).

The settling behavior for varying doses of sodium henicosapolyphosphate ($Na_{23}P_{21}O_{64}$, Glass-H) is shown in Figure 3.8. Again, without calcium in the slurry, the dispersive stability remains constant at the same level as distilled water regardless of the amount of Glass-H added. This shows that theory 1 as described above does not apply for silicate or phosphate based dispersants. When calcium is added at 20 ppm, the dispersive stability is again lowered drastically. When Glass-H is added as a dispersant to the calcium-rich

slurry, the dispersive stability increased; however, not as much as when SHMP was added. When Glass-H was added at 0.1 lb/ton and 0.2 lb/ton, the final total suspended solids increased by 8 mg/L and 25 mg/L, respectively. This shows that Glass-H will re-disperse the ore in the presence of calcium with little to no diminish in returns upon increased dosages. Glass-H may also conform to theory 2, theory 3 or both because the dispersive effect of the Glass-H changed progressively with increased dispersant dose.

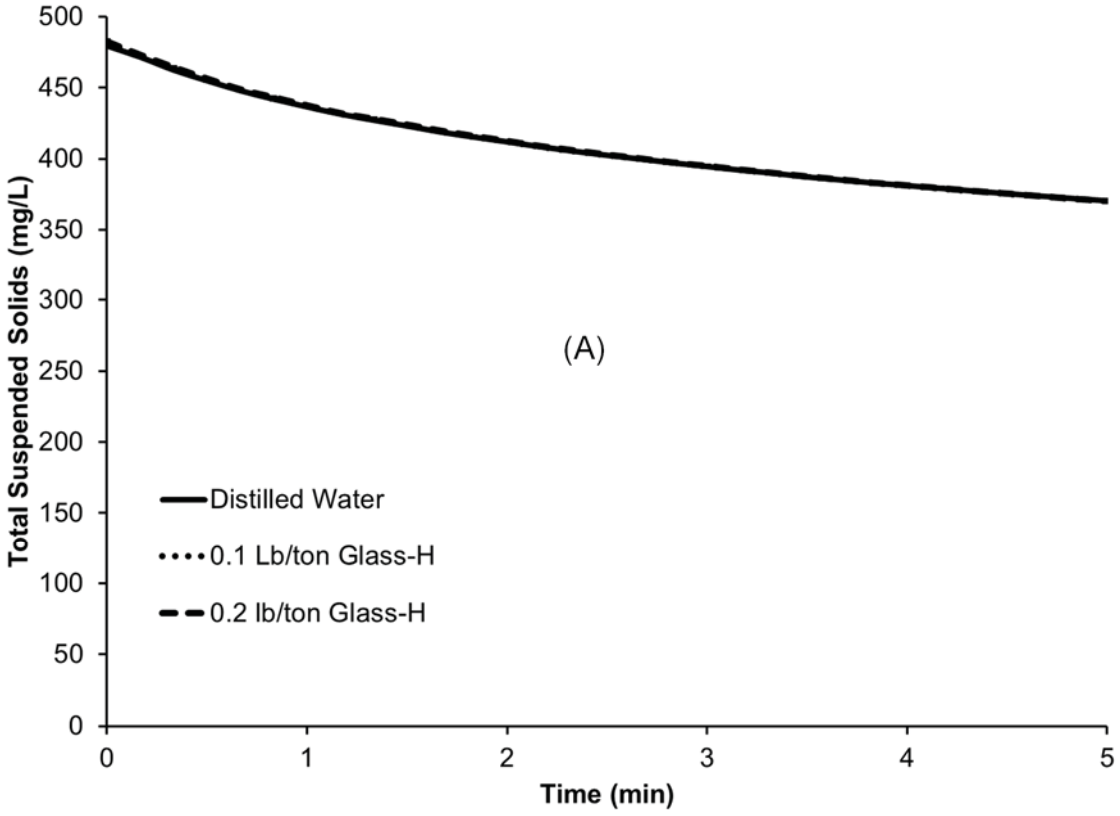

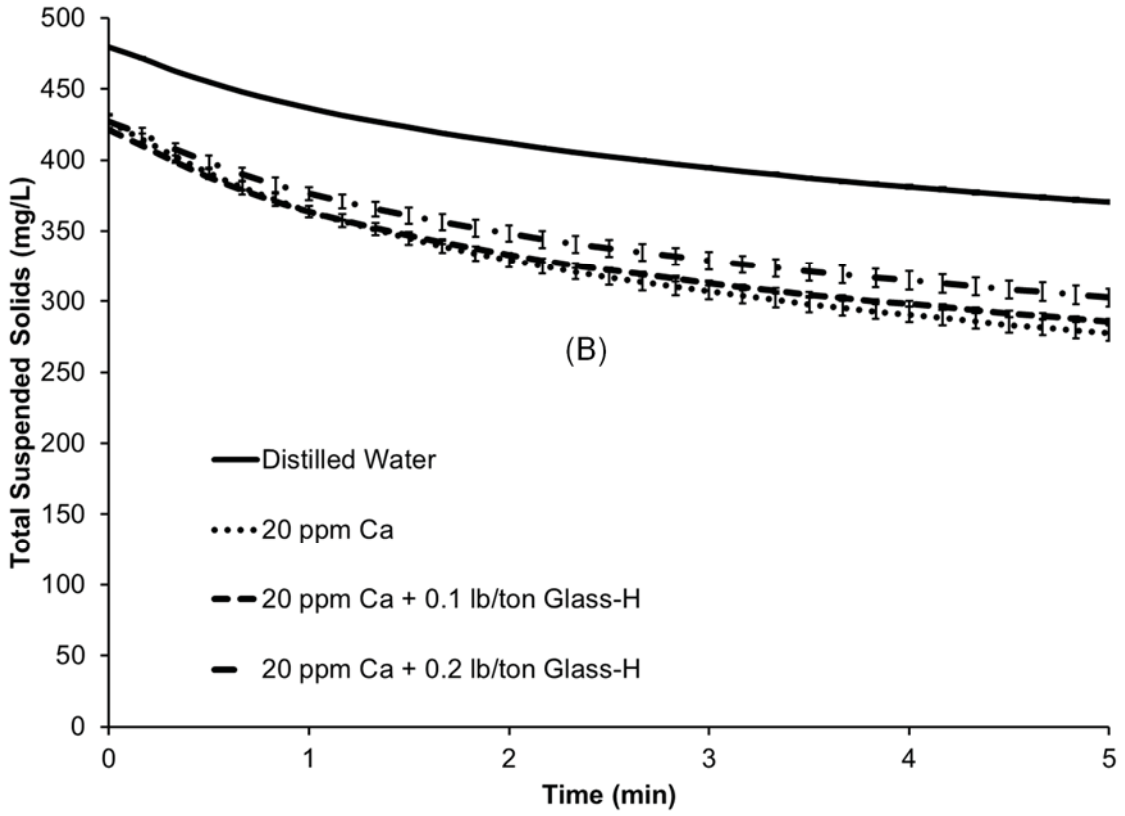

Figure 3.8: Sodium henicosapolyphosphate effectiveness as a dispersant. Total suspended solids over time of hematite ore in a distilled water solution at a pH of 11. Sodium henicosapolyphosphate (Glass-H) dispersant added without calcium present (a) and after calcium had been added (b).

The settling behavior for varying doses of ethylenediaminetetraacetic acid ($C_{10}H_{16}N_2O_8$, EDTA) is shown in Figure 3.9. Unlike the silicate and phosphate dispersants, EDTA causes a slight increase in dispersive stability without the addition of calcium in the slurry. This shows that theory 1 as described above could be applied in this situation. As before, when calcium is added at 20 ppm the dispersive stability is lowered drastically; however, when EDTA is added as a dispersant to the calcium-rich slurry, the dispersive

stability further decreases. When EDTA was added at 0.1 lb/ton, the final total suspended solids decreased by 37 mg/L; however, when EDTA was added at 0.2 lb/ton there was no change in final total suspended solids. This shows that in the presence of calcium, EDTA will cause flocculation, and in the absence of calcium EDTA will cause slight dispersion. Also, this shows that EDTA does not follow theory 2 or 3, as mentioned above.

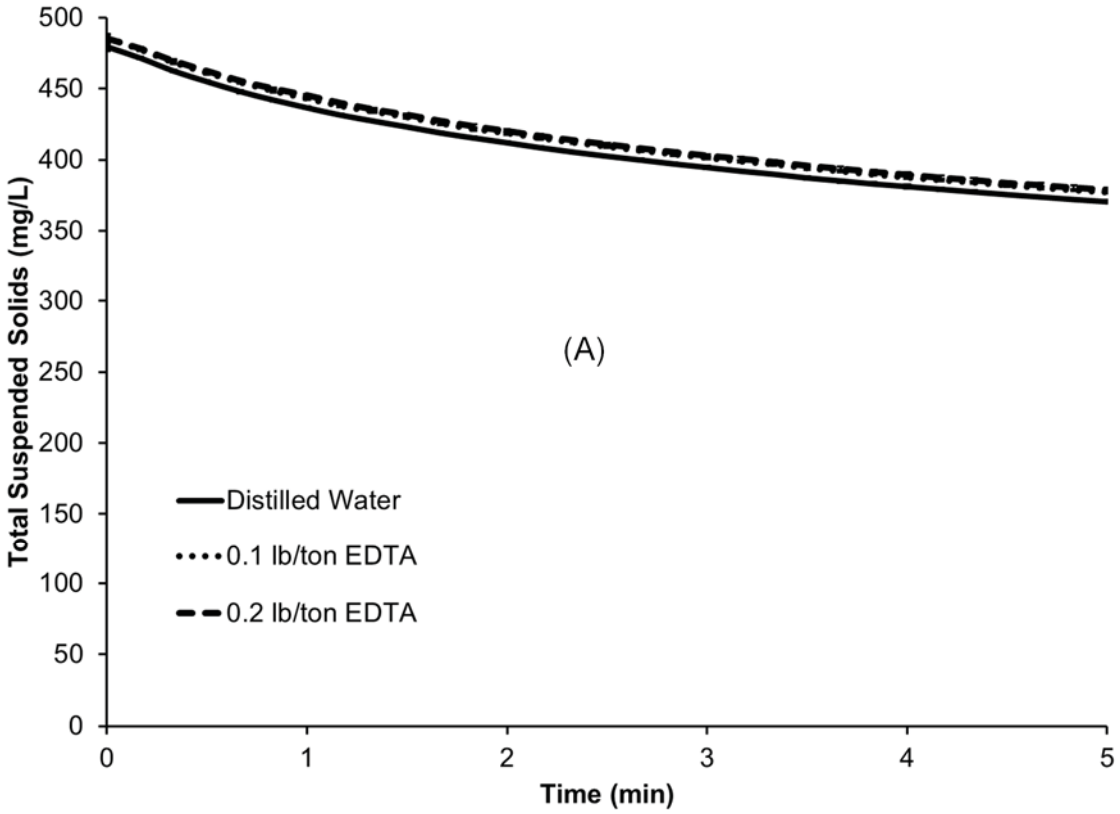

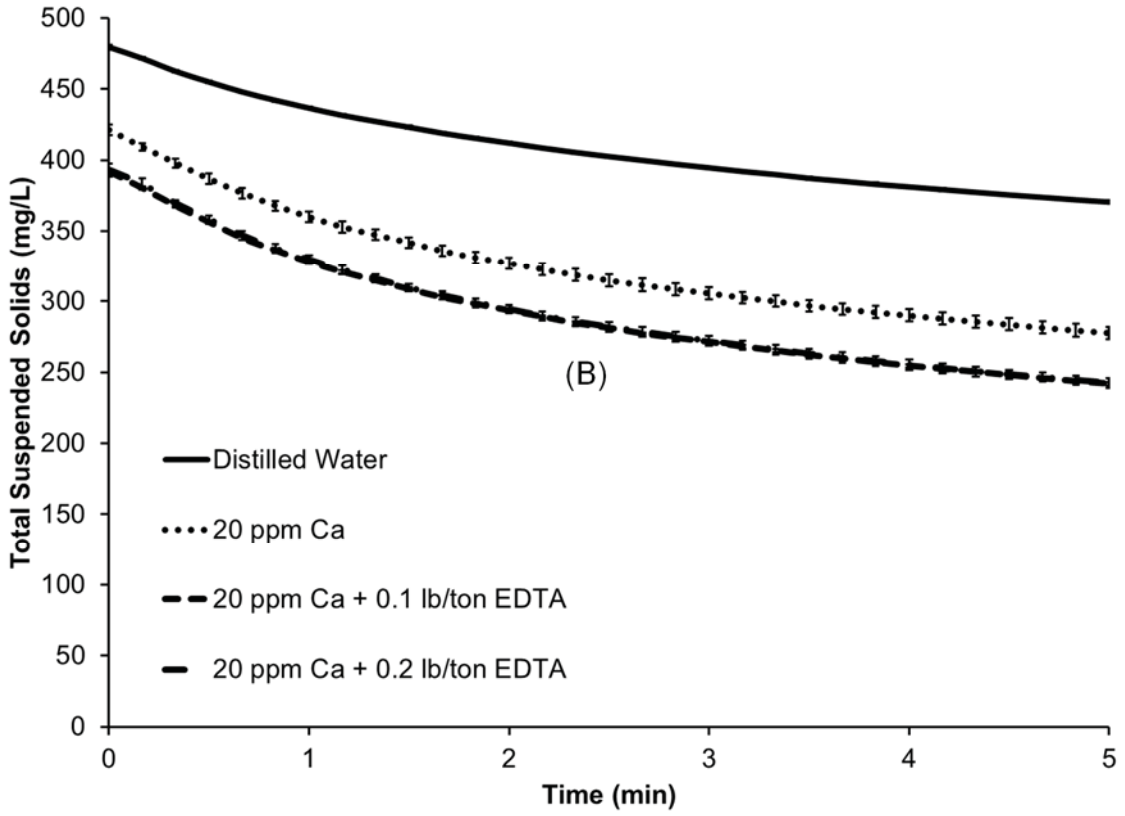

Figure 3.9: Ethylenediaminetetraacetic acid effectiveness as a dispersant. Total suspended solids over time of hematite ore in a distilled water solution at a pH of 11. Ethylenediaminetetraacetic acid (EDTA) dispersant added without calcium present (a) and after calcium had been added (b).

3.1.5 Conclusions

The settling behavior of ground hematite-rich iron ore at a pH of 11 was assessed in the presence of calcium and several common dispersants used in iron ore concentration processes. Three possible adsorption mechanisms for these dispersants have been shown in literature:

1. The dispersive anions coat surfaces with inner-sphere complexes by displacing hydroxyl groups at the oxide surfaces (Stumm et al., 1992)
2. The anions form stable complexes with calcium in solution causing these ions to dissolve from the particle surfaces (Ding et al., 2007)
3. The anions form stable surface complexes with positively charged calcium inner-sphere complexes at the surface thereby neutralizing calcium surface complexes (Green et al., 1984)

The dispersive ability of sodium silicate, sodium tripolyphosphate (STPP), sodium hexametaphosphate (SHMP), sodium henicosapolyphosphate (Glass-H), and ethylenediaminetetraacetic acid (EDTA) was evaluated with and without aqueous calcium present in the slurry. Without calcium, the dispersants had no effect on the dispersive stability of the ore, with EDTA being the only exception. This suggests that the inorganic dispersants do not adsorb to the oxide surfaces at a pH of 11 due to their inability to displace the negatively charged hydroxyl groups at the oxide-water interface. EDTA did cause slight dispersion of the ore, indicating it can displace the hydroxyl groups forming a stable complex.

Calcium was found to lower the dispersive stability of the ore by flocculating fine particles. Each dispersant affected the dispersive stability differently when calcium was present. Sodium silicate caused little to no dispersion in the presence of 20 ppm calcium. All of the phosphate based dispersants effectively re-dispersed the ore in the presence of 20 ppm calcium. STPP re-dispersed the ore slightly with diminishing returns upon increased dosage. This shows that STPP likely adsorbs to positively charged calcium

inner-sphere complexes thereby reversing the charge of the surface site. SHMP re-dispersed the ore with little diminishing returns at the dosages tested. This shows that SHMP may complex and remove calcium from the surface, complex with calcium inner-sphere complexes without removing the calcium from the surface, or a combination of both adsorption mechanisms. Glass-H re-dispersed the ore with little to no diminishing returns at the dosages tested. The adsorption mechanism of Glass-H follows that of SHMP. EDTA causes further flocculation suggesting that an aqueous EDTA molecule may bind with two calcium complexes; sometimes, one calcium being bound to a neighboring particle. This could form a more stable EDTA complex at the particle surface resulting in flocculation.

It has been concluded that anionic dispersants require positively charged surface sites, such as calcium inner-sphere complexes, to adsorb and cause dispersion of an iron ore pulp at a pH of 11. The order of dispersant effectiveness from lowest to highest in the presence of 20 ppm calcium at a pH of 11 was found to be ethylenediaminetetraacetic acid < sodium silicate < sodium tripolyphosphate < sodium henicosapolyphosphate < sodium hexametaphosphate.

3.1.6 References

ASTM, 2006, *D1971-02 Standard Practices for Digestion of Water Samples for Determination of Metals by Flame Atomic Absorption, Graphite Furnace Atomic Absroption, Plasma Emission Spectroscopy, or Plasma Mass Spectroscopy,* Water and Environmental Technology, ASTM International, Pennsylvania.

Benner, B. R., and Goetzman, H. E., 1994, “Reagent Use in the Iron Ore Industry,” *Reagents for Better Metallurgy,* Society for Mining, Metallurgy and Exploration, pp. 143-153.

Ding, H., Lin, H., and Deng, Y., 2007, "Depressing effect of sodium hexametaphosphate on apatite in flotation of rutile," *Journal of University of Science and Technology Beijing,* Vol. 14, No. 3, pp. 200-203.

Dzombak, D. A., and Morel, F., 1990, *Surface complexation modeling : hydrous ferric oxide,* Wiley, 393 pp.

Green, R. E., and Colombo, A. F., 1984, “Dispersion-Selective Flocculation-Desliming Characteristics of Oxidized Taconites,” US Bureau of Mines, Report of Investigations, RI 8867, 24 pp.

Hach, 2010, “Method 8006: Suspended Solids - Photometric Method,” Hach Methods

Iwasaki, I., 1989, “Bridging Theory and Practice in Iron Ore Flotation,” *Advances in Coal and Mineral Processing Using Flotation,* Society for Mining, Metallurgy and Exploration, pp. 177-190.

Kinniburgh, D. G., Jackson, M. L., and Syers, J. K., 1976, "Adsorption of Alkaline Earth, Transition, and Heavy Metal Cations by Hydrous Oxide Gels of Iron and Aluminum," *Soil Science Society of America Journal,* Vol. 40, No. 5, pp. 796-799.

Krawczyk, D., and Gonglewski, N., 1959, "Determining Suspended Solids Using a Spectrophotometer," *Sewage and Industrial Wastes,* Vol. 31, No. 10, pp. 1159-1164.

Potapova, E., Yang, X., Grahn, M., Holmgren, A., Forsmo, S. P. E., Fredriksson, A., and Hedlund, J., 2011, "The effect of calcium ions, sodium silicate and surfactant on charge and wettability of magnetite," *Colloids and Surfaces A: Physicochemical and Engineering Aspects,* Vol. 386, No. 1–3, pp. 79-86.

Ryden, J. C., Syers, J. K., and Tillman, R. W., 1987, "Inorganic anion sorption and interactions with phosphate sorption by hydrous ferric oxide gel," *Journal of Soil Science,* Vol. 38, No. 2, pp. 211-217.

Stumm, W., Sigg, L., and Sulzberger, B., 1992, *Chemistry of the solid-water interface,* Wiley, 448 pp.

3.2 Comparison of Dispersants for Selective Flocculation of Hematite Ore at a Pilot Scale[6]

3.2.1 Abstract

Selective flocculation and dispersion is a process used to separate finely liberated (<25μm) hematite ore from gangue minerals. It requires a specific water chemistry, a selective flocculant and a dispersant to yield an effective separation. This research focused on finding the most effective dispersant for the hematite concentration process using a laboratory scale continuous deslime thickener. The dispersants studied were sodium silicate, sodium henicosapolyphosphate (21-member polyphosphate), 2000 molecular weight (MW) polyacrylic acid (PAA), 4000 MW PAA and 7000 MW PAA. It was found that sodium henicosapolyphosphate at 0.05 pounds of dispersant per ton of ore yielded the best grade/recovery curve for iron. The 4000 MW polyacrylic acid at 0.25 pounds of PAA per ton of ore had an iron grade/recovery curve nearly that of sodium henicosapolyphosphate but yielded a lower phosphorus concentration in the product (down to 0.022% P).

3.2.2 Introduction

The United States produced 53.2 million metric tons of concentrated iron ore in 2012 (Tuck, 2013). As iron ore reserves containing high grade iron ore have been depleted for

---

[6] The material contained in this chapter is under review in the journal *"Minerals and Metallurgical Processing."* It is included in this dissertation with permission from the journal.
Citation:
Haselhuhn, H. J., Kawatra, S. K., 2015, "Design of a Continuous Pilot Scale Deslime Thickener," *Minerals & Metallurgical Processing*, Accepted.

over five decades, the U.S. has relied on lower grade ores for all domestic production. Most of the ore has been obtained in the form of low-grade unoxidized magnetite; this ore has been selected because Fe_3O_4 is easily separated from the gangue minerals using low-intensity wet magnetic separation. Fully oxidized iron ores containing hematite and goethite are very abundant throughout the world; however, beneficiation of these ores has been a stumbling block, both technologically and economically (Colombo, 1980). Recently, there has been much recent interest in the beneficiation and processing of these ores (Bolen, 2014; Carlson et al., 2010, 2013; Carlson, 2008; Halt, 2014; Halt et al., 2014a; Halt et al., 2014b; Haselhuhn, 2012, 2013; Haselhuhn et al., 2012a; Haselhuhn et al., 2012b; Kawatra et al., 2011; Liu et al., 2014; Manouchehri, 2014; Sandvik et al., 2014; Semberg et al., 2014)

One commercial facility has been capable of economically separating low-grade fully oxidized ores since 1974 (Colombo, 1980). This facility accounted for about 15% of U.S. production in 2012 and relied on a process known as selective flocculation and dispersion (Cliffs Natural Resources, 2011; Tuck, 2013). Selective flocculation and dispersion is a process used to concentrate fine, non-magnetic mineral particles such as hematite. The process relies on both water chemistry and surface chemistry to separate mineral particles. It requires two types of reagents: a selective flocculant and a dispersant. For concentrating hematite ore, cooked acid-modified cornstarch has been used as a selective flocculant. The dispersant used has varied over time as polymer technology has developed.

To facilitate adequate dispersion, sodium hydroxide has been used to increase slurry pH and create a negatively charged zeta potential at mineral surfaces. The negative zeta potential of all mineral surfaces is important to prevent the natural flocculation of the mineral particles. Both high pH and low concentration of polyvalent cations are necessary to achieve adequate natural dispersion of the particles (Haselhuhn, 2012).

In addition to sodium hydroxide, a number of different dispersants have been used to increase the dispersion of the ore. Many of these dispersants have been chosen to combat the effects of polyvalent cations in the process water (Haselhuhn, 2013). Since the inception of the process in 1974 at a plant scale, these dispersants have included sodium silicate, sodium tripolyphosphate, several experimental phosphate-based dispersants and a phosphate polymer averaging 21 phosphate groups known as Glass-H (Siirak et al., 1988).

Sodium silicate was the most widely used dispersant in the world for iron ore beneficiation (Ma, 2011a). Sodium silicate was used as the dispersant of choice in selective flocculation and dispersion processes until it was recognized that phosphorus rejection could be accomplished using phosphate-based dispersants. Siirak and Hancock (1988) showed that phosphorus occurred in the Lake Superior district ore body in two forms: approximately 50% as apatite ($Ca_5(PO_4)_3(F,Cl,OH)$) grains and the remainder as non-liberatable phosphorus highly disseminated throughout the iron oxide grains. Sodium tripolyphosphate was the first phosphate dispersant tested with some success at rejecting phosphorus during desliming (Siirak et al., 1988). The work of Siirak and Hancock (1988) went on to show that longer polyphosphate chain lengths (P6, P13 and P21 chain

lengths) increased rejection of phosphorus during desliming. It was found that a 21 member sodium polyphosphate could be used economically to reject phosphorus during desliming (Siirak et al., 1988). This dispersant has been used since that time at the only selective flocculation and dispersion iron ore beneficiation plant in North America.

Recently, the use of polyacrylic acids were researched as a suitable replacement for sodium polyphosphate dispersants in iron oxide – kaolinite systems (Ma, 2011a; Ma, 2011b). The studies performed by Ma (2011a,b) suggested that a low molecular weight dispersant could perform nearly as well as polyphosphates to disperse kaolinite in iron ore over a wide pH range. This study did not assess the dispersants ability to reject phosphorus from the ore. More research was needed to determine if low molecular weight polyacrylic acids could both meet the dispersion capabilities of polyphosphates while still rejecting phosphorus during the desliming stage.

This study compared the effectiveness of sodium silicate, sodium henicosapolyphosphate (21 member polyphosphate) and three different polyacrylic acid dispersants with varying molecular weights (2,000, 4,000, 7,000 Da). Unlike previous studies, this research was conducted in a laboratory scale continuous deslime thickener. Iron recovery and phosphorus rejection was reported for each dispersant over varying flocculant dosages. The novel design of this thickener and the experimental procedures used were capable of replicating the grade and recovery seen at an industrial hematite beneficiation plant using the same technology and reagents.

3.2.3 Materials and Methods

3.2.3.1 Thickener Design

A laboratory scale deslime thickener was constructed using a 3 inch diameter, 50 inch tall acrylic column with an acrylic overflow collector and a stainless steel cone bottom. The feed slurry basin consisted of a powder-coated conical tank and a mixer on a small variac to adjust the mixer speed. The feed slurry was pumped into the feed well of the thickener using a Masterflex Easy-Load 7518-12 peristaltic pump. The thickener overflow was gravity drained from the thickener overflow collector back into the feed basin. The thickener underflow was pumped back into the feed basin using a Manostat Veristaltic Pump Jr. peristaltic pump. This experimental setup, including pertinent dimensions, can be seen in Figure 3.10. This thickener design was used to simulate a continuous deslime thickener without the need for excessive amounts of iron ore by recycling the underflow and overflow of the column back into the feed basin.

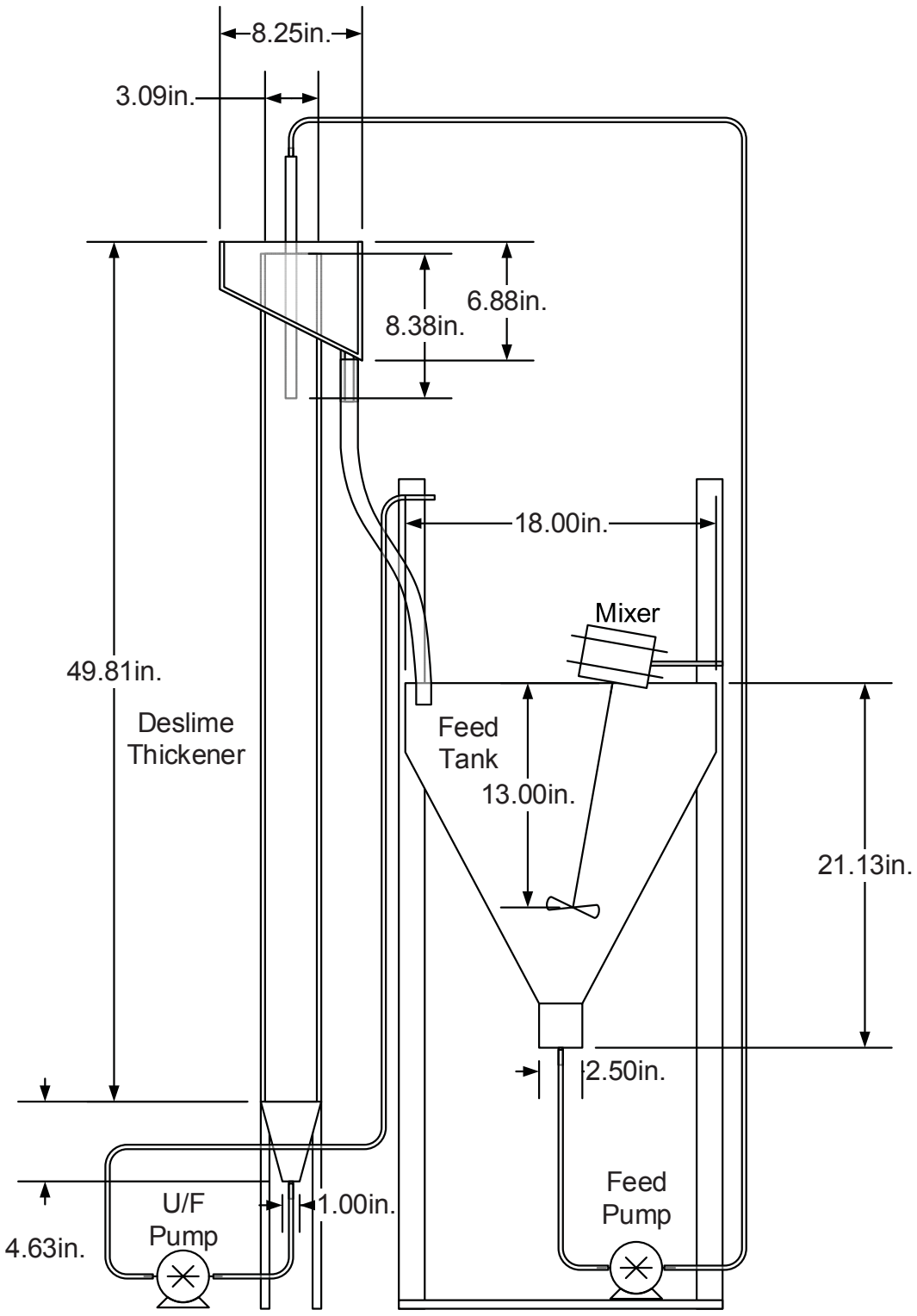

Figure 3.10: Scaled diagram of the continuous laboratory scale deslime thickener

3.2.3.2 Ore Preparation

Fully oxidized (hematite) iron ore was collected at an operating hematite beneficiation plant prior to any dispersant or flocculant addition in the circuit. The ore was collected using a cross-flow sample cutter on a falling stream of slurry between primary autogenous grinding and the dispersant addition point as can be seen in Figure 1.2. This sample point was chosen because no reagents aside from caustic soda (NaOH) had been added up to that point. Sampling at this location also allowed for a smaller sample to be representative of the bulk ore body due to the reduced particle size. Once sampled, the slurry was dewatered and dried in a convection oven at 107°°C for 24 hours. Once dry, the material was processed in a roll mill to break up chunks of dried material. A particle size analysis on this material showed an 80% passing size of 1.41 mm. The particle size required to liberate the iron oxide grains from the gangue minerals was known to be 82% passing at 25 μm (Siirak et al., 1988). To reach this particle size, the dried ore was ground in a laboratory rod mill for 70 minutes. The resultant ore was analyzed for particle size using a laser scattering particle size analyzer. This gave an 80% passing size of 23.1 μm.

Once the ore was ground, it was split using a rotary riffle splitter into 400 gram samples. The samples were placed in plastic bags and immediately inerted under argon to prevent oxidation of any cleaved iron grains. One sample was saved and analyzed for both iron and phosphorus concentration. The ore contained 39.7% iron and 0.0268% phosphorus.

3.2.3.3 Water Chemistry and Reagent Selection

The water used for these experiments was made using distilled water and laboratory grade salts to match the water chemistry found at an operating hematite beneficiation plant (Haselhuhn et al., 2012a). The water chemistry was held constant for each trial and can be found in Table 3.3. Laboratory grade reagents of sodium hydroxide (NaOH), sodium chloride (NaCl), potassium chloride (KCl), magnesium chloride ($MgCl_2 \cdot 6H_2O$), calcium chloride ($CaCl_2 \cdot 2H_2O$), sodium carbonate (Na_2CO_3, anhydrous), and sodium sulfate (Na_2SO_4, anhydrous) were used to reach the desired levels of ionic constituents in the simulated process water.

An ~400 gram sample of ground iron ore was mixed in the feed basin at 2% solids in simulated process water. A dispersant was added at a fixed dose and cooked acid-modified cornstarch was added at 0.05 lb/ton[7] increments up to 0.20 lb/ton. The tested dispersants included 0.3 lb/ton sodium silicate, 0.05 lb/ton Glass-H, 0.05 lb/ton Glass-H + 0.3 lb/ton sodium silicate, 0.25 lb/ton 2000 MW PAA, 0.25 lb/ton 4000 MW PAA, and 0.25 lb/ton 7000 MW PAA. The dosages of the dispersants were selected based upon operational data from an operating beneficiation plant and from manufacturer recommendations. The structures of these dispersants can be seen in Table 3.4. Overflow and underflow samples were taken 30 minutes (~1.6 underflow residence times) after each starch addition. These samples were filtered and dried. The filtrate volume was measured in a 500 mL graduated cylinder and the dried solids were weighed on an

[7] lb/ton refers to pounds (U.S.) of the reagent per ton of ore in the feed material of the thickener. This applies for every instance of lb/ton within this document.

analytical balance. Iron and phosphorus analysis using acid digestion of the dried solids and UV-VIS spectroscopy in conjunction with solids concentrations yielded grade/recovery curves for each dispersant at each starch dose.

Table 3.3: Water chemistry used during laboratory thickening tests

Component	**Concentration**
Sodium	495 ppm
Potassium	10 ppm
Magnesium	2 ppm
Calcium	3 ppm
Chloride	20.2 ppm
Carbonate	396.5 ppm
Sulfate	399.3 ppm
pH	11

Table 3.4: Chemical structures of dispersants used in this study

Dispersant	Structure
Silicate	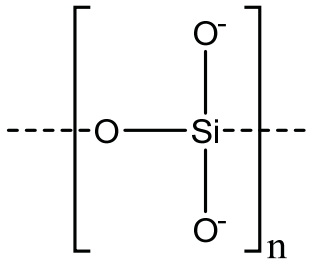
Henicosapolyphosphate (21-member polyphosphate)	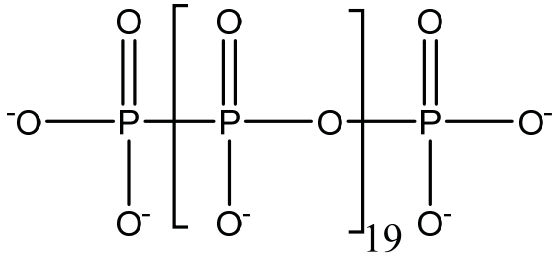
Polyacrylic Acid	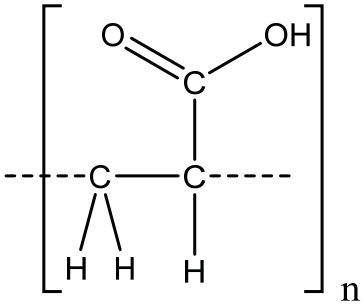

3.2.3.4 *Iron and Phosphorus Analyses*

The iron content of samples was measured using a UV-VIS spectrometer. A small sample of dried solids (<0.4 grams) was digested in 20 mL of hydrochloric acid for 20 minutes. The iron-bearing liquid was transferred to a 100 mL class-A volumetric flask and diluted using distilled water. This was allowed to cool to room temperature. To prepare the indicator solution, 5 mL of 0.1 M ammonium acetate solution, 5 mL of 10% hydroxylamine hydrochloride solution and 5 mL of 0.1% 1,10-phenanthroline solution

were added to a 50 mL class- A volumetric flask. Once cool, 100 µL of the digested solution was added to the indicator solution. The indicator solution was diluted to 50 mL with distilled water. The absorbance at 510 nm of the indicator solution was correlated to the iron concentration within the sample using a calibration curve prepared with an atomic absorption spectroscopy standard. Phosphorus concentration was measure using a phosphor-molybdenum-blue indicator and UV-VIS spectroscopy according to ASTM standard E1070-11 (2011).

3.2.4 Results and Discussion

3.2.4.1 Iron Beneficiation

The laboratory deslime thickener was run with six different dispersants to determine which dispersant yielded the best grade/recovery curve for iron beneficiation. Curves were constructed by incrementally increasing the starch flocculant dose from 0.0 to 0.2 lb/ton. The grade and recovery curves for these tests can be seen in Figure 3.11 and 3.12. As expected, with no flocculant the recovery of iron for all dispersants was low (42%-52%). As starch dose was increased, the iron recovery increased; however, the grade decreased.

The type of inorganic dispersant had a significant impact on the grade/recovery curve for iron. Sodium silicate had the least desirable grade/recovery curve. Sodium henicosapolyphosphate (21-member polyphosphate) had a significantly higher grade and recovery at each starch dose. The addition of sodium silicate to the sodium henicosapolyphosphate did not result in a better grade/recovery curve than the sodium

henicosapolyphosphate alone. This suggests that sodium silicate negatively impacts the dispersive stability achieved by other dispersants when mixed.

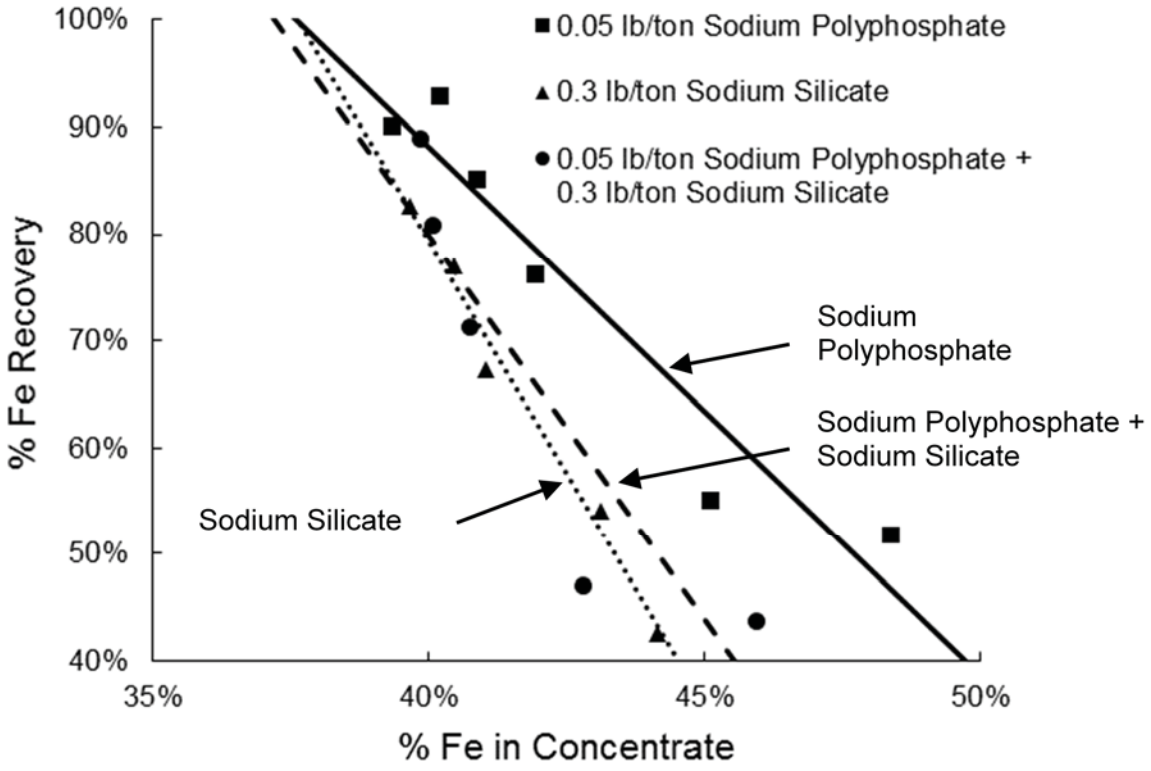

Figure 3.11: Iron grade/recovery using inorganic dispersants with varying flocculant concentration

The molecular weight of the polyacrylic acids used as dispersants did not significantly alter the effectiveness of the dispersant, as shown in Figure 3.12. All three dispersants resulted in grade/recovery curves that were very close to each other. The polyacrylic acids did not perform as well as sodium henicosapolyphosphate for the recovery of iron during desliming. However, the polyacrylic acids did out-perform sodium silicate and the

mixture of sodium silicate and sodium henicosapolyphosphate. This conclusion may be different at different dosages of polyacrylic acid and sodium henicosapolyphosphate.

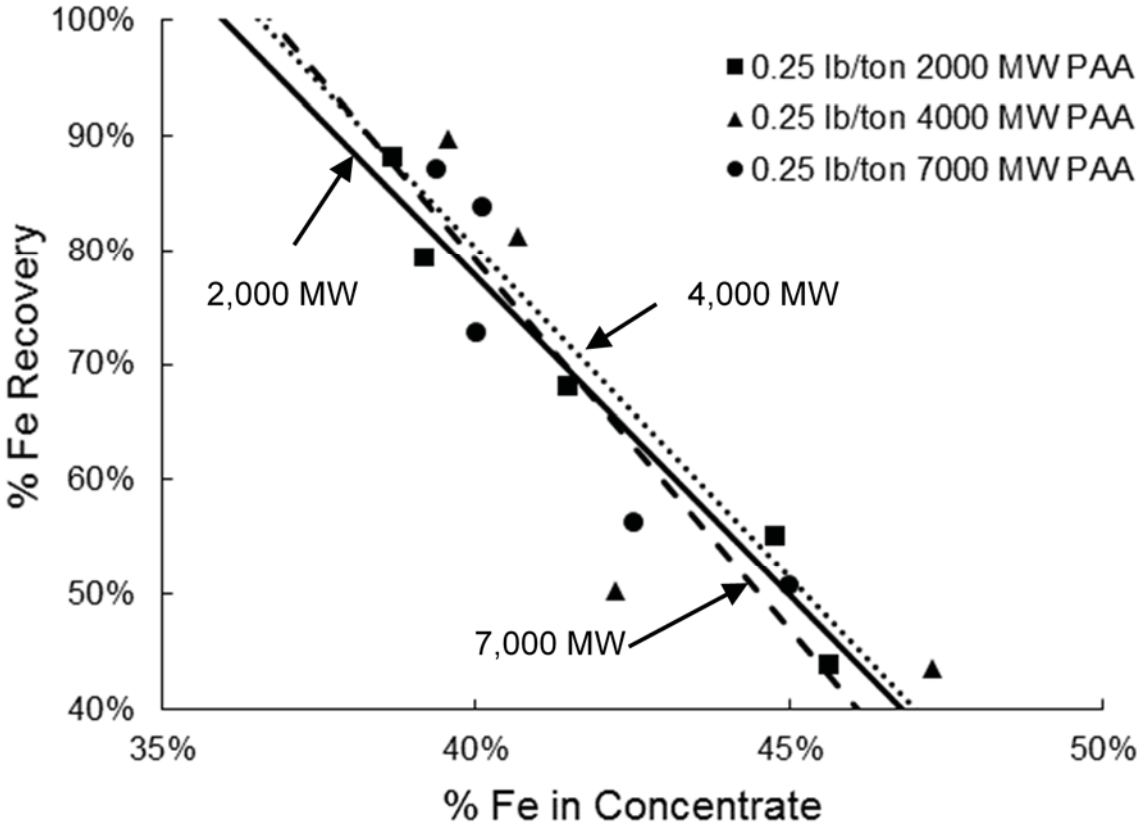

Figure 3.12: Iron grade/recovery using polyacrylic acid dispersants with varying flocculant concentration

3.2.4.2 Phosphorus Rejection

The phosphorus concentration of both the thickener overflow and underflow solids was analyzed to perform a mass balance around phosphorus in the process. This allowed for a comparison to be made between the six different dispersants used in the study. Since both

the phosphorus rejection and the iron recovery were the two most important factors in this study, they were plotted against each other for each dispersant. These plots can be found in Figure 3.13 and 3.14.

As expected and reported by Siirak and Hancock (1988), the use of sodium henicosapolyphosphate yielded the best phosphorus rejection and iron recovery at each starch dose. The lowest phosphorus concentration achieved in the thickener underflow using sodium henicosapolyphosphate as the dispersant was 0.0245% at an iron recovery of 51.8%. Sodium silicate yielded the poorest phosphorus rejection and iron recovery at each starch dose. The mixture of the two dispersants fell between the two, again suggesting that the addition of sodium silicate is detrimental to the effectiveness of the sodium henicosapolyphosphate dispersant.

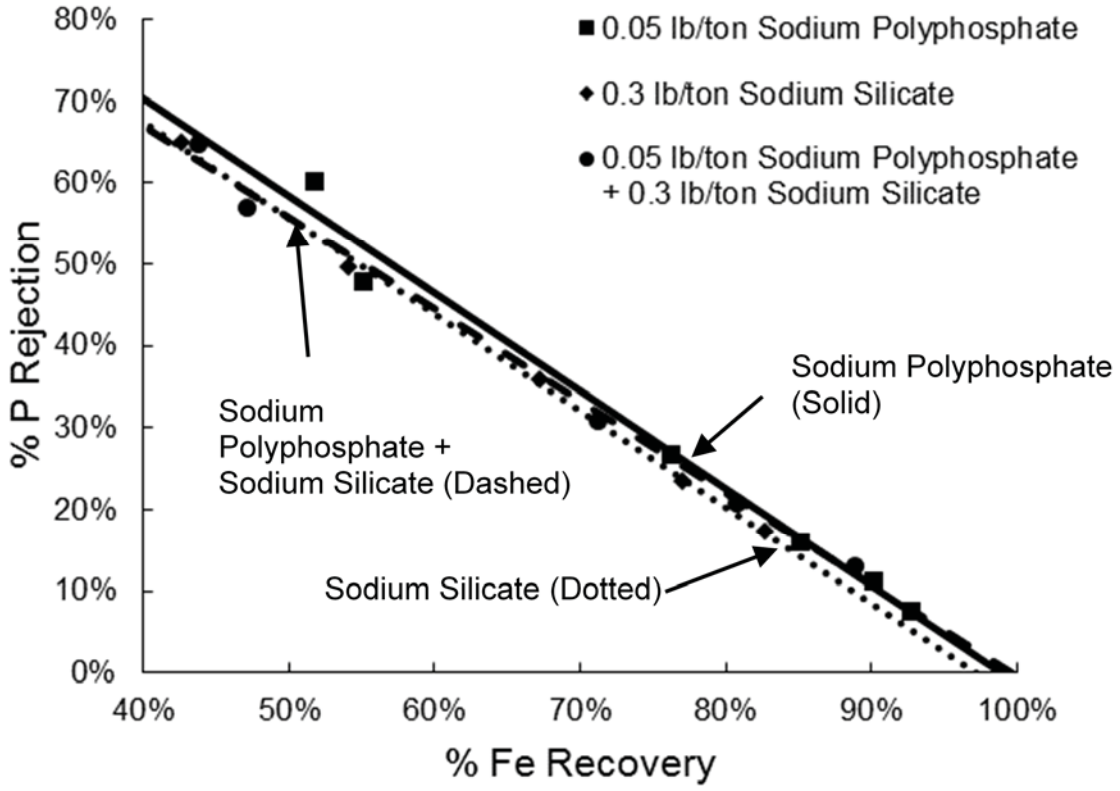

Figure 3.13: Phosphorus rejection versus iron recovery for inorganic dispersants with varying flocculant dose

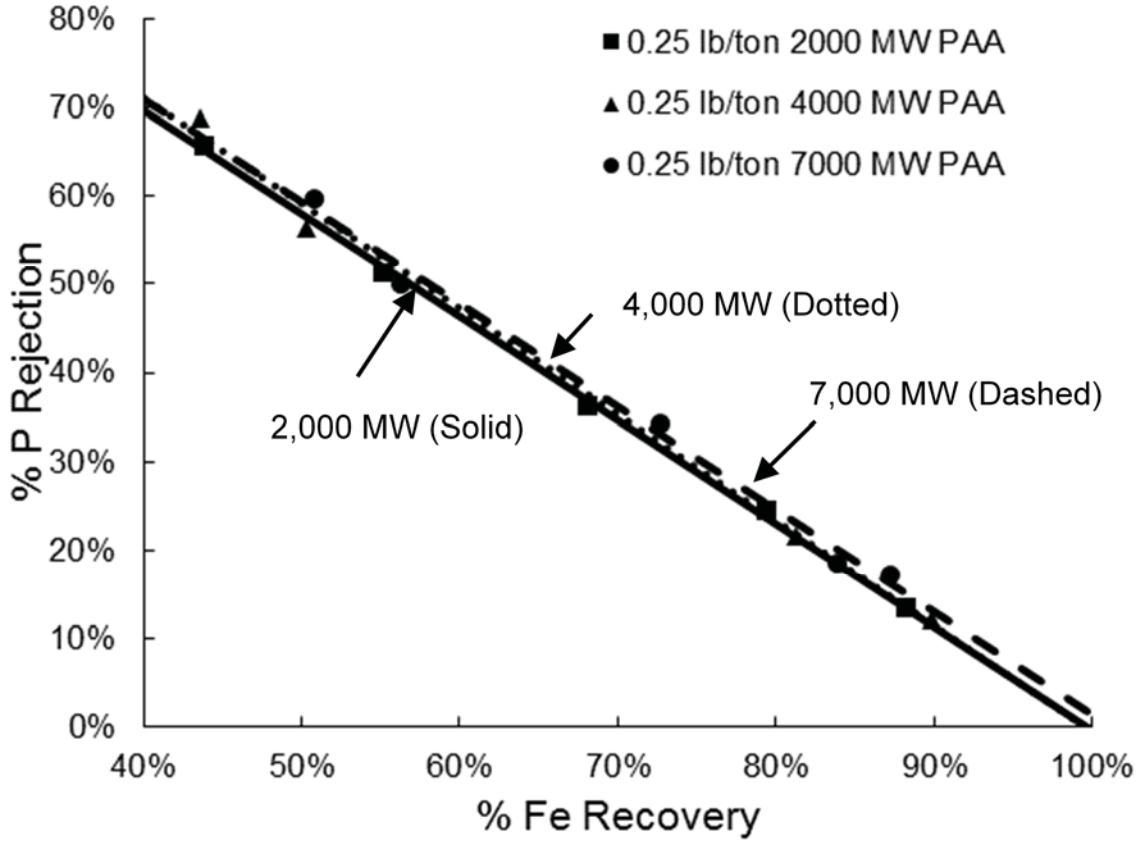

Figure 3.14: Phosphorus rejection versus iron recovery for polyacrylic acid dispersants with varying flocculant dose

3.2.5 Conclusions

A laboratory scale deslime thickener was used to compare the effectiveness of six different dispersants ability to both enhance iron recovery and phosphorus rejection in the selective flocculation-dispersion desliming process. The six dispersants tested included sodium silicate, sodium henicosapolyphosphate (21-member polyphosphate), a mixture of both sodium silicate and sodium henicosapolyphosphate, 2,000 MW polyacrylic acid, 4,000 MW polyacrylic acid, and 7,000 MW polyacrylic acid. The dosages of the

dispersants were selected based upon operational data from an operating beneficiation plant and from manufacturer recommendations.

Of the inorganic dispersants tested, sodium henicosapolyphosphate yielded the best grade/recovery curve for iron and was able to reject the most phosphorus during desliming. Sodium silicate and a mixture of the two dispersants did not yield grade/recovery curves comparable to that of sodium henicosapolyphosphate alone. The sodium silicate seemed to lessen the dispersive ability of the sodium henicosapolyphosphate.

All three polyacrylic acids, varying in molecular weight from 2,000 to 7,000 Da, performed nearly identically in the process for both iron recovery and phosphorus rejection. It was found that sodium henicosapolyphosphate, at 0.05 lb/ton of ore, yielded the best grade/recovery curve for iron; however, 0.25 lb/ton 4000 MW PAA was able to reject up to 40% more phosphorus with concentrate phosphorus concentrations as low as 0.022%. The iron grade/recovery curve for the sodium henicosapolyphosphate was only slightly better than the 4000 MW PAA.

3.2.6 References

ASTM, 2011, *E1070-11 Standard Test Method for Determination of Phosphorus in Iron Ores by Phospho-Molybdenum-Blue Spectrophotometry*, ASTM Interantional, Conshohocken, PA.

Bolen, J., 2014, "Modern Air Pollution Control for Iron Ore Induration," *Minerals & Metallurgical Processing,* Vol. 31, No. 2, pp. 103-114.

Carlson, J. J. and Kawatra, S. K., 2008, "Effect of Particle Shape on the Filtration Rate in an Industrial Iron Ore Processing Plant," *Minerals & Metallurgical Processing,* Vol. 25, No. 3, pp. 165-168.

Carlson, J. J., and Kawatra, S. K., 2010, "Effects of CO_2 on the Zeta Potential of Hematite," *International Journal of Mineral Processing,* Vol. 98, No. 1-2, pp. 8-14.

Carlson, J. J., and Kawatra, S. K., 2013, "Factors Affecting Zeta Potential of Iron Oxides," *Mineral Processing and Extractive Metallurgy Review,* Vol. 34, No. 5, pp. 269-303.

Cliffs Natural Resources, 2011, *Steel Starts Here*, Operations Data Fact Sheet, 4 pp.

Colombo, A. F., 1980, "Selective Flocculation and Flotation of Iron-Bearing Materials," *Fine Particles Processing,* AIME, pp. 1034-1056.

Halt, J. A., 2014, "Increasing the preheat strength of cornstarch-bonded pellets," *Minerals & Metallurgical Processing,* Vol. 31, No. 3, pp. 179.

Halt, J. A., and Kawatra, S. K., 2014a, "Review of organic binders for iron ore concentrate agglomeration," *Minerals & Metallurgical Processing,* Vol. 31, No. 2, pp. 73-94.

Halt, J. A., Nitz, M. C., Kawatra, S. K., and Dube, M., 2014b, "Iron Ore Pellet Dustiness Part I: Factors Affecting Dust Generation," *Mineral Processing and Extractive Metallurgy Review,* Vol. 36, No. 4, pp. 258-266.

Haselhuhn, H. J., 2012, "Water Chemistry Effects on the Zeta Potential of Concentrated Hematite Ore," *Minerals & Metallurgical Processing,* Vol. 29, No. 2, pp. 135-136.

Haselhuhn, H. J., 2013, "Dispersant Adsorption and Effects on Settling Behavior of Iron Ore," *Minerals & Metallurgical Processing,* Vol. 30, No. 3, pp. 188-189.

Haselhuhn, H. J., Carlson, J. J., and Kawatra, S. K., 2012a, "Water chemistry analysis of an industrial selective flocculation dispersion hematite ore concentrator plant," *International Journal of Mineral Processing,* Vol. 102–103, pp. 99-106.

Haselhuhn, H. J., Swanson, K. P., and Kawatra, S. K., 2012b, "The effect of CO_2 sparging on the flocculation and filtration rate of concentrated hematite slurries," *International Journal of Mineral Processing,* Vol. 112-113, pp. 107-109.

Kawatra, S. K., and Halt, J. A., 2011, "Binding effects in hematite and magnetite concentrates," *International Journal of Mineral Processing,* Vol. 99, No. 1-4, pp. 39-42.

Liu, S., Zhau, Y., Wang, W., and Wen, S., 2014, "Beneficiation of a Low-grade, Hematite-Magnetite Ore in China," *Minerals & Metallurgical Processing,* Vol. 31, No. 2, pp. 136-142.

Ma, X., 2011a, "The Dispersion of Kaolinite," *Proceeding of the Iron Ore Conference,* The Australian Institute of Mining and Metallurgy, Perth, Australia, pp. 471-474.

Ma, X., 2011b, "Effect of a low-molecular-weight polyacrylic acid on the coagulation of kaolinite particles," *International Journal of Mineral Processing,* Vol. 99, No. 1–4, pp. 17-20.

Manouchehri, H. R., 2014, "Pyrrhotite Flotation and its Selectivity against Pentlandite in the Beneficiation of Nickeliferous Ores: An Electrochemistry Perspective," *Minerals & Metallurgical Processing,* Vol. 31, No. 2, pp. 115-125.

Sandvik, K. L., and Larsen, E., 2014, "Iron Ore Flotation with Environmentally Friendly Reagents," *Minerals & Metallurgical Processing,* Vol. 31, No. 2, pp. 95-102.

Semberg, P., Andersson, C., and Bjorkman, B., 2014, "Interaction between Iron Oxides and Olivine in Magnetite Pellets during Reduction at 500°-1,300°C," *Minerals & Metallurgical Processing,* Vol. 31, No. 2, pp. 126-135.

Siirak, J., and Hancock, B. A., 1988, “Progress in Developing a Flotation Phosphorus Reduction Process at the Tilden Iron Ore Mine,” *Proceedings of the XVI International Mineral Processing Congress,* Stockholm, Sweden, pp. 1393-1404.

Tuck, C. A., 2013, “Mineral Commodity Studies - Iron Ore,” US Geological Survey.

Conclusions

This dissertation discussed the importance of water chemistry, surface chemistry, and reagent selection on the hematite dispersion and selective flocculation process. The majority of the dissertation focused on the dependence of the previously under-studied desliming process on water chemistry and surface chemistry phenomena. Experiments were performed in a laboratory setting, in a pilot scale deslime thickener, and at a full scale beneficiation process making this work the first of its kind to show these effects at all three process scales.

These studies proved many hypotheses proposed throughout literature and found new phenomena that had been previously untested in other literature studies. The links between water chemistry, surface chemistry and reagent selection that are critical to the only hematite beneficiation process successfully implemented at a full scale have been shown and proven. In particular, it was shown that decreasing the sodium ion concentration in the process increases both iron grade and recovery. This is an important finding because increasing both the grade and the recovery is a very rare phenomenon and is extraordinarily beneficial to this process. It was also proven that calcium causes non-selective flocculation resulting in increased iron recovery at the expense of iron grade in the product, a typical scenario for process changes. The optimal pH for the process was found to be dependent upon the water chemistry during the separation but is typically optimal between 10.5 and 11. These findings have shown the importance of

certain water chemistry and surface chemistry parameters on the hematite beneficiation process.

Various dispersants were also tested at a laboratory and pilot scale for their effectiveness in the selective flocculation and dispersion deslime process. It was found that the polyphosphate (glass-H, sodium henicosapolyphosphate) dispersant yielded both high iron recovery and phosphorus rejection. Polyacrylic acid dispersants yielded the highest phosphorus rejection of tested dispersants and have the potential to replace polyphosphates in the full scale plant in the near future.

Appendix A – Zeta Potential Analyses from Plant Scale Studies

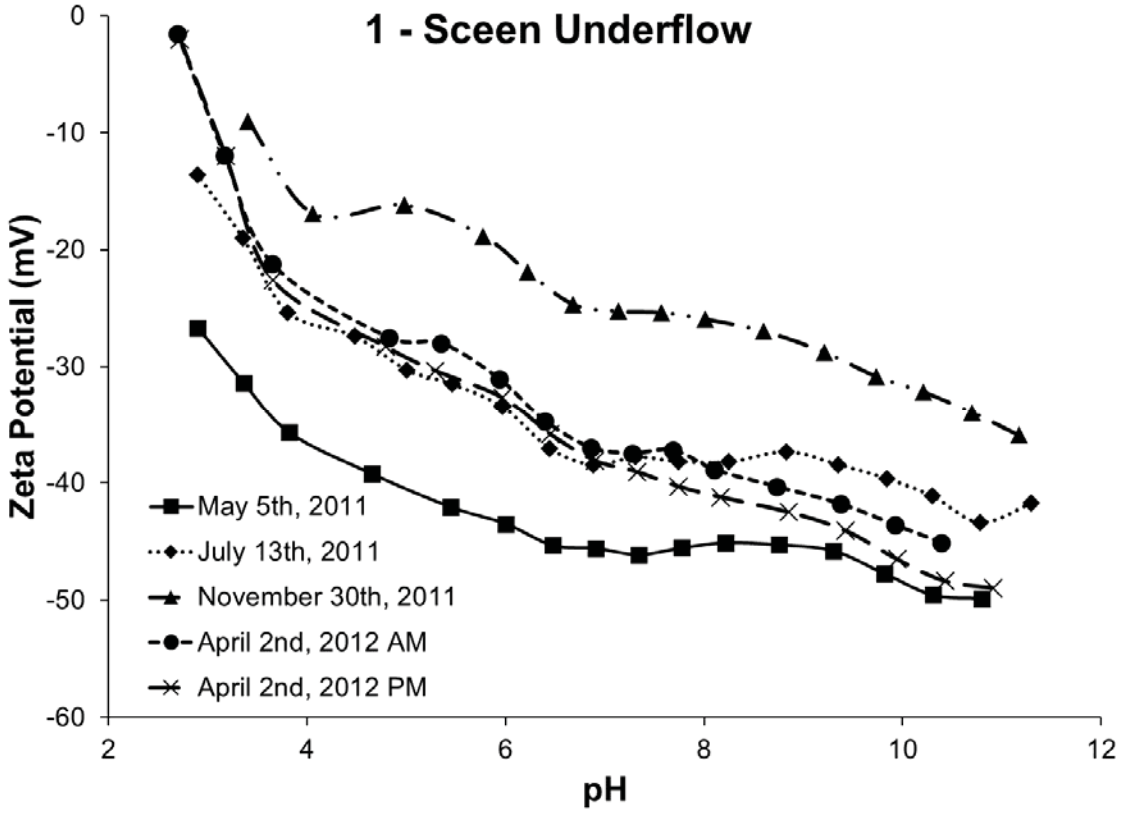

Figure A.1: Zeta potential as a function of pH for screen underflow solids at process conditions for each sample set

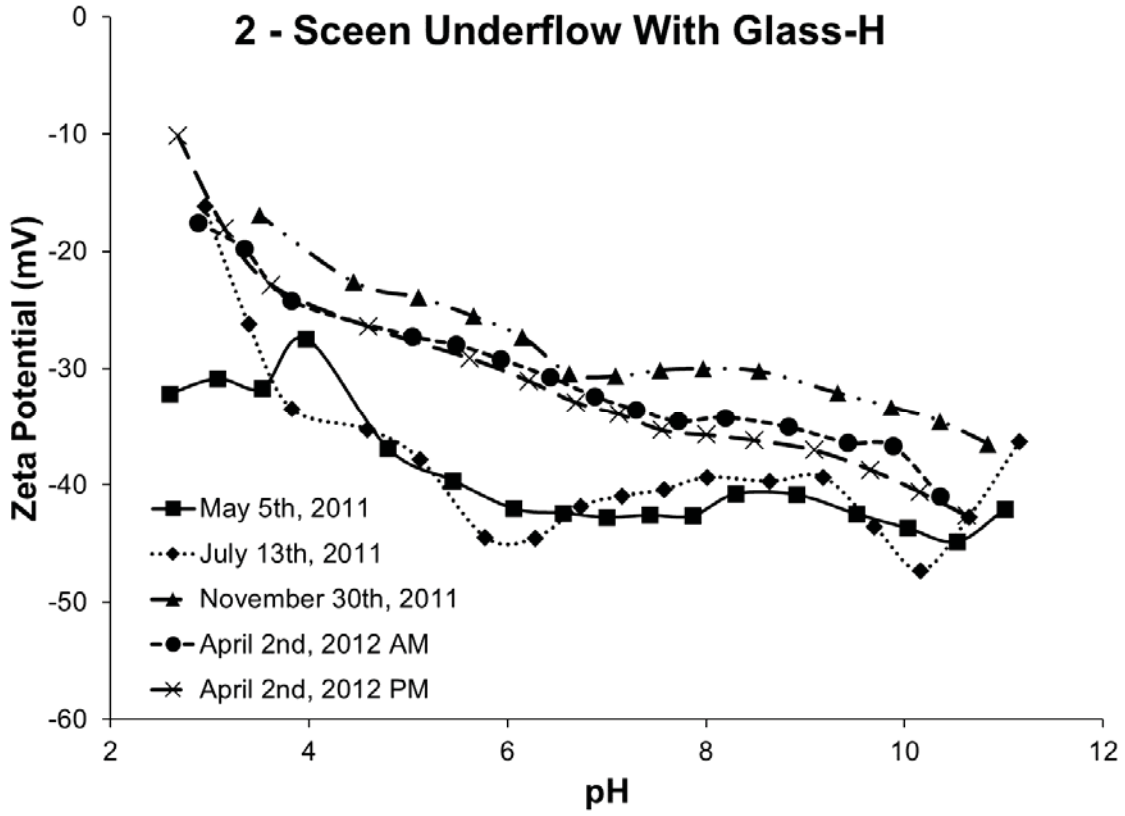

Figure A.2: Zeta potential as a function of pH for screen underflow with Glass-H solids at process conditions for each sample set

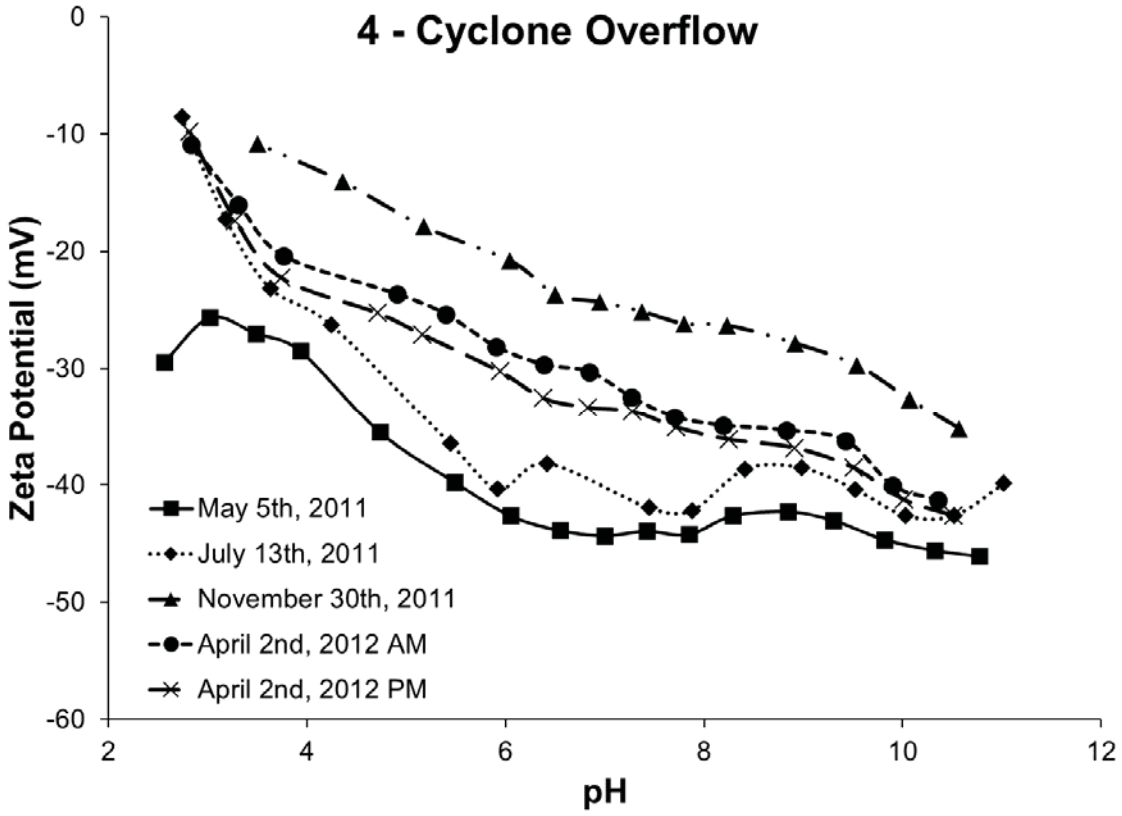

Figure A.3: Zeta potential as a function of pH for cyclone overflow solids at process conditions for each sample set

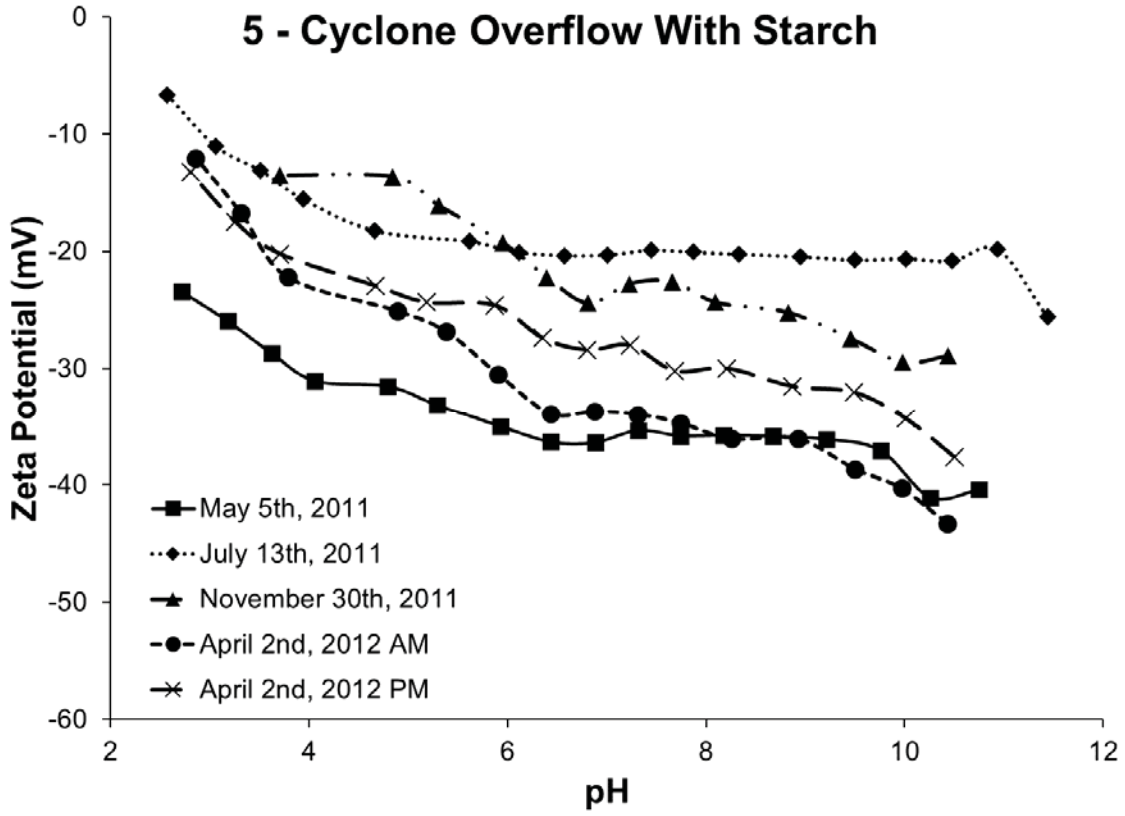

Figure A.4: Zeta potential as a function of pH for cyclone overflow with starch solids at process conditions for each sample set

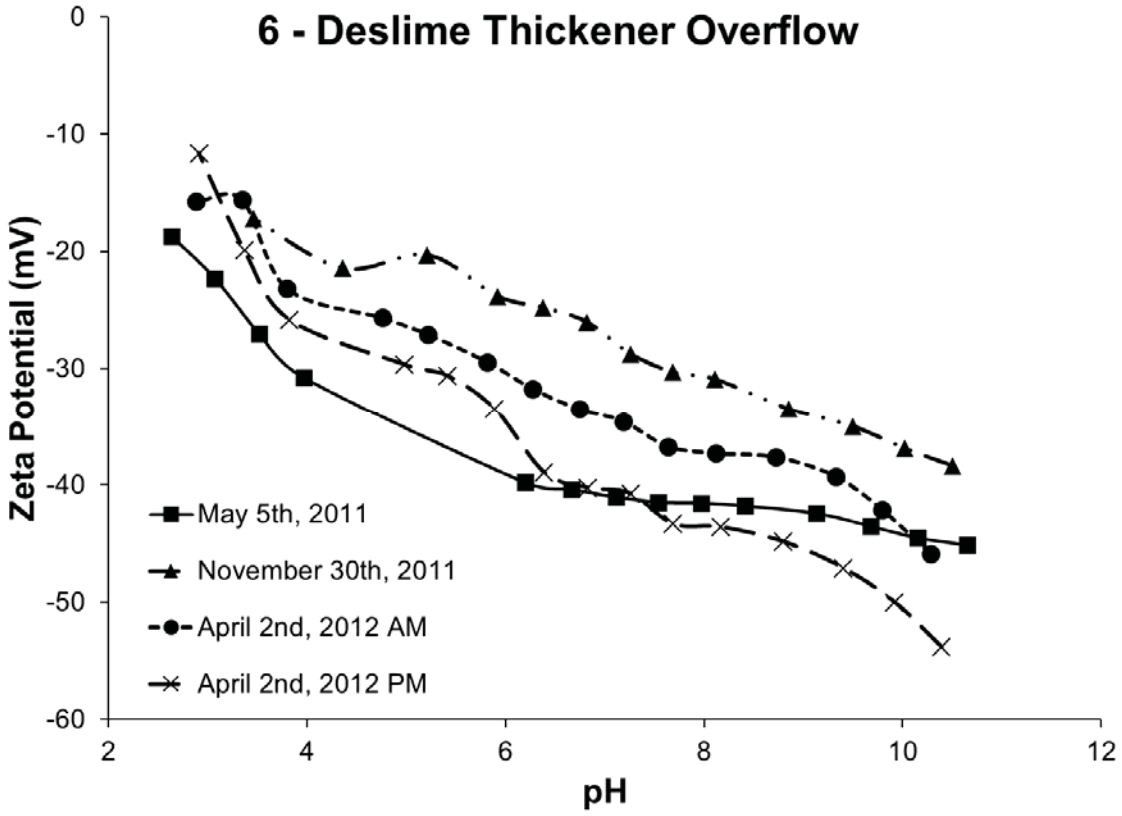

Figure A.5: Zeta potential as a function of pH for deslime thickener overflow solids at process conditions for each sample set

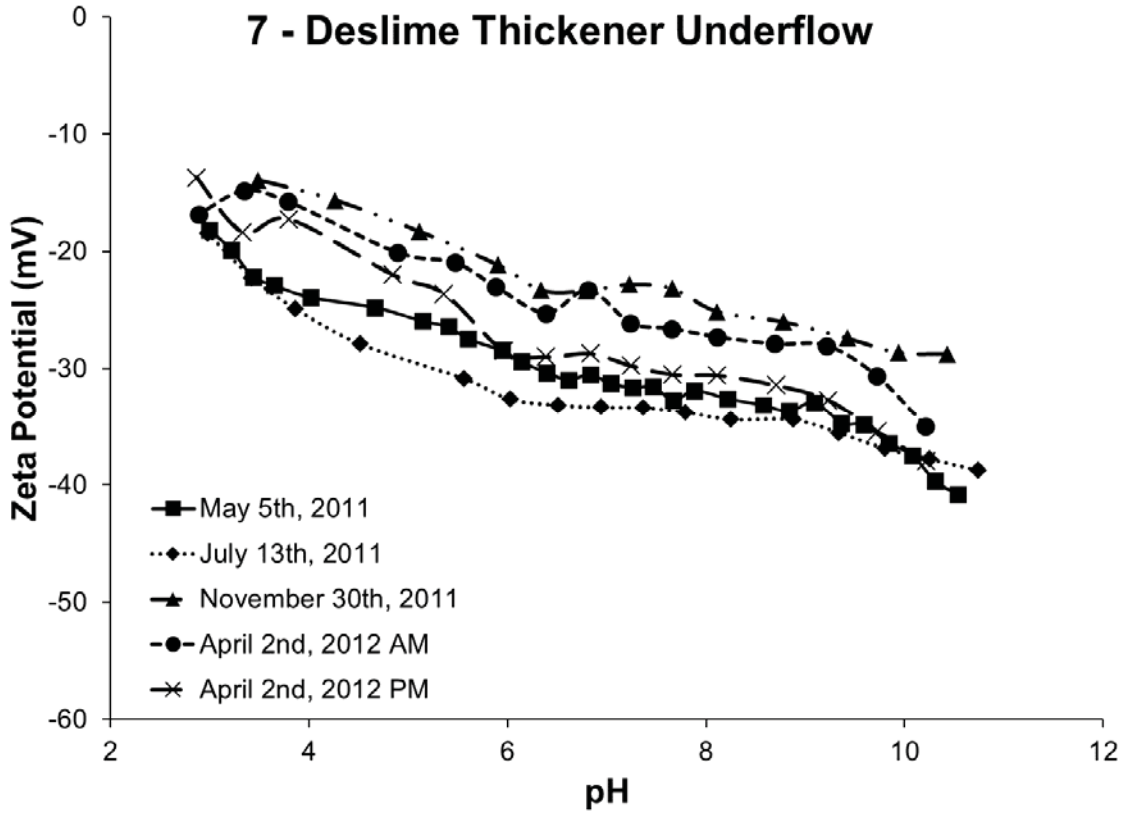

Figure A.6: Zeta potential as a function of pH for deslime thickener underflow solids at process conditions for each sample set

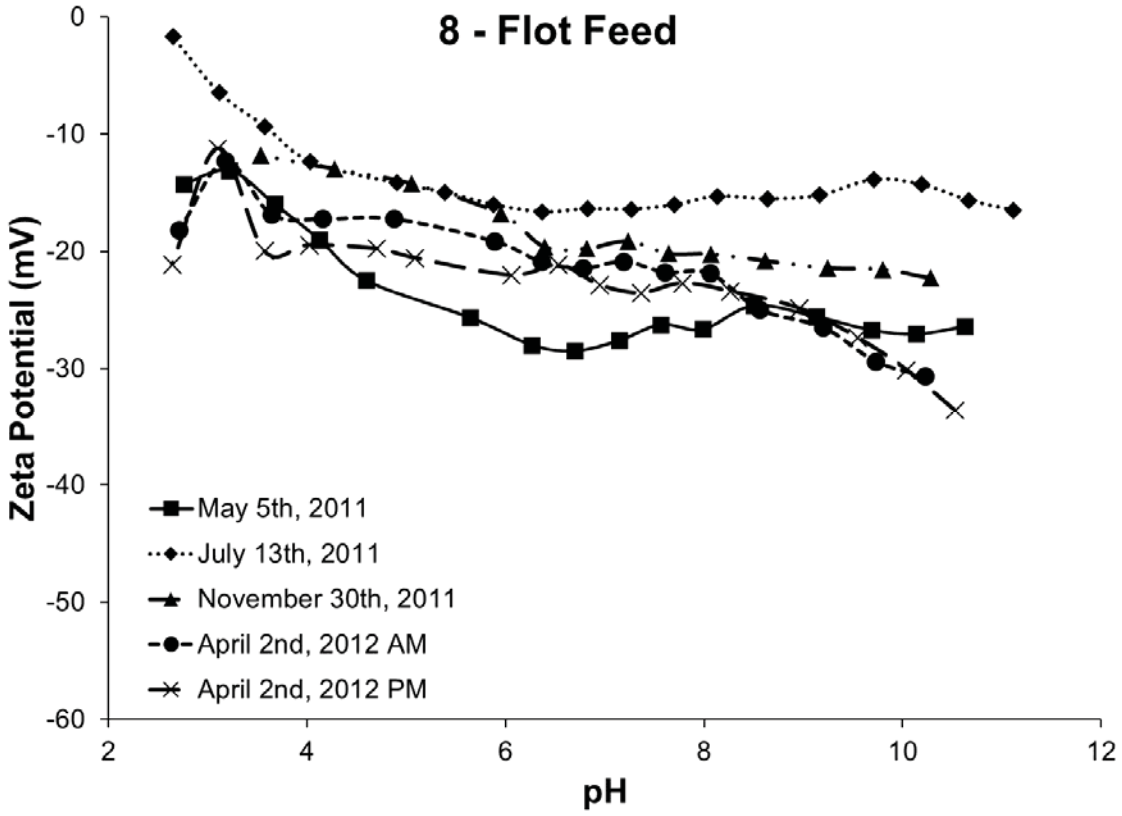

Figure A.7: Zeta potential as a function of pH for flotation feed solids at process conditions for each sample set

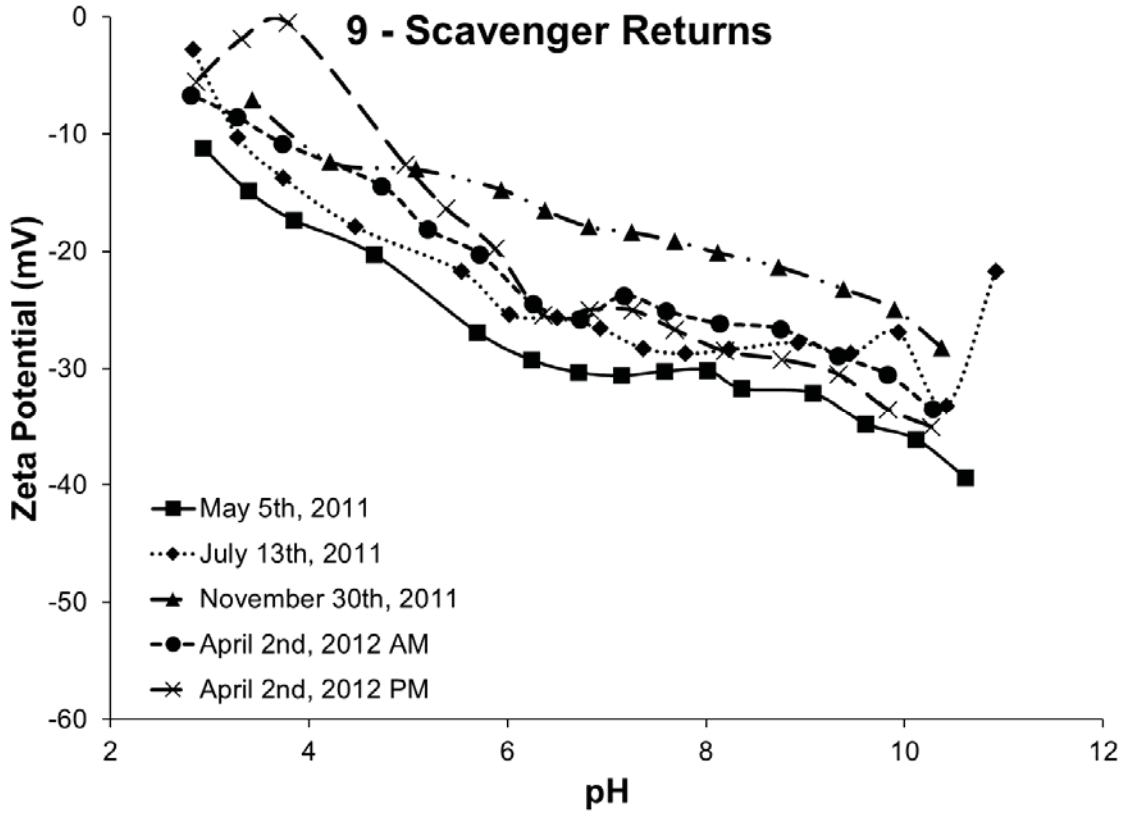

Figure A.8: Zeta potential as a function of pH for scavenger returns solids at process conditions for each sample set

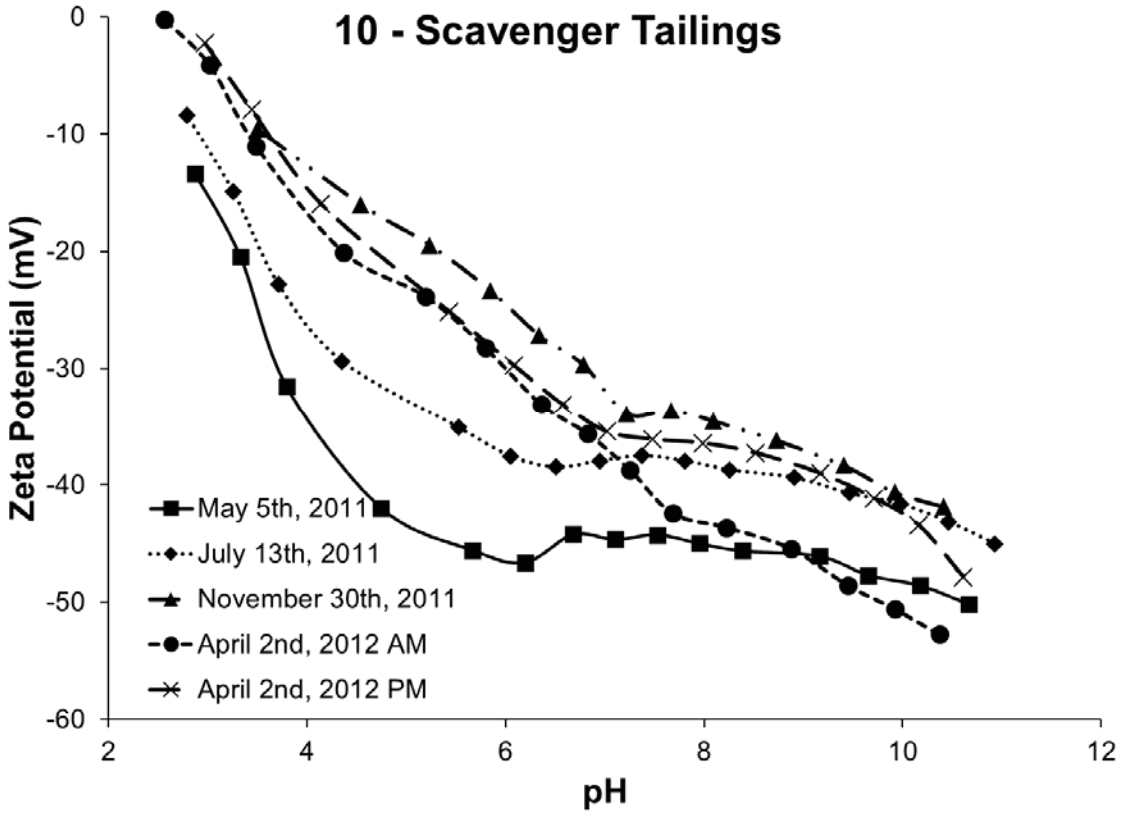

Figure A.9: Zeta potential as a function of pH for scavenger tailings solids at process conditions for each sample set

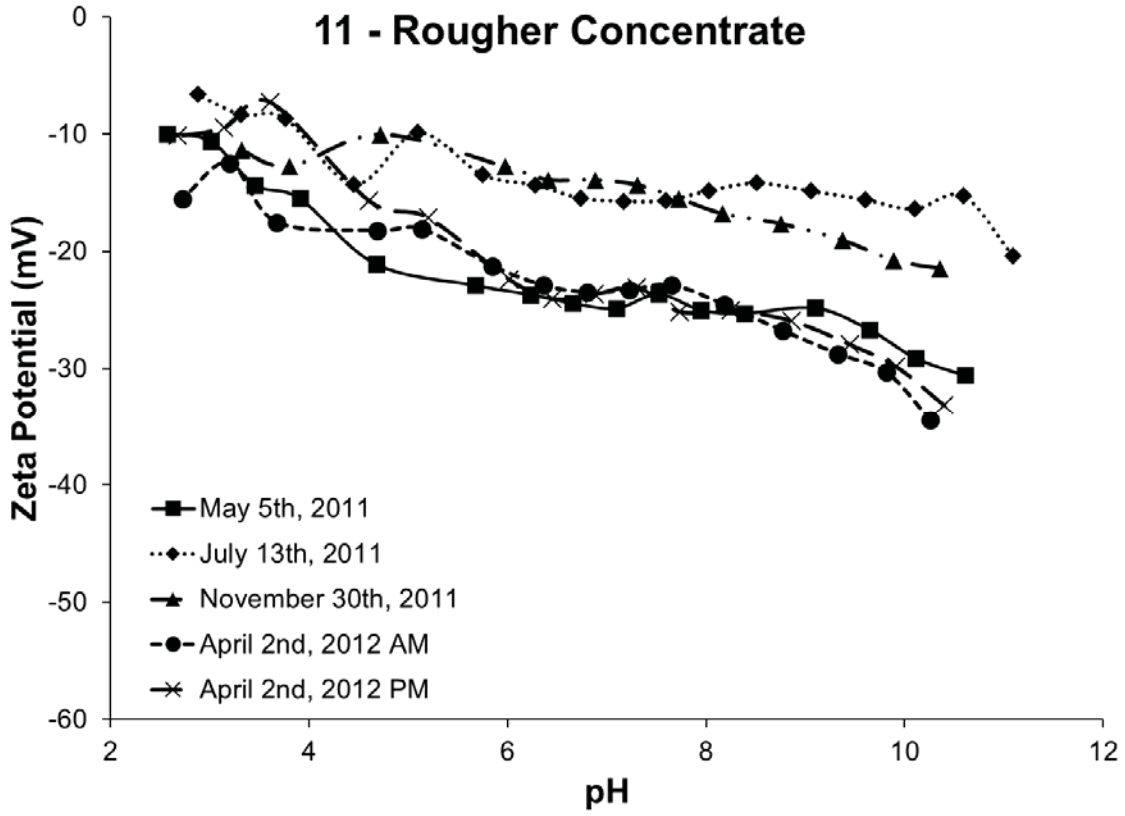

Figure A.10: Zeta potential as a function of pH for rougher concentrate solids at process conditions for each sample set

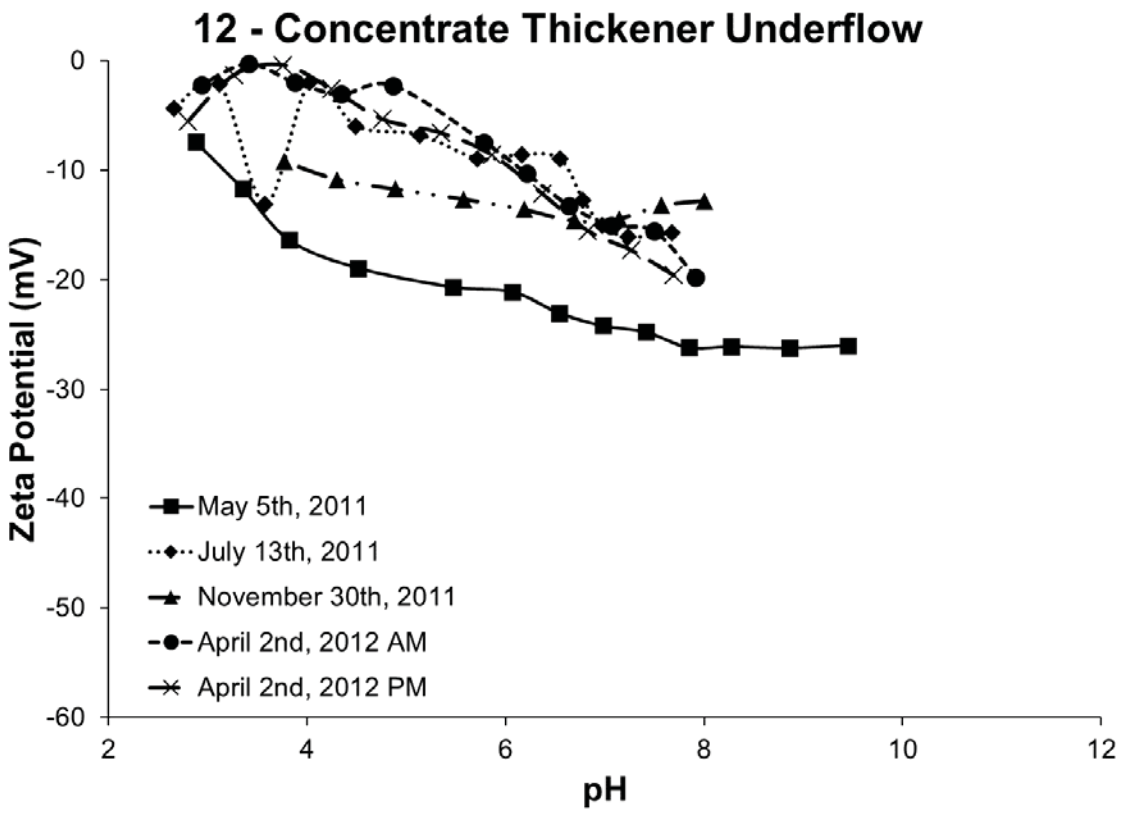

Figure A.11: Zeta potential as a function of pH for concentrate thickener underflow solids at process conditions for each sample set

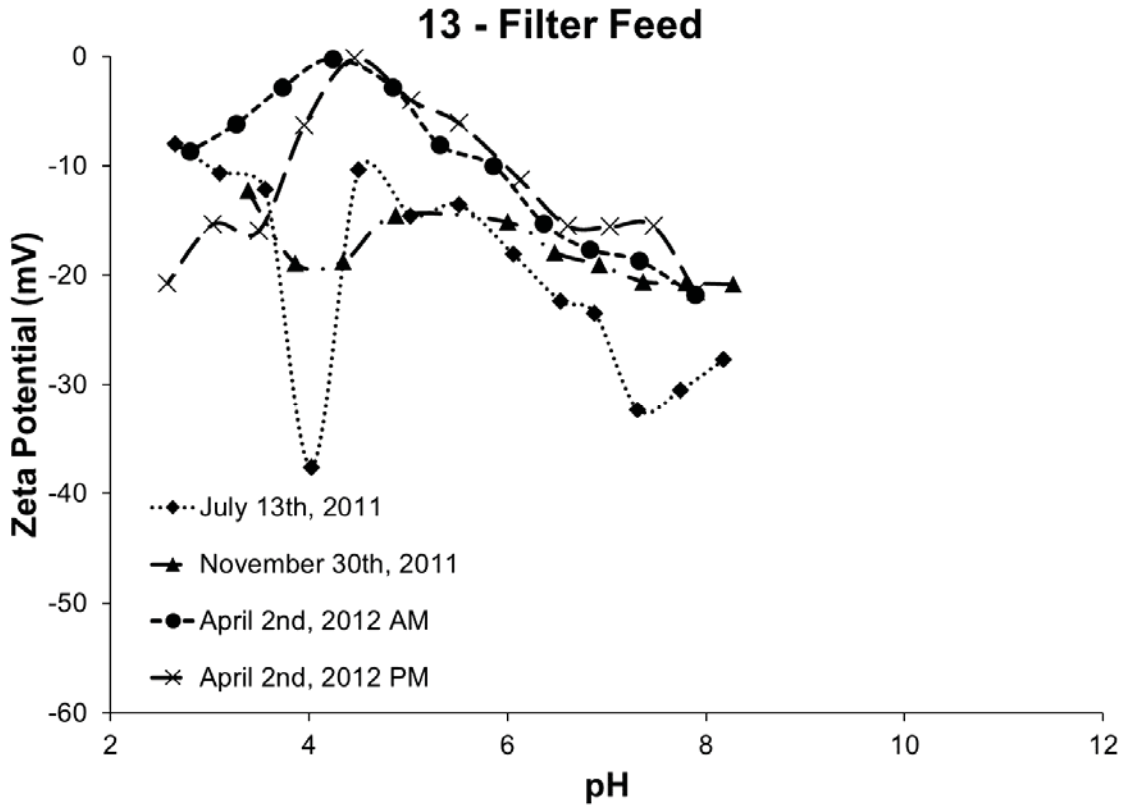

Figure A.12: Zeta potential as a function of pH for filter feed solids at process conditions for each sample set. Note: filter feed sample was not taken on May 5th, 2011.

Appendix B - Thermogravimetric Analysis for Plant Scale Studies

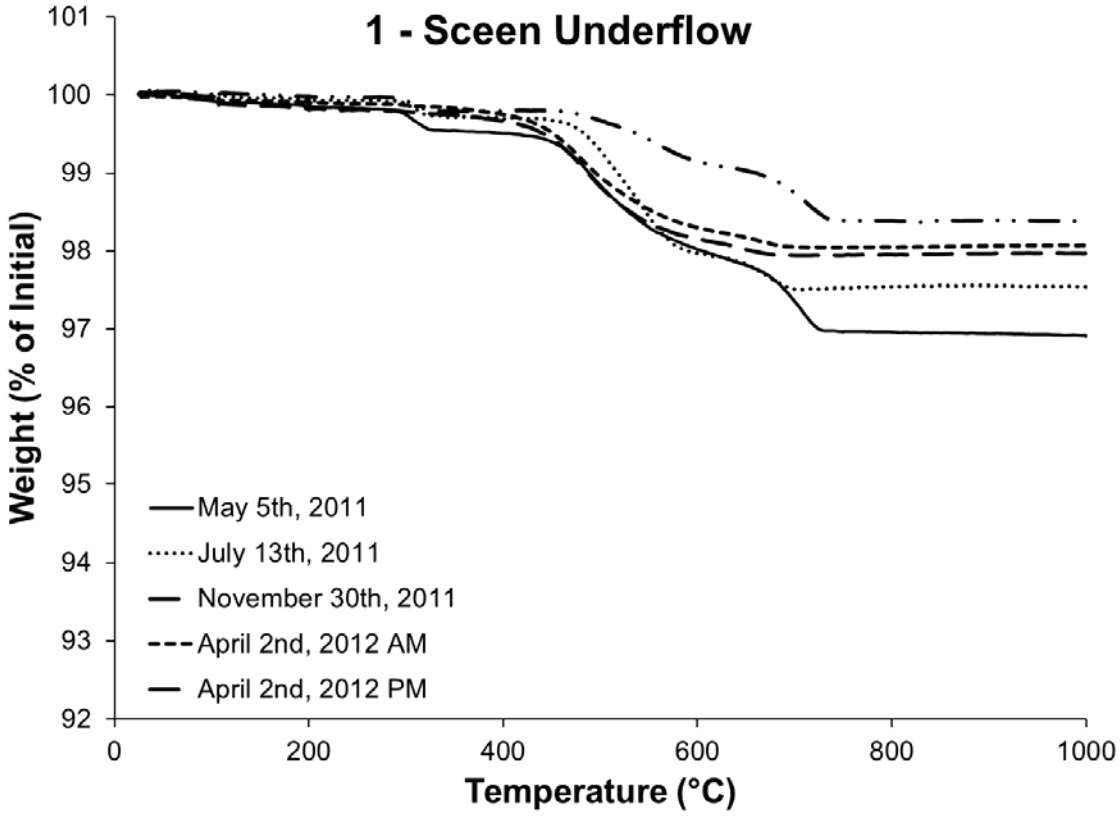

Figure B.1: Thermolysis curves for screen underflow solids. Thermal decomposition prior to 200°C is primarily due to moisture and loosely bound water at mineral surfaces. Decomposition near 300°C is due to the dehydration of goethite into hematite. Decomposition from 400 to 700°C is due to the decarbonation of dolomite, ankerite, calcite and siderite.

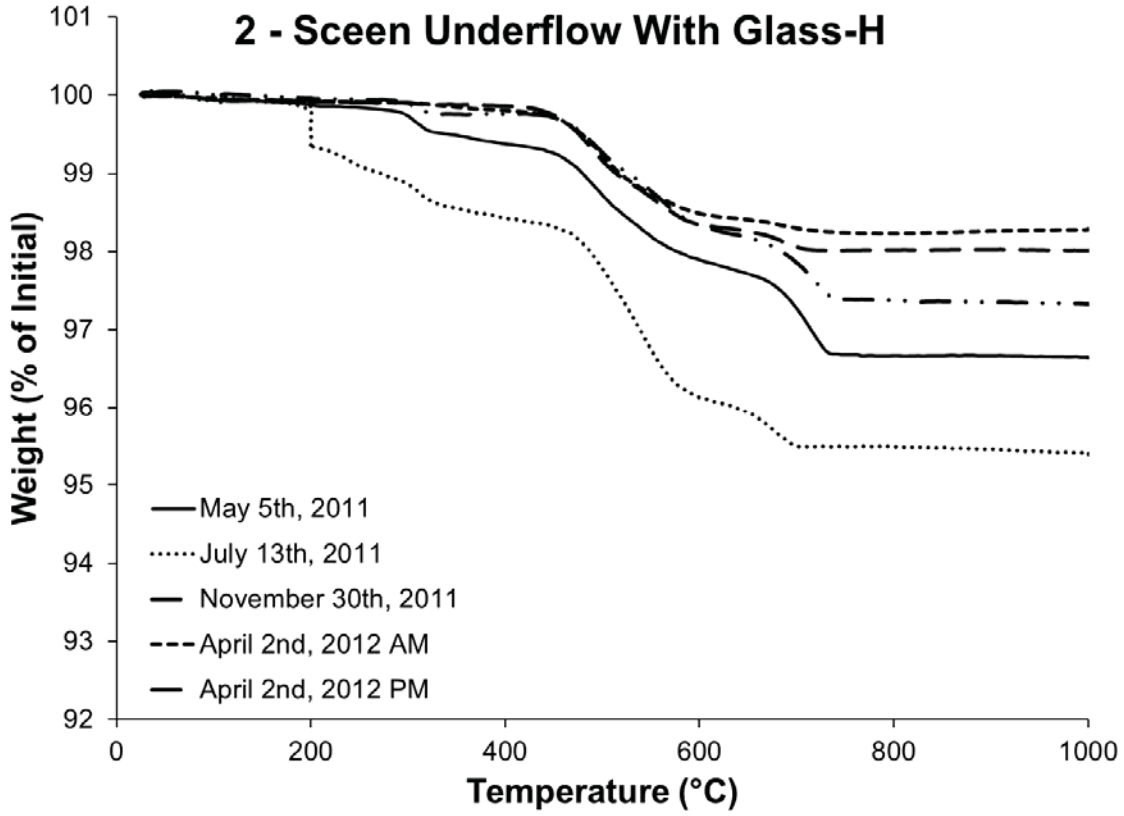

Figure B.2: Thermolysis curves for screen underflow with Glass-H solids. Thermal decomposition prior to 200°C is primarily due to moisture and loosely bound water at mineral surfaces. Decomposition near 300°C is due to the dehydration of goethite into hematite. Decomposition from 400 to 700°C is due to the decarbonation of dolomite, ankerite, calcite and siderite.

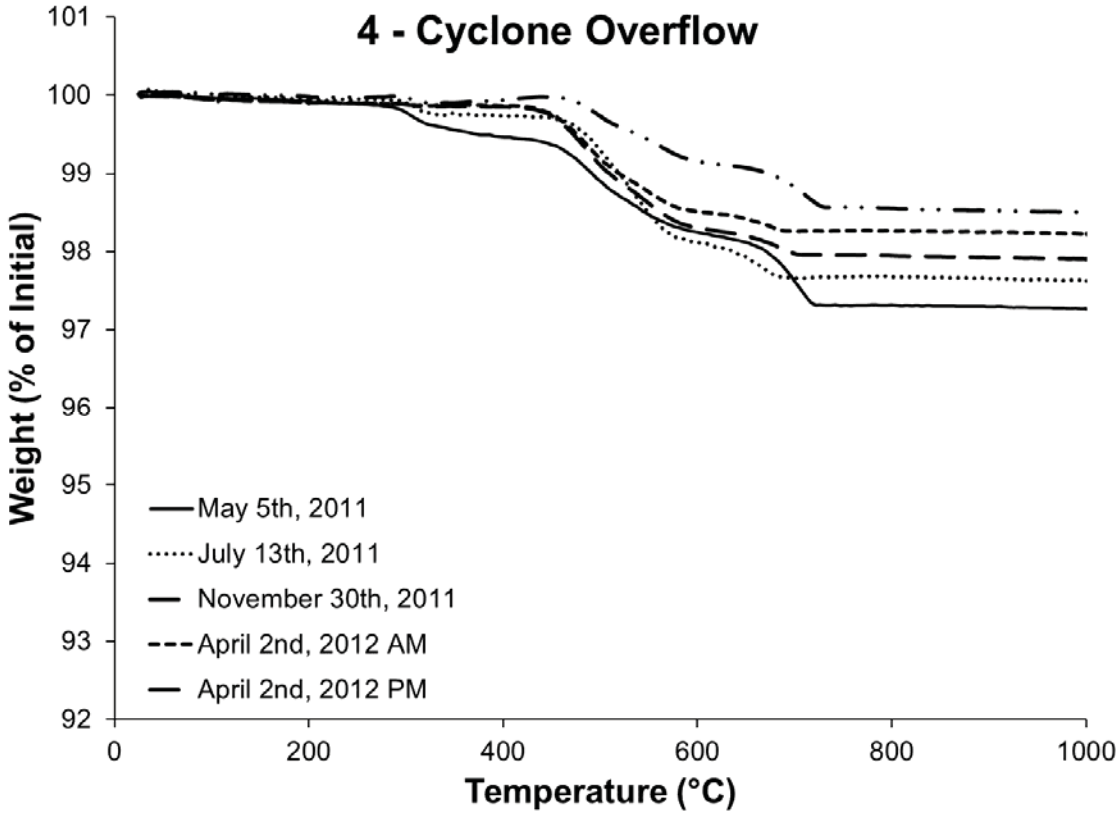

Figure B.3: Thermolysis curves for cyclone overflow solids. Thermal decomposition prior to 200°C is primarily due to moisture and loosely bound water at mineral surfaces. Decomposition near 300°C is due to the dehydration of goethite into hematite. Decomposition from 400 to 700°C is due to the decarbonation of dolomite, ankerite, calcite and siderite.

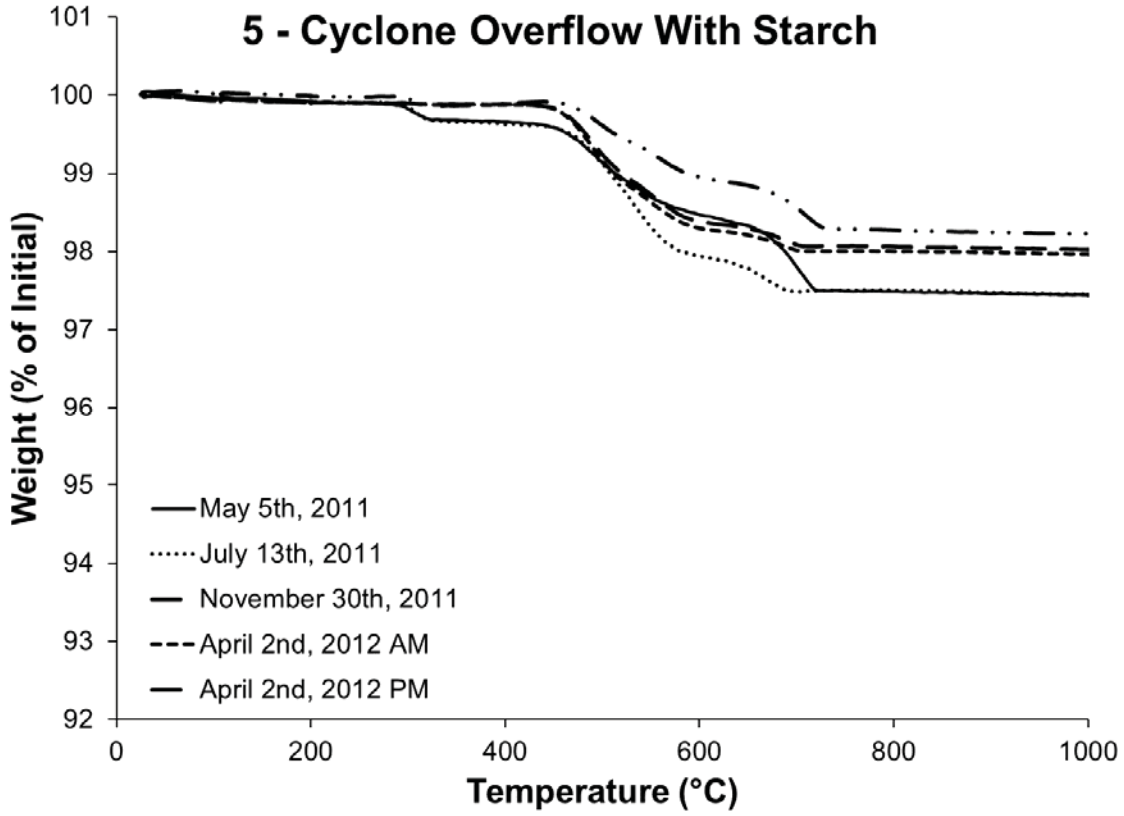

Figure B.4: Thermolysis curves for cyclone overflow with starch solids. Thermal decomposition prior to 200°C is primarily due to moisture and loosely bound water at mineral surfaces. Decomposition near 300°C is due to the dehydration of goethite into hematite. Decomposition from 400 to 700°C is due to the decarbonation of dolomite, ankerite, calcite and siderite.

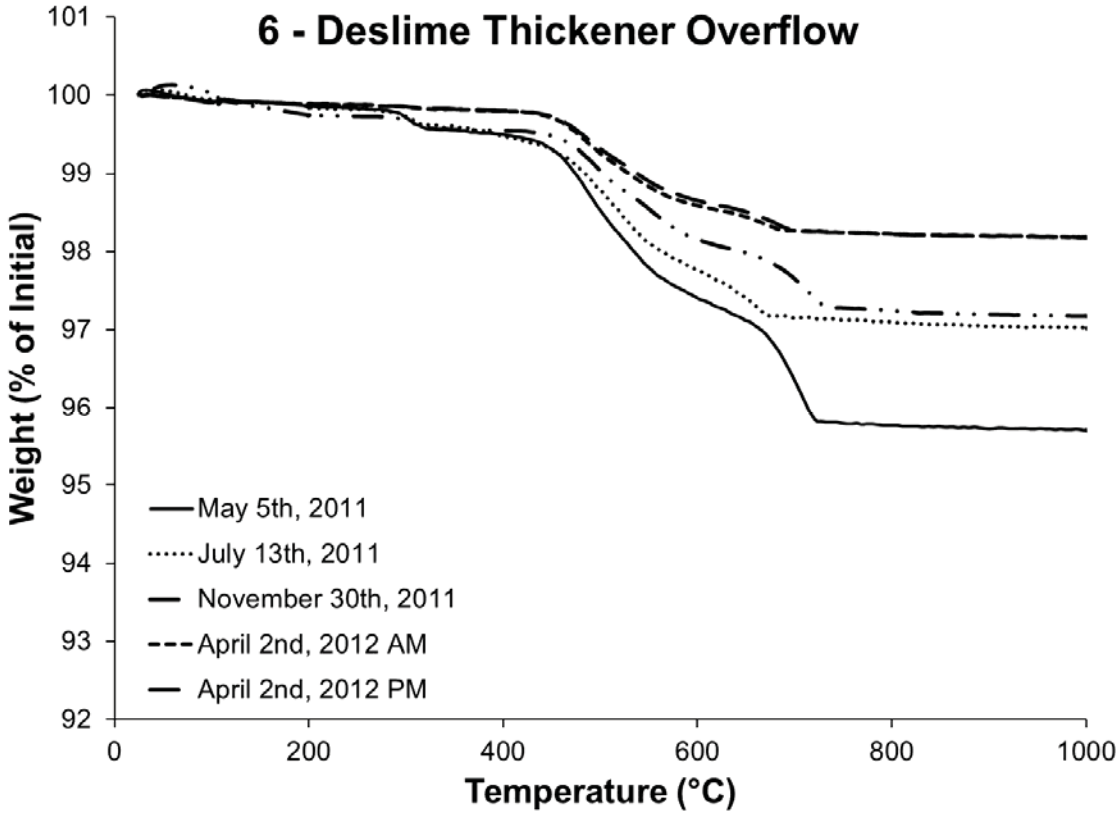

Figure B.5: Thermolysis curves for deslime thickener overflow solids. Thermal decomposition prior to 200°C is primarily due to moisture and loosely bound water at mineral surfaces. Decomposition near 300°C is due to the dehydration of goethite into hematite. Decomposition from 400 to 700°C is due to the decarbonation of dolomite, ankerite, calcite and siderite.

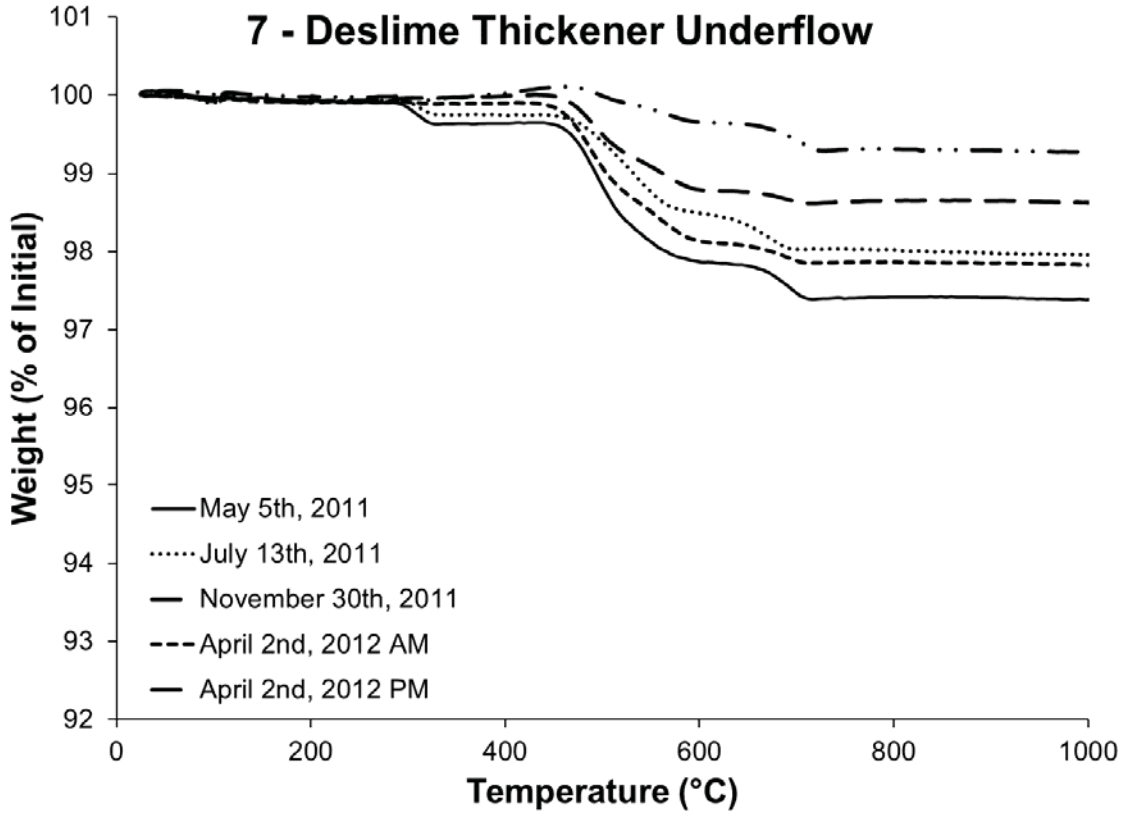

Figure B.6: Thermolysis curves for deslime thickener underflow solids. Thermal decomposition prior to 200°C is primarily due to moisture and loosely bound water at mineral surfaces. Decomposition near 300°C is due to the dehydration of goethite into hematite. Decomposition from 400 to 700°C is due to the decarbonation of dolomite, ankerite, calcite and siderite.

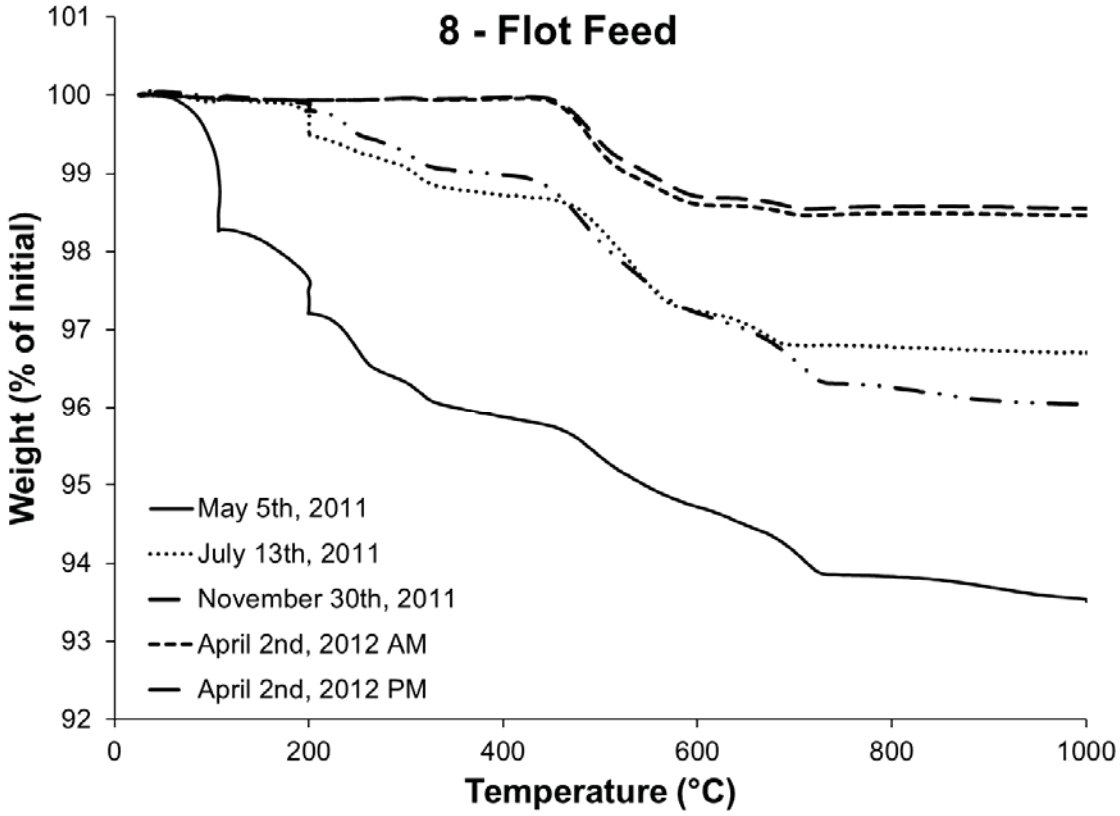

Figure B.7: Thermolysis curves for flotation feed solids. Thermal decomposition prior to 200°C is primarily due to moisture and loosely bound water at mineral surfaces. Decomposition near 300°C is due to the dehydration of goethite into hematite. Decomposition from 400 to 700°C is due to the decarbonation of dolomite, ankerite, calcite and siderite.

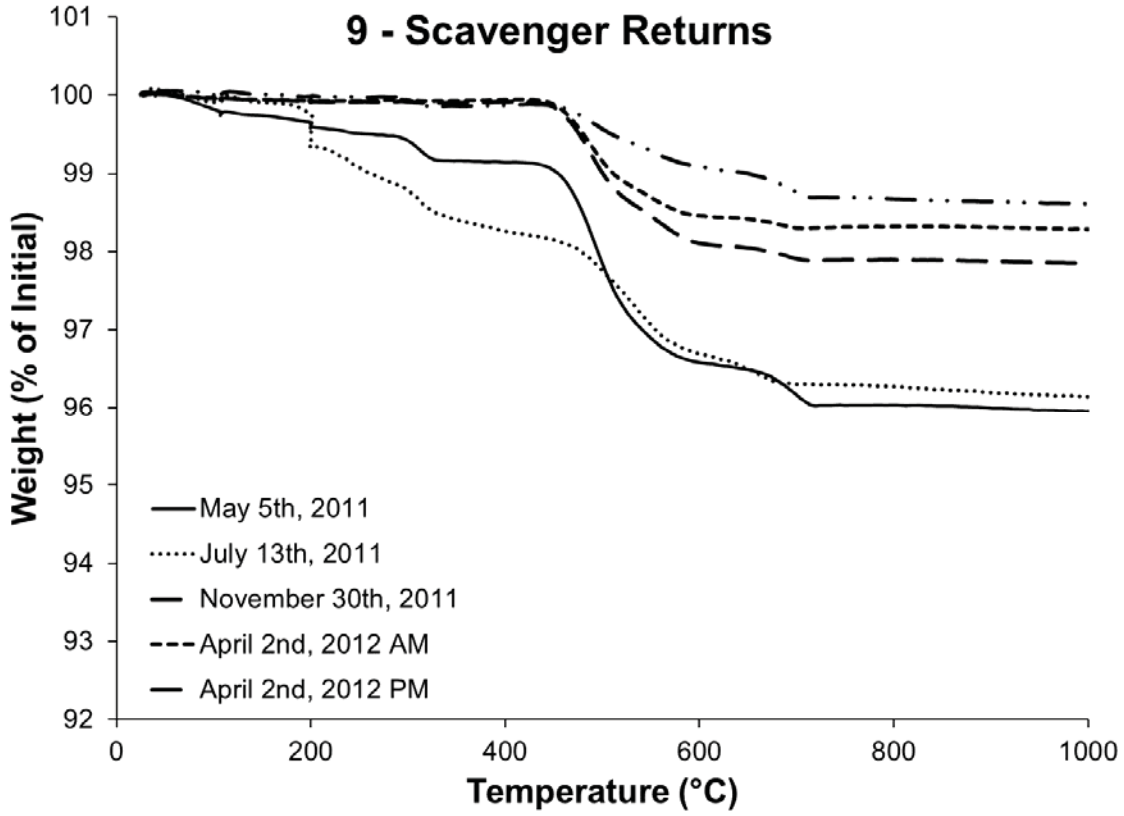

Figure B.8: Thermolysis curves for scavenger returns solids. Thermal decomposition prior to 200°C is primarily due to moisture and loosely bound water at mineral surfaces. Decomposition near 300°C is due to the dehydration of goethite into hematite. Decomposition from 400 to 700°C is due to the decarbonation of dolomite, ankerite, calcite and siderite.

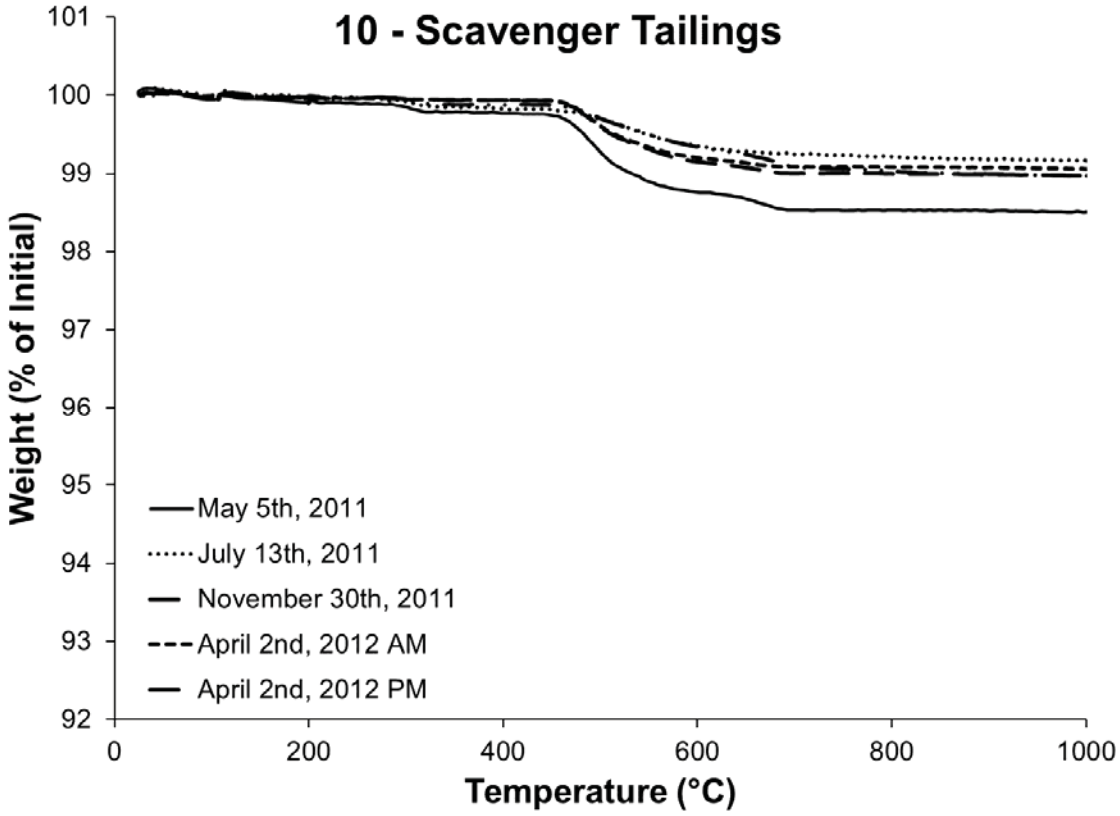

Figure B.9: Thermolysis curves for scavenger tailings solids. Thermal decomposition prior to 200°C is primarily due to moisture and loosely bound water at mineral surfaces. Decomposition near 300°C is due to the dehydration of goethite into hematite. Decomposition from 400 to 700°C is due to the decarbonation of dolomite, ankerite, calcite and siderite.

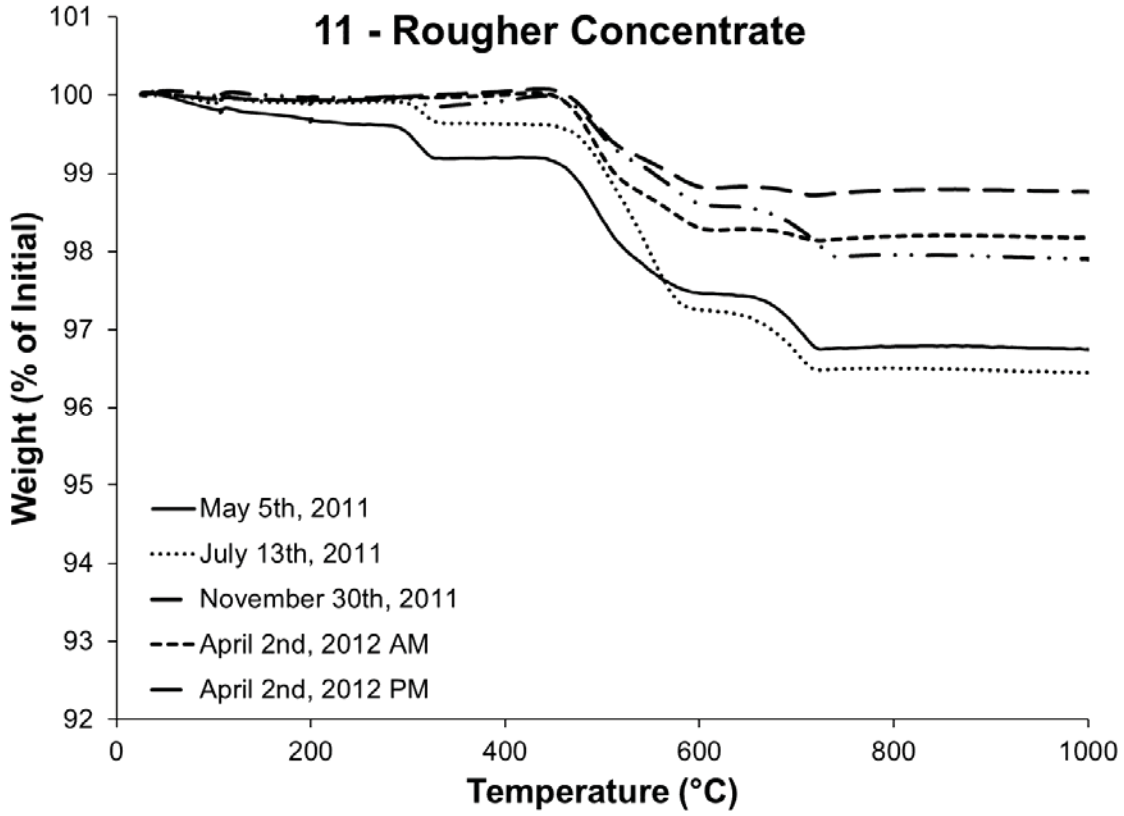

Figure B.10: Thermolysis curves for rougher concentrate solids. Thermal decomposition prior to 200°C is primarily due to moisture and loosely bound water at mineral surfaces. Decomposition near 300°C is due to the dehydration of goethite into hematite. Decomposition from 400 to 700°C is due to the decarbonation of dolomite, ankerite, calcite and siderite.

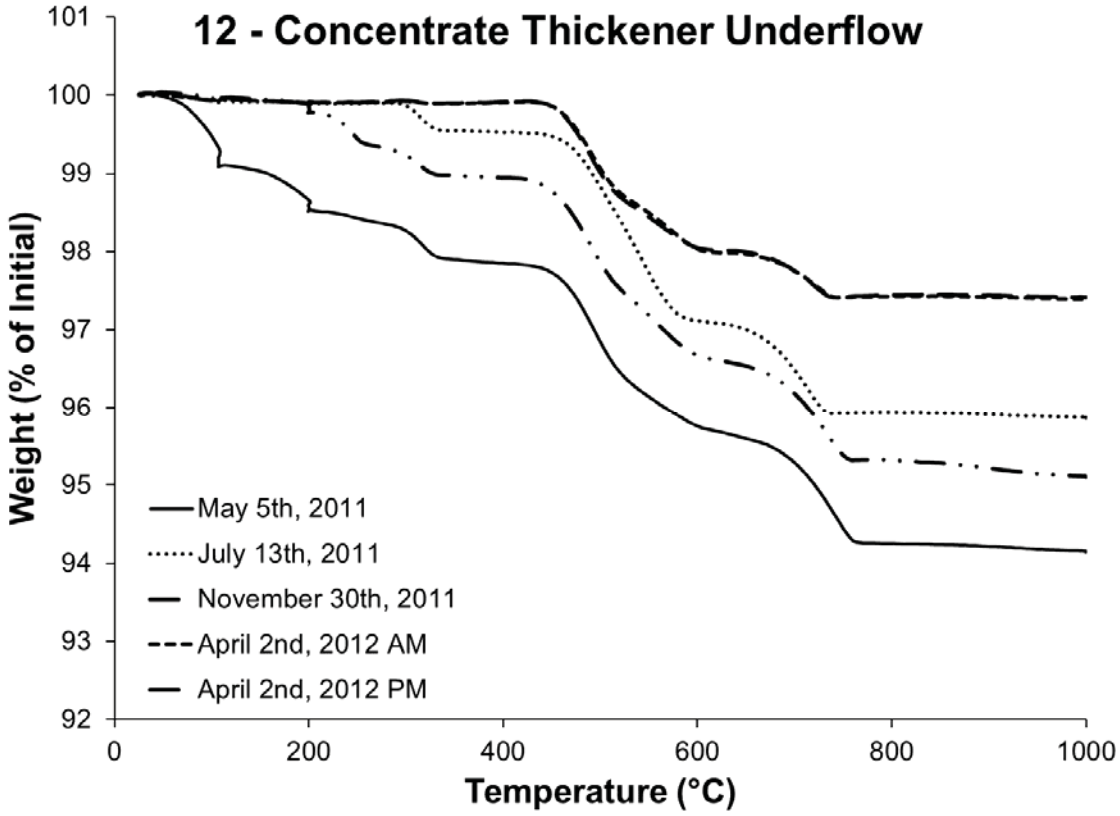

Figure B.11: Thermolysis curves for concentrate thickener underflow solids. Thermal decomposition prior to 200°C is primarily due to moisture and loosely bound water at mineral surfaces. Decomposition near 300°C is due to the dehydration of goethite into hematite. Decomposition from 400 to 700°C is due to the decarbonation of dolomite, ankerite, calcite and siderite.

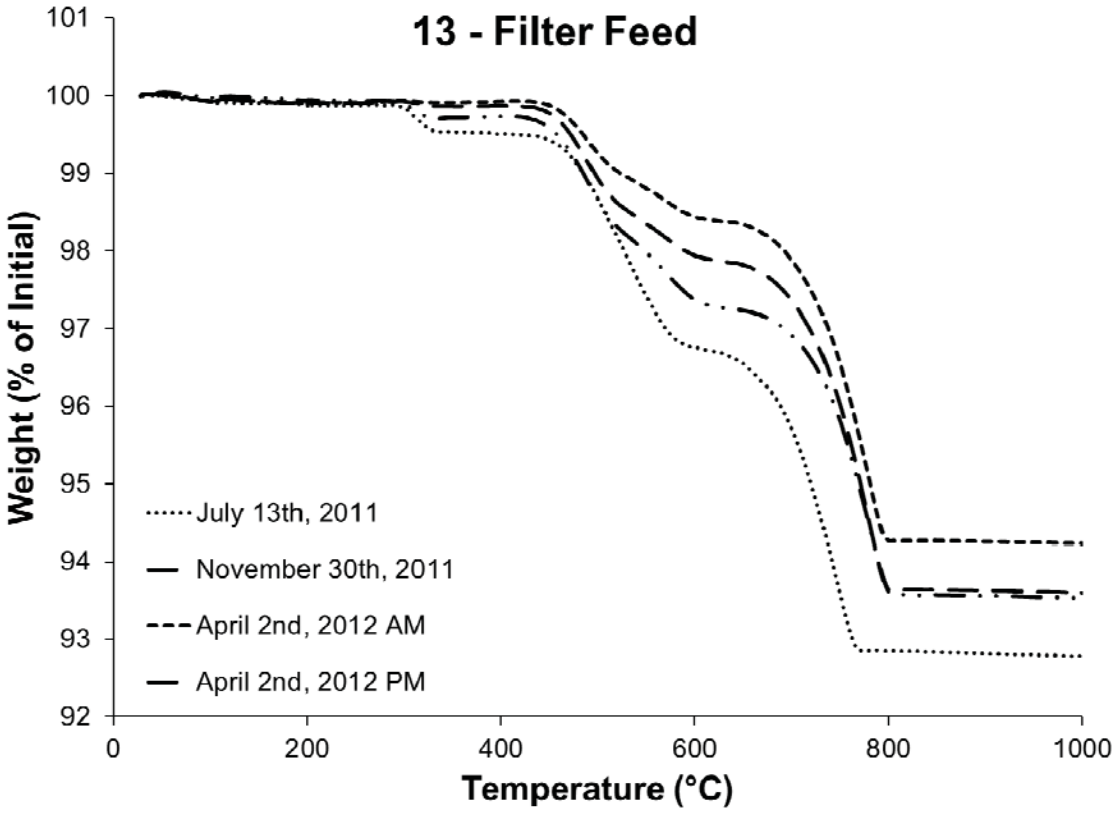

Figure B.12: Thermolysis curves for filter feed solids. Thermal decomposition prior to 200°C is primarily due to moisture and loosely bound water at mineral surfaces. Decomposition near 300°C is due to the dehydration of goethite into hematite. Decomposition from 400 to 700°C is due to the decarbonation of dolomite, ankerite, calcite and siderite. Note: filter feed sample was not taken on May 5th, 2011.

Appendix C – Particle Size Analyses for Plant Scale Studies

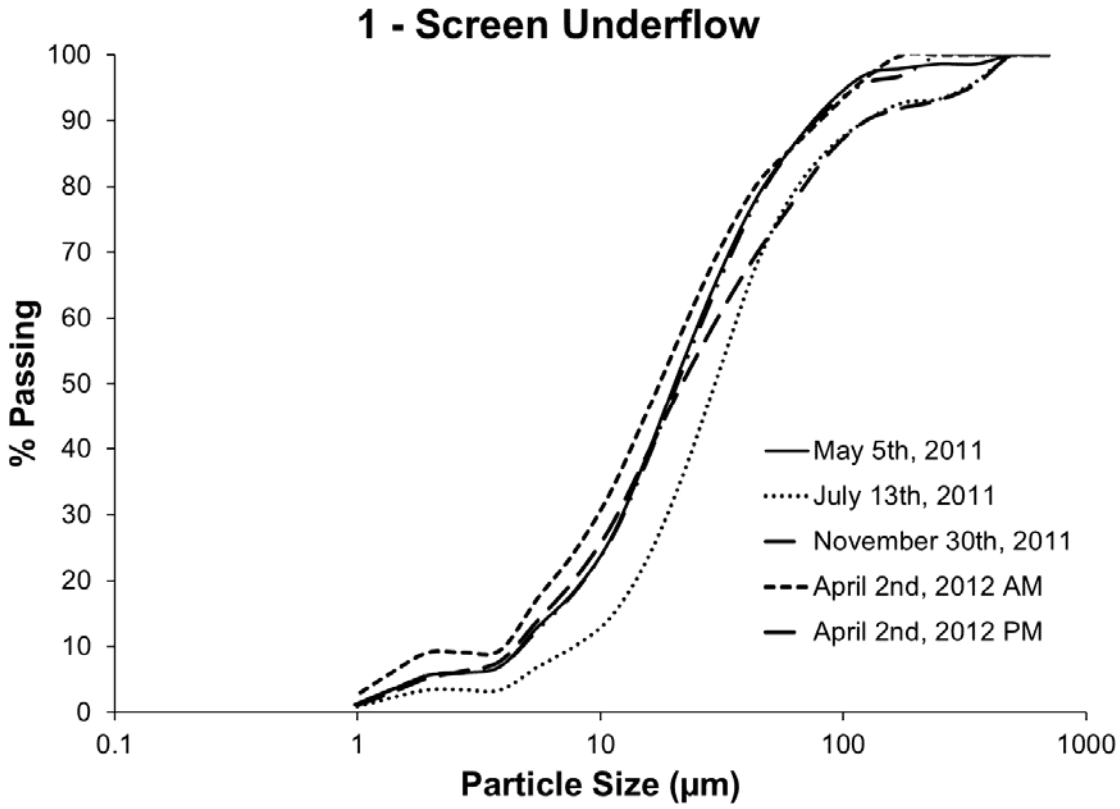

Figure C.1: Particle size distribution of screen underflow solids for each sample set.

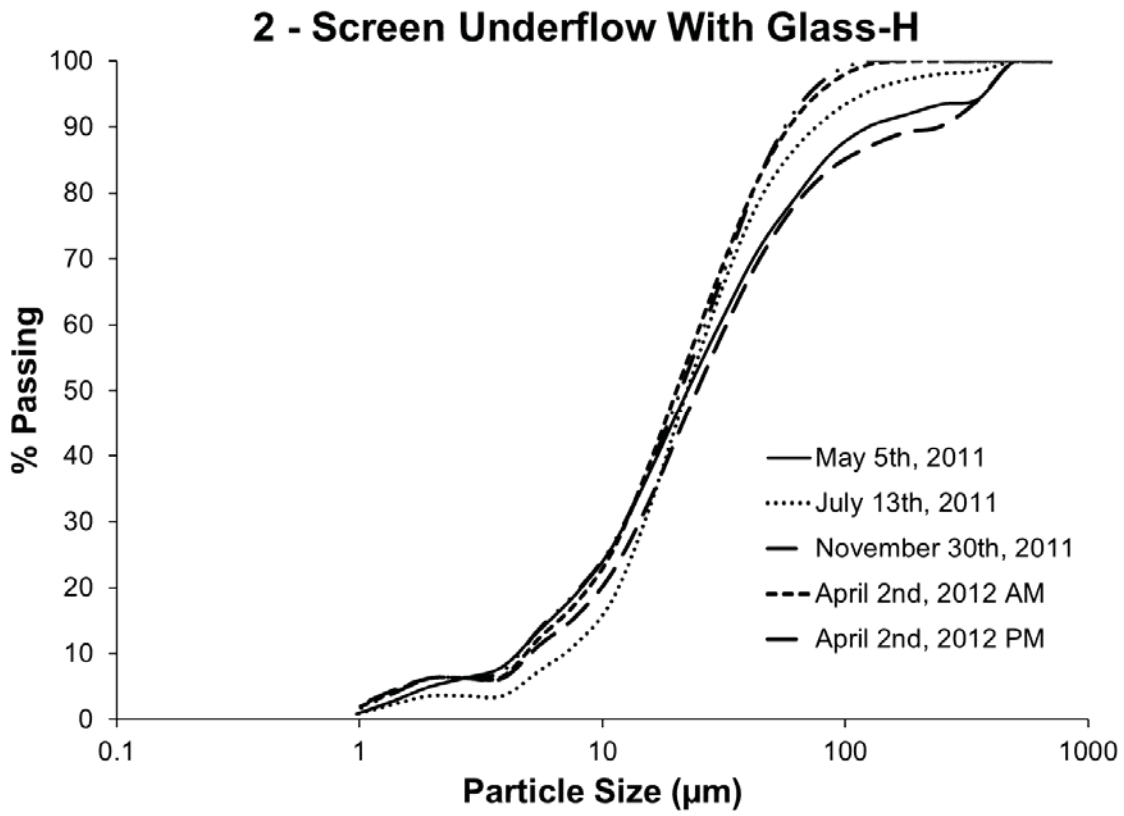

Figure C.2: Particle size distribution of screen underflow with Glass-H solids for each sample set.

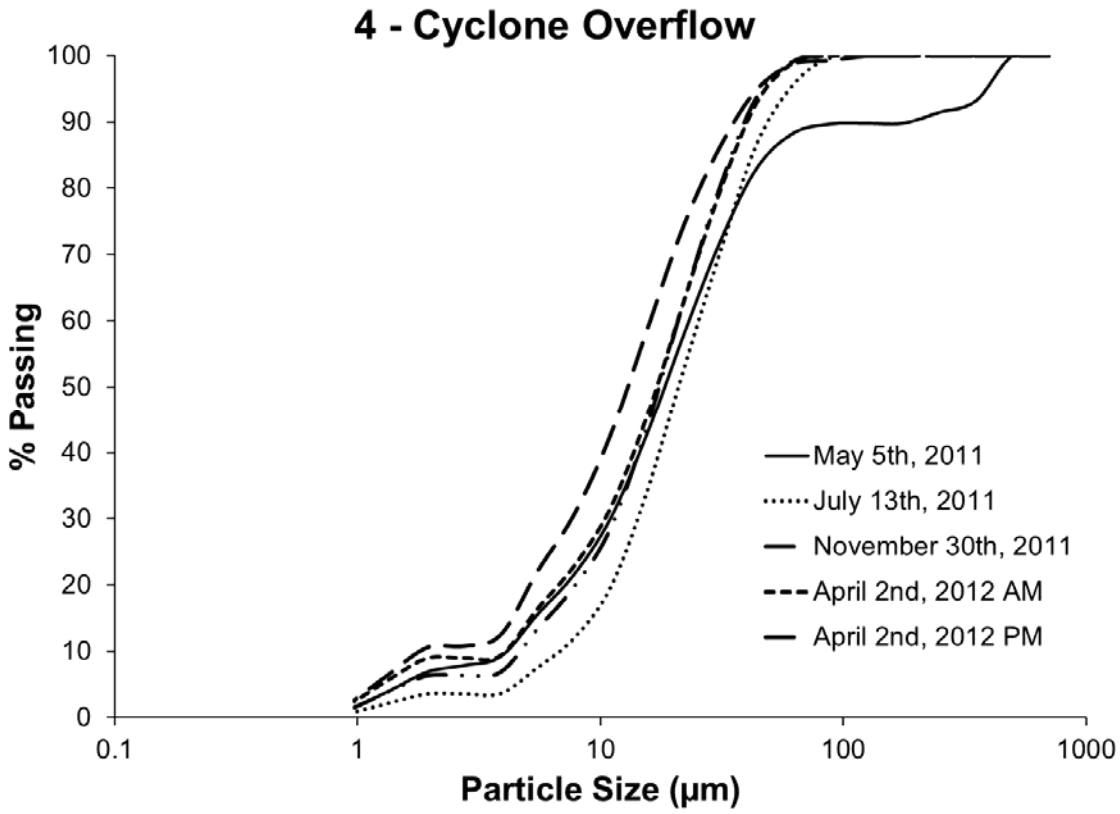

Figure C.3: Particle size distribution of cyclone overflow solids for each sample set.

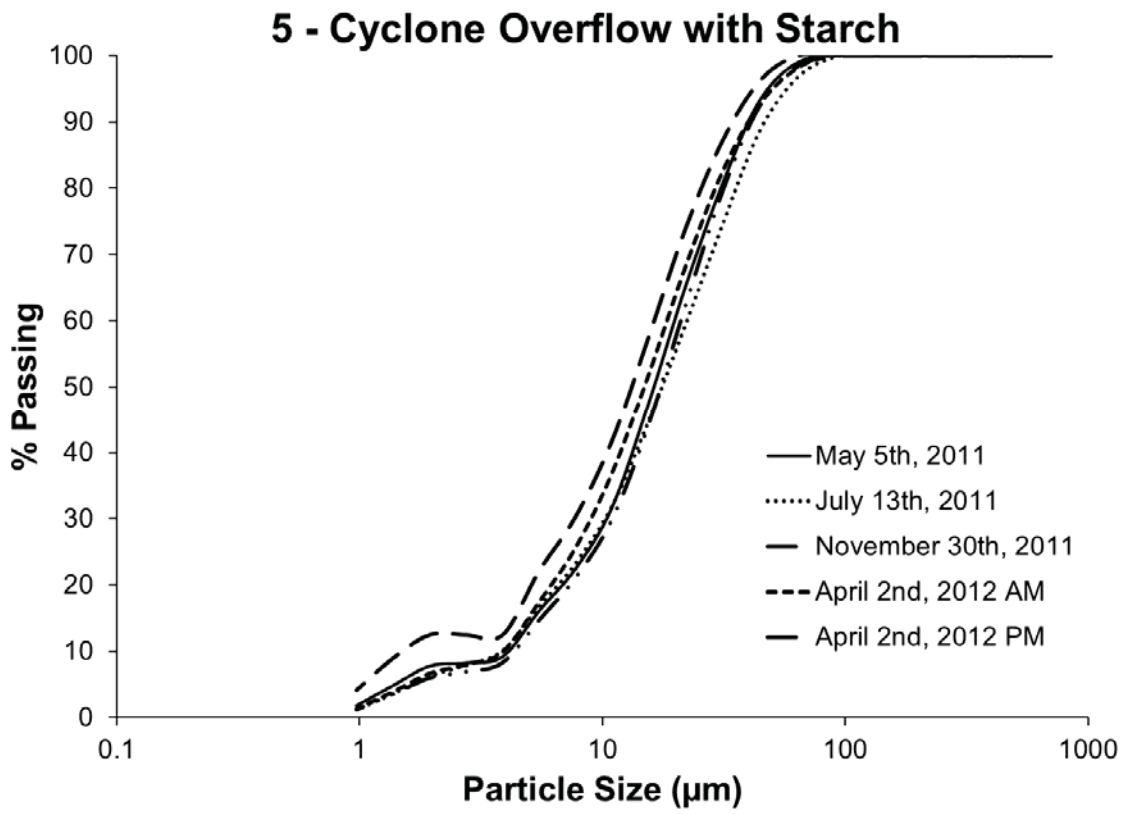

Figure C.4: Particle size distribution of cyclone overflow with starch solids for each sample set.

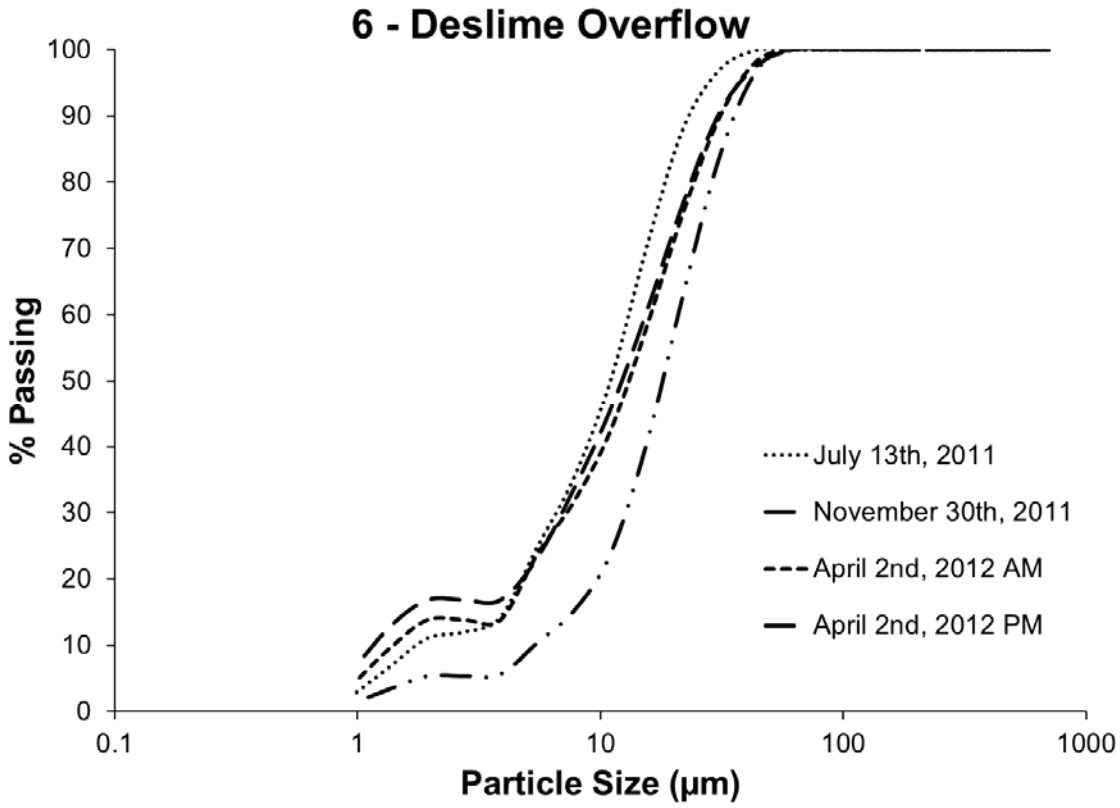

Figure C.5: Particle size distribution of deslime overflow solids for each sample set.

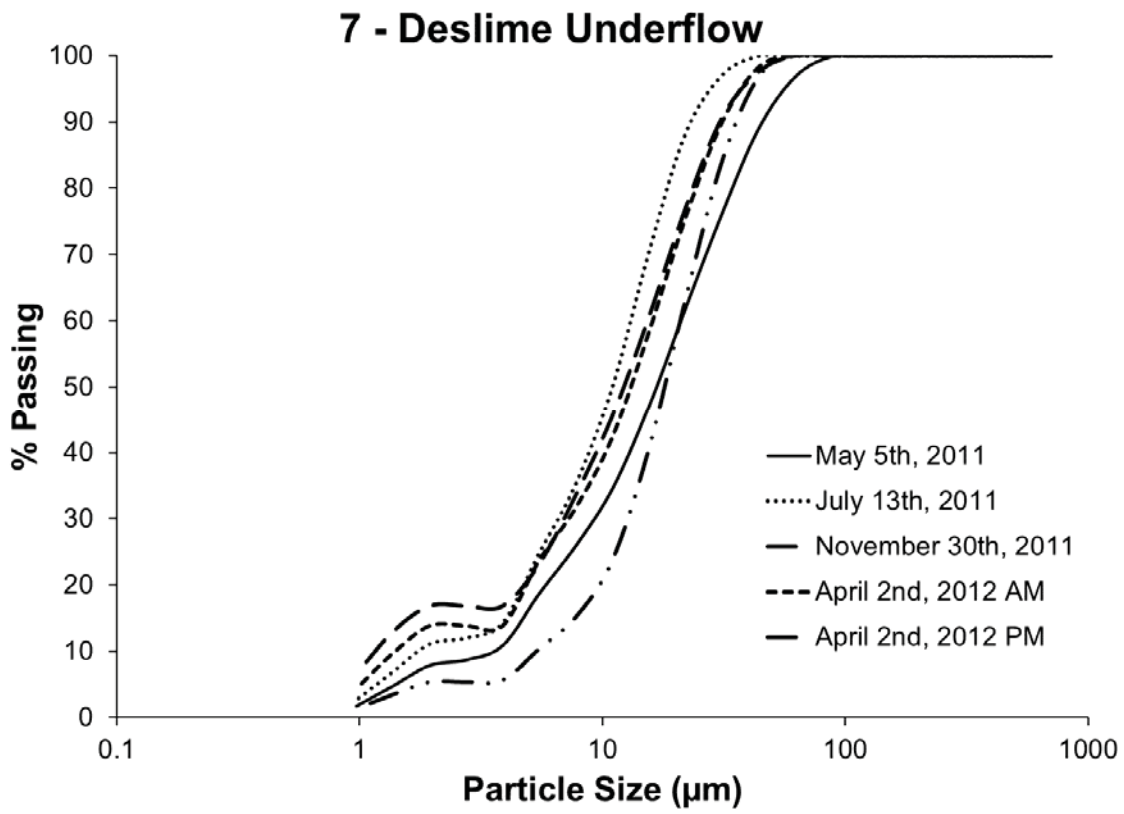

Figure C.6: Particle size distribution of deslime underflow solids for each sample set.

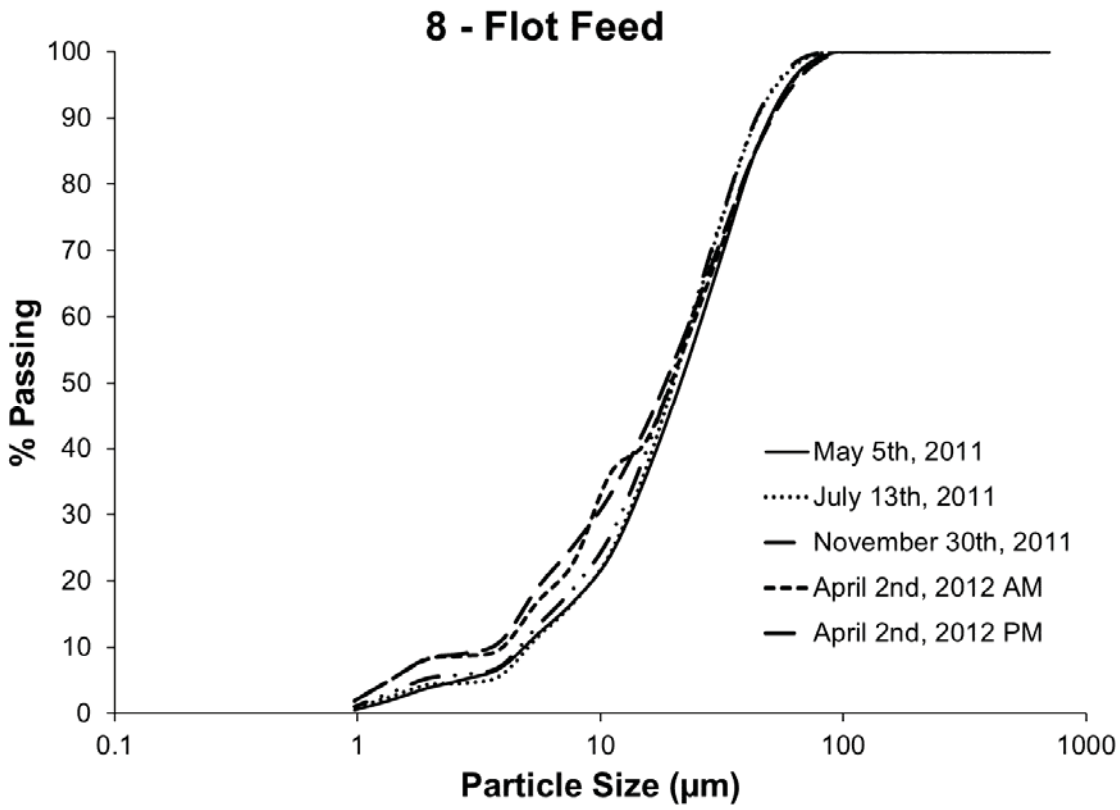

Figure C.7: Particle size distribution of flotation feed solids for each sample set.

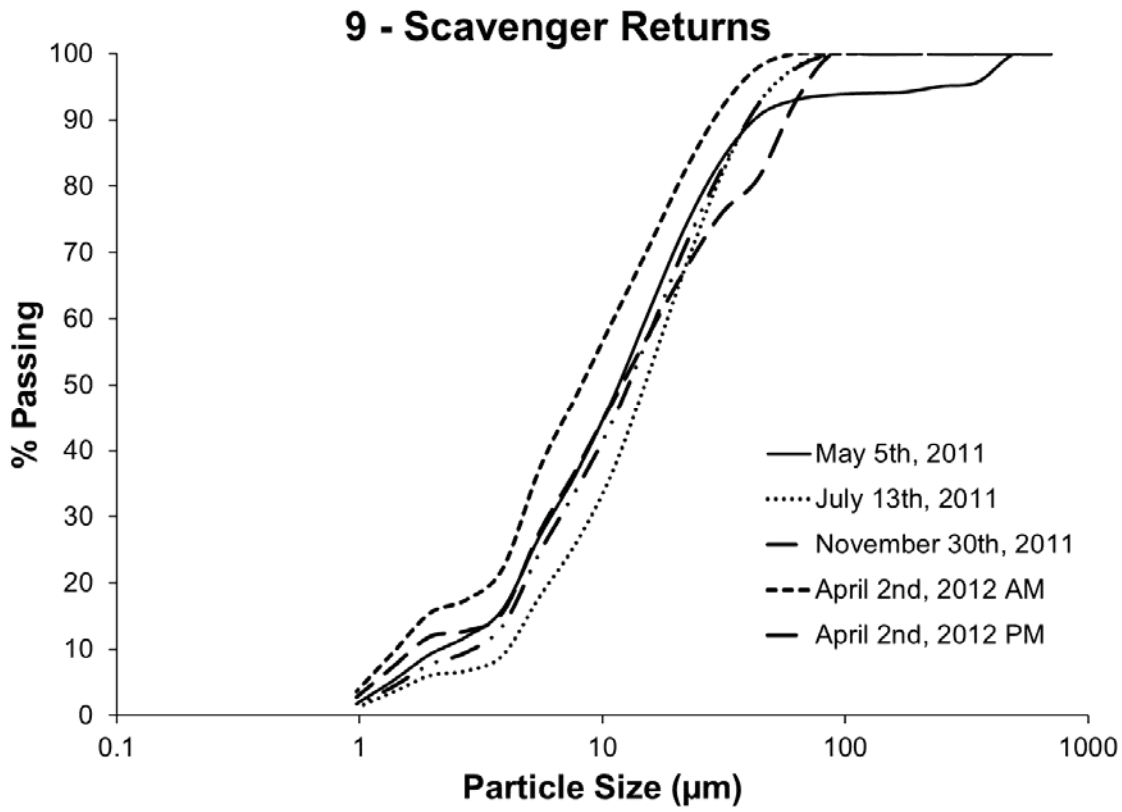

Figure C.8: Particle size distribution of scavenger returns solids for each sample set.

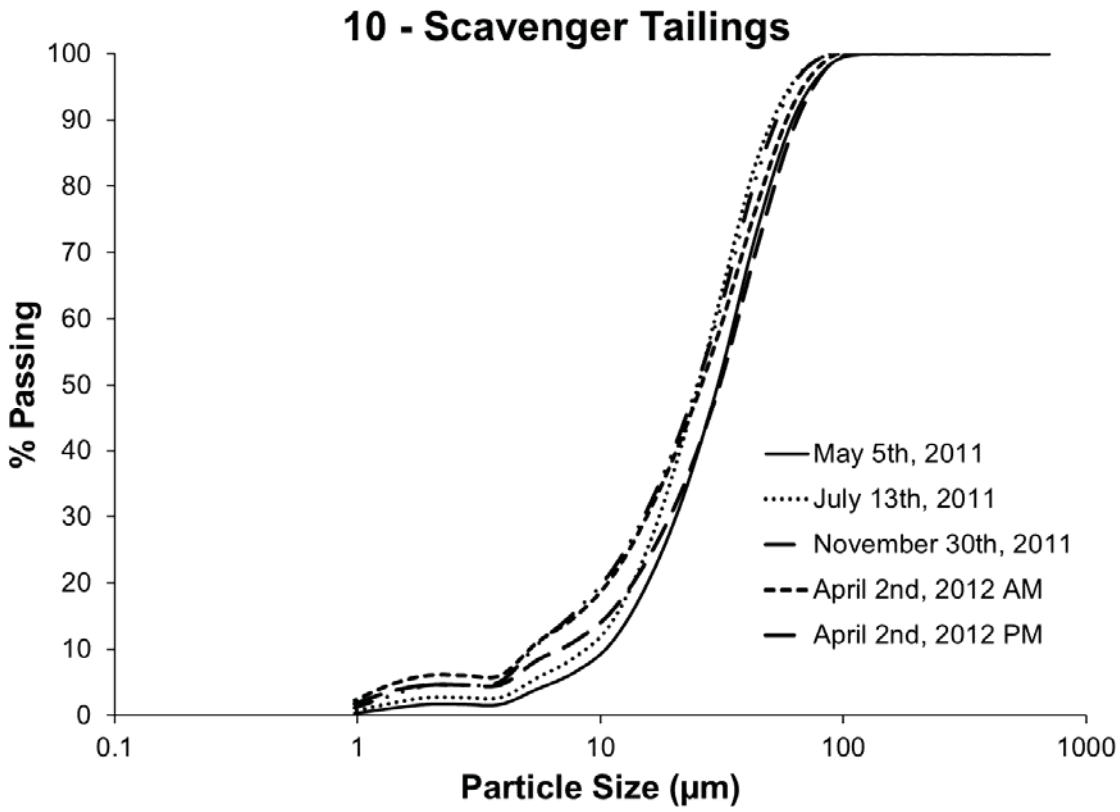

Figure C.9: Particle size distribution of scavenger tailings solids for each sample set.

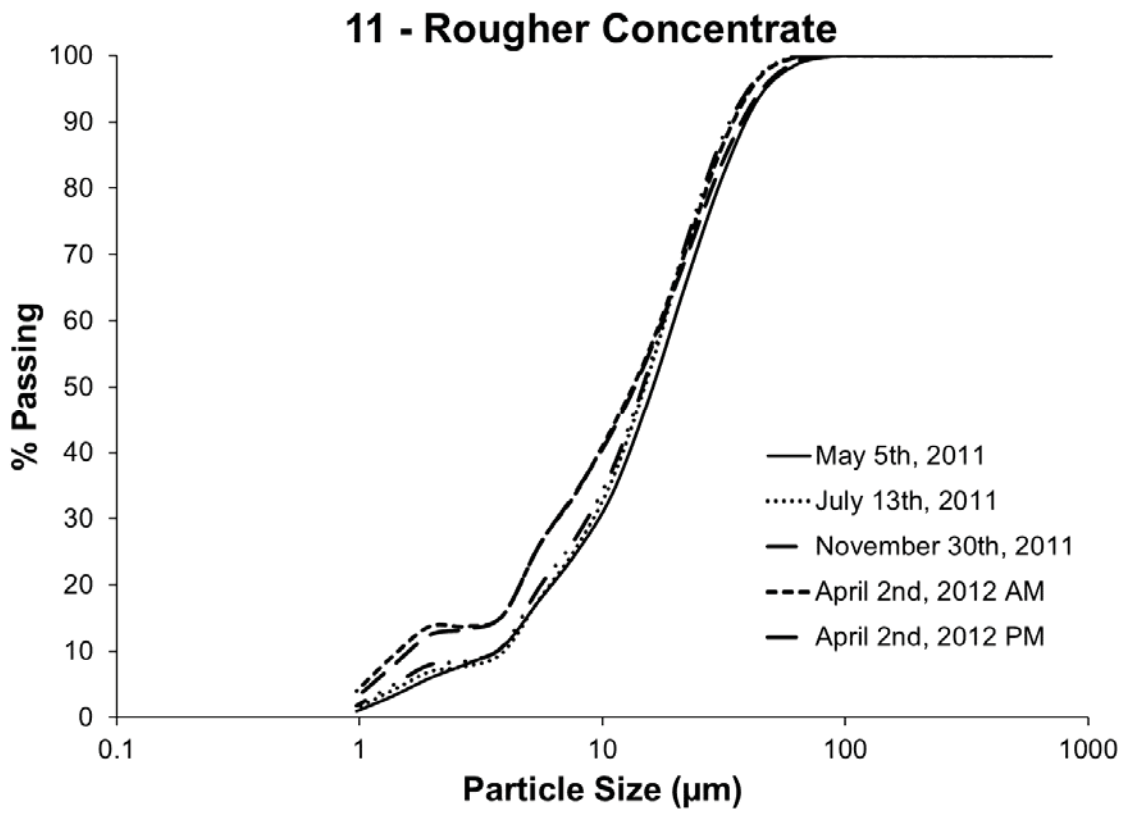

Figure C.10: Particle size distribution of rougher concentrate solids for each sample set.

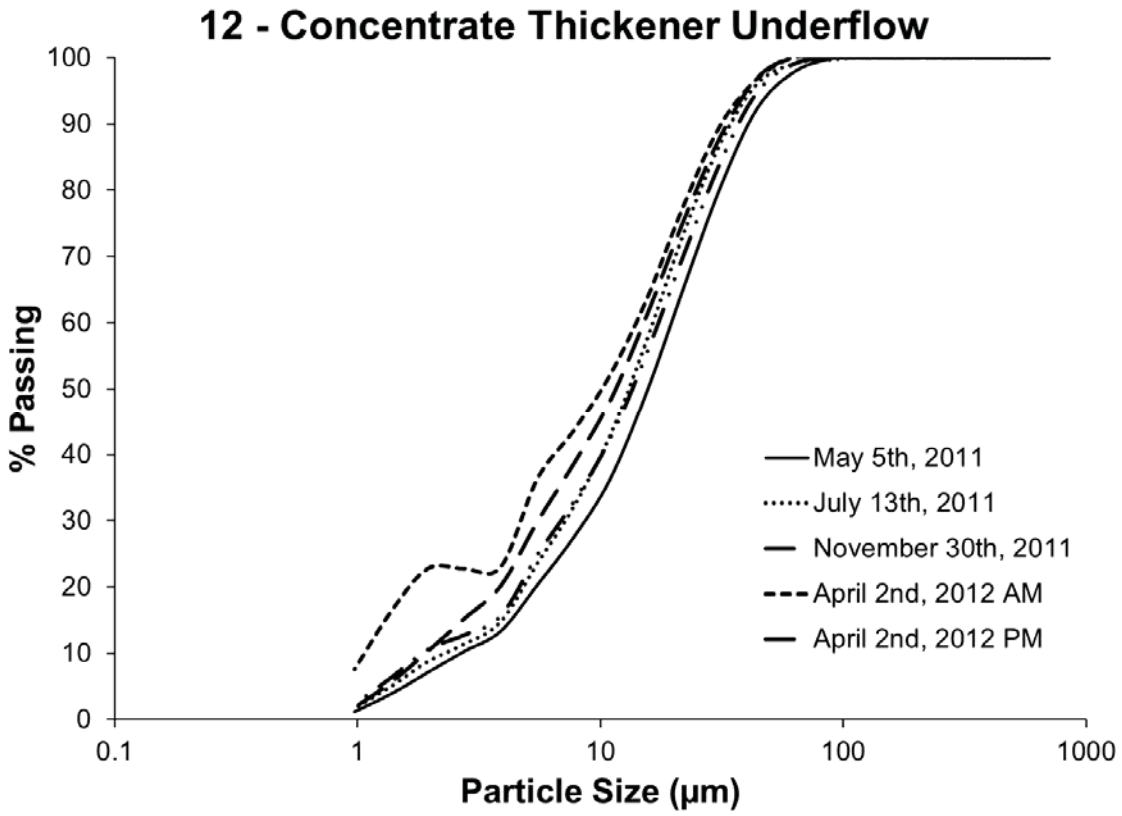

Figure C.11: Particle size distribution of concentrate thickener underflow solids for each sample set.

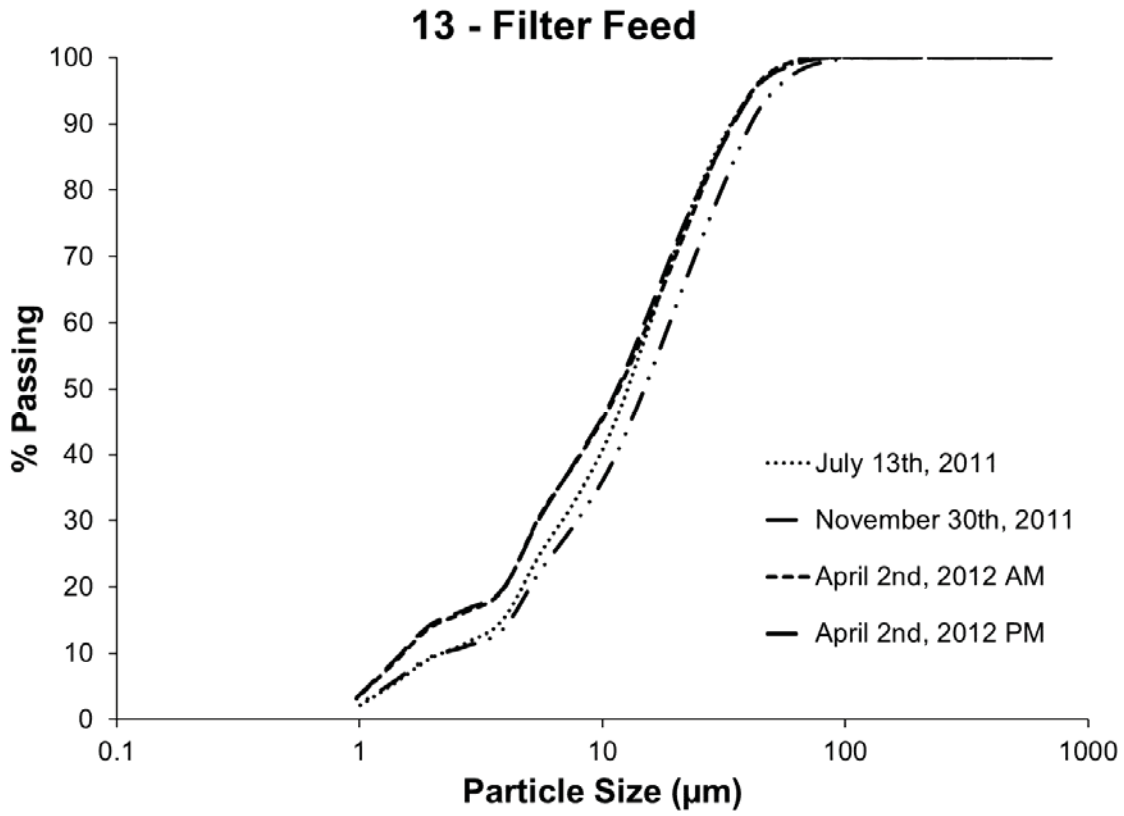

Figure C.12: Particle size distribution of Filter Feed solids for each sample set.